University of Nottingham
UK | CHINA | MALAYSIA

Circular motion Unruh effect: in spacetime and in the laboratory

Cameron Richard David Bunney

Supervised by Jorma Louko

School of Mathematical Sciences
University of Nottingham

Thesis submitted to the University of Nottingham
for the degree of Doctor of Philosophy

September 2024

To my mum and my sister

Abstract

Quantum Field Theory in Curved Spacetime (QFTCS) is an approximation to the union of General Relativity (GR) and Quantum Field Theory (QFT). Born out of Parker's investigations into cosmological particle creation, QFTCS has since flourished into a productive field in its own right, giving rise to predictions such as black-hole evaporation and the Unruh effect, which states that a uniformly linearly accelerated observer will react to the Minkowski vacuum as if it were a thermal state in temperature $T = \hbar a/(2\pi c k_{\mathrm{B}})$. Later, in 1981, Unruh demonstrated that acoustic perturbations in a fluid may equivalently be described as a scalar field propagating on a curved spacetime, whose geometry is characterised by the background fluid flow. Furthermore, Unruh found that "the same arguments which lead to black-hole evaporation also predict a thermal spectrum of sound waves should be given out from the sonic horizon in transsonic fluid flow." With this discovery, analogue gravity was born. Over the past forty years, several analogue-gravity and early-Universe simulators have been devised, using physical systems such as ultracold atoms, optical devices, and fluid interfaces. Motivated by the inherent temperature and finite size of the spacetimes provided by these analogue systems, this Thesis extends the theoretical modelling of an accelerated observer to include the effect of thermality and spatial confinement.

Particle detectors in non-inertial motion will register particles in the Minkowski vacuum. A non-inertial trajectory of theoretical and experimental interest is uniform circular motion, in which motion a detector will remain within a finite-size laboratory for an arbitrarily long interaction time. We replace the Minkowski vacuum by a thermal state, breaking the Lorentz invariance of the system and introducing a Doppler effect in the response of the detector. We identify a measure to isolate the acceleration-dependent, rather than velocity-dependent, contribution to the response of a detector. We then apply this modelling to the analogue spacetime provided by thin films of superfluid helium-4 and propose an experiment to extract the observer dependence in the response of a detector probing a quantum field prepared in a thermal state.

We consider the robustness of the duality between an accelerated observer in the Minkowski vacuum and a static observer in a thermal bath by introducing circular motion; we compare the experience of a detector undergoing uniform circular motion through a thermal bath with that of a detector undergoing uniform circular motion whilst linearly accelerating orthogonal to the plane of rotation, known as hypertor motion. Linear acceleration, hypertor motion, and circular motion are all examples of "stationary trajectories", for which motions there exist Unruh-like phenomena. We provide a geometric and algebraic classification of the stationary trajectories in $(n+1)$-dimensional Minkowski spacetime.

We investigate how the presence of a cylindrical boundary affects the response

of a detector undergoing uniform circular motion both through the Minkowski vacuum and through a thermal bath. Our modelling includes the effects of spatial confinement, thermality, a modified dispersion relation, and a finite-time interaction between the quantum field and the detector. We consider the asymptotic behaviour of the response of the detector in the limit of a large boundary. We examine to what extent the spacetimes of constant positive and negative curvature, de Sitter (dS) and anti-de Sitter (AdS) spacetimes, may be considered curved-spacetime analogues of thermality and spatial confinement in the limit of a small cosmological constant and compare with the corresponding results in Minkowski spacetime.

We present two results concerning Bessel functions, which we have not found in the existing literature.

Acknowledgements

First and foremost, I would like to thank my supervisor, Jorma, for your continued support and guidance throughout my PhD; it is difficult to even conceive of a supervisor more dedicated to their students than you and I am grateful to have learned so much from you. I have a deep respect and admiration for you and for your rigorous approach to mathematics. If I have improved as a mathematician and scientist, it is all thanks to you.

Next, and in equal measure, I would like to thank my second supervisor, Silke; your scientific drive and vision are inspiring and infectious. Thank you for welcoming me into the Gravity Laboratory and thank you for your confidence in me, encouraging me to be the best physicist I can be.

I want also to thank my previous mentors, without whom this Thesis would not be here today. Thank you, Dr Stokes, for your support throughout school and belief in me that I could become a mathematician. I thank also my Bachelor's and Master's supervisors, Kirill Krasnov and Alexander Schenkel, for instilling in me a love of mathematical physics and opening my eyes to the beauty of geometry.

To all members and visitors of the Gravity Laboratory, past and present, I thank you for our discussions, your feedback, and support during my PhD. I would like to thank especially Vitor and Patrik. Vitor, I have learnt much from you and I am sincerely grateful for the time we have spent together. In musical theatre, a "triple threat" is a performer of skill in singing, dancing, and acting. I extend this title to you for your theoretical, experimental, and numerical skills. Patrik, your ability to lead a team, from designing a cryostat, through to the impeccable execution of the experiment and subsequent publication in Nature is beyond impressive. Thank you for letting a mathematician into your laboratory and taking the time to answer all of my questions about helium and experimental physics. I thank you both for your comments, your thoughts, and your time; this Thesis is all the stronger because of you.

Being at University of Nottingham has afforded me many wonderful friends, both within the research group and without, some with whom I was able to work during my PhD. Leo and Rick, thank you for your friendship and for our many discussions, I have always left them feeling motivated and driven to learn, to improve, and to do more maths. Beyond academia, Aleena, thank you for your friendship, our caffeinated catch-ups, and for being the most considerate friend a person could wish for.

To my family. To my mum, my greatest cheerleader, thank you for your unconditional love and support. As long as I tried my best, that was more than enough for you and I can say that I have put my heart and soul into this PhD and into this Thesis; I feel secure in the knowledge that you are proud of that. To my sister, Megan, my earliest best friend. Thank you for your consistent support, the care packages you sent when the PhD was overwhelming during the pandemic meant more than you could know and thank you for always being there. To Graham, thank you for all of the (poor) jokes, the laughter, and the help over the years, I appreciate it more than I express.

Finally, to Kuba, my better half. Thank you for your selfless support during my PhD and during the writing of this Thesis. Without your support, I cannot be certain that I would have completed this stage. Thank you for you constancy, your grounding, and your rationality. You have been my rock and I am a better person because of you.

To everyone who has supported me during this time, thank you.

Preface

IN *principio erat universitas iuxta Minkowski. Universitas erat inanis et vacua. Omnes spectatores sine acceleratione erant concordes. Tum venit Rindler. Dixitque Rindler fiat acceleratio et facta est acceleratio. Tamen universitas iuxta Rindler erat quoque inanis et vacua. Tum venit Unruh. Rogavitque Unruh spectatores Rindlerosos quomodo videtur universitatem Minkowskiosam? Dixeruntque calida est. Viditque Unruh effectum et quod esset bonum.*

IN the beginning, there was the Universe according to Minkowski. The Universe was void and empty. All inertial observers were in agreement. Then came Rindler. And Rindler said "let there be acceleration". And acceleration was made. However, the Universe according to Rindler was also void and empty. Then came Unruh. And Unruh asked the Rindler observers "how does the Minkowski Universe appear?" And they said "it is hot." And Unruh saw this effect and saw that it was good.

List of Publications

[1] Bunney, C R D and Louko, J
Circular motion analogue Unruh effect in a thermal bath: robbing from the rich and giving to the poor
Classical and Quantum Gravity, **40** 155001, June 2023. [Chapter 3]

[2] Bunney, C R D, Barroso, V S, Biermann, S, Geelmuyden, A, Gooding, C, Ithier, G, Rojas, X, Louko, J, and Weinfurtner, S
Third sound detectors in accelerated motion.
New Journal of Physics, **26** 065001, June 2024. [Chapter 4]

[3] Bunney, C R D, Parry, L, Perche, T R, and Louko, J
Ambient temperature versus ambient acceleration in the circular motion Unruh effect
Physical Review D, **109** 065001, March 2024. [Chapter 5]

[4] Bunney, C R D
Stationary trajectories in Minkowski spacetimes
Journal of Mathematical Physics, **65** 052501, May 2024. [Chapter 6]

[5] Bunney, C R D and Louko, J
Circular motion in (anti-)de Sitter spacetime: thermality versus finite size
arXiv preprint, June 2024. [Chapter 8]

List of Figures

List of Abbreviations

AdS	Anti-de Sitter
BEC	Bose-Einstein condensate
BH	Black Hole
CAdS	Universal Covering Space of Anti-de Sitter
dS	de Sitter
ESU	Einstein Static Universe
FLRW	Friedmann – Lemaître – Robertson – Walker
GEMS	Global Embedding Minkowski Spacetime
GR	General Relativity
KG	Klein-Gordon
PSD	Power Spectral Density
QFT	Quantum Field Theory
QFTCS	Quantum Field Theory in Curved Spacetimes
RdS	Rindler-de Sitter
SNR	Signal-to-Noise
UDW	Unruh-DeWitt

List of Symbols

Physical Constants

$\hbar$	Reduced Planck constant	$1.054\,571\,82 \times 10^{-34}\,\mathrm{J\,s}$
h	Planck constant	$6.626\,070\,15 \times 10^{-34}\,\mathrm{J\,s}$
k_B	Boltzmann constant	$1.380\,649 \times 10^{-23}\,\mathrm{J\,K^{-1}}$
ϵ_0	Permittivity of free space	$8.854\,187\,812\,8 \times 10^{-12}\,\mathrm{F\,m^{-1}}$
μ_0	Permeability of free space	$1.256\,637\,062\,1 \times 10^{-6}\,\mathrm{N\,A^{-2}}$
c	Speed of light in vacuum	$2.997\,924\,58 \times 10^{8}\,\mathrm{m\,s^{-1}}$
G	Gravitational constant	$6.674\,30 \times 10^{-11}\,\mathrm{N\,kg^{-2}\,m^{2}}$
g_0	Acceleration of gravity on Earth	$9.806\,65\,\mathrm{m\,s^{-2}}$

Sets of Numbers, Sets of Functions, and Groups

$\mathbb{N}$	Natural numbers	
$\mathbb{N}_0$	Natural numbers with zero $\mathbb{N} \cup \{0\}$	
$\mathbb{Z}$	Integers	
$\mathbb{Q}$	Rational numbers	
$\mathbb{R}$	Real numbers	
$\mathbb{C}$	Complex numbers	
$\mathbb{S}^n$	n-dimensional sphere	
$C(\mathbb{R})$	Space of real-valued functions	
$C_0^\infty(\mathbb{R})$	Space of smooth, real-valued functions of compact support	
$\mathrm{O}(n)$	Orthogonal group in dimension n	113

Functions and Operators

Other Symbols

Contents

Chapter 1

Introduction

"By his theory of relativity Albert Einstein has provoked a revolution of thought in physical science.
... Physical space and time are found to be closely bound up with [the] motion of the observer; and only an amorphous combination of the two is left inherent in the external world."

Arthur Eddington
Space Time and Gravitation (1920)

TWO of the greatest triumphs of mathematical physics of the twentieth century are General Relativity (GR) and Quantum Field Theory (QFT), together illuminating the four fundamental forces of Nature. Whilst gravity is the domain of GR, the unified electromagnetic, strong, and weak interactions are governed by the framework of QFT. From the general relativistic explanation of the precession of the perihelion of Mercury [6] and the observation of the deflection of light by the Sun [7], to the prediction [8–10] and subsequent detection [11] of the Higgs boson, GR and QFT have stood resolute in the face of many tests.

The union of the four fundamental forces though a quantum theory of gravity is, however, the subject of ongoing research. This notwithstanding, significant progress has been made in the theory of Quantum Field Theory in Curved Spacetimes (QFTCS), in which one promotes the Minkowski metric in QFT to a general Lorentzian metric with either a minimally or non-minimally coupled quantum field [12–14]. Minimal coupling is simply the promotion of the Minkowski metric to a general Lorentzian metric, whereas non-minimal coupling is the subsequent inclusion of an additional term in the action, coupling the quantum field to the Ricci scalar curvature of the underlying spacetime.

The nascence of QFTCS began in 1968 with the discovery of cosmological particle production by Parker [15–17]. As recalled by Parker [18], "to investigate the creation of particles by the metric of an expanding universe in general relativity, it was first necessary to extend the quantum field theory of elementary particles from the well-established flat Minkowski spacetime of special relativity to the context of a classical general relativistic expanding universe with a general expansion scale-factor." In his calculations, Parker considered a Friedmann – Lemaître – Robertson – Walker (FLRW) Universe with a scale factor $a(t)$. Assuming that the scale factor was constant at early times $a(t) = a_1$ and constant at late times $a(t) = a_2$ with $a_1 \neq a_2$, Parker modelled a smoothly expanding Minkowski spacetime. Since it was known, "from the experimentally established interpretation of quantum field theory in flat spacetime, how to identify the particles that were created and annihilated during any period when $a(t)$ was constant, [Parker] could unambiguously interpret the effect of the expansion of the Universe on the particle number," [18] finding that the particle content of the Universe at early times did not agree with the particle content of the Universe at late times: cosmological expansion produces particles.

The framework of QFTCS was extended by Hawking in 1975 to generally curved spacetimes, rather than just those that are flat at early and late times, leading to the discovery that not only expanding Universes, but black holes too, create particles [19]. By considering the Schwarzschild solution [20] with mass M, Hawking showed that "quantum mechanical effects cause black holes to create and emit particles as if they were hot bodies with temperature $T = \hbar c^3/(8\pi G M k_{\mathrm{B}})$", a temperature which has come to be known as the Hawking temperature.

A year later in 1976, in studying black hole evaporation, Unruh considered a uniformly linearly accelerated observer in Minkowski spacetime [21]. From two perspectives, Unruh demonstrated that an accelerated observer with proper acceleration a would experience the Minkowski vacuum as if it were a thermal state in temperature $T = \hbar a/(2\pi c k_{\mathrm{B}})$, a temperature which has come to be known as the Unruh temperature. This effect is known as the Unruh effect and highlights the observer-dependence of the perception of particles within QFT. First, Unruh demonstrated that the Minkowski vacuum may be written as a thermal state in the Unruh temperature from the perspective of a uniformly accelerated observer. Second, Unruh considered a two-level system interacting with a quantum field, modelling a simple detector, where the two states represent the detector's ground and excited states. The detector model quantifies the excitations and de-excitations in the quantum field and, as such, may also be used as a thermometer. Unruh demonstrated that the ratio of excitation and de-

excitation probabilities of the detector fit a Boltzmann distribution in the Unruh temperature: an accelerated detector reacts to a quantum field in the Minkowski vacuum as if it were a thermal bath in the Unruh temperature. Later refined by DeWitt [22], this detector model has come to be known as the Unruh-DeWitt (UDW) detector model.

The UDW detector model has become an indispensable theoretical tool for exploring quantum fields, with applications such as: probing Hawking radiation [21, 23] and the Unruh effect [21, 24–30]; probing quantum fields outside of black holes [23, 31–36]; probing entanglement in quantum field theory [37–42]; accessing the correlation function of quantum fields [43, 44]; and the implementation of numerous quantum information protocols [45–49].

A further year later in 1977, Gibbons and Hawking discovered a third thermal effect in QFTCS. In their studies of cosmological particle production in the de Sitter (dS) Universe, Gibbons and Hawking found it to be thermal with temperature $T = \hbar\sqrt{\Lambda}/(2\sqrt{3}\pi k_{\mathrm{B}})$, where $\Lambda > 0$ is the cosmological constant [50]. The Hawking, Unruh, and Gibbons-Hawking temperatures may all be written in the form $T = \hbar\kappa/(2\pi k_{\mathrm{B}})$ for some κ. Further linking the Hawking, Unruh, and Gibbons-Hawking effects is the presence of a horizon: an event horizon, an acceleration horizon, and a cosmological horizon respectively. In their work, Gibbons and Hawking found the more general result that a temperature may be associated to each spacetime with a Killing horizon. Indeed, this temperature is given by $T = \hbar\kappa/(2\pi k_{\mathrm{B}})$, where κ is the surface gravity of the horizon.

Whilst the early studies in QFTCS were purely theoretical, in 1981 the discipline of analogue gravity emerged and with it opened new avenues for empirical verification. In the seminal work "*Experimental Black Hole Evaporation?*" [51], Unruh considered the Euler equation [52] and demonstrated that acoustic perturbations in an inviscid fluid may be interpreted as a massless scalar field propagating on a curved spacetime background, whose metric is determined by the background velocity field of the fluid flow, and in which metric the speed of light is replaced by the speed of sound in the fluid. The guiding principle of this equivalence is that "the same equations have the same solutions" [53]. Unruh found that "the same arguments which lead to black hole evaporation also predict that a thermal spectrum of sound waves should be given out from the sonic horizon in transsonic fluid flow."

A hydrodynamical black hole in $1{+}1$ dimensions may be visualised as a stream ending in a tall waterfall; light rays and the speed of light may be replaced by ripples on the surface of the water and the speed of surface wave propagation respectively. Far away from the waterfall, ripples on the surface of the water may travel both upstream and downstream. However, as one approaches the

waterfall, the flow speed of the water increases. Eventually, there will be a point at which the speed of surface wave propagation is equal to the flow speed of the water, representing the analogue event horizon. Any ripples on the surface beyond this point are carried downstream and may not escape upstream.

The theory of hydrodynamical black holes was further developed in 2002 by Schützhold and Unruh [54], in which work rotating black hole analogues and related phenomena such as superradiance were investigated. Furthermore, Visser and Weinfurtner [55] demonstrated in 2004 that the geometry of the equatorial slice of the Kerr spacetime may be reproduced by a rotational draining vortex flow. Subsequent to this major work, the field of analogue gravity soon developed further in several directions. Studies by Novello et al. [56] and Volovik [57] considered analogue simulators for gravity and cosmology in condensed-matter systems such as Bose-Einstein condensates (BECs) and superfluid helium, both experimentally realisable inviscid fluids.

After an era of predictions of phenomena in analogue systems came the era of empirical verification. The first analogue horizons were observed in 2008, both using pulsed light in an optical fibre [58] and in open-channel water flow [59]. Later in 2011, Weinfurtner et al. [60] made an observation of the stimulated Hawking spectrum and in the following years, several further black hole phenomena were observed in $(2+1)$-dimensional hydrodynamical systems, such as: superradiance around an analogue rotating black hole [61]; the relaxation of an analogue black hole through the emission of quasinormal modes [62]; and the observation of bound states in a giant superfluid helium vortex flow [63].

The experimental verification of phenomena predicted in QFT has not been the domain solely of analogue gravity. In 1983, Bell and Leinaas [64] proposed the spin of an electron in a magnetic field as a possible candidate for a detector of the Unruh effect. However, the use of electron spin as a detector of the perceived thermal bath requires a long period of acceleration to produce an effect and so Bell and Leinaas proposed using a circular orbit, rather than a uniformly linearly accelerated trajectory. Furthermore, Bell and Leinaas suggested that the residual polarisation of electrons in an electron storage ring is therefore a measure of the temperature of the thermal bath perceived by the electrons. Jackson [65], however, raised doubts about the use of thermality to explain the residual polarisation of the electrons in such storage rings.

Motivated by Jackson's response, Unruh [66] investigated the experience of an accelerated electron in circular motion. Unruh found that a detector in uniform circular motion will react to the Minkowski vacuum through excitations and de-excitations, but with an effective temperature that depends on the energy gap between the two levels of the detector. In the case of an accelerated electron,

however, the circular orbit is not strictly uniform due to oscillations of the electron perpendicular to the plane of circular motion. Unruh found that the electron will indeed respond to this approximately thermal bath, however, due to complications in the theoretical understanding of rotating electrons interacting with an electromagnetic field [67], finding a direct connection between the observation of the residual polarisation of electrons in an electron storage ring and the circular motion Unruh effect remains elusive [68].

Whilst the residual polarisation of electrons remains inconclusive as an observation of the Unruh effect, the studies of Bell, Leinaas, and Unruh predict the existence of other related effects such as the circular motion Unruh effect. Circular motion holds a key advantage over linear acceleration in an experimental realisation of the effect: the experiment can remain within a finite-size laboratory for an arbitrarily long interaction time. As such, the circular motion Unruh effect remains a strong candidate for the observation of observer-dependence of the perception of particles in QFT. In the following Chapters, we study the circular motion Unruh effect, modelling several experimentally relevant features, bridging the gap between theory and experiment, and laying the foundations for an experimental realisation of the effect.

1.1 Outline

The Chapters of this Thesis are organised as follows.

In Chapter 2, we present the theoretical and mathematical foundations that will be present throughout this work. We begin by presenting three derivations of the Unruh effect, each highlighting a unique aspect of the effect. We consider the effect geometrically and quantum field theoretically and finally in the UDW detector formulation. The central object of the detector formalism is the detector transition probability, a measure of detector excitation and de-excitation. We then introduce explicitly the analogue spacetime provided by inviscid hydrodynamical systems. We reproduce some key results from the analysis of the circular motion Unruh effect in $2+1$ and $3+1$ dimensions in [69] in both a genuinely relativistic spacetime and analogue spacetime formulation. Finally, we introduce a generalisation of the UDW detector, the continuous quasiparticle detector model [70], in which the two-level UDW detector is replaced by a continuous probing field.

Motivated by the inherent temperature in any experimental realisation of the circular motion Unruh effect, we replace in Chapter 3 the initial vacuum state of the quantum field by a thermal state. A key observation is that the inclusion of

a thermal bath breaks the Lorentz invariance of the system. In particular, not all inertial observers will agree on the particle content of the spacetime; there will be velocity-dependent phenomena in the response of a detector. As such, we develop measures to isolate the acceleration-dependence and demonstrate that, independent of the ambient temperature, acceleration-dependence may be identified in some range of the parameter space in the response of a UDW detector, even when the ambient temperature is so high that the detector's response is dominated by the ambient thermal bath.

In Chapter 4, we develop an experimental proposal for the realisation of acceleration-dependent response in thin-film superfluid helium-4. We introduce superfluid phenomenology and demonstrate that, within experimentally viable regimes, thin films of superfluid helium may be considered as analogue spacetimes. Samples of superfluid helium exist at very low but nonzero temperatures. As such, we apply the thermal field theory developed in Chapter 3 to incorporate the sample temperature into our model. Furthermore, we demonstrate that a laser may act as a local detector of fluctuations on the surface of thin-film superfluid helium. Then, through an experimentally accessible measure, we demonstrate that observer-dependence persists in a system with a significant ambient temperature and, furthermore, that the background temperature enhances the signature of this effect.

In Chapter 5, we probe the robustness of the Unruh effect. At its heart, the Unruh effect is the duality between the experience of an accelerated observer through the Minkowski vacuum and a static observer in a thermal bath. We compare the experience of an observer undergoing uniform circular motion through a thermal bath in $3+1$ Minkowski spacetime with that of an observer undergoing uniform circular motion and linear acceleration orthogonal to the plane of rotation. We compare the two motions in a range of asymptotic regimes and find that the addition of circular motion in general breaks the duality; any circular perturbation would enable a particle detector to distinguish between a genuine thermal bath and the thermal bath provided by linear acceleration.

In Chapter 6, we discuss stationary trajectories, a class of trajectory for which the two-point function is time-translation invariant. It was shown in [71, 72] that Unruh-like phenomena exist for all six stationary trajectories in $3+1$ Minkowski spacetime. Furthermore, all trajectories considered in the preceding Chapters are stationary. In this Chapter, we provide an algebraic and geometric classification of the stationary trajectories in $n+1$ Minkowski spacetime. Finally, by considering dS spacetime as embedded in Minkowski spacetime of one higher spatial dimension, we provide a classification of the stationary trajectories in the static patch of dS spacetime.

Motivated by the finite size of the analogue spacetimes provided by condensed matter systems such as thin-film superfluid helium, we consider in Chapter 7 a detector undergoing uniform circular motion in analogue $2+1$ Minkowski spacetime with a cylindrical boundary. We consider a quantum field in its vacuum state and also when the field is prepared in a thermal state. Allowing for full generality, we also include a finite-time interaction and allow for a field with a modified (nonlinear) dispersion. After specialising to a Klein-Gordon (KG) field and an infinite interaction time, we consider the asymptotic behaviour of the response of the UDW detector in the limit of a large cylindrical boundary and find the leading and subleading terms. At subleading order, we find resonance peaks when the detector's energy gap is equal to the angular frequency of the circular trajectory — resonant detectors are more sensitive to a cylindrical boundary.

Finally, having analysed the effect of an ambient temperature in Chapter 3 and a cylindrical boundary in Chapter 7, we investigate in Chapter 8 to what extent dS and Anti-de Sitter (AdS), the spacetimes of constant positive and negative curvature respectively, may be considered curved-spacetime analogues of thermality and finite size. Positive curvature provides a notion of an ambient temperature, via the Euclidean vacuum, whereas negative curvature provides a notion of spatial confinement. dS and AdS spacetimes are solutions to Einstein's field equations with a positive and negative cosmological constant respectively, which tend to Minkowski spacetime in the limit of a vanishing cosmological constant. In terms of thermality and spatial confinement, a small cosmological constant corresponds to the limit of a low ambient temperature and a large boundary.

We consider a UDW detector undergoing uniform circular motion in the static patch of dS and in AdS and find the leading and subleading contributions to the response of the detector. We find that dS does indeed act as a curved-spacetime analogue of Minkowski spacetime with a low ambient temperature. However, we find that AdS serves as a curved-spacetime analogue of Minkowski spacetime with a large cylindrical boundary only when the field is prepared in the global static vacuum. When the field is prepared in a thermal state, we find a resonance peak in the detector's response with no corresponding term in the corresponding Minkowski spacetime calculation in Chapter 7; we find that thermal states in AdS exhibit richer features than their Minkowski spacetime counterparts.

1.2 Mathematical conventions

We use metric signature $(-,+,\ldots,+)$. Except in Chapter 4, we use units in which $c = \hbar = k_{\mathrm{B}} = 1$, where c represents the speed of light in a relativistic spacetime setting and the speed of sound in an analogue spacetime setting. Sans serif letters (x) denote spacetime points and boldface Italic letters ($\boldsymbol{k}$) denote spatial vectors. Quantum operators are denoted by a circumflex, $\hat{a}$. In asymptotic formulae, $f(x) = \mathcal{O}(g(x))$ denotes that $f(x)/g(x)$ remains bounded in the limit considered, $f(x) = o(g(x))$ denotes that $f(x)/g(x)$ tends to zero in the limit considered, and $f(x) \sim g(x)$ denotes that $f(x)/g(x)$ tends to unity in the limit considered.

1.3 Statement of originality

This Thesis is a result of my own work, done in collaboration with members of the research group and other academic partners, in and out of the University of Nottingham. Below, I disclaim the related publications and contributions to the work in each chapter.

- Chapter 2 is a review of well-established work.
- Chapter 3 is based on [1]. I played a significant role in all aspects of this project.
- Chapter 4 is based on [2]. This work is the result of an extended collaboration. I led the project and actively contributed to the development of the theoretical framework and mapping between the QFT and hydrodynamical descriptions, and the interpretation of the results. The Figures in this Chapter were produced by Vitor S Barroso.
- Chapter 5 is based on [3]. I played a significant role in all aspects of this project.
- Chapter 6 is based on [4]. I completed this project in its entirety.
- Chapter 7 is based on [5]. I played a significant role in all aspects of this project.
- Chapter 8 is based on a publication in progress [73]. I play a significant role in all aspects of this project.

Chapter 2

Unruh effect: Uniform linear acceleration and circular motion

"A particle is what a particle detector detects."

William G Unruh

2.1 Unruh effect: Uniform linear acceleration

THE Fulling-Davies-Unruh effect [21, 74, 75] is the remarkable prediction of Quantum Field Theory (QFT) that a uniformly accelerating observer in Minkowski spacetime reacts to a quantum field in its Minkowski vacuum through excitations and de-excitations with the characteristics of a thermal state at the Unruh temperature,

$$T_U = \frac{\hbar a}{2\pi c k_{\mathrm{B}}} . \tag{2.1}$$

Fulling (1972 [74]) demonstrated first the inequivalence of the particle content of vacua in static spacetimes, summarised as "the particles or quanta of the Rindler-Fock (rus. Фок) representation cannot be identified with the physical particles described by the usual quantum theory of the free field." Davies (1975 [75]) then showed that a fixed inertial mirror in an accelerating coordinate system would emit thermal radiation with temperature (2.1), interpreting that "the concept of a particle is ill-defined and observer-dependent". Finally, Unruh (1976 [21]) provided an explanation for Davies' conclusion [27], expressing the Minkowski vacuum in terms of a Gibbs state from the perspective of a uniformly accelerated observer, and introduced the particle detector, now known as the Unruh-DeWitt (UDW) detector.

In this Section, we demonstrate different perspectives of the Unruh effect. First we outline the geometric origin of the Unruh effect and its relation to

phenomena such as the Hawking effect [19]. We then demonstrate its grounding with QFT. Finally, we introduce the UDW particle detector model and show how the Unruh effect arises from the excitations and de-excitations of a particle detector.

Except in (2.1), we will use units in which $\hbar = c = G = k_{\mathrm{B}} = 1$.

2.1.1 Geometric perspective

We consider first the geometric interpretation of the Unruh effect before exploring its foundation within QFT. As a toy model, we consider $(1+1)$-dimensional Minkowski spacetime in inertial coordinates (t, x) with the metric

$$\mathrm{d}s^2 \;=\; -\mathrm{d}t^2 + \mathrm{d}x^2 \,. \tag{2.2}$$

Everything that follows generalises easily to the case of arbitrary dimension. We consider an observer on a trajectory $\mathsf{x}(\tau)$ parametrised by its proper time τ,

$$t(\tau) \;=\; \frac{1}{A}\sinh(A\tau)\,, \quad x(\tau) \;=\; \frac{1}{A}\cosh(A\tau)\,. \tag{2.3}$$

This is the trajectory of a uniformly accelerated observer with proper acceleration A. One may, however, use coordinates (η, ξ) adapted to this trajectory,

$$t \;=\; \frac{1}{a}\mathrm{e}^{a\xi}\sinh(a\eta)\,, \quad x \;=\; \frac{1}{a}\mathrm{e}^{a\xi}\cosh(a\eta)\,, \tag{2.4}$$

where $\eta,\ \xi \in \mathbb{R}$.

The coordinates (η, ξ) only cover the region $x > |t|$ in Minkowski spacetime, a region known as the right Rindler wedge, depicted as region **I** in Figure 2.1. In these coordinates, trajectories of constant ξ are trajectories of constant proper acceleration. In particular, an observer with constant proper acceleration $a = A$ moves along the path $\eta = \tau$, $\xi = 0$. The pullback of the metric (2.2) to the right Rindler wedge (2.4) is

$$\mathrm{d}s^2 \;=\; \mathrm{e}^{2a\xi}\left(-\mathrm{d}\eta^2 + \mathrm{d}\xi^2\right)\,. \tag{2.5}$$

From the metric (2.5), one identifies ∂_η as a Killing vector. Let f be a smooth map (coordinate transformation) from the right Rindler wedge in coordinates (η, ξ) to Minkowski spacetime in coordinates (t, x). Then, the pushforward of the Killing vector ∂_η to Minkowski spacetime through the function f is

$$f_*(\partial_\eta) \;=\; a(x\partial_t + t\partial_x) \;=:\; \Xi^\mu \partial_\mu\,. \tag{2.6}$$

This is the Killing vector in Minkowski spacetime associated with boosts parallel

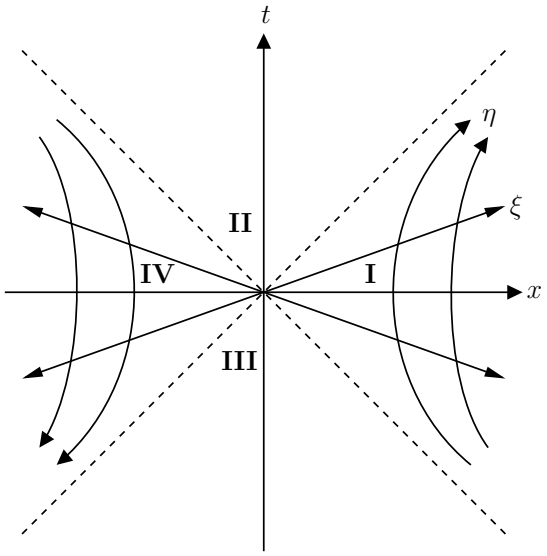

Figure 2.1: Spacetime diagram of Minkowski spacetime. Regions **I** and **IV** represent the right and left Rindler wedges respectively, in which the coordinates (η, ξ) (2.4) may be used, pointing in opposite directions in each wedge. Dashed lines represent the Killing horizons $x = \pm|t|$.

to the x-axis. The magnitude of this Killing vector is $a^2(-x^2 + t^2)$: this is timelike for $x > |t|$ and $x < -|t|$; spacelike for $-|t| < x < |t|$; and null for $x = \pm|t|$.

We have already identified the region $x > |t|$ with the right Rindler wedge. We now identify the region $x < -|t|$ as the left Rindler wedge (region **IV** in Figure 2.1) with coordinates

$$t \;=\; -\frac{1}{a}\mathrm{e}^{a\xi}\sinh(a\eta)\,, \quad x \;=\; -\frac{1}{a}\mathrm{e}^{a\xi}\cosh(a\eta)\,. \tag{2.7}$$

The null hypersurfaces $x = \pm|t|$, on which the Killing vector Ξ^μ (2.6) is null, are Killing horizons [13], known in this context as "acceleration" or "Rindler" horizons, and together they form a bifurcate Killing horizon. Associated with any Killing horizon Σ is its surface gravity κ, which is defined as [13, 76]

$$\Xi^\nu \nabla_\nu \Xi^\mu\big|_\Sigma \;=\; \kappa\, \Xi^\mu\big|_\Sigma\,, \tag{2.8}$$

and given explicitly by

$$\kappa^2 \;=\; -\frac{1}{2}(\nabla^\mu \Xi^\nu)(\nabla_\mu \Xi_\nu)\big|_\Sigma\,. \tag{2.9}$$

We may further associate a temperature, the Hawking temperature, to a spacetime with a bifurcate Killing horizon [50, 77, 78], proportional to the surface

gravity of the horizon. This temperature is given by [13]

$$T \;=\; \frac{\kappa}{2\pi}\,. \tag{2.10}$$

We find this relation now in the case of static, spherically symmetric spacetimes.

Example 2.1. We consider an $(n+1)$-dimensional, static, spherically symmetric spacetime described by the metric

$$\mathrm{d}s^2 \;=\; -f(r)\mathrm{d}t^2 + \frac{1}{f(r)}\mathrm{d}r^2 + r^2\mathrm{d}\Omega^2\,, \tag{2.11}$$

where $\mathrm{d}\Omega^2$ is the metric on the $(n-1)$-sphere. We assume that there exists r_h such that $f(r_h)=0$ and $f'(r_h)\neq 0$.

We first show that $r=r_h$ is a bifurcate Killing horizon. The normal to the hypersurface Σ defined by $r=r_h$ is given by $n_\mu = \partial_\mu(r-r_h)$, which has magnitude $n_\mu\, n^\mu|_\Sigma = f(r_h) = 0$; hence, Σ is a null hypersurface. Furthermore, $\Xi = \partial_t$ is a Killing vector of the metric (2.11) with norm $\Xi^\mu\Xi_\mu = -f(r)$ that vanishes on Σ; hence, Σ is a Killing horizon. Finally, by employing Kruskal–Szekeres-like coordinates, one finds that there exist both a past and a future horizon, which comprise the bifurcate Killing horizon.

By direct calculation using (2.9), we find the surface gravity

$$\kappa^2 \;=\; -\frac{1}{2}\left[g_{rr}g^{tt}(\Gamma^r_{tt})^2 + g_{tt}g^{rr}\left(\Gamma^t_{rt}\right)^2\right]\Big|_\Sigma \;=\; \frac{1}{4}\left(f'(r_h)\right)^2\,. \tag{2.12}$$

We next show that one may associate the temperature $T=\kappa/(2\pi)$ with the horizon. Near the horizon, it is convenient to introduce a new radial coordinate ρ measuring the proper distance from the Killing horizon. For spacetimes with $r>r_h$, such as Schwarzschild and Reissner-Nordström, we write

$$\rho(r) \;=\; \int_{r_h}^{r} \mathrm{d}r'\,\frac{1}{\sqrt{f(r')}}\,. \tag{2.13a}$$

Whereas for spacetimes with $r<r_h$, such as the static patch of de Sitter (dS), we write

$$\rho(r) \;=\; \int_{r}^{r_h} \mathrm{d}r'\,\frac{1}{\sqrt{f(r')}}\,. \tag{2.13b}$$

Close to the horizon, we have $f(r) = |r-r_h||f'(r_h)| + \mathcal{O}((r-r_h)^2)$, allowing us to evaluate the integral (2.13). To leading order, we find the relation

$$\rho^2(r) \;=\; \frac{2}{\kappa}|r-r_h|\,, \tag{2.14}$$

where we have identified $\kappa = \frac{1}{2}|f'(r_h)|$.

We write the (t, r) part of the metric (2.11) as

$$\mathrm{d}s^2 \;=\; \Xi^\mu \Xi_\mu \mathrm{d}t^2 + \mathrm{d}\rho^2\,, \tag{2.15}$$

where we have used $\Xi^\mu \Xi_\mu = g_{tt}$ and the relation $\mathrm{d}\rho^2 = \mathrm{d}r^2/f(r)$. Near to the horizon, we have

$$\Xi^\mu \Xi_\mu \;=\; -f(r) \;=\; -|r - r_h||f'(r_h)| + \mathcal{O}((r-r_h)^2) \;=\; -\kappa^2\rho^2 + \mathcal{O}(\rho^4)\,, \tag{2.16}$$

where, in the final equality, we have used (2.14). The metric then reads

$$\mathrm{d}s^2 \;=\; -\kappa^2\rho^2 \mathrm{d}t^2 + \mathrm{d}\rho^2\,. \tag{2.17}$$

We perform a Wick rotation $t = -\mathrm{i}\tau$, leading to

$$\mathrm{d}s^2 \;=\; \mathrm{d}\rho^2 + \rho^2 \mathrm{d}(\kappa\tau)^2\,. \tag{2.18}$$

This is simply the flat metric in polar coordinates. To avoid a conical singularity at $\rho = 0$, we require $\kappa\tau$ to be an angle with period 2π; hence, τ is periodic with period $2\pi/\kappa$. In the Euclidean formalism, the periodicity β of imaginary time is related to the inverse temperature $\beta = 1/T$ [79–81] and we find $T = \kappa/(2\pi)$. ■

Returning to the metric (2.5), the surface gravity of the acceleration horizon is simply $\kappa = a$, leading to the well-known Unruh temperature [21],

$$T_U \;=\; \frac{a}{2\pi}\,. \tag{2.19}$$

We may connect this result with Example 2.1. In this example, we found that, close to the horizon, the metric describing a static, spherically symmetric spacetime may be written as

$$\mathrm{d}s^2 \;=\; -\kappa^2\rho^2 \mathrm{d}t^2 + \mathrm{d}\rho^2\,. \tag{2.20}$$

In addition to the coordinates (2.4), we may also cover the right Rindler wedge with the coordinates $(t, x) = (R\sinh(aT), R\cosh(aT))$. Identifying $\kappa = a$, the pullback of the Minkowski metric (2.2) to the right Rindler wedge reads

$$\mathrm{d}s^2 \;=\; -\kappa^2 R^2 \mathrm{d}T^2 + \mathrm{d}R^2\,. \tag{2.21}$$

Comparing (2.20) and (2.21), we see that near to the horizon, the geometry of a static, spherically symmetric spacetime is that of the right Rindler wedge.

With the geometric foundations set, we will move to the QFT interpretation

of this effect in Section 2.1.2. In this Section, we saw that the geometry of a static, spherically symmetric spacetime near to a Killing horizon may be described by the geometry of Rindler spacetime. As such, this connects the Unruh effect with other known phenomena; the event horizon around a black hole is another such Killing horizon. For a Schwarzschild black hole with mass M, the surface gravity is $\kappa = 1/(4M)$, leading to the Hawking temperature $T_H = 1/(8\pi M)$ [19, 50, 77, 82, 83]. A second example is found in dS spacetime [84] with positive cosmological constant Λ. Restricting to the static patch of dS, one finds the presence of a cosmological horizon with associated temperature $T = \sqrt{\frac{\Lambda}{3}}/(2\pi)$ [50].

2.1.2 Quantum field theoretic perspective

In this Section, we give a more standard treatment of the Unruh effect, expressed in terms of expectation values. Results in this Section will be stated without proof. For a detailed account of this calculation, see [27]. In particular, we consider a massless scalar field in $(1+1)$-dimensional Minkowski spacetime. This is an infrared-divergent theory [12]; however, one need not deal with this divergence for the purpose of explicating the Unruh effect [27].

We consider a massless scalar field $\hat{\Phi}(t,x)$ in $(1+1)$ dimensions, satisfying the Klein-Gordon (KG) equation,

$$\left(-\frac{\partial^2}{\partial t^2}+\frac{\partial^2}{\partial x^2}\right)\hat{\Phi}(t,x) \;=\; 0\,. \tag{2.22}$$

This field can be expanded in terms of plane waves. However, it is convenient to introduce null coordinates $U = t - x$, $V = t + x$ and expand the field $\hat{\Phi}$ as

$$\hat{\Phi}(t,x) \;=\; \hat{\Phi}_-(U) + \hat{\Phi}_+(V)\,, \tag{2.23a}$$

$$\hat{\Phi}_\pm(W) \;=\; \int_0^\infty \mathrm{d}k\, \hat{b}_{\pm k} f_k(W) + \mathrm{Hc}\,, \tag{2.23b}$$

$$f_k(W) \;=\; \frac{1}{\sqrt{4\pi k}}\mathrm{e}^{-\mathrm{i}kW}\,, \tag{2.23c}$$

where the annihilation and creation operators satisfy $[\hat{b}_{\pm k}, \hat{b}^\dagger_{\pm k'}] = \delta(k-k')$, $\delta(k)$ is the Dirac delta, and Hc stands for Hermitian conjugate. The left-moving $\hat{\Phi}_+$ and right-moving $\hat{\Phi}_-$ sectors of the field are independent and hence one may consider, without loss of generality, only the left-moving section $\hat{\Phi}_+(V)$. The (global) Minkowski vacuum $|0_\mathrm{M}\rangle$ is defined by $\hat{b}_{+k}\,|0_\mathrm{M}\rangle = 0$ for all k.

One may solve the KG equation in the right Rindler wedge, shown in Figure 2.1. Again, the solutions can be separated into left and right-moving modes

with respect to $u = \eta - \xi$ and $v = \eta + \xi$. For $V > 0$,

$$\hat{\Phi}_+(V) \;=\; \int_0^\infty \mathrm{d}\omega\, \hat{a}^{\mathrm{R}}_{+\omega} g_\omega(v) + \mathrm{Hc}\,, \tag{2.24a}$$

$$g_\omega(v) \;=\; \frac{1}{\sqrt{4\pi\omega}} \mathrm{e}^{-\mathrm{i}\omega v}\,, \tag{2.24b}$$

where the annihilation and creation operators satisfy $[\hat{a}^{\mathrm{R}}_{+\omega}, \hat{a}^{\mathrm{R}\dagger}_{+\omega'}] = \delta(\omega - \omega')$.

The field $\hat{\Phi}_+(V)$ can also be expressed in the left Rindler wedge. Using Rindler coordinates defined by (2.7), one defines $\widetilde{v} = \widetilde{\eta} - \widetilde{\xi}$ such that

$$\hat{\Phi}_+(V) \;=\; \int_0^\infty \mathrm{d}\omega\, \hat{a}^{\mathrm{L}}_{+\omega} g_\omega(\widetilde{v}) + \mathrm{Hc}\,, \tag{2.25}$$

where the annihilation and creation operators satisfy $[\hat{a}^{\mathrm{L}}_{+\omega}, \hat{a}^{\mathrm{L}\dagger}_{+\omega'}] = \delta(\omega - \omega')$. The vacuum state in the left and right Rindler wedges $|0_{\mathrm{R}}\rangle$ is then defined by $\hat{a}^{\mathrm{R}}_{+\omega}|0_{\mathrm{R}}\rangle = \hat{a}^{\mathrm{L}}_{+\omega}|0_{\mathrm{R}}\rangle = 0$.

One may find a Bogoliubov (rus. Боголюбов) transformation to express the Minkowski annihilation and creation operators in terms of those in the left and right Rindler wedges. In particular, one has

$$\left(\hat{a}^{\mathrm{R}}_{+\omega} - \mathrm{e}^{-\pi\omega/a}\hat{a}^{\mathrm{L}\dagger}_{+\omega}\right)|0_{\mathrm{M}}\rangle \;=\; 0\,, \tag{2.26a}$$

$$\left(\hat{a}^{\mathrm{L}}_{+\omega} - \mathrm{e}^{-\pi\omega/a}\hat{a}^{\mathrm{R}\dagger}_{+\omega}\right)|0_{\mathrm{M}}\rangle \;=\; 0\,. \tag{2.26b}$$

These two relations uniquely define the Minkowski vacuum $|0_{\mathrm{M}}\rangle$. Importantly, the Minkowski vacuum is defined in terms of the annihilation and creation operators in *both* the right and left Rindler wedges. The correlation between the right and left Rindler wedges in the global Minkowski vacuum state plays an important role in the Unruh effect [27].

For simplicity, we use box quantisation in which the Rindler energy levels ω are discrete, thereby writing ω_i in place of ω and letting $[\hat{a}^{\mathrm{R}}_{+\omega_i}, \hat{a}^{\mathrm{R}\dagger}_{+\omega_j}] = [\hat{a}^{\mathrm{L}}_{+\omega_i}, \hat{a}^{\mathrm{L}\dagger}_{+\omega_j}] = \delta_{ij}$, where δ_{ij} is the Kronecker delta. The discrete version of (2.26) then allows one to calculate

$$\langle 0_{\mathrm{M}}|\hat{a}^{\mathrm{R}\dagger}_{+\omega_i}\hat{a}^{\mathrm{R}}_{+\omega_i}|0_{\mathrm{M}}\rangle \;=\; \langle 0_{\mathrm{M}}|\hat{a}^{\mathrm{L}\dagger}_{+\omega_i}\hat{a}^{\mathrm{L}}_{+\omega_i}|0_{\mathrm{M}}\rangle \;=\; \frac{1}{\mathrm{e}^{2\pi\omega_i/a} - 1}\,. \tag{2.27}$$

That is to say the expectation value of the number of Rindler particles with respect to the Minkowski vacuum follows a Bose-Einstein distribution at temperature T_U, the Unruh temperature (2.19). This result follows equally without discretisation, in which case one expresses the Rindler annihilation and creation operators using the wave-packet formalism [27]. Furthermore, using this result,

one may show that if one probes only the right Rindler wedge, the Minkowski vacuum is described by a density matrix for a system of free bosons at temperature T_U (2.1). One may perform the calculation for the right-moving modes in a similar fashion, arriving at the same result. Further, this calculation can be generalised easily to higher dimensions [27].

This perspective of the Unruh effect highlights the importance of both the left and right Rindler wedges. In Section 2.1.3, we will consider the response of a detector undergoing uniform linear acceleration and introduce the "response function", an object which will be the main focus of this thesis.

We now end this subsection with the following remark: the Unruh temperature is the same for every field and every coupling, which follows from the Kubo-Martin-Schwinger property of the Minkowski vacuum when written in terms of excitations on the Rindler vacuum, or, at a general level, from the behaviour of the Minkowski vacuum correlation functions under boosts, a property known as the Bisognano-Wichmann theorem [85, 86].

2.1.3 Unruh-DeWitt detector model

In this Section, we review the UDW detector model [21, 22]; a two-level system — a qubit — undergoing a smooth timelike trajectory $\mathsf{x}(\tau)$ in Minkowski spacetime, parametrised by its proper time τ. We present the theory in arbitrary dimensions and give examples in $(3+1)$-dimensional Minkowski spacetime, paralleling [12].

In d spacetime dimensions, the Minkowski metric in inertial coordinates $(t, x^1, x^2, \ldots, x^{d-1})$ reads

$$\mathrm{d}s^2 \;=\; -\mathrm{d}t^2 + (\mathrm{d}x^1)^2 + (\mathrm{d}x^2)^2 + \cdots + (\mathrm{d}x^{d-1})^2 \,. \tag{2.28}$$

We consider a real, massless scalar field $\hat{\Phi}$ satisfying the KG equation,

$$\eta^{\mu\nu}\partial_\mu\partial_\nu\hat{\Phi} \;=\; \left(-\frac{\partial^2}{\partial t^2} + \delta^{ij}\partial_i\partial_j\right)\hat{\Phi} \;=\; 0\,, \tag{2.29}$$

where $\eta_{\mu\nu} = \mathrm{diag}(-1, 1, \ldots, 1)$ and $i,\ j = 1, \ldots, d-1$. The field may be expanded in terms of Minkowski plane-wave modes

$$\hat{\Phi}(\mathsf{x}) \;=\; \int_{\mathbb{R}^{d-1}} \mathrm{d}^{d-1}\boldsymbol{k}\, \phi_{\boldsymbol{k}}(\mathsf{x})\hat{a}_{\boldsymbol{k}} + \mathrm{Hc}\,, \tag{2.30a}$$

$$\phi_{\boldsymbol{k}}(\mathsf{x}) \;=\; \frac{1}{(2\pi)^{(d-1)/2}}\frac{\mathrm{e}^{\mathrm{i}\mathsf{k}\cdot\mathsf{x}}}{\sqrt{2|\boldsymbol{k}|}}\,, \tag{2.30b}$$

where $\mathsf{k} = (|\boldsymbol{k}|, \boldsymbol{k})$, $\mathsf{x} = (t, \boldsymbol{x})$, and $\mathsf{k}\cdot\mathsf{x} = \eta_{\mu\nu}\mathsf{k}^\mu\mathsf{x}^\nu$. The field modes $\phi_{\boldsymbol{k}}(\mathsf{x})$ are

normalised with respect to the KG norm

$$(\phi_{\boldsymbol{k}}, \phi_{\boldsymbol{k}'}) = -\mathrm{i}\int_{\mathbb{R}^{d-1}} \mathrm{d}^{d-1}\boldsymbol{x}\,(\phi_{\boldsymbol{k}}\partial_t\phi^*_{\boldsymbol{k}'} - \phi^*_{\boldsymbol{k}'}\partial_t\phi_{\boldsymbol{k}})\,, \tag{2.31a}$$

$$(\phi_{\boldsymbol{k}}, \phi_{\boldsymbol{k}'}) = -(\phi^*_{\boldsymbol{k}}, \phi^*_{\boldsymbol{k}'}) = \delta^{(d-1)}(\boldsymbol{k}-\boldsymbol{k}')\,, \tag{2.31b}$$

$$(\phi_{\boldsymbol{k}}, \phi^*_{\boldsymbol{k}'}) = 0\,. \tag{2.31c}$$

The annihilation $\hat{a}_{\boldsymbol{k}}$ and creation $\hat{a}^\dagger_{\boldsymbol{k}}$ operators satisfy $[\hat{a}_{\boldsymbol{k}}, \hat{a}^\dagger_{\boldsymbol{k}'}] = \delta^{(d-1)}(\boldsymbol{k}-\boldsymbol{k}')$. The Poincaré-invariant Minkowski vacuum $|0_{\mathrm{M}}\rangle$ is defined by $\hat{a}_{\boldsymbol{k}}\,|0_{\mathrm{M}}\rangle = 0$ for all $\boldsymbol{k}$.

We assume the field (2.30) is initially prepared in a state $|\Psi\rangle$ with standard Fock space $\mathcal{H}_\Phi$, in which the positive frequencies are defined with respect to the timelike Killing vector ∂_t of metric (2.28). In this work, we will consider only the cases when the field (2.30) is initially prepared in its vacuum $|\Psi\rangle = |0_{\mathrm{M}}\rangle$ or in a thermal state $|\beta\rangle$ in inverse temperature $\beta = 1/T$.

The Hilbert space of the detector $\mathcal{H}_{\mathrm{D}} \simeq \mathbb{C}^2$ is spanned by the orthonormal basis $\{|0_{\mathrm{D}}\rangle, |1_{\mathrm{D}}\rangle\}$. The internal dynamics of the detector are described by the Hamiltonian $\hat{H}_{\mathrm{D}}$ with respect to τ, whose action on $\mathcal{H}_{\mathrm{D}}$ is $\hat{H}_{\mathrm{D}}\,|0_{\mathrm{D}}\rangle = 0$ and $\hat{H}_{\mathrm{D}}\,|1_{\mathrm{D}}\rangle = E\,|1_{\mathrm{D}}\rangle$. The constant $E \in \mathbb{R}$ is the detector's energy gap. For $E > 0$, $|0_{\mathrm{D}}\rangle$ is the ground state and $|1_{\mathrm{D}}\rangle$ is the excited state. For $E < 0$, the roles are reversed. The total Hilbert space of the system is $\mathcal{H}_{\mathrm{D}} \otimes \mathcal{H}_\Phi$.

The detector-field interaction is described by the Hamiltonian

$$\hat{H}_{\mathrm{int}} = \lambda\chi(\tau)\hat{\mu}(\tau) \otimes \hat{\Phi}(\mathsf{x}(\tau))\,, \tag{2.32}$$

where λ is a coupling constant, $\chi \in C(\mathbb{R})$ is the real-valued switching function determining the temporal profile of the interaction. We will be interested in the long-interaction limit $\chi \to 1$. $\hat{\mu}$ is the time-evolved monopole moment operator in the interaction picture $\hat{\mu}(\tau) = \mathrm{e}^{\mathrm{i}\hat{H}_{\mathrm{D}}\tau}\hat{\mu}(0)\mathrm{e}^{-\mathrm{i}\hat{H}_{\mathrm{D}}\tau}$, where $\hat{\mu}(0) = \hat{\sigma}^+ + \hat{\sigma}^-$ and $\hat{\sigma}^\pm$ are the raising and lowering operators in $\mathcal{H}_{\mathrm{D}}$,

$$\hat{\sigma}^+\,|0_{\mathrm{D}}\rangle = |1_{\mathrm{D}}\rangle\,, \qquad \hat{\sigma}^-\,|0_{\mathrm{D}}\rangle = 0\,, \tag{2.33a}$$

$$\hat{\sigma}^+\,|1_{\mathrm{D}}\rangle = 0\,, \qquad \hat{\sigma}^-\,|1_{\mathrm{D}}\rangle = |0_{\mathrm{D}}\rangle\,. \tag{2.33b}$$

The time-evolved raising and lowering operators read $\hat{\sigma}^\pm(\tau) = \mathrm{e}^{\pm\mathrm{i}E\tau}\hat{\sigma}^\pm$, such that $\hat{\mu}(\tau) = \mathrm{e}^{\mathrm{i}E\tau}\hat{\sigma}^+ + \mathrm{e}^{-\mathrm{i}E\tau}\hat{\sigma}^-$.

We take the initial state of the joint system to be $|0_{\mathrm{D}}\rangle \otimes |\Psi\rangle = |0_{\mathrm{D}}, \Psi\rangle$ and consider the case in which the detector transitions to $|1_{\mathrm{D}}\rangle$ whilst the field transitions to an excited state $|\Upsilon\rangle$. We assume the coupling constant λ is small such that first-order perturbation theory is a valid approximation. The joint-state of the

detector-field system evolves according to the time-evolution operator

$$\hat{U} \;=\; \mathcal{T}\exp\!\left(-\mathrm{i}\int_{-\infty}^{\infty}\mathrm{d}\tau\,\hat{H}_{\mathrm{int}}(\tau)\right)\,, \tag{2.34a}$$

where $\mathcal{T}\,\exp$ is the time-ordered exponential, which may be expanded as a Dyson series, leading to

$$\hat{U} \;=\; \hat{\mathbb{1}} - \mathrm{i}\int_{-\infty}^{\infty}\mathrm{d}\tau\hat{H}_{\mathrm{int}}(\tau) + \mathcal{O}(\lambda^2)\,. \tag{2.34b}$$

Then, the amplitude $\mathcal{A}_{|\Upsilon\rangle}$ for the joint system to transition from its initial state $|0_{\mathrm{D}},\Psi\rangle$ to final state $|1_{\mathrm{D}},\Upsilon\rangle$ is given by

$$\begin{aligned}\mathcal{A}_{|\Upsilon\rangle} \;&=\; -\mathrm{i}\int_{-\infty}^{\infty}\mathrm{d}\tau\;\langle 1_{\mathrm{D}},\Upsilon|\hat{H}_{\mathrm{int}}|0_{\mathrm{D}}\Psi\rangle\;,\\ &=\; -\mathrm{i}\lambda\,\langle 1_{\mathrm{D}}|\hat{\mu}(0)|0_{\mathrm{D}}\rangle\int_{-\infty}^{\infty}\mathrm{d}\tau\,\chi(\tau)\mathrm{e}^{\mathrm{i}E\tau}\,\langle\Upsilon|\hat{\Phi}(\mathsf{x}(\tau))|\Psi\rangle\;.\end{aligned} \tag{2.35}$$

Example 2.2 (Inertial detector)**.** Let us consider the transition amplitude $\mathcal{A}_{|1_{\boldsymbol{k}}\rangle}$ (2.35) of a detector undergoing inertial motion in the long-interaction-time limit $\chi\to 1$.

We assume the field is initially prepared in the Minkowski vacuum $|\Psi\rangle = |0_{\mathrm{M}}\rangle$, in which case to first order in perturbation theory, the field can only transition to the state $|1_{\boldsymbol{k}}\rangle$. We use the field expansion (2.30), noting that $\langle\Upsilon|\hat{\Phi}(\mathsf{x}(\tau))|0_{\mathrm{M}}\rangle = \langle 1_{\boldsymbol{k}}|\hat{\Phi}(\mathsf{x}(\tau))|0_{\mathrm{M}}\rangle = \phi^*_{\boldsymbol{k}}(\mathsf{x}(\tau))$ such that

$$\mathcal{A}_{|1_{\boldsymbol{k}}\rangle} \;=\; -\mathrm{i}\frac{\lambda\,\langle 1_{\mathrm{D}}|\hat{\mu}(0)|0_{\mathrm{D}}\rangle}{(2\pi)^{\frac{3}{2}}\sqrt{2|\boldsymbol{k}|}}\int_{\mathbb{R}}\mathrm{d}\tau\,\mathrm{e}^{\mathrm{i}(E\tau-\mathsf{k}\cdot\mathsf{x})}\,. \tag{2.36a}$$

Specialising to the inertial trajectory $\boldsymbol{x} = \boldsymbol{x}_0 + \boldsymbol{v}t = \boldsymbol{x}_0 + \boldsymbol{v}\gamma\tau$, where $\boldsymbol{x}_0$ and $\boldsymbol{v}$ are real constants and γ is the Lorentz gamma factor defined by $\mathrm{d}t = \gamma\mathrm{d}\tau$, we have

$$\mathcal{A}_{|1_{\boldsymbol{k}}\rangle} \;=\; -\mathrm{i}\mathrm{e}^{-\mathrm{i}\boldsymbol{x}_0\cdot\boldsymbol{k}}\frac{\lambda\,\langle 1_{\mathrm{D}}|\hat{\mu}(0)|0_{\mathrm{D}}\rangle}{(2\pi)^{\frac{3}{2}}\sqrt{2|\boldsymbol{k}|}}\int_{\mathbb{R}}\mathrm{d}\tau\,\mathrm{e}^{\mathrm{i}E\tau}\mathrm{e}^{\mathrm{i}(|\boldsymbol{k}|-\boldsymbol{v}\cdot\boldsymbol{k})\gamma\tau}\,, \tag{2.36b}$$

$$\;=\; -\mathrm{i}\mathrm{e}^{-\mathrm{i}\boldsymbol{x}_0\cdot\boldsymbol{k}}\frac{\lambda\,\langle 1_{\mathrm{D}}|\hat{\mu}(0)|0_{\mathrm{D}}\rangle}{\sqrt{4\pi|\boldsymbol{k}|}}\delta(E+(|\boldsymbol{k}|-\boldsymbol{v}\cdot\boldsymbol{k})\gamma)\;. \tag{2.36c}$$

In a relativistic spacetime setting, we have $|\boldsymbol{v}|<1$; therefore, $|\boldsymbol{k}|-\boldsymbol{v}\cdot\boldsymbol{k}>0$. For a detector transitioning to an excited state $(E>0)$, the argument of the delta is strictly positive in which case $\mathcal{A}_{|1_{\boldsymbol{k}}\rangle}$ vanishes — a direct consequence of the Poincaré invariance of the Minkowski vacuum. As such, an inertial detector probing the Minkowski vacuum does not get excited. An inertial detector may, however, de-excite: if the detector begins in an excited state and de-excites to its ground state $(E<0)$, the transition amplitude is nonzero.

By contrast, if this calculation were performed again but in a dielectric

medium, in which the trajectory is parametrised by the coordinate time t, then the speed of light c_0 would be replaced by the effective speed of light in the medium c_{eff}, in which case it is possible to have "superluminal" observers with $1 < \frac{|\boldsymbol{v}|}{c_{\text{eff}}} < \frac{c_0}{c_{\text{eff}}}$. For such observers, the transition amplitude to an excited state ($E > 0$) (2.36) would not vanish for all $\boldsymbol{k}$, an effect known as Cherenkov (rus. Черенков) radiation [87, 88]. ■

For more complicated trajectories than the inertial motion considered in Example 2.2, a quantity of interest is the transition probability $\mathcal{P}(E)$, found by summing over (the complete basis of) final states,

$$\mathcal{P}(E) = \sum_{|\Upsilon\rangle} |\mathcal{A}_{|\Upsilon\rangle}|^2 , \tag{2.37a}$$

$$= \lambda^2 |\langle 1_{\text{D}}|\hat{\mu}(0)|0_{\text{D}}\rangle|^2 \int_{\mathbb{R}^2} \mathrm{d}\tau \mathrm{d}\tau' \, \chi(\tau)\chi(\tau') \mathrm{e}^{-\mathrm{i}E(\tau-\tau')} \langle \Psi|\hat{\Phi}(\mathsf{x}(\tau))\hat{\Phi}(\mathsf{x}(\tau'))|\Psi\rangle \ . \tag{2.37b}$$

The quantity $\langle \Psi|\hat{\Phi}(\mathsf{x})\hat{\Phi}(\mathsf{x}')|\Psi\rangle$ is the two-point function or Wightman function. We assume this to be a distribution with a controlled singularity structure, which includes the Hadamard property in the coincidence limit $\mathsf{x} \to \mathsf{x}'$ [89, 90]. When the field is initially prepared in either its vacuum state or in a thermal state in inverse temperature β, we denote the pullback of the field's Wightman function to the trajectory $\mathsf{x}(\tau)$ by

$$\mathcal{W}(\tau,\tau') = \langle 0_{\text{M}}|\hat{\Phi}(\mathsf{x}(\tau))\hat{\Phi}(\mathsf{x}(\tau'))|0_{\text{M}}\rangle \ , \tag{2.38a}$$

$$\mathcal{W}_\beta(\tau,\tau') = \langle \beta|\hat{\Phi}(\mathsf{x}(\tau))\hat{\Phi}(\mathsf{x}(\tau'))|\beta\rangle \ . \tag{2.38b}$$

By abuse of terminology, we will refer to (2.38) as the Wightman function. The strength of the coincidence-limit singularity of the Wightman function $\mathcal{W}$ depends on the spacetime dimension [69]. We assume that χ has sufficiently strong early and late-time falloff so that the integral in (2.37b) converges.

In Minkowski spacetime (2.28), the Wightman functions $\mathcal{W}$ and $\mathcal{W}_\beta$ are given by [26, 69]

$$\mathcal{W}(\mathsf{x},\mathsf{x}') = \frac{\Gamma(\frac{d}{2}-1)}{4\pi^{d/2}[(\boldsymbol{x}-\boldsymbol{x}')^2-(t-t'-\mathrm{i}\varepsilon)^2]^{(d-2/2)}} , \tag{2.39a}$$

$$\mathcal{W}_\beta(\mathsf{x},\mathsf{x}') = \int_{\mathbb{R}^{d-1}} \mathrm{d}^{d-1}\boldsymbol{k}[(1+n(\beta|\boldsymbol{k}|))\phi_{\boldsymbol{k}}(\mathsf{x})\phi^*_{\boldsymbol{k}}(\mathsf{x}') + n(\beta|\boldsymbol{k}|)\phi^*_{\boldsymbol{k}}(\mathsf{x})\phi_{\boldsymbol{k}}(\mathsf{x}')] \ , \tag{2.39b}$$

$$= \mathcal{W}(\mathsf{x},\mathsf{x}') + \int_{\mathbb{R}^{d-1}} \mathrm{d}^{d-1}\boldsymbol{k}\, n(\beta|\boldsymbol{k}|)(\phi_{\boldsymbol{k}}(\mathsf{x})\phi^*_{\boldsymbol{k}}(\mathsf{x}') + \phi^*_{\boldsymbol{k}}(\mathsf{x})\phi_{\boldsymbol{k}}(\mathsf{x}')) \ , \tag{2.39c}$$

where

$$n(x) \;=\; \frac{1}{\mathrm{e}^{x}-1}\,, \tag{2.40}$$

is the Bose thermal factor. The distributional limit $\varepsilon \to 0^{+}$ in (2.39) is understood. The thermal Wightman function (2.39c) splits into a vacuum contribution and a thermal contribution, in which only the vacuum Wightman function $\mathcal{W}$ has a distributional behaviour. For odd d, the denominator in (2.39) is positive for spacelike separations and the $\mathrm{i}\varepsilon$ specifies the branch in its continuation through to timelike separations.

The constant prefactor in front of the integral in the transition probability (2.37b) is determined by the internal degrees of freedom of the detector and the coupling strength, whereas the interaction information is entirely determined by the integral. As such, we introduce the switching-dependent response function

$$\mathcal{F}_{\chi}(E) \;=\; \int_{\mathbb{R}^2} \mathrm{d}\tau \mathrm{d}\tau'\, \chi(\tau)\chi(\tau')\mathrm{e}^{-\mathrm{i}E(\tau-\tau')}\mathcal{W}(\tau,\tau')\,. \tag{2.41}$$

Throughout this work, we will specialise to the class of stationary trajectories $\mathsf{x}(\tau)$, members of which include inertial motion, uniform linear acceleration, and circular motion [4, 71, 91]. In situations in which the state $|\Psi\rangle$ and trajectory $\mathsf{x}(\tau)$ are stationary, the pullback of the Wightman function $\mathcal{W}$ depends on its two arguments only through their difference,

$$\mathcal{W}(\tau,\tau') \;=\; \mathcal{W}(\tau-\tau',0)\,. \tag{2.42}$$

The Wightman function with respect to the Minkowski vacuum $|0_{\mathrm{M}}\rangle$ (2.39a) simplifies to

$$\mathcal{W}(\tau,0) \;=\; \frac{1}{4\pi^2}\frac{1}{(\Delta\mathsf{x}(\tau-\mathrm{i}\varepsilon))^2}\,, \tag{2.43}$$

where $(\Delta\mathsf{x}(\tau))^2 = (\mathsf{x}(\tau)-\mathsf{x}(0))^2$ and the square is a Minkowski square, $\mathsf{x}^2 = \eta_{\mu\nu}\mathsf{x}^{\mu}\mathsf{x}^{\nu}$.

We further specialise to the case of long interaction time $\chi \to 1$; however, the switching-dependent response function $\mathcal{F}_{\chi}$ (2.41) and hence transition probability diverges. Instead, by first dividing by the total interaction time and then letting the interaction time tend to infinity, we find that the transition probability per unit time is proportional to the stationary response function [13],

$$\mathcal{F}(E) \;=\; \int_{\mathbb{R}} \mathrm{d}\tau\, \mathrm{e}^{-\mathrm{i}E\tau}\mathcal{W}(\tau,0)\,. \tag{2.44}$$

The subtleties in the infinite duration limit are discussed in [90]; in particular, the limit assumes the coupling to tend to zero sufficiently fast for the first order

perturbative treatment to remain valid in the limit.

Example 2.3 (Inertial detector in a thermal bath)**.** We consider as an example an inertial detector in a $(3+1)$-dimensional thermal bath at temperature T in Minkowski spacetime probing a real, massless, KG field $\hat{\Phi}$. The field decomposition (2.30) in $3+1$ dimensions is given by

$$\hat{\Phi}(\mathsf{x}) = \int_{\mathbb{R}^3} \mathrm{d}^3\boldsymbol{k}\, \phi_{\boldsymbol{k}}(\mathsf{x})\hat{a}_{\boldsymbol{k}} + \mathrm{Hc}\,, \tag{2.45a}$$

$$\phi_{\boldsymbol{k}}(\mathsf{x}) = \frac{1}{(2\pi)^{\frac{3}{2}}}\frac{\mathrm{e}^{\mathrm{i}\mathsf{k}\cdot\mathsf{x}}}{\sqrt{2|\boldsymbol{k}|}}\,, \tag{2.45b}$$

where $\eta_{\mu\nu} = \mathrm{diag}(-1,1,1,1)$. In even spacetime dimensions, one can re-express the thermal Wightman function $\mathcal{W}_\beta$ (2.39c) by method of an image sum [23] or by direct calculation of the integral (2.39b). In $3+1$ dimensions, one finds

$$\mathcal{W}_\beta(\mathsf{x},\mathsf{x}') = \frac{1}{4\pi^2}\frac{\pi T\sinh(2\pi T|\Delta\boldsymbol{x}|)}{|\Delta\boldsymbol{x}|(\cosh(2\pi T|\Delta\boldsymbol{x}|)-\cosh(2\pi T\Delta t))}\,, \tag{2.46}$$

where $|\Delta\boldsymbol{x}| = |\boldsymbol{x}-\boldsymbol{x}'|$ and $\Delta t = t - t' - \mathrm{i}\varepsilon$.

The thermal bath is stationary with respect to the Killing vector ∂_t of (2.28) and isotropic in the spatial coordinates, so the Wightman function is again stationary in the sense of (2.42). However, a thermal bath has a preferred rest frame because of the role of ∂_t in the construction of the state $|\beta\rangle$. Therefore, $\mathcal{W}_\beta$ (2.39c) is not Lorentz invariant [1] and observers with a non-zero constant velocity will experience a Doppler shift.

We specialise to a static observer at the origin, $\mathsf{x}(\tau) = (\tau,0,0,0)$, on which trajectory the thermal Wightman function (2.46) reads [3, 26]

$$\mathcal{W}_\beta(\tau,0) = -\frac{1}{4\beta^2\sinh^2\left(\frac{\pi}{\beta}(\tau-\mathrm{i}\varepsilon)\right)}\,. \tag{2.47}$$

The (stationary) response function is then

$$\mathcal{F}(E,\beta) = \int_{\mathbb{R}}\mathrm{d}\tau\,\mathrm{e}^{-\mathrm{i}E\tau}\mathcal{W}_\beta(\tau,0)\,, \tag{2.48a}$$

$$= \frac{E}{2\pi}\frac{1}{\mathrm{e}^{E\beta}-1}\,. \tag{2.48b}$$

We see that, in the absence of the Doppler effect ($\boldsymbol{v}=\boldsymbol{0}$), the static observer experiences a thermal bath at temperature β^{-1}. ■

We consider now a detector undergoing a uniform linear acceleration trajec-

tory in $3+1$ Minkowski spacetime

$$(t,x,y,z) \;=\; \left(\frac{1}{a}\sinh(a\tau),\frac{1}{a}\cosh(a\tau),0,0\right)\,. \tag{2.49}$$

The pullback of the Wightman function (2.43) to the trajectory (2.49) reads

$$\mathcal{W}(\tau,0) \;=\; -\frac{1}{4\pi^2}\frac{1}{\frac{4}{a^2}\sinh^2(\frac{a}{2}(\tau-\mathrm{i}\varepsilon))}\,. \tag{2.50}$$

The response function $\mathcal{F}$ (2.44) for an accelerated detector can be expressed explicitly in terms of elementary functions,

$$\mathcal{F}(E) \;=\; -\frac{1}{4\pi^2}\int_{\mathbb{R}}\mathrm{d}\tau\,\mathrm{e}^{-\mathrm{i}E\tau}\frac{1}{\frac{4}{a^2}\sinh^2(\frac{a}{2}(\tau-\mathrm{i}\varepsilon))}\,, \tag{2.51a}$$

$$\;=\; \frac{E}{2\pi}\frac{1}{\mathrm{e}^{2\pi E/a}-1}\,. \tag{2.51b}$$

Comparing this result with Example 2.3, one sees that the response of a detector undergoing linearly accelerated motion and a static detector in a $3+1$ thermal bath is identical under the identification $\beta = 2\pi/a$.

To interpret this result, we recall that in a local system in equilibrium with a thermal bath, the excitation and de-excitation probabilities satisfy Einstein's *detailed balance* condition [92, 93],

$$\frac{P_\downarrow(\Delta)}{P_\uparrow(\Delta)} \;=\; \mathrm{e}^{\Delta/T}\,, \tag{2.52}$$

where $P_\uparrow(\Delta)$ is the excitation probability, $P_\downarrow(\Delta)$ is the de-excitation probability, $\Delta > 0$ is the energy difference between the two states under consideration, and T is the temperature of the thermal bath. Solving (2.52) for T gives

$$T \;=\; \frac{\Delta}{\ln\left(\dfrac{P_\downarrow(\Delta)}{P_\uparrow(\Delta)}\right)}\,, \tag{2.53}$$

giving an operational way to determine the bath's temperature in terms of the probabilities $P_\uparrow(\Delta)$ and $P_\downarrow(\Delta)$ that are observable in the local system. Note that while both $P_\uparrow(\Delta)$ and $P_\downarrow(\Delta)$ depend on the energy gap Δ, the temperature T in (2.52) and (2.53) does not: the temperature T sets the ratio of the excitation and de-exitation probabilities for all energy gaps. This is the characteristic feature of a local system in equilibrium with a thermal bath.

Using the language of response functions, the detailed balance tempera-

ture (2.53) then reads

$$T = \frac{E}{\ln\left(\frac{\mathcal{F}(-E)}{\mathcal{F}(E)}\right)} . \tag{2.54}$$

For the response functions (2.48) and (2.51), we find the corresponding detailed balance temperatures (2.54)

$$T = \begin{cases} \frac{1}{\beta} & \text{static detector in thermal bath} , \\ \frac{a}{2\pi} & \text{linearly accelerated detector} . \end{cases} \tag{2.55}$$

A static detector therefore behaves as a perfect thermometer for the thermal bath, whereas the linearly accelerated detector responds as if it were in a thermal bath at a temperature proportional to its acceleration — the Unruh effect.

The reason behind this phenomenon is that the Minkowski vacuum is a genuine thermal state in the Fock space adapted to the boost Killing vector whose one orbit the linearly accelerated observer follows [21], and the detector consequently responds to this thermality by excitations and de-excitations that obey detailed balance.

By contrast, the Minkowski vacuum does not have a similar description as a genuine thermal state in a Fock space adapted to non-linear accelerations. Indeed, the excitation and de-excitation probabilities are affected by the acceleration, the ratio of these probabilities, however, depends on the energy gap Δ in a way that does not follow the detailed balance exponential law (2.52) in terms of a single parameter T. These motions, therefore, do not have a conventional notation of temperature and the physical phenomenon behind the acceleration effect may be described as a combination of synchrotron radiation as well as the conventional Unruh effect, as reviewed in [67]. In particular, the quantity T given by (2.53) depends on the gap Δ.

The probabilities $P_{\uparrow}(\Delta)$ and $P_{\downarrow}(\Delta)$ are still, however, observable quantities in the local quantum system, affected by the acceleration, even when the acceleration is not linear. For a given value of Δ, the excitation and de-excitation probabilities in the local system are related as if the system were in equilibrium with a thermal bath in the temperature given by (2.53). The Δ-dependent quantity given by (2.53) thus provides a useful quantifier of the system's response to the acceleration at energy gap Δ, and hence an operational notion of an effective temperature at a given energy scale. We call this quantity the *detailed balance temperature*.

This concludes our final perspective on the uniform linear acceleration Unruh effect, all of which highlight the uniqueness of linear acceleration in their

construction, either through the presence of an acceleration horizon, the behaviour of Minkowski vacuum correlation functions under boosts according to the Bisognano-Wichmann theorem, or the description of the Minkowski vacuum as a thermal state in the Fock space adapted to the boost Killing vector $x\partial_t + t\partial_x$.

The UDW detector model will serve as the main tool throughout this work and the response function and detailed balance temperature will act as useful quantifiers of the response of the local quantum system at a given energy scale. In this way, the UDW model allows for the study of both the Unruh effect, as well as Unruh-like phenomena [71, 72, 94, 95], such as an observer in uniform circular motion [26, 91, 96–98]. Experimental interest in the circular motion Unruh effect has a long standing [64, 66, 99–101], in which a new avenue is opened by recent proposals [2, 70, 102, 103] to utilise the analogue spacetime that occurs in nonrelativistic laboratory systems [57, 104]. In Section 2.2, we will introduce nonrelativistic analogue spacetimes and the circular motion Unruh effect.

2.2 Unruh effect: Circular motion

"Noli turbare circulos meos!"
(Do not disturb my circles!)

Last words of Archimedes

We introduce the analogue spacetime setting, the effective description of perturbations around a background flow within a hydrodynamical system as a scalar field propagating in a curved spacetime. We focus on the circular motion Unruh effect in $2+1$ and $3+1$ spacetime dimensions and continue with the UDW model, using the response function of the detector to quantify the experience of the detector. Finally, we consider the continuous-detector model as a generalisation of the two-state UDW detector model.

2.2.1 Analogue spacetimes

The concept of an analogue spacetime originates in Unruh's seminal work "*Experimental Black-Hole Evaporation?*" [51] and has since flourished into the discipline of analogue gravity. In this Section, we introduce the mathematical analogy between fluid perturbations on a background flow and scalar fields on a curved spacetime.

We begin with the equations of motion for an inviscid, irrotational fluid [52],

$$\nabla \times \boldsymbol{v} \;=\; 0\,, \tag{2.56a}$$

$$\rho\left(\frac{\partial \boldsymbol{v}}{\partial t} + (\boldsymbol{v}\cdot\nabla)\boldsymbol{v}\right) \;=\; -\nabla p - \rho\nabla V\,, \tag{2.56b}$$

$$\frac{\partial \rho}{\partial t} + \nabla\cdot(\rho\boldsymbol{v}) \;=\; 0\,, \tag{2.56c}$$

where $\boldsymbol{v}$ is the velocity field of the fluid, ρ is the fluid density, $p(\rho)$ is the fluid pressure, and V is an external force potential. The first equation ensures the fluid is irrotational, the second is the Euler equation, the equation of motion for an inviscid fluid, and the third equation is the continuity equation. For a fluid whose density is steady ($\partial_t\rho = 0$) and uniform ($\nabla\rho = 0$), the continuity equation (2.56c) reduces to the familiar incompressibility condition $\nabla\cdot\boldsymbol{v} = 0$.

We introduce the velocity potential ψ such that $\boldsymbol{v} = \nabla\psi$ and define new variables ξ and g,

$$\xi \;=\; \ln\rho\,, \qquad\qquad g(\xi) \;=\; \int^{\mathrm{e}^{\xi}} \mathrm{d}\rho'\,\frac{1}{\rho'}\frac{\mathrm{d}p(\rho')}{\mathrm{d}\rho'}\,. \tag{2.57}$$

The velocity potential guarantees that the fluid is irrotational (2.56a). The equations (2.56b) and (2.56c) in these new variables now read

$$\frac{\partial\psi}{\partial t} + \frac{1}{2}|\boldsymbol{v}|^2 + g(\xi) + V \;=\; 0\,, \tag{2.58a}$$

$$\frac{\partial\xi}{\partial t} + \boldsymbol{v}\cdot\nabla\xi + \nabla\cdot\boldsymbol{v} \;=\; 0\,. \tag{2.58b}$$

We next linearise the fluid equations (2.58) about some background velocity field $\boldsymbol{v}_0 = \nabla\psi_0$ by perturbing ξ and ψ,

$$\xi = \xi_0 + \widetilde{\xi}\,, \qquad\qquad \psi = \psi_0 + \widetilde{\psi}\,. \tag{2.59}$$

Combining the resulting two linearised equations into a single equation for the velocity potential perturbation $\widetilde{\psi}$, we find

$$\frac{1}{\rho_0}\Bigg[\frac{\partial}{\partial t}\frac{\rho_0}{g'(\xi_0)}\frac{\partial\widetilde{\psi}}{\partial t} + \frac{\partial}{\partial t}\frac{\rho_0\boldsymbol{v}_0}{g'(\xi_0)}\cdot\nabla\widetilde{\psi} + \nabla\cdot\left(\frac{\rho_0\boldsymbol{v}}{g'(\xi_0)}\frac{\partial\widetilde{\psi}}{\partial t}\right) - \nabla\cdot\left(\rho_0\nabla\widetilde{\psi}\right) + \nabla\cdot\left(\boldsymbol{v}\frac{\rho_0}{g'(\xi_0)}\boldsymbol{v}\cdot\nabla\widetilde{\psi}\right)\Bigg] \;=\; 0\,. \tag{2.60}$$

Recast into a more familiar form, this equation reads

$$0 = \frac{1}{\sqrt{-g}}\partial_\mu\left(\sqrt{-g}g^{\mu\nu}\partial_\nu\right)\widetilde{\psi}\,, \tag{2.61a}$$

$$\begin{aligned} \mathrm{d}s^2 &= g_{\mu\nu}\mathrm{d}x^\mu \mathrm{d}x^\nu\,, \\ &= -(c_s^2 - \boldsymbol{v}_0\cdot\boldsymbol{v}_0)\mathrm{d}t^2 - 2\mathrm{d}t(\boldsymbol{v}_0\cdot\mathrm{d}\boldsymbol{x}) + \mathrm{d}\boldsymbol{x}\cdot\mathrm{d}\boldsymbol{x}\,, \end{aligned} \tag{2.61b}$$

where $c_s^2 = \frac{\mathrm{d}p}{\mathrm{d}\rho}|_{\rho=\rho_0}$ is the (local) speed of sound. Equation 2.61 describes a KG field $\widetilde{\psi}$ propagating on a nonrelativistic curved spacetime background, determined by the background velocity field $\boldsymbol{v}_0$. An important class is $\rho_0 = const$ and $\boldsymbol{v}_0 = 0$, describing an analogue Minkowski spacetime with a constant speed of sound.

In a nonrelativistic analogue spacetime setting, it is appropriate to parametrise an observer's trajectory by the 'lab time' t, with respect to which any frequencies will be measured. The energy gap of the detector is also adapted to the analogue spacetime system and is defined with respect to the Minkowski time and denoted by $\overline{E}$. The lab frame energy gap $\overline{E}$ is related to the energy gap of a relativistic detector by $\overline{E} = E/\gamma$. The response function adapted to the lab frame reads

$$\mathcal{F}(\overline{E}) = \int_{\mathbb{R}} \mathrm{d}t\, \mathrm{e}^{-\mathrm{i}\overline{E}t}\mathcal{W}(t - \mathrm{i}\varepsilon, 0)\,, \tag{2.62}$$

and is related to the relativistic spacetime setting by multiplication by $1/\gamma$ (cf. $\mathrm{d}t = \gamma\mathrm{d}\tau$).

By utilising an analogue Minkowski spacetime, one may repeat the calculations of Section 2.1.3 and arrive at the analogue Unruh temperature,

$$T_U = \frac{\hbar a}{2\pi c_s k_\mathrm{B}}\,. \tag{2.63}$$

The key difference between (2.19) and (2.63) is the replacement of the speed of light c by the speed of sound c_s. In a Bose-Einstein condensate (BEC), the speed of sound can be 12 orders of magnitude lower than the speed of light [70]: an analogue-spacetime implementation brings the Unruh effect much closer to experimental realisation.

The work in [21] initiated the field of analogue gravity and has since been extended to describe gravity wave perturbations on a range of curved spacetimes, from black hole backgrounds [54] through to cosmological spacetimes [105]. This framework now resonates with several areas throughout physics [104, 106], with experimental and theoretical efforts in classical fluids [61, 107], ultracold atoms systems [70, 108], superfluids [2, 63], and optical systems [109, 110]. In Sec-

tion 2.2.2, we will explore a particular example, the circular motion Unruh effect.

2.2.2 Circular motion Unruh effect

We consider a UDW detector as modelled in Section 2.1.3 undergoing uniform circular motion in Minkowski spacetime. Its worldline is

$$\mathsf{x}(\tau) \;=\; (\gamma\tau, R\cos(\gamma\Omega\tau), R\sin(\gamma\Omega\tau), \dots)\,, \tag{2.64}$$

where the dots are not present in $2+1$ dimensions and denote zeros in higher dimensions. The parameters $R, \Omega > 0$ satisfy $R\Omega < 1$, ensuring the trajectory is timelike. The Lorentz factor is given by $\gamma = (1-v^2)^{-1/2}$. R is the orbital radius, Ω is the angular velocity with respect to Minkowski time t, $\Omega = \mathrm{d}\theta/\mathrm{d}t$, we denote the orbital speed by $v = R\Omega$, and the acceleration by $a = v^2\gamma^2/R$.

In an analogue spacetime, circular motion enjoys two main advantages over linear acceleration. First, the trajectory can remain within a finite-size laboratory for an arbitrarily long interaction time. Second, the Lorentz factor γ remains constant in time. On an experimental level, this allows for the inclusion of the gamma factor by appropriately scaling the energies during the theoretical analysis of an experiment. On a theoretical level, one can readily transition results between a genuinely relativistic spacetime and an analogue spacetime setting by a rescaling of the energy gap E.

There are two fundamental differences between the Unruh effect presented in Section 2.1 and the circular motion Unruh effect. First geometrically (cf. Section 2.1.1), no horizons form in uniform circular motion. Second, the Minkowski vacuum does not have a description as a thermal state in a Fock space adapted to the circular motion Killing vector (cf. Section 2.1.2). Therefore, we now analyse the circular motion Unruh effect in a relativistic spacetime, first in $3+1$ and then in $2+1$ dimensions using the UDW detector model (cf. Section 2.1.3), as analysed in [69], with previous earlier analyses given in [23, 66, 72].

$(3+1)$-dimensional Minkowski spacetime

In $(3+1)$-dimensional Minkowski spacetime, the Wightman function (2.39a) reads

$$\mathcal{W}(\tau,0) \;=\; \frac{1}{4\pi^2}\frac{1}{(\Delta\mathsf{x}(\tau-\mathrm{i}\varepsilon))^2}\,. \tag{2.65}$$

We can isolate the distributional contribution of the Wightman function at $\tau = 0$ to the response function (2.44) by adding and subtracting the singular behaviour

at $\tau = 0$,

$$\mathcal{F}(E) \;=\; -\frac{1}{4\pi^2}\int_{\mathbb{R}} \mathrm{d}\tau\, \mathrm{e}^{-\mathrm{i}E\tau}\frac{1}{(\tau-\mathrm{i}\varepsilon)^2} + \frac{1}{4\pi^2}\int_{\mathbb{R}} \mathrm{d}\tau\, \mathrm{e}^{-\mathrm{i}E\tau}\left(\frac{1}{\tau^2}+\frac{1}{(\Delta \mathsf{x}(\tau))^2}\right)\,. \tag{2.66a}$$

We note that the second integral is free from $\mathrm{i}\varepsilon$ regularisation and the decomposition (2.66) is independent of the trajectory $\mathsf{x}(\tau)$ due to the short-distance Hadamard property of the Wightman function. We evaluate the first integral by means of a contour integral in the complex plane,

$$\mathcal{F}(E) \;=\; -\frac{E}{2\pi}\Theta(-E) + \frac{1}{4\pi^2}\int_{\mathbb{R}} \mathrm{d}\tau\, \mathrm{e}^{-\mathrm{i}E\tau}\left(\frac{1}{\tau^2}+\frac{1}{(\Delta \mathsf{x}(\tau))^2}\right)\,, \tag{2.66b}$$

where Θ is the Heaviside step function [111]. The first term is the response function of a detector undergoing inertial motion in $3+1$ Minkowski spacetime,

$$\mathcal{F}_0(E) \;=\; -\frac{E}{2\pi}\Theta(-E)\,. \tag{2.67}$$

As in Example 2.2, the inertial detector (2.67) only responds via de-excitations and has a detailed balance temperature $T = 0$.

Specialising to the circular trajectory (2.64), we have

$$(\Delta \mathsf{x}(z))^2 \;=\; -4\frac{R^2}{v^2}\big(z^2 - v^2\sin^2(z)\big)\,, \tag{2.68}$$

where $z = \gamma v\tau/(2R)$. The response function (2.66) is given by

$$\mathcal{F}(E) \;=\; -\frac{E}{2\pi}\Theta(-E) + \frac{v}{4\pi^2\gamma R}\int_0^\infty \mathrm{d}z\, \cos\left(\frac{2ER}{\gamma v}z\right)\left(\frac{\gamma^2}{z^2} - \frac{1}{z^2 - v^2\sin^2 z}\right)\,. \tag{2.69}$$

This expression is useful for numerical implementation and for some limits such as the small energy gap limit; however, it can also be useful to write the integral as a contour integral in the complex plane,

$$\mathcal{F}(E) \;=\; -\frac{E}{2\pi}\Theta(-E) - \frac{v}{8\pi^2\gamma R}\int_C \mathrm{d}z\, \frac{\exp\left(\mathrm{i}\frac{2|E|R}{\gamma v}z\right)}{z^2 - v^2\sin^2 z}\,, \tag{2.70}$$

where the contour C lies along the real axis from $-\infty$ to $+\infty$, passes the pole at $z = 0$ in the upper half-plane, and is closed in the upper half-plane. The distributional contribution at $z = 0$ is already contained in the inertial term and should therefore be left outside the contour. The residue theorem then allows one to rewrite the integral as a sum over the (infinitely many) residues.

Two limits of interest are the large and small energy gap limits. Considering

first the large-gap limit $|E| \to \infty$, one sees from (2.70) that the leading-order behaviour is determined by the zero of

$$z^2 - v^2 \sin^2 z \;=\; 0\,, \tag{2.71}$$

with the smallest positive imaginary part. This zero is purely imaginary and is denoted in [69] by α_0, defined implicitly by

$$v \;=\; \frac{\alpha_0}{\sinh \alpha_0}\,. \tag{2.72}$$

This leads to the detailed balance temperature (2.54)

$$T_{\text{circ}} \;=\; \frac{\gamma v}{2\alpha_0 R}\,. \tag{2.73}$$

We consider now the small-gap limit $E \to 0$. In Appendix A, we detail a dominated convergence argument to calculate the leading and subleading contributions to the integral (2.69) as $E \to 0$,

$$\mathcal{F}(E) \;=\; \frac{v\gamma}{4\pi^2 R}\int_0^\infty \mathrm{d}z \left(\frac{1}{z^2} - \frac{1}{\gamma^2(z^2 - v^2\sin^2 z)}\right) - \frac{1}{4\pi}\left(1 - \frac{1}{\gamma^2}\mathrm{sgn}(E)\right) E + \mathcal{O}(E^2)\,, \tag{2.74}$$

where $\mathrm{sgn}(E) = E/|E|$ is the signum function. An application of the detailed balance formula (2.54) leads to

$$T_{\text{circ}} \;=\; \frac{v\gamma}{2\pi R}\int_0^\infty \mathrm{d}z \left(\frac{1}{z^2} - \frac{1}{\gamma^2(z^2 - v^2\sin^2 z)}\right) + \mathcal{O}(E^2)\,. \tag{2.75}$$

$(2+1)$-dimensional Minkowski spacetime

The Wightman function (2.39a) in $(2+1)$-dimensional Minkowski spacetime is given by

$$\mathcal{W}(\tau, 0) \;=\; \frac{1}{4\pi}\frac{1}{\sqrt{(\Delta\mathsf{x}(\tau - \mathrm{i}\varepsilon))^2}}\,. \tag{2.76}$$

The square root in the denominator is positive imaginary for $\tau > 0$ and negative imaginary for $\tau < 0$. The associated response function (2.44) admits a simple decomposition in two ways, both of which ways isolate the distributional behaviour at $\tau = 0$. In the first, we separate the odd and even contributions to the

response function,

$$\mathcal{F}(E) \;=\; \frac{1}{4} - \frac{1}{2\pi}\int_0^\infty \mathrm{d}\tau\, \frac{\sin(E\tau)}{\sqrt{-(\Delta \mathsf{x}(\tau))^2}}\,. \tag{2.77}$$

In the second, we add and subtract the singular behaviour under the integral as in (2.66),

$$\mathcal{F}(E) \;=\; \frac{1}{2}\Theta(-E) + \frac{1}{2\pi}\int_0^\infty \mathrm{d}\tau\, \sin(E\tau)\left(\frac{1}{\tau} - \frac{1}{\sqrt{-(\Delta \mathsf{x}(\tau))^2}}\right)\,. \tag{2.78}$$

In this decomposition, the first term is the detector response for an inertial detector in $(2+1)$-dimensional Minkowski spacetime,

$$\mathcal{F}_0(E) \;=\; \frac{1}{2}\Theta(-E)\,. \tag{2.79}$$

As in $3+1$ dimensions, these two decompositions are independent of the trajectory chosen, following from the short-distance Hadamard property of the Wightman function.

The response function in the two decompositions (2.77) and (2.78) is given by

$$\mathcal{F}(E) \;=\; \frac{1}{4} - \frac{1}{2\pi\gamma}\int_0^\infty \mathrm{d}z\, \frac{\sin\left(\frac{2ER}{\gamma v}z\right)}{\sqrt{z^2 - v^2\sin^2 z}}\,, \tag{2.80a}$$

$$\;=\; \frac{1}{2}\Theta(-E) + \frac{1}{2\pi\gamma}\int_0^\infty \mathrm{d}z\, \sin\left(\frac{2ER}{\gamma v}z\right)\left(\frac{\gamma}{z} - \frac{1}{\sqrt{z^2 - v^2\sin^2 z}}\right)\,. \tag{2.80b}$$

We rewrite the integral in (2.80b) as a contour integral in the complex plane,

$$\mathcal{F}(E) \;=\; \frac{1}{2}\Theta(-E) + \frac{\mathrm{i}\,\mathrm{sgn}(E)}{4\pi\gamma}\int_C \mathrm{d}z\, \frac{\exp\left(\mathrm{i}\frac{2|E|R}{\gamma v}z\right)}{\sqrt{z^2 - v^2\sin^2 z}}\,, \tag{2.81}$$

where the contour C lies along the real axis from $-\infty$ to $+\infty$ and passes the branch point at $z=0$ in the upper half-plane. By deforming the contour C in the upper half-plane around each of the branch points, one can re-express the integral as an infinite sum, the details of which are given in [69].

The dominant contribution in the large gap limit is again given by the zero of (2.71) with smallest positive imaginary part. It follows that the detailed balance temperature is the same as in $3+1$ dimensions (2.73).

In the small energy gap regime, it is shown in [69] that the detailed balance

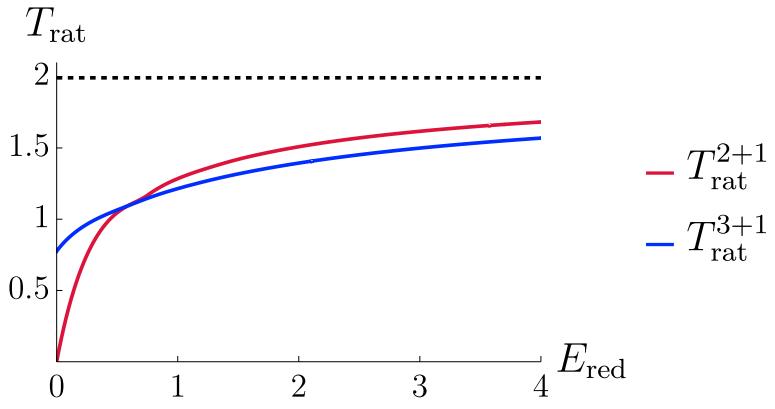

Figure 2.2: (Relativistic spacetime for $v = 0.8$) Ratio of circular motion and linear acceleration detailed balance temperatures $T_{\rm rat} \coloneqq T_{\rm circ}/T_{\rm lin}$ as a function of the reduced energy gap $E_{\rm red} \coloneqq E/a$ with all other parameters fixed. The red curve shows $T_{\rm rat}$ in $2+1$ dimensions. The blue curve shows $T_{\rm rat}$ in $3+1$ dimensions. The dashed black curve shows the asymptotic large energy gap temperature (2.73) $T_{\rm rat} \to 1.99$ in both $2+1$ and $3+1$ dimensions, evaluated from (2.73). In $2+1$ dimensions, the effective temperature vanishes as $E_{\rm red} \to 0$ as seen in the analytic formula (2.82). In $3+1$ dimensions, $T_{\rm rat} \to 0.78$ as $E_{\rm red} \to 0$, evaluated from (2.75).

temperature is given by

$$T_{\rm circ} = \frac{|E|}{\ln\left(\frac{\gamma+1}{\gamma-1}\right)} + o(E)\,, \tag{2.82}$$

which vanishes as $E \to 0$, in contrast to the corresponding limit in $3+1$ dimensions (2.75).

Numerical results: $3+1$ **and** $2+1$

In the previous Section, only the asymptotically large and small energy gaps were amenable to analytic techniques. We now interpolate numerically between these regions and compare the circular motion Unruh effect in both a relativistic and analogue spacetime setting. We recall that the time dilation Lorentz factor $\gamma = (1-v^2)^{-1/2}$ is constant along the circular trajectory, hence we can map the relativistic spacetime results into an analogue spacetime setting by the following identifications: $\overline{E} = E/\gamma$ and $\overline{a} = a/\gamma^2$ are the energy gap and acceleration measured with respect to Minkowski time t and $\overline{T} = T/\gamma$ is the temperature measured with respect to $\overline{E}$.

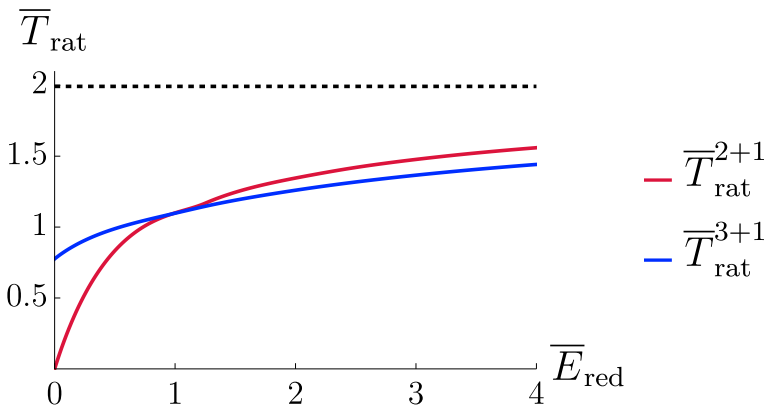

Figure 2.3: (Analogue spacetime for $v = 0.8$) Ratio of circular motion and linear acceleration detailed balance temperatures $\overline{T}_{\text{rat}} \coloneqq \overline{T}_{\text{circ}}/\overline{T}_{\text{lin}}$ as a function of the reduced energy gap $\overline{E}_{\text{red}} \coloneqq \overline{E}/\overline{a}$ with all other parameters fixed. The red curve shows $\overline{T}_{\text{rat}}$ in $2+1$ dimensions. The blue curve shows $\overline{T}_{\text{rat}}$ in $3+1$ dimensions. The dashed black curve shows the asymptotic large energy gap temperature (2.73) $\overline{T}_{\text{rat}} \to 1.99$ in both $2+1$ and $3+1$ dimensions, evaluated from (2.73).

In the relativistic spacetime setting, we plot the ratio $T_{\text{circ}}/T_{\text{lin}}$ as a function of the dimensionless variable E/a, whereas in the analogue spacetime setting, we plot $\overline{T}_{\text{circ}}/\overline{T}_{\text{lin}}$ as a function of the dimensionless variable $\overline{E}/\overline{a}$.

In Figure 2.2, we compare the effective temperature experienced by a UDW undergoing uniform circular motion in $3+1$ and $2+1$ dimensions with respect to the Unruh temperature in a relativistic spacetime setting. We interpolate between the large and small gap limits in Figure 2.2. The effective temperature in $2+1$ and $3+1$ dimensions is bounded from above (in the chosen parameters) by $2T_{\text{lin}}$. As seen in the formula (2.75), the effective temperature in $3+1$ dimensions remains of order unity with respect to the Unruh temperature throughout the parameter space. In $2+1$ dimensions, however, this is only true for $|E/a| \gtrsim 0.5$ as T^{2+1}_{circ} tends linearly to zero as $|E/a| \to 0$. The plot shows incipient growth of T_{circ} towards the large energy gap limit (2.73). In general, for away from the small-gap limit, the detailed balance temperature in both $3+1$ and $2+1$ dimensions behaves similarly and is of order unity with respect to the linear uniform acceleration Unruh temperature T_{lin}.

In Figure 2.3, we compare the effective temperature experienced by a UDW undergoing uniform circular motion in $3+1$ and $2+1$ dimensions with respect to the Unruh temperature in an analogue spacetime setting. The plot is qualitatively

similar to the relativistic spacetime as the quantity $T_{\text{circ}}/T_{\text{lin}}$ is invariant under $T \to T/\gamma$. However, the data is now plotted as a function of $\overline{E}/\overline{a} = \gamma E/a$.

The UDW model underpins the circular motion Unruh effect and any observation thereof requires a realisation of a UDW detector. However, in [70], it was shown that the characteristics of a UDW detector can be obtained by using a continuous field — rather than a two-level system — such as a laser field. In Section 2.2.3, we will review the continuous quasiparticle detector.

2.2.3 Continuous quasiparticle detectors

We consider the field theory as described in [70] comprising of a $(2{+}1)$-dimensional KG field $\Phi(t, \boldsymbol{x})$, where $\boldsymbol{x} = (x, y)$, and a $(1+1)$-dimensional probing KG field $\psi(t, z)$. In an analogue system such as a BEC, the field Φ represents density perturbations [70], whereas in thin-film superfluid helium, the field Φ represents height fluctuations [2].

The field Φ is confined to the $\boldsymbol{x}$ plane, whereas the probing field ψ can move on an interaction trajectory $\boldsymbol{X}(t)$ parameterised by its coordinate time t. The two fields have a pointlike interaction such that, before quantisation, the field theory is described by the Lagrangian

$$\begin{aligned} L \;=\; -\frac{1}{2}\int \mathrm{d}^2\boldsymbol{x}\, \partial_\mu\Phi\partial^\mu\Phi - \frac{1}{2}\int \mathrm{d}z\, \partial_\mu\psi\partial^\mu\psi \\ - \lambda \int \mathrm{d}^2\boldsymbol{x}\mathrm{d}z\, \partial_t(\psi(t,z))\Phi(t,\boldsymbol{x})\delta(z)\delta^{(2)}(\boldsymbol{x}-\boldsymbol{X}(t))\,, \end{aligned} \tag{2.83}$$

where λ is a small coupling constant and the delta functions restrict the interaction to $(\boldsymbol{x}, z) = (\boldsymbol{X}(t), 0)$. Upon quantisation, the effective interaction Hamiltonian is

$$\hat{H}_{\text{int}} \;=\; \lambda\partial_t\hat{\psi}(t,0)\otimes\hat{\Phi}(t,\boldsymbol{X}(t))\,. \tag{2.84}$$

We assume the field $\hat{\Phi}$ and $\hat{\psi}$ admit a decomposition into plane waves. At the point of interaction, the fields $\hat{\Phi}$ and $\hat{\psi}$ are then decomposed as

$$\hat{\Phi}(t,\boldsymbol{X}(t)) \;=\; \int_{\mathbb{R}^2} \mathrm{d}^2\boldsymbol{k}\, \frac{1}{2\pi\sqrt{2\omega}} \mathrm{e}^{-\mathrm{i}\omega t + \boldsymbol{k}\cdot\boldsymbol{X}(t)}\hat{a}_{\boldsymbol{k}} + \mathrm{Hc}\,, \tag{2.85a}$$

$$\hat{\psi}(t,0) \;=\; \int_{\mathbb{R}} \mathrm{d}\ell\, \frac{1}{\sqrt{4\pi\widetilde{\omega}}} \mathrm{e}^{-\mathrm{i}\widetilde{\omega}t}\hat{b}_\ell + \mathrm{Hc}\,, \tag{2.85b}$$

where $\omega = |\boldsymbol{k}|$, $\widetilde{\omega} = |\ell|$, $\hat{a}_{\boldsymbol{k}}$ and $\hat{a}^\dagger_{\boldsymbol{k}}$ are the annihilation and creation operators for quasiparticles in the analogue system, and $\hat{b}_\ell$ and $\hat{b}^\dagger_\ell$ are the annihilation and creation operators for the probing field.

We assume the field $\hat{\Phi}$ is prepared in a vacuum state $|0_\Phi\rangle$ and the field $\hat{\psi}$

is prepared in an initial state $|0_\psi\rangle$. To first order in perturbation theory, the fields $\hat{\Phi}$ and $\hat{\psi}$ can transition only to their first excited states $|1_{\boldsymbol{k}}\rangle = \hat{a}^\dagger_{\boldsymbol{k}}|0_\Phi\rangle$ and $|1_\ell\rangle = \hat{b}^\dagger_\ell|0_\psi\rangle$.

In an analogue system, the time-evolution operator (2.34) is given in terms of the coordinate time t,

$$\hat{U} \;=\; \hat{\mathbb{1}} - \mathrm{i}\int_{-\infty}^{\infty} \mathrm{d}t\, \hat{H}_{\mathrm{int}}(t) + \mathcal{O}(\lambda^2)\,, \tag{2.86}$$

where λ is the small coupling constant in the interaction. The transition amplitude for the joint state to transition from $|0_\Phi, 0_\psi\rangle$ to $|1_{\boldsymbol{k}}, 1_\ell\rangle$ is given by

$$\mathcal{A}_{|1_{\boldsymbol{k}}\rangle} \;=\; -\mathrm{i}\int \mathrm{d}t\ \langle 1_{\boldsymbol{k}}, 1_\ell|\hat{H}_{\mathrm{int}}|0_\Phi, 0_\psi\rangle\ , \tag{2.87}$$

where $\hat{H}_{\mathrm{int}}$ is the interaction Hamiltonian (2.84), leading to

$$\mathcal{A}_{|1_{\boldsymbol{k}}\rangle} \;=\; \lambda\sqrt{\frac{\widetilde{\omega}}{4\pi}}\int \mathrm{d}t \mathrm{e}^{-\mathrm{i}\widetilde{\omega}t}\,\langle 1_{\boldsymbol{k}}|\hat{\Phi}(t,\boldsymbol{X}(t))|0_\Phi\rangle\ . \tag{2.88}$$

On an inertial trajectory $\boldsymbol{X}(t) = \boldsymbol{x}_0 + \boldsymbol{v}_0 t$, where $\boldsymbol{x}_0$ and $\boldsymbol{v}_0$ are constants, the transition amplitude $\mathcal{A}_{|1_{\boldsymbol{k}}\rangle}$ is

$$\mathcal{A}_{|1_{\boldsymbol{k}}\rangle} \;=\; \frac{\lambda}{2}\sqrt{\frac{\widetilde{\omega}}{2\pi\omega}}\mathrm{e}^{\mathrm{i}\boldsymbol{k}\cdot\boldsymbol{x}_0}\delta(\widetilde{\omega}+\omega-\boldsymbol{k}\cdot\boldsymbol{v}_0)\,. \tag{2.89}$$

Note the transition amplitude vanishes for $\widetilde{\omega} > 0$, akin to the two-level UDW detector in Example 2.2.

By considering $|\mathcal{A}_{|1_{\boldsymbol{k}}\rangle}|^2$ and summing over the complete set of final states $|1_{\boldsymbol{k}}\rangle$, we find the transition probability,

$$\mathcal{P}(\widetilde{\omega}) \;=\; \frac{\lambda^2\widetilde{\omega}}{4\pi}\int \mathrm{d}t\mathrm{d}t'\,\mathrm{e}^{-\mathrm{i}\widetilde{\omega}(t'-t)}\mathcal{W}(t',t)\,, \tag{2.90}$$

where $\mathcal{W}(t',t) = \langle 0_\Phi|\hat{\Phi}(t',\boldsymbol{X}(t'))\hat{\Phi}(t,\boldsymbol{X}(t))|0_\Phi\rangle$ is the pullback of the Wightman function to the trajectory $\boldsymbol{X}(t)$. For a stationary Wightman function in the sense of (2.42), we divide by the total interaction time to find the response function

$$\mathcal{F}(\widetilde{\omega}) \;=\; \int_{\mathbb{R}} \mathrm{d}t\,\mathrm{e}^{-\mathrm{i}\widetilde{\omega}t}\mathcal{W}(t,0)\,. \tag{2.91}$$

When the field $\hat{\Phi}$ is initially prepared in a thermal state in inverse temperature β, we find also

$$\mathcal{F}(\widetilde{\omega},\beta) \;=\; \int_{\mathbb{R}} \mathrm{d}t\,\mathrm{e}^{-\mathrm{i}\widetilde{\omega}t}\mathcal{W}_\beta(t,0)\,. \tag{2.92}$$

In summary, the continuous quasiparticle detector model parallels the two-state UDW model of Section 2.1.3 in two fundamental ways. First, an inertial detector does not register any particles. Second, both model lead to the description of detector excitation and de-excitation in terms of the Fourier transform of the Wightman function, the response functions (2.44) and (2.91). As such, all calculations in Section 2.1.3 could be repeated with the continuous detector model and lead to the same results. In Chapter 4, we will see an example of the continuous detector model in which a laser field acts as a continuous quasiparticle detector of fluctuations in the height of thin-film superfluid helium.

2.3 Summary

In this Chapter, we have reviewed the (linearly accelerated) Unruh effect from three separate perspectives. First, in Section 2.1.1 we considered the geometric origins of the Unruh effect in which the presence of acceleration horizons play a key role in deriving the Unruh temperature. Then in Section 2.1.2, we considered the expected particle content for an inertial observer and an accelerated observer in Minkowski spacetime, finding that the expected particle number for an accelerated observer in the Minkowski vacuum is described by a thermal spectrum. The origins of the Unruh effect within QFT highlight the importance of both the left and right Rindler wedges. After, we considered the UDW detector model, in which the experience of a two-state detector is encoded in the response function $\mathcal{F}$. When the detector is linearly accelerated, the response function obeys Einstein's detailed balance condition describing an exact thermal state in the Unruh temperature. However, this model allows for the extension of the Unruh effect to other motions such as circular motion. No horizons form when an observer undergoes uniform circular motion in Minkowski spacetime and the Minkowski vacuum does not have a description as a genuine thermal state in a Fock space adapted to uniform circular motion. However, one can fit an effective, energy-gap-dependent temperature to satisfy Einstein's detailed balance condition. In this sense, one can consider other Unruh-like phenomena by investigating the excitation and de-excitation rates of the detector.

In Section 2.2.1, we reviewed Unruh's seminal work "*Experimental Black-Hole Evaporation?*" [51], finding that perturbations around a background flow in a fluid admit a description in terms of a scalar field propagating on a curved spacetime background, giving rise to the discipline of analogue gravity. In Section 2.2.2, we considered a UDW detector undergoing uniform circular motion. We saw that for small energy gaps, the experience of the detector depends on the

spatial dimensions: in $2+1$ dimensions, the detailed balance temperature tends to zero, whereas in $3+1$ dimensions, the detailed balance temperature tends to a nonzero constant. For large energy gaps, however, the detailed balance temperature tends to a constant, describing an approximately thermal state. Finally, in Section 2.2.3, we considered an interacting field theory between a $(2+1)$-dimensional KG field and a $(1+1)$-dimensional KG field, in which the latter acted as a probe field for the former. The $(1+1)$-dimensional field lay perpendicular to the $(2+1)$-dimensional field and was permitted to move along an interaction trajectory. For inertial motion, the probability of excitation was zero, as in the case of a UDW undergoing inertial motion. However, for general stationary motions, the excitation probability led to the response function of Section 2.1.3.

In the succeeding Chapters, we will develop further the ideas considered within this Chapter and the response function $\mathcal{F}$ will serve as the main tool to investigate detector response.

Chapter 3

Circular motion analogue Unruh effect in a $2+1$ thermal bath: Robbing from the rich and giving to the poor

"Poor men's goodes hee spared, aboundantly releeving them with that, which by thefte he gote from Abbeyes and the houses of riche Carles."

John Stow
The Annales of England (1592) [112]

THE analogue spacetimes offered by condensed-matter systems have inherent ambient temperatures that may not be neglected; hence, we build upon the discussion in Section 2.2.2 of a detector undergoing uniform circular motion probing a scalar field and replace the Minkowski vacuum by an ambient thermal bath. However, the presence of a thermal bath breaks the Lorentz invariance of the system, introducing a Doppler shift in the response of the detector. As such, it is not *a priori* clear what are the respective velocity-dependent and acceleration-dependent contributions to the detector response. We compare the response of a detector in circular motion with that of an inertial detector at a constant velocity matching the orbital speed of the detector in circular motion to isolate acceleration effects. The contents of this Chapter were extracted from, or based on, the journal article "Circular motion analogue Unruh effect in a $2+1$ thermal bath: Robbing from the rich and giving to the poor" [1] in collaboration with Jorma Louko.

3.1 Spacetime, field, and detector preliminaries

We work in $(2+1)$-dimensional analogue Minkowski spacetime in inertial coordinates (t, x, y) with the metric $\mathrm{d}s^2 = -\mathrm{d}t^2 + \mathrm{d}x^2 + \mathrm{d}y^2$. We consider a quantised, real scalar field $\hat{\Phi}$, with a dispersion relation that is isotropic in (x, y) and subject to the mild monotonicity conditions specified in Section 3.1.1, but otherwise arbitrary; in particular, we do not assume the dispersion relation to be Lorentz invariant.

We assume that the field has been initially prepared in a thermal state in inverse temperature $\beta > 0$, where the notion of thermality is with respect to the time evolution generated by ∂_t.

We first assume that the thermal state has a Wightman two-point function (2.39), denoted by

$$\widetilde{\mathcal{W}}_\beta(\mathsf{x}', \mathsf{x}'') = \langle \hat{\Phi}(\mathsf{x}')\hat{\Phi}(\mathsf{x}'')\rangle_\beta \,, \tag{3.1}$$

possibly modulo infrared subtleties that we shall describe shortly. Because of the role in ∂_t in the construction of the thermal state, $\widetilde{\mathcal{W}}_\beta$ is not Lorentz invariant. In particular, it is not invariant under Lorentz boosts, not even when the dispersion relation is Lorentz invariant. A thermal bath has a distinguished rest frame.

We probe the field by a pointlike detector in uniform circular motion, on the worldline (2.64) in $2+1$ dimensions in the lab frame,

$$\mathsf{x}(t) = \big(t, R\cos(\Omega t), R\sin(\Omega t)\big) \,. \tag{3.2}$$

The orbital speed is $v = R\Omega$. We assume that the worldline is timelike, $v < 1$.

As in Section 2.1.3, the detector's Hilbert space is $\mathcal{H}_\mathrm{D} \simeq \mathbb{C}^2$ and is spanned by the orthonormal basis $\{|0\rangle, |1\rangle\}$. In the analogue spacetime setting, the detector energy gap is given by $\overline{E}$, defined with respect to lab time t.

In the interaction picture, we take the interaction Hamiltonian to be

$$\hat{H}_\mathrm{int} = \lambda\chi(t)\hat{\mu}(t) \otimes \frac{\mathrm{d}}{\mathrm{d}t}\hat{\Phi}\big(\mathsf{x}(t)\big) \,, \tag{3.3}$$

where $\hat{\mu}$ is the detector's monopole moment operator, χ is a real-valued switching function that specifies how the interaction is turned on and off, and λ is a real-valued coupling constant. As we shall see later, the derivative coupling renders the detector's Wightman function well defined and divergence free.

Working to first order in perturbation theory in λ as in Section 2.2.3, one may calculate the probability $\mathcal{P}(\overline{E})$ for the detector to transition from $|0\rangle$ to $|1\rangle$, regardless of the final state of the field [12, 21].

As the thermal state is stationary with respect to the Killing vector ∂_t and

isotropic in (x, y), the Wightman function is stationary in the sense of (2.42). By dividing the transition probability $\mathcal{P}(\overline{E})$ by the total interaction time and letting the duration tend to infinity, one recovers the stationary response function,

$$\mathcal{F}(\overline{E}, \beta) = \int_{\mathbb{R}} \mathrm{d}t\, \mathrm{e}^{-\mathrm{i}\overline{E}t} \mathcal{W}_\beta(t, 0)\,, \tag{3.4a}$$

$$\mathcal{W}_\beta(t', t'') = \left\langle \frac{\mathrm{d}}{\mathrm{d}t'}\hat{\Phi}\big(\mathsf{x}(t')\big) \frac{\mathrm{d}}{\mathrm{d}t''}\hat{\Phi}\big(\mathsf{x}(t'')\big) \right\rangle_\beta . \tag{3.4b}$$

Had we not included the time derivative in $\hat{H}_{\mathrm{int}}$ (3.3), i.e. had we replaced the interaction Hamiltonian by (2.32), then $\mathcal{W}_\beta$ would have been replaced by the pullback of the Wightman function $\widetilde{\mathcal{W}}_\beta$ (3.1) to the trajectory (3.2) given by $\widetilde{\mathcal{W}}_\beta(t', t'') = \langle \hat{\Phi}(\mathsf{x}(t'))\hat{\Phi}(\mathsf{x}(t''))\rangle_\beta$. For a massless Klein-Gordon (KG) field, however, $\widetilde{\mathcal{W}}_\beta$ is infrared divergent [26]. The derivative-coupled detector model is often employed to sidestep a similar infrared divergence that occurs for a massless field in $1+1$ spacetime dimensions already in zero temperature [31–33, 113–115].

3.1.1 Response function mode sum

By assumption, the field's dispersion relation is spatially isotropic. As such, the field mode frequency with respect to ∂_t can be written as $\omega(|\boldsymbol{k}|)$, where $\omega(K)$ is a function of a non-negative argument and ω is positive everywhere except possibly at $K = 0$. We write $\omega'(K) = \mathrm{d}\omega(K)/\mathrm{d}K$ and assume that $\omega'(K) > 0$ for $K > 0$. If $\omega(0) = 0$, we assume that $\omega'(0) > 0$.

In the analogue spacetime setting, there are two dispersion relations of particular interest satisfying these assumptions, the Bogoliubov (rus. Боголюбов) dispersion relation for quasiparticle excitations in a Bose-Einstein condensate (BEC) [116] and the dispersion relation for waves on the free surface of a liquid [52, 105]. Both dispersion relations satisfy $\omega(0) = 0$. The second assumption is then interpreted as $\omega(K)$ being linear around zero. Introducing for a moment dimensionful units, we have $\omega(K) = c_s K$, where c_s is the speed of sound in these systems.

We show in Appendix B that the response function (3.4) has the mode sum expression

$$\mathcal{F}(\overline{E}, \beta) = \frac{\overline{E}^2}{2}\Bigg(\sum_{m > (\overline{E}+\omega(0))/\Omega} \frac{K_m^+}{\omega'(K_m^+)\omega(K_m^+)} \Big(1 + n\big(\beta\omega(K_m^+)\big)\Big) J_m^2(RK_m^+) + \sum_{m > (-\overline{E}+\omega(0))/\Omega} \frac{K_m^-}{\omega'(K_m^-)\omega(K_m^-)}\, n\big(\beta\omega(K_m^-)\big) J_m^2(RK_m^-) \Bigg)\,, \tag{3.5}$$

where n is the Bose thermal factor (2.40), J_m are the Bessel functions of the first kind [111], and $K_m^\pm$ is defined for $m > (\pm\overline{E} + \omega(0))/\Omega$, as the unique solution to

$$\omega(K) - m\Omega \pm \overline{E} \;=\; 0\,. \tag{3.6}$$

The uniqueness of $K_m^\pm$ follows from the positivity of $\omega'(K)$, and the notation suppresses the $\overline{E}$-dependence of $K_m^\pm$.

If $\omega(0) = 0$, the factors $n\big(\beta\omega(K_m^\pm)\big)/\omega(K_m^\pm)$ have singularities, but, by the assumption $\omega'(0) > 0$, these singularities are more than outweighed by the factors $K_m^\pm J_m^2(RK_m^\pm)$ for $m \neq 0$, whereas the $m = 0$ term is not singular because $\overline{E} \neq 0$ by assumption; $\mathcal{F}(\overline{E},\beta)$ is hence continuous in $\overline{E}$, but it is not smooth. We shall comment on this in more explicitly with the massless KG field below.

3.1.2 Massless Klein-Gordon field

We now specialise to the massless KG field, for which $\omega(K) = K$, $\omega'(K) = 1$ and $K_m^\pm = m\Omega \mp \overline{E}$. The response function (3.5) then simplifies to

$$\mathcal{F}(\overline{E},\beta) \;=\; \mathcal{F}_\infty(\overline{E}) + \Delta\mathcal{F}_\beta(\overline{E})\,, \tag{3.7a}$$

$$\mathcal{F}_\infty(\overline{E}) \;=\; \frac{\overline{E}^2}{2}\sum_{m>\overline{E}/\Omega} J_m^2\big((m\Omega - \overline{E})R\big)\,, \tag{3.7b}$$

$$\begin{aligned}\Delta\mathcal{F}_\beta(\overline{E}) \;=\; \frac{\overline{E}^2}{2}\Bigg(&\sum_{m>|\overline{E}|/\Omega} n\big((m\Omega - |\overline{E}|)\beta\big)J_m^2\big((m\Omega - |\overline{E}|)R\big)\\ &+ \sum_{m>-|\overline{E}|/\Omega} n\big((m\Omega + |\overline{E}|)\beta\big)J_m^2\big((m\Omega + |\overline{E}|)R\big)\Bigg)\,,\end{aligned} \tag{3.7c}$$

where $\mathcal{F}_\infty$ is the vacuum contribution, independent of β, while $\Delta\mathcal{F}_\beta$ is the additional contribution due to the ambient temperature. The notation $\mathcal{F}_\infty$ indicates the contribution remaining in the limit as $\beta \to \infty$ (equivalently $T \to 0$). We note that $\Delta\mathcal{F}_\beta(\overline{E})$ is even in $\overline{E}$, and we have written (3.7c) in a way that makes this manifest. Note also that both $\mathcal{F}_\infty$ and $\Delta\mathcal{F}_\beta$ are manifestly positive.

Recall that by assumption $\overline{E} \neq 0$ and $0 < v < 1$, where $v = R\Omega$. It follows from the uniform asymptotic expansion 10.20.4 in [111] that the sums in (3.7b) and (3.7c) converge, and $\mathcal{F}(\overline{E},\beta)$ is hence well defined. $\mathcal{F}(\overline{E},\beta)$ is however not smooth in $\overline{E}$ at integer values of $\overline{E}/\Omega$, where new terms enter the sums: at $|\overline{E}|/\Omega = n \in \{1,2,\ldots\}$, $\Delta\mathcal{F}_\beta(\overline{E})$ has a discontinuity in its $(2n-1)^{\text{th}}$ derivative and $\mathcal{F}_\infty(\overline{E})$ has a discontinuity in its $(2n)^{\text{th}}$ derivative.

$\mathcal{F}_\infty$ has the integral representation

$$\mathcal{F}_\infty(\overline{E}) \;=\; \overline{E}^2\left(\frac{\gamma}{4} - \frac{1}{2\pi}\int_0^\infty dz\, \frac{\sin\bigl(2(\overline{E}/\Omega)z\bigr)}{\sqrt{z^2 - v^2\sin^2 z}}\right), \tag{3.8}$$

where $\gamma = (1-v^2)^{-1/2}$, which follows by translating (2.80a) to our analogue spacetime conventions and to our derivative-coupled interaction. This representation will be useful for discussing some of the limits in Section 3.2.

3.1.3 Cooling inequality

In an analogue spacetime setting, we consider the detailed balance temperature (2.54) as a function of the lab-frame energy gap $\overline{E}$, defined with respect to the lab time t. To distinguish the detailed balance temperature from the ambient temperature, we write

$$T_{\rm DB}(\overline{E}) \;=\; \frac{\overline{E}}{\ln\left(\frac{\mathcal{F}(-\overline{E},\beta)}{\mathcal{F}(\overline{E},\beta)}\right)}\,. \tag{3.9}$$

We shall find in Section 3.2.1 and Section 3.3 that there are regimes where the circular motion detailed balance temperature $T_{\rm DB}$ is *lower* than the ambient temperature β^{-1}. Here we make preliminary observations as to where such parameter regimes might be found.

The definition of the detailed balance temperature $T_{\rm DB}$ (3.9) may be rearranged as

$$\mathcal{F}(\overline{E},\beta)\mathrm{e}^{\overline{E}/T_{\rm DB}} \;=\; \mathcal{F}(-\overline{E},\beta)\,. \tag{3.10}$$

Whilst (3.10) holds for either sign of $\overline{E}$, let us assume here $\overline{E} > 0$, for simplicity of the notation. As $\mathcal{F}$ is by construction positive, (3.10) then shows that the condition for $T_{\rm DB}$ to be lower than β^{-1} is

$$\mathcal{F}(\overline{E},\beta)\mathrm{e}^{\beta\overline{E}} \;<\; \mathcal{F}(-\overline{E},\beta)\,. \tag{3.11}$$

Using (3.7), and the evenness of $\Delta\mathcal{F}_\beta(\overline{E})$, this becomes

$$\mathcal{F}_\infty(\overline{E})\mathrm{e}^{\beta\overline{E}} + \Delta\mathcal{F}_\beta(\overline{E})(\mathrm{e}^{\beta\overline{E}} - 1) \;<\; \mathcal{F}_\infty(-\overline{E})\,. \tag{3.12}$$

In the low temperature limit, $\beta \to \infty$, with the other parameters fixed, the leftmost term in (3.12) shows that (3.12) cannot hold.

In the high temperature limit, $\beta \to 0^+$, with the other parameters fixed, we shall see in Section 3.2.1 that the left-hand side of (3.12) has a finite limit, and

the possibility of satisfying (3.12) arises. We shall return to this analytically in Section 3.2.1 and numerically in Section 3.3.

3.1.4 Inertial motion response function

In this Section, we consider the response function of a detector undergoing inertial motion but with a nonvanishing (constant) velocity with respect to the heat bath. We shall use this in the later sections to distinguish the acceleration contribution from the velocity contribution in the circular motion response.

Time evolution for an inertial observer with nonvanishing velocity is generated by the Killing vector ∂_t, the same timelike Killing vector used in the construction of a thermal state. As such, this is a stationary situation. By contrast, the time evolution for a uniformly accelerating observer, say, parallel to the x-axis is generated by the Lorentz boost $x\partial_t + t\partial_x$. The notions of time evolution between the accelerated observer and the thermal bath therefore disagree and the Wightman function is no long stationary, as pointed out in [24].

Specialising to the massless KG field, the inertial motion response function may be obtained from (3.4) with (B.1) and (B.2) in a straightforward way, using identities $6.671.1$ and $6.671.2$ in [117]. The outcome is

$$\mathcal{F}_{\rm Lin}(\overline{E},\beta) \;=\; \frac{\overline{E}^2}{2}\left(\gamma\Theta(-\overline{E}) + \frac{1}{\pi}\int_{\frac{|\overline{E}|}{1+v}}^{\frac{|\overline{E}|}{1-v}} \frac{\mathrm{d}x}{(\mathrm{e}^{\beta x}-1)\sqrt{(vx)^2-\left(x-|\overline{E}|\right)^2}}\right)\,, \tag{3.13}$$

where v is the detector's velocity in the rest frame of the thermal bath, satisfying $0 < v < 1$, and $\gamma = (1-v^2)^{-1/2}$ is the Lorentz factor. The subscript "Lin" stands for "linear", emphasising that the inertial motion may be viewed as the $R\to\infty$ limit of the circular motion (3.2) with fixed orbital speed $v = R\Omega$; as a consistency check, we have verified that (3.13) may be obtained from (3.7) in this limit, viewing the sum as the Riemann sum of an integral and using the asymptotic expansions of the Bessel functions [111]. The integrand in (3.13) is singular at the upper and lower limits, but these singularities are integrable and the integral is well defined.

Alternatively, one may re-express $\mathcal{F}_{\rm Lin}(\overline{E},\beta)$ as

$$\mathcal{F}_{\rm Lin}(\overline{E},\beta) \;=\; \frac{\overline{E}^2\gamma}{2}\left(\Theta(-\overline{E}) + \frac{1}{\pi}\int_{-\frac{\pi}{2}}^{\frac{\pi}{2}} \frac{\mathrm{d}\theta}{\mathrm{e}^{\beta|\overline{E}|\gamma^2(1+v\sin\theta)}-1}\right)\,, \tag{3.14}$$

obtained from (3.13) by the substitution $x = \gamma^2|\overline{E}|(1+v\sin\theta)$. (3.14) is more convenient for extracting some asymptotic limits and for numerical evaluation, as the integrand is nonsingular over the whole integration range.

3.2 Asymptotic regimes

In this Section, we examine the behaviour of the response function (3.7) and corresponding detailed balance temperature (3.9) in the asymptotic regimes of high and low ambient temperature, small energy gap, small orbital radius with fixed speed, and near-sonic speed. We also give the corresponding results for inertial motion, including in this case the regime of large energy gap. We demonstrate that for both circular motion and inertial motion there are regimes in which the detailed balance temperature is lower than the ambient temperature.

3.2.1 High ambient temperature

Consider the high ambient temperature limit, $\beta \to 0^+$, with Ω, R and $\overline{E}$ fixed.

By 24.2.1 in [111], the Bose factor $n(x)$ (2.40) has the small argument Laurent expansion

$$n(x) \;=\; \sum_{k=0}^{\infty} \frac{B_k}{k!}\, x^{k-1} \;=\; \frac{1}{x} - \frac{1}{2} + \frac{x}{12} + \cdots\,, \tag{3.15}$$

which is convergent for $0 < x < 2\pi$ and where B_k are the Bernoulli numbers. The Bessel functions in (3.7c) exhibit exponential decay for large m, by 10.20.4 in [111]. It follows, by a dominated convergence argument, that the asymptotic expansion of $\Delta\mathcal{F}_\beta(\overline{E},\beta)$ at $\beta \to 0^+$ may be found from (3.7c) by using (3.15) under the sum over m and exchanging the order of the sums. As the Bernoulli numbers B_k vanish for odd $k > 1$, the expansion proceeds in powers β^p with $p = -1, 0, 1, 3, 5, \ldots$. To leading order we have

$$\Delta\mathcal{F}_\beta(\overline{E}) \;=\; \frac{\overline{E}^2}{2\beta}\Bigg(\sum_{m>|\overline{E}|/\Omega} \frac{J_m^2\big((m\Omega - |\overline{E}|)R\big)}{m\Omega - |\overline{E}|} + \sum_{m>-|\overline{E}|/\Omega} \frac{J_m^2\big((m\Omega + |\overline{E}|)R\big)}{m\Omega + |\overline{E}|} \Bigg) + \mathcal{O}(1)\,. \tag{3.16}$$

For the detailed balance temperature, we combined (3.7), (3.9), and (3.16) to give

$$T_{\mathrm{DB}} \;=\; \frac{1}{\beta}\mathcal{Q}(v, |\overline{E}|/\Omega) + \mathcal{O}(1)\,, \tag{3.17}$$

where

$$\mathcal{Q}(v,k) \;=\; \frac{\displaystyle\sum_{m>-k} \frac{J_m^2\big((m+k)v\big)}{m+k} \;+\; \sum_{m>k} \frac{J_m^2\big((m-k)v\big)}{m-k}}{\displaystyle\sum_{m>-k} J_m^2\big((m+k)v\big) \;-\; \sum_{m>k} J_m^2\big((m-k)v\big)}\,, \tag{3.18}$$

k is assumed positive, and we recall that $0 < v < 1$.

The function $\mathcal{Q}(v,k)$ (3.18) is well defined: the sums over m converge by the exponential falloff of the Bessel functions as seen from 10.20.4 in [111], and the denominator is positive, which one may see in the following way. We first write the denominator as

$$\frac{2}{\pi}\int_0^\infty dz\, \frac{\sin(2kz)}{\sqrt{z^2 - v^2\sin^2 z}}\,, \tag{3.19}$$

using (3.7b) and (3.8). Then, one may see that (3.19) is positive by breaking the integral into a sum of integrals over the intervals $\frac{\pi p}{2k} < z < \frac{\pi(p+1)}{2k}$, $p = 0, 1, 2, \ldots$ and then combining each even p interval with the next odd p interval. The combined integrand in each term is then positive because the denominator in (3.19) is a strictly increasing function of z, and finally one observes that these rearrangements are justified by the convergence of (3.19) as an improper Riemann integral.

In the limit $v \to 0^+$ with fixed k, $\mathcal{Q}(v,k)$ has the asymptotic behaviour

$$\mathcal{Q}(v,k) \;=\; \begin{cases} \dfrac{1}{k} - \frac{1}{2}v^2 + \mathcal{O}(v^4) & \text{for } 0 < k < 1\,, \\[2ex] \dfrac{1}{k\gamma}\big(1 + \mathcal{O}(v^4)\big) & \text{for } 1 \le k\,, \end{cases} \tag{3.20}$$

which can be verified by expanding the sums in (3.18) in v term by term. Interchanging the sum and the expansion is justified by the falloff 10.20.4 in [111] allows one to differentiate the sums with respect to v term by term for $0 < v < 1$. It follows that for fixed $k \ge 1$, $\mathcal{Q}(v,k) < 1$ for sufficiently small v.

In the limit $v \to 1$ with fixed k, $\mathcal{Q}(v,k)$ tends to zero and decays proportionally to $1/\ln\gamma$. To see this, we note that the numerator in (3.18) remains bounded as $v \to 1$, by 10.20.4 in [111], whereas the denominator diverges, with the leading term $\frac{4\sqrt{3}}{\pi} k \ln\gamma$, as is seen using the integral representation (3.19) and the asymptotic expansion in Appendix E of [69].

Given these observations about $\mathcal{Q}(v,k)$, we see that for sufficiently high ambient temperatures (so that (3.17) is a good approximation of the detailed balance temperature), T_{DB} (3.17) is lower than the ambient temperature for any fixed $|\overline{E}|$

and sufficiently large v, and also for any fixed $|\overline{E}| \geq \Omega$ and sufficiently small v. We shall return to $\mathcal{Q}(v,k)$ numerically in Section 3.3.

While the sums arising from $\Delta\mathcal{F}_\beta$ do not appear to be expressible in terms of elementary functions, $\Delta\mathcal{F}_\beta(\overline{E})$ admits an elementary analytic bound at the particular value $\overline{E} = \pm\Omega$, at the boundary between the two asymptotic behaviours shown in (3.20): from (3.7c) we have

$$\begin{aligned}\Delta\mathcal{F}_\beta(\pm\Omega) \;&<\; \frac{\Omega^2}{2} n(v\beta/R) \sum_{m=1}^{\infty} \big(J_{m+1}^2(mv) + J_{m-1}^2(mv)\big) \\ &=\; \frac{\Omega^2}{2} \frac{n(v\beta/R)}{\sqrt{1-v^2}}\,,\end{aligned} \tag{3.21}$$

and the bound is sharper at lower values of β. The inequality in (3.21) follows by renaming the summation index and replacing the Bose factor (2.40) by its value at the lowest summand. The equality follows from the identity

$$\sum_{m=1}^{\infty} \big(J_{m-1}^2(mv) + J_{m+1}^2(mv)\big) \;=\; \frac{1}{\sqrt{1-v^2}}\,, \tag{3.22}$$

which we verify in Appendix C. We have not found this identity in the existing literature.

3.2.2 Low ambient temperature

We consider now the low ambient temperature limit, $\beta \to \infty$, with Ω, R and $\overline{E}$ fixed.

The Bose factor $n(x)$ (2.40) has the following large-argument expansion

$$n(x) \;=\; \sum_{k=1}^{\infty} \mathrm{e}^{-kx}\,, \tag{3.23}$$

which is convergent for $x > 0$. By the exponential decay of the Bessel functions in (3.7c), it follows by a dominated convergence argument that the asymptotic expansion of $\Delta\mathcal{F}_\beta(\overline{E},\beta)$ as $\beta \to \infty$ may be found from (3.7c) by using (3.23) and rearranging the sums. We find

$$\begin{aligned}\Delta\mathcal{F}_\beta(\overline{E}) \;=\; \frac{\overline{E}^2}{2}\Big(&\mathrm{e}^{-\beta(m^+\Omega - |\overline{E}|)}\, J_{m^+}^2\big((m^+\Omega - |\overline{E}|)R\big) \\ &+ \mathrm{e}^{-\beta(m^-\Omega + |\overline{E}|)}\, J_{m^-}^2\big((m^-\Omega + |\overline{E}|)R\big)\Big) \\ &+ \mathcal{O}\Big(\mathrm{e}^{-2\beta\min\left(m^+\Omega - |\overline{E}|,\, m^-\Omega + |\overline{E}|\right)}\Big)\,,\end{aligned} \tag{3.24}$$

where

$$m^{\pm} \;=\; 1 + \big\lfloor \pm|\overline{E}|/\Omega \big\rfloor \;, \tag{3.25}$$

$\lfloor \cdot \rfloor$ is the floor function, and the notation suppresses the $\overline{E}$-dependence of $m^{\pm}$. Note that since

$$0 < m^{\pm}\Omega \mp |\overline{E}| \leq \Omega \,, \tag{3.26}$$

(3.24) shows that $\Delta\mathcal{F}_\beta(\overline{E})$ has an exponential decay in β. Note that whilst the coefficients $m^{\pm}\Omega \mp |\overline{E}|$ in the exponent are by construction positive, they are not continuous in E and the parameters of the motion, and they may take arbitrarily small positive values.

The dependence of the exponents in (3.24) on $\overline{E}$ determines the dominant term in the exponential decay. There are three qualitatively different cases:

1. For $0 < \big||\overline{E}| - n\Omega\big| < \frac{1}{2}\Omega$, $n \in \{0, 1, 2, \ldots\}$:

$$\Delta\mathcal{F}_\beta(\overline{E}) \;=\; \tfrac{1}{2}\overline{E}^2\, \mathrm{e}^{-\beta\big||\overline{E}|-n\Omega\big|}\, J_n^2\big((|\overline{E}| - n\Omega)R\big) + \mathcal{O}\Big(\mathrm{e}^{-\beta \min\left(2\big||\overline{E}|-n\Omega\big|,\,\Omega-\big||\overline{E}|-n\Omega\big|\right)}\Big) \;. \tag{3.27}$$

2. For $|\overline{E}| = (n + \frac{1}{2})\Omega$, $n \in \{0, 1, 2, \ldots\}$:

$$\Delta\mathcal{F}_\beta\big((n+\tfrac{1}{2})\Omega\big) \;=\; \tfrac{1}{2}(n+\tfrac{1}{2})^2\Omega^2\, \mathrm{e}^{-\beta\Omega/2}\big(J_{n+1}^2(\Omega R/2) + J_n^2(\Omega R/2)\big) + \mathcal{O}\big(\mathrm{e}^{-\beta\Omega}\big) \;. \tag{3.28}$$

3. For $|\overline{E}| = n\Omega$, $n \in \{1, 2, 3, \ldots\}$:

$$\Delta\mathcal{F}_\beta(n\Omega) \;=\; \tfrac{1}{2}n^2\Omega^2\, \mathrm{e}^{-\beta\Omega}\big(J_{n+1}^2(\Omega R) + J_{n-1}^2(\Omega R)\big) \;+\; \mathcal{O}\big(\mathrm{e}^{-2\beta\Omega}\big) \;. \tag{3.29}$$

The detailed balance temperature differs from the zero ambient temperature value by a correction that is exponentially decaying in β, with the same leading exponent as in (3.27)–(3.29).

3.2.3 Small energy gap

We consider now the limit $\overline{E} \to 0$, with fixed Ω, R and β.

Without loss of generality, we can assume $|\overline{E}| < \Omega$. Then, in $\Delta\mathcal{F}_\beta(\overline{E}, \beta)$ (3.7c), we have

$$\Delta\mathcal{F}_\beta(\overline{E}) = \frac{\overline{E}^2}{2}\Big\{n(|\overline{E}|\beta)J_0^2(|\overline{E}|R) + \sum_{m=1}^{\infty}\Big[n\big((m\Omega-|\overline{E}|)\beta\big)J_m^2\big((m\Omega-|\overline{E}|)R\big)+ n\big((m\Omega+|\overline{E}|)\beta\big)J_m^2\big((m\Omega+|\overline{E}|)R\big)\Big]\Big\}$$

$$= \frac{|\overline{E}|}{2\beta} + \left(-\frac{1}{4}+\sum_{m=1}^{\infty} n(m\Omega\beta)J_m^2(m\Omega R)\right)|\overline{E}|^2 + \left(\frac{\beta}{24}-\frac{R^2}{4\beta}\right)|\overline{E}|^3 + \mathcal{O}\big(|\overline{E}|^4\big)\,, \quad (3.30)$$

where we have used the expansion (3.15) and we have expanded in $|\overline{E}|$ under the sum, justified by the falloff seen from 10.20.4 in [111]. We note that the assumption $|\overline{E}| < \Omega$ allowed us to simply the lower limits of the summations in (3.7c).

Considering now the vacuum contribution $\mathcal{F}_\infty(\overline{E})$, we have

$$\mathcal{F}_\infty(\overline{E}) = \frac{\overline{E}^2\gamma}{4} - \frac{\overline{E}^2\mathrm{sgn}(\overline{E})}{4} + \frac{\overline{E}^3}{\pi\Omega}\int_0^\infty dz\left(1-\frac{z}{\sqrt{z^2-v^2\sin^2 z}}\right) + \mathcal{O}\big(\overline{E}^4\big)\,, \quad (3.31)$$

obtained by applying to (3.8) the method of Appendix B of [69] and proceeding to one order higher to verify that the error term is as shown in (3.31).

We therefore calculate the asymptotic behaviour of the detailed balance temperature (3.9), by combining (3.7), (3.30), and (3.31) to give

$$T_{\mathrm{DB}} = \frac{1}{\beta} + \left[\frac{\gamma-1}{2} + 2\sum_{m=1}^{\infty} n(m\Omega\beta)J_m^2(m\Omega R) + \frac{4}{\pi\Omega\beta}\int_0^\infty dz\left(1-\frac{z}{\sqrt{z^2-v^2\sin^2 z}}\right)\right]|\overline{E}| + \mathcal{O}\big(|\overline{E}|^2\big)\,. \quad (3.32)$$

We see that in the limit $\overline{E}\to 0$, the detector acts as a thermometer, probing the ambient temperature $1/\beta$.

3.2.4 Large energy gap

We consider now the limit $\overline{E}\to\pm\infty$, with fixed Ω, R and β.

We can adapt the analysis of the vacuum contribution to the response function $\mathcal{F}_\infty(\overline{E})$ given in [69] to our derivative coupled, analogue spacetime conventions

using the integral representation (3.8). This shows that $\mathcal{F}_\infty(\overline{E})$ consists of the inertial motion contribution and a piece that is exponentially suppressed in $|\overline{E}|$.

Estimating $\Delta\mathcal{F}_\beta(\overline{E})$ (3.7c) at $|\overline{E}| \to \infty$, however, would require new techniques and we do not pursue this estimate here.

3.2.5 Small radius with fixed speed

We consider the limit $R \to 0$ with fixed v, β and $\overline{E}$. In $\Delta\mathcal{F}_\beta(\overline{E},\beta)$ (3.7c), writing $\Omega = v/R$ gives, for $R < v/|\overline{E}|$,

$$\begin{aligned}\Delta\mathcal{F}_\beta(\overline{E}) &= \frac{\overline{E}^2}{2}\Big\{n(|\overline{E}|\beta)J_0^2(|\overline{E}|R) \\ &\quad + \sum_{m=1}^{\infty}\Big[n(mv/R-|\overline{E}|\beta)J_m^2(mv-|\overline{E}|R)+n(mv/R+|\overline{E}|\beta)J_m^2(mv+|\overline{E}|R)\Big]\Big\} \\ &= \frac{\overline{E}^2 n(|\overline{E}|\beta)}{2}+\mathcal{O}\big(R^2\big)\,. \end{aligned} \tag{3.33}$$

For $\mathcal{F}_\infty(\overline{E})$, we have

$$\mathcal{F}_\infty(\overline{E}) = \frac{\overline{E}^2\gamma}{4}-\frac{\overline{E}^2\mathrm{sgn}(\overline{E})}{4}+\frac{\overline{E}^3 R}{\pi v}\int_0^\infty dz\left(1-\frac{z}{\sqrt{z^2-v^2\sin^2 z}}\right)+\mathcal{O}\big(R^2\big)\,, \tag{3.34}$$

obtained from (3.8) by writing $\Omega = v/R$ and proceeding as with (3.31).

Combining (3.7), (3.33) and (3.34), we find the leading asymptotic behaviour of the detailed balance temperature (3.9),

$$T_{\mathrm{DB}} = \frac{|\overline{E}|}{\ln\left(\dfrac{\gamma+1+2n(|\overline{E}|\beta)}{\gamma-1+2n(|\overline{E}|\beta)}\right)}+\mathcal{O}(R)\,. \tag{3.35}$$

We remark that despite the acceleration $a = v^2/R$ diverging as $R \to 0$, both the response function $\mathcal{F}$ and the detailed balance temperature T_{DB} remain finite.

3.2.6 Large radius with fixed speed

Consider the limit $R \to \infty$ with fixed v, β and $\overline{E}$. This is the limit of inertial motion with speed v, as discussed in Section 3.1.4. The leading term in $\mathcal{F}$ is $\mathcal{F}_{\mathrm{Lin}}$ (3.13). We have not pursued the subleading corrections.

3.2.7 Machian limit

In this analogue spacetime setting, we consider now the Machian, or near-sonic limit $v \to 1$, equivalently $R \to 1/\Omega$ with fixed Ω, β, and $\overline{E}$.

In $\Delta\mathcal{F}_\beta(\overline{E},\beta)$ (3.7c), the Bose thermal factors n exhibit an exponential large m falloff, while the falloff of the Bessel function factors is exponential for $0 < v < 1$ and $m^{-2/3}$ for $v = 1$, as seen from 10.20.4 in [111]. It follows that $\Delta\mathcal{F}_\beta(\overline{E},\beta)$ has a finite limit as $v \to 1$,

$$\Delta\mathcal{F}_\beta(\overline{E},\beta) \;=\; \frac{\overline{E}^2}{2}\left(\sum_{m>|\overline{E}|/\Omega} n\big(\beta(m\Omega-|\overline{E}|)\big)\,J_m^2(m-|\overline{E}|/\Omega) + \sum_{m>-|\overline{E}|/\Omega} n\big(\beta(m\Omega+|\overline{E}|)\big)\,J_m^2(m+|\overline{E}|/\Omega)\right) + o(1)\,. \tag{3.36}$$

Again, using the integral representation (3.8) and the formulas in Appendix E of [69] adapted to our derivative coupled, analogue spacetime conventions, we find

$$\mathcal{F}_\infty(\overline{E}) \;=\; \overline{E}^2\left[\frac{\gamma}{4}+\frac{\sqrt{3}\,\overline{E}}{\pi\Omega}\ln\left(\frac{\sqrt{3}\,\mathrm{e}^{\gamma_E-1}|\overline{E}|}{\gamma\Omega}\right)-\frac{1}{2\pi}h(2\overline{E}/\Omega)\right]+o(1)\,, \tag{3.37}$$

where γ_E is the Euler-Mascheroni constant and

$$h(x) \;=\; \int_0^\infty dz\,\frac{\sin(xz)}{z}\left(\frac{1}{\sqrt{1-(\sin^2 z)/z^2}}-\frac{\sqrt{3}}{z}\right)\,. \tag{3.38}$$

The detailed balance temperature (3.9), is given by collecting (3.7), (3.36), and (3.37) to give

$$T_{\mathrm{DB}} \;=\; \frac{\pi\Omega}{8\sqrt{3}}\left(\frac{\gamma}{\ln\gamma}\right)\left\{1+\frac{1}{\ln\gamma}\left[\ln\left(\frac{\sqrt{3}\,\mathrm{e}^{\gamma_E-1}|\overline{E}|}{\Omega}\right)-\frac{\Omega}{2\sqrt{3}\,|\overline{E}|}h(2|\overline{E}|/\Omega)\right]+o\left(\frac{1}{\ln\gamma}\right)\right\}. \tag{3.39}$$

All terms shown arise from $\mathcal{F}_\infty$: the contribution due to the ambient temperature only appears at lower orders and is redshifted away.

3.2.8 Inertial motion

In this Section, we record the corresponding asymptotic results for inertial motion.

For large/small β and large/small $|\overline{E}|$, we use (3.14) and note that the expansions depend on β and $|\overline{E}|$ only through the combination $\beta|\overline{E}|$. At high ambient temperature and/or small gap, $\beta|\overline{E}| \to 0$, we find

$$\mathcal{F}_{\mathrm{Lin}}(\overline{E},\beta) = \frac{\overline{E}^2}{2}\left(\frac{1}{\beta|\overline{E}|} + \gamma\Theta(-\overline{E}) + \frac{\gamma^3\beta|\overline{E}|}{12} + \mathcal{O}\big(\beta^2\overline{E}^2\big)\right), \tag{3.40a}$$

$$T_{\mathrm{DB}}^{\mathrm{Lin}} = \frac{1}{\gamma\beta}\left[1 + \frac{(\gamma-1)\gamma^2\beta^2\overline{E}^2}{12} + \mathcal{O}\big(\beta^4\overline{E}^4\big)\right], \tag{3.40b}$$

using (3.15). In the low ambient temperature and/or large gap limit, $\beta|\overline{E}| \to \infty$, we find

$$\mathcal{F}_{\mathrm{Lin}}(\overline{E},\beta) = \frac{\overline{E}^2}{2}\left[\gamma\Theta(-\overline{E}) + \frac{\mathrm{e}^{-\beta|\overline{E}|/(1+v)}}{\sqrt{2\pi v\beta|\overline{E}|}} + \mathcal{O}\Big(\big(\beta|\overline{E}|\big)^{-3/2}\mathrm{e}^{-\beta|\overline{E}|/(1+v)}\Big)\right], \tag{3.41a}$$

$$T_{\mathrm{DB}}^{\mathrm{Lin}} = \frac{(1+v)}{\beta}\left[1 + \frac{(1+v)\ln(\beta|\overline{E}|)}{2\beta|\overline{E}|} + \mathcal{O}\left(\frac{1}{\beta|\overline{E}|}\right)\right], \tag{3.41b}$$

using (3.23) and the properties 10.32.1 and 10.40.1 from [111] of the modified Bessel function I_0.

Considering the Machian limit, $v \to 1$, we start from (3.13), change variables by $\omega = |\overline{E}|\,(1+z^2)\,/(1+v)$, use a dominated convergence argument to take the $v \to 1$ limit under the integral, and use 25.12.11 in [111]. We find

$$\mathcal{F}_{\mathrm{Lin}}(\overline{E},\beta) = \frac{\overline{E}^2}{2}\left(\gamma\Theta(-\overline{E}) + \frac{1}{\sqrt{2\pi\beta|\overline{E}|}}\,\mathrm{Li}_{\frac{1}{2}}\big(\mathrm{e}^{-\frac{1}{2}\beta|\overline{E}|}\big) + o(1)\right), \tag{3.42a}$$

$$T_{\mathrm{DB}}^{\mathrm{Lin}} = \frac{|\overline{E}|}{\ln\gamma}\left[1 + \frac{1}{\ln\gamma}\ln\left(\frac{\mathrm{Li}_{\frac{1}{2}}\big(\mathrm{e}^{-\frac{1}{2}\beta|\overline{E}|}\big)}{\sqrt{2\pi\beta|\overline{E}|}}\right) + o\left(\frac{1}{\ln\gamma}\right)\right], \tag{3.42b}$$

where Li is the polylogarithm [111].

In the limit $\beta|\overline{E}| \to \infty$, corresponding to either the low ambient temperature and/or the large energy gap regime, we find that the detailed balance temperature T_{DB} is always higher than the ambient temperature, see (3.41b). By contrast, the detailed balance temperature T_{DB} is always lower than the ambient temperature in the in limit $\beta|\overline{E}| \to 0$, corresponding to the high ambient temperature

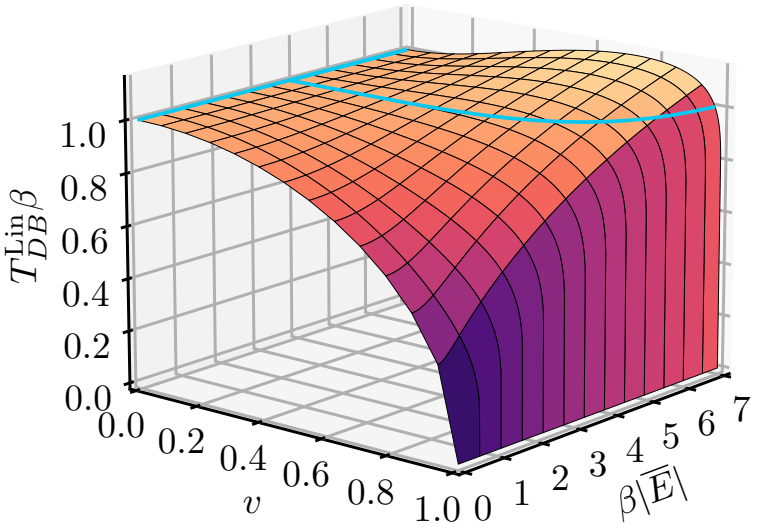

Figure 3.1: Inertial motion detailed balance temperature $T_{\mathrm{DB}}^{\mathrm{Lin}}$, plotted from (3.9) and (3.14). The graph shows $\beta T_{\mathrm{DB}}^{\mathrm{Lin}}$ as a function of v and $\beta|\overline{E}|$, which contains all the independent information. The horizontal (blue) curve is at $\beta T_{\mathrm{DB}}^{\mathrm{Lin}} = 1$, at the boundary between a heating effect and a cooling effect. The large $\beta|\overline{E}|$ heating effect (3.41b), the small $\beta|\overline{E}|$ cooling effect (3.40b) and the large v cooling effect (3.42b) are evident in the plot; note in particular the abrupt $1/\ln\gamma$ cooling effect (3.42b) as $v \to 1$. The interpolation between the large $\beta|\overline{E}|$ heating effect and the large v cooling effect is showing in the region where both of these these quantities are large, with the horizontal (blue) curve $\beta T_{\mathrm{DB}}^{\mathrm{Lin}} = 1$ receding into the distance.

and/or the small energy gap regime by (3.40b), and similarly in the Machian limit, by (3.42b).

3.3 Numerical results

In this Section, we plot the detailed balance temperature for a detector in uniform circular motion and in inertial motion, interpolating between the asymptotic regimes considered in Section 3.2.

3.3.1 Detailed balance temperature in inertial motion

We consider first inertial motion. We plot the dimensionless quantity $\beta T_{\mathrm{DB}}^{\mathrm{Lin}}$, which encompasses all the independent information about $T_{\mathrm{DB}}^{\mathrm{Lin}}$, as a function of the dimensionless variables v and $\beta|\overline{E}|$ using (3.9) and (3.14). We plot this in Figure 3.1. The plot displays the interpolation between the large $\beta|\overline{E}|$ heating effect (3.41b), the small $\beta|\overline{E}|$ cooling effect (3.40b) and the large v cooling effect (3.42b).

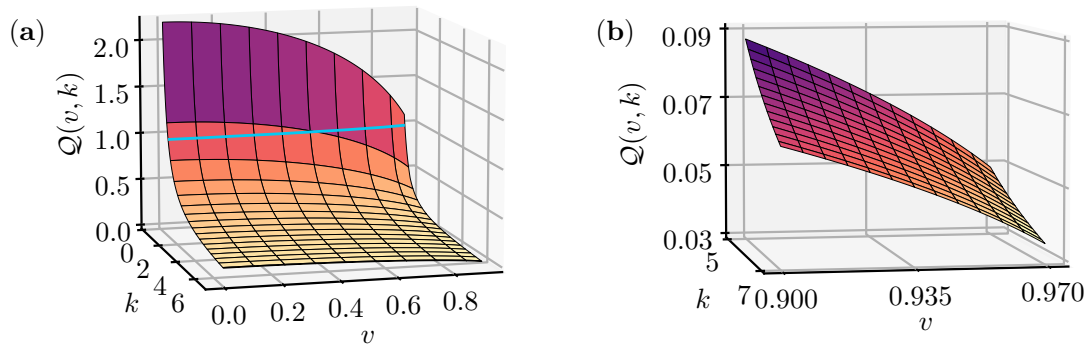

Figure 3.2: Plots of the function $\mathcal{Q}(v,k)$ (3.18), determining the high ambient temperature asymptotic behaviour of T_{DB} by (3.17). **(a)** Plotting parameters: $0.45 \leq k \leq 7$ and $0 < v \leq 0.9$. Horizontal (blue) curve is at $\mathcal{Q}(v,k) = 1$, at the boundary between a heating effect and a cooling effect at high ambient temperature. **(b)** Plotting parameters: $5 \leq k \leq 7$ and $0.9 \leq v \leq 0.97$. Incipient evidence of the $1/\ln\gamma$ falloff at $v \to 1$; closer to $v = 1$ the numerics becomes slow because of the sums in the denominator in (3.18). If the pattern shown in the plots continues beyond the plotted range, there is a high ambient temperature cooling effect for all $|\overline{E}|/\Omega \geq 1$, regardless of v.

3.3.2 Detailed balance temperature in circular motion

We consider now circular motion. As a preliminary, we recall from (3.17) that asymptotic behaviour of T_{DB} in the limit of a high ambient temperature is determined by the function $\mathcal{Q}(v,k)$ (3.18), with $k = |\overline{E}|/\Omega$. We found in Section 3.2.1 that in this limit, there is a cooling effect for any fixed $|\overline{E}|/\Omega$ and sufficiently large v, and also for any fixed $|\overline{E}|/\Omega \geq 1$ and sufficiently small v. The plot of $\mathcal{Q}(v,k)$ in Figure 3.2 confirms numerically these findings, and indicates that there is a cooling effect when $|\overline{E}|/\Omega \geq 1$ for any v.

Returning to finite ambient temperature, we address the interpolation between the asymptotic regimes analysed in Section 3.2. In Figure 3.3**(a)**, we plot the detailed balance temperature as a function of the ambient temperature and the energy gap, for fixed $v = 0.6$ and a fixed orbital radius, and in Figure 3.3**(b)** the difference between the detailed balance temperature and the ambient temperature. The orbital radius R enters the plots only in that it sets the scales of the axes, and the range of the variables is chosen to cover the main transitional region of interest and to indicate the onset of asymptotics.

As one would expect, Figure 3.3**(a)** shows that the contribution from the ambient temperature dominates when the ambient temperature is high, consistent with the analytic estimates of Section 3.2. The key information in Figure 3.3 is the interpolation between the heating and cooling effects due to motion: while we know from Section 3.2 and Figure 3.2 that a high ambient temperature cooling

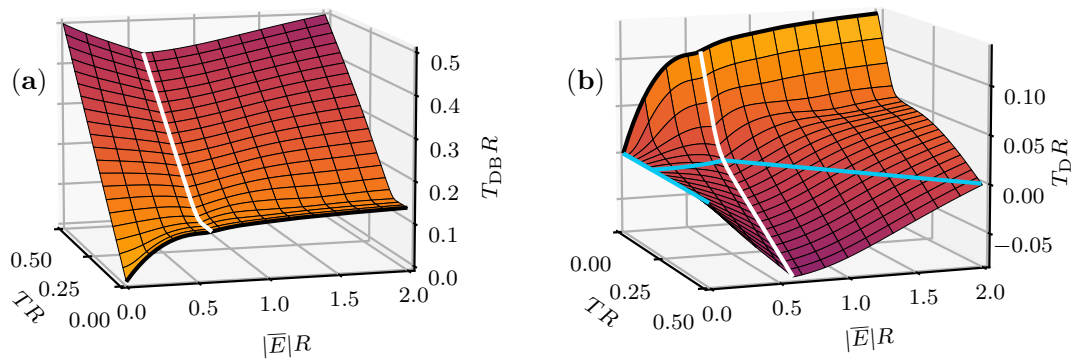

Figure 3.3: (a) Circular motion detailed balance temperature as a function of the ambient temperature and the energy gap, at fixed $v = 0.6$. The orbital radius R enters only in that it sets the scale of the axes: the vertical axis is $T_{\mathrm{DB}}R$, the ambient temperature horizontal axis is TR where $T = 1/\beta$, and the energy gap horizontal axis is $|\overline{E}|R$. The white curve marks the discontinuity in the first derivative at $|\overline{E}|R = v$, coming from the discontinuity in the first derivative of $\mathcal{F}(\overline{E}, \beta)$ (3.7) at $|\overline{E}| = \Omega = v/R$.
(b) As in (a), but showing the difference of the detailed balance temperature and the ambient temperature: the vertical axis is $T_{\mathrm{D}}R$, where $T_{\mathrm{D}} = T_{\mathrm{DB}} - T$. Note that the horizontal TR axes in (a) and (b) increase in opposite directions, for the benefit of the visual perspective. The horizontal (blue) curve is at $T_{\mathrm{D}}R = 0$, at the boundary between a heating effect and a cooling effect, and the white curve at $|\overline{E}|R = v$ is at the discontinuity in the first derivative, as in (a). A cooling effect near $|\overline{E}|R = v$ sets in at moderate ambient temperature, from where it extends to high ambient temperature for $|\overline{E}|R \geq v$.

occurs for $|\overline{E}| \geq \Omega$, Figure 3.3 shows that this cooling effect occurs already for moderate values of the ambient temperature when $|\overline{E}| \lesssim \Omega$.

3.4 Acceleration versus speed in circular motion

By the introduction of a thermal bath, we also broke the Lorentz invariance of the system. In particular, this introduced a Doppler shift. We can see the effect of this in the detailed balance temperature for an inertial detector, plotted in Figure 3.1. We see that only a detector at rest ($v = 0$) will act as a perfect thermometer, measuring the ambient temperature for all energy gaps $\overline{E}$. When the velocity is nonzero, the detector experiences both a heating and cooling effect depending on the energy gap. As such, the response of the detector due to its acceleration versus response due to the Doppler effect in Figure 3.3 is unclear. In this Section, we ask how much of the circular motion effect in the detector's response can be attributed to the detector's speed and how much to the acceleration.

3.4.1 Acceleration quantifiers

A primary quantity indicating the significance of acceleration is the difference in the transition rates between the circular motion and inertial motion at the same speed. We quantify this difference by the ratio

$$\mathcal{N}_v(\overline{E}\beta, R/\beta) \;=\; \frac{\mathcal{F}(\overline{E},\beta) - \mathcal{F}_{\text{Lin}}(\overline{E},\beta)}{\mathcal{F}_{\text{Lin}}(\overline{E},\beta)}\,. \tag{3.43}$$

The notation suppresses that, on the right-hand side, the velocity v in $\mathcal{F}_{\text{Lin}}$ is taken to be equal to $R\Omega$ in $\mathcal{F}$. The notation on the left-hand side makes explicit that the ratio $\mathcal{N}_v$ depends on the parameters only through the dimensionless triple $(v, \overline{E}\beta, R/\beta)$, as seen from (3.7) and (3.14). $\mathcal{N}_v$ is interpreted as the relative excess transition rate due to the acceleration at a given speed. This excess, however, may *a priori* be positive or negative. When the response due to the Doppler shift dominates, we have $\mathcal{F} \to \mathcal{F}_{\text{Lin}}$. Therefore, the contribution due to acceleration is insignificant if and only if $|\mathcal{N}_v| \ll 1$.

Throughout the analysis in Section 3.2, we investigated the asymptotic behaviour of both the response function and also the detailed balance temperature as quantifiers of detector response. As such, a second quantity indicating the significance of acceleration is the ratio of the circular motion detailed balance temperature and the inertial motion detailed balance temperature, $T_{\text{DB}}/T_{\text{DB}}^{\text{Lin}}$, at the same speed. Just like the difference in response (3.43), the ratio of detailed balance temperatures depends on the parameters through the dimensionless triple $(v, \overline{E}\beta, R/\beta)$. The main question we will be addressing is where in parameter space is $T_{\text{DB}}/T_{\text{DB}}^{\text{Lin}}$ approximately unity, and where is it significantly different from unity?

3.4.2 Asymptotic regimes

Using the results of Section 3.2, we consider now four asymptotic regimes.

First, in the limit $R \to \infty$ with fixed v, β and $\overline{E}$, the circular motion trajectory becomes inertial, and the effects due to acceleration become insignificant by construction, as discussed in Section 3.2.6. Trivially, we have $\mathcal{N}_v \to 0$ and $T_{\text{DB}}/T_{\text{DB}}^{\text{Lin}} \to 1$.

Second, we consider the limiting behaviour as $\overline{E} \to 0$ with v, R and β fixed. From Section 3.2.3 and Section 3.2.8, we obtain

$$\mathcal{N}_v(\overline{E}\beta, R/\beta) \;=\; \beta|\overline{E}|\left((\gamma-1)\Theta(\overline{E}) + 2\sum_{m=1}^{\infty} n(mv\beta/R)J_m^2(mv)\right) + \mathcal{O}\big(\overline{E}^2\big)\,, \tag{3.44a}$$

$$\frac{T_{\mathrm{DB}}}{T_{\mathrm{DB}}^{\mathrm{Lin}}} = \gamma + \mathcal{O}(\overline{E})\,. \tag{3.44b}$$

The contribution due to acceleration in the response function $\mathcal{F}$ hence tends to zero linearly in $\overline{E}$, but with different coefficients for excitations and de-excitations. The acceleration effect in the detailed balance temperature, however, remains nontrivial in this limit, increasing the temperature from $T_{\mathrm{DB}}^{\mathrm{Lin}}$ by the factor γ (as $\gamma > 1$).

Third, we consider the limit $R \to 0$ with fixed v, $\overline{E}$ and β. From Section 3.2.5 and Section 3.2.8, we see that both $\mathcal{N}_v$ and $T_{\mathrm{DB}}/T_{\mathrm{DB}}^{\mathrm{Lin}}$ remain finite as $R \to 0$, despite the diverging acceleration. The limits depend on the remaining variables only through the dimensionless pair $(v, \overline{E}\beta)$, but in a complicated way:

$$\begin{aligned}
\lim_{R\to 0} \mathcal{N}_v(\overline{E}\beta, R/\beta) &= \frac{\big(\gamma - \mathrm{sgn}(\overline{E}) + 2n(|\overline{E}|\beta)\big)}{\big(4/\overline{E}^2\big)\mathcal{F}_{\mathrm{Lin}}(\overline{E},\beta)} - 1\,, \\
&= \begin{cases}
(\gamma-1)\overline{E}\beta + \mathcal{O}\big((\overline{E}\beta)^2\big) & \text{for } \overline{E}\beta \to 0^+\,, \\
-\dfrac{\gamma^3-1}{12}(\overline{E}\beta)^2 + \mathcal{O}\big((\overline{E}\beta)^3\big) & \text{for } \overline{E}\beta \to 0^-\,, \\
\dfrac{\gamma-1}{2}\sqrt{2\pi v\overline{E}\beta}\,\mathrm{e}^{\overline{E}\beta/(1+v)}\left(1 + \mathcal{O}\left(\dfrac{1}{\overline{E}\beta}\right)\right) & \text{for } \overline{E}\beta \to \infty\,, \\
-\dfrac{1}{2}\left(1 - \dfrac{1}{\gamma}\right) + \mathcal{O}\left(\dfrac{\mathrm{e}^{-|\overline{E}|\beta/(1+v)}}{\sqrt{|\overline{E}|\beta}}\right) & \text{for } \overline{E}\beta \to -\infty\,,
\end{cases}
\end{aligned} \tag{3.45a}$$

$$\begin{aligned}
\lim_{R\to 0} \frac{T_{\mathrm{DB}}}{T_{\mathrm{DB}}^{\mathrm{Lin}}} &= \frac{\ln\left(\dfrac{\mathcal{F}_{\mathrm{Lin}}(-|\overline{E}|,\beta)}{\mathcal{F}_{\mathrm{Lin}}(|\overline{E}|,\beta)}\right)}{\ln\left(\dfrac{\gamma+1+2n(|\overline{E}|\beta)}{\gamma-1+2n(|\overline{E}|\beta)}\right)}\,, \\
&= \begin{cases}
\gamma + \mathcal{O}(|\overline{E}|\beta) & \text{for } |\overline{E}|\beta \to 0\,, \\
\dfrac{|\overline{E}|\beta}{(1+v)\ln\left(\frac{\gamma+1}{\gamma-1}\right)} + \mathcal{O}\big(\ln(|\overline{E}|\beta)\big) & \text{for } |\overline{E}|\beta \to \infty\,,
\end{cases}
\end{aligned} \tag{3.45b}$$

where we have used the large and small $|\overline{E}|\beta$ results from Section 3.2.8. The limit of $\mathcal{N}_v$ as $R \to 0$ hence takes a wide range of values, from much less than unity to much larger than unity, depending on $\overline{E}\beta$. The limit of $T_{\mathrm{DB}}/T_{\mathrm{DB}}^{\mathrm{Lin}}$ as $R \to 0$ is, by contrast, larger than unity for both small and large $|\overline{E}|\beta$. In particular, for large $|\overline{E}|\beta$, the ratio is much larger than unity and for small $|\overline{E}|\beta$, the ratio agrees

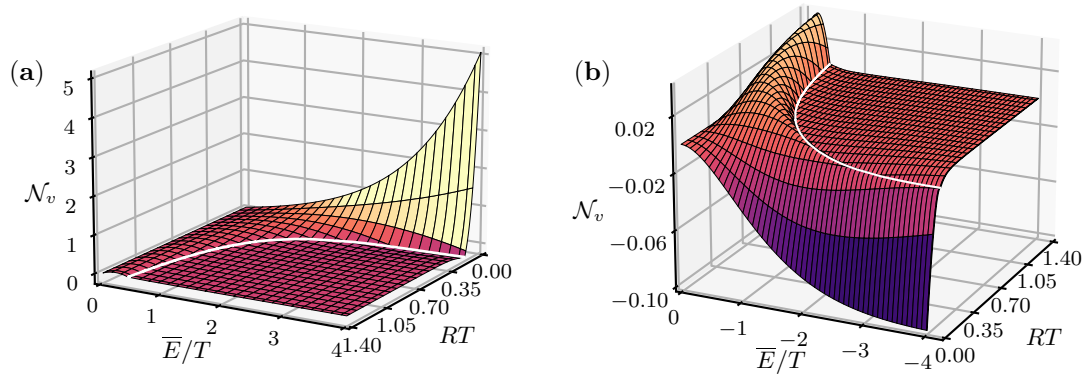

Figure 3.4: Relative excess transition rate $\mathcal{N}_v$ (3.43) due to acceleration as a function of the circular trajectory radius R and the excitation energy $\overline{E}$, at fixed $v = 0.6$. The ambient temperature $T = 1/\beta$ enters only in that it sets the scale of the horizontal axes. **(a)** Excitations, $\overline{E} > 0$. **(b)** De-excitations, $\overline{E} < 0$. White curve at $\overline{E}R = v$, demarcating the discontinuity of the first derivative, as in Figure 3.3. At $|\overline{E}|R \gg v$ we have $|\mathcal{N}_v| \ll 1$, but $\mathcal{N}_v$ starts to show nontrivial behaviour near $|\overline{E}|R \approx v$. The behaviour for $|\overline{E}|R \ll v$ is consistent with the asymptotic estimates (3.44a) and (3.45a). In particular, as $\overline{E}/T \to 0$, N_v decays to zero linearly, by (3.44a).

with (3.44b).

Finally, we consider the near-sonic or Machian limit, $v \to 1$, with fixed R, $|\overline{E}|$ and β. From Section 3.2.7 and Section 3.2.8, we find

$$\mathcal{N}_v(\overline{E}\beta, R/\beta) = \begin{cases} \dfrac{\sqrt{2\pi\overline{E}\beta}}{2\,\mathrm{Li}_{\frac{1}{2}}\left(\mathrm{e}^{-\frac{1}{2}\overline{E}\beta}\right)}\gamma + o(\gamma) & \text{for } \overline{E} > 0\,, \\ -\dfrac{1}{2} + \mathcal{O}\left(\dfrac{\ln\gamma}{\gamma}\right) & \text{for } \overline{E} < 0\,, \end{cases} \tag{3.46a}$$

$$\frac{T_{\mathrm{DB}}}{T_{\mathrm{DB}}^{\mathrm{Lin}}} = \frac{\pi\gamma}{8\sqrt{3}\,|\overline{E}|R}\left[1 + \mathcal{O}\left(\frac{1}{\ln\gamma}\right)\right], \tag{3.46b}$$

which shows a significant acceleration effect in $T_{\mathrm{DB}}/T_{\mathrm{DB}}^{\mathrm{Lin}}$, and in the excess excitation rate, but only a moderate suppression of the de-excitation rate.

3.4.3 Numerical results

We interpolate between the asymptotic regimes we have just analysed. We present numerical results for $v = 0.6$, plotting $\mathcal{N}_v$ and $T_{\mathrm{DB}}/T_{\mathrm{DB}}^{\mathrm{Lin}}$ as functions of the independent dimensionless variables $\overline{E}\beta$ and R/β.

In Figure 3.4, we plot the excess transition rate $\mathcal{N}_v$, both for excitation $\overline{E} > 0$ and for de-excitations $\overline{E} < 0$. In both cases, the plot indicates that $|\mathcal{N}_v| \ll 1$ for $|\overline{E}|R \gg v$ and hence a response dominated by its contribution due to the Doppler effect. However, near $|\overline{E}|R \approx v$, significant deviations appear and there are regions of positive $\mathcal{N}_v$ and regions of negative $\mathcal{N}_v$.

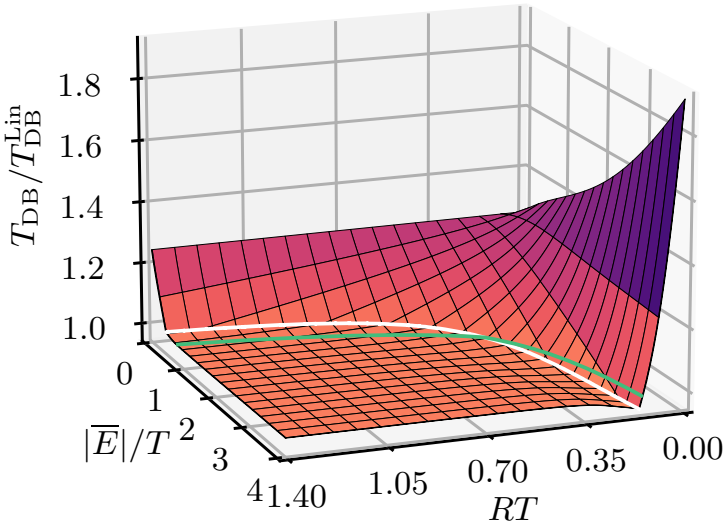

Figure 3.5: Ratio of the circular motion detailed balance temperature T_{DB} and the inertial motion detailed balance temperature $T_{\mathrm{DB}}^{\mathrm{Lin}}$, as a function of the circular trajectory radius R and the excitation energy $|\overline{E}|$, at fixed $v = 0.6$. The ambient temperature $T = 1/\beta$ again enters only in the scales of the horizontal axes. White curve at $|\overline{E}|R = v$, at the discontinuity of the first derivative. $T_{\mathrm{DB}}/T_{\mathrm{DB}}^{\mathrm{Lin}}$ is close to unity for $|\overline{E}|R \gg v$, but starts to deviate significantly from unity near $|\overline{E}|R \approx v$. Green curve at $T_{\mathrm{DB}}/T_{\mathrm{DB}}^{\mathrm{Lin}} = 1$. Behaviour in region $|\overline{E}|R \ll v$ is consistent with the asymptotic estimates (3.44b) and (3.45b); in particular, at $\overline{E}/T \to 0$, $T_{\mathrm{DB}}/T_{\mathrm{DB}}^{\mathrm{Lin}} \to \gamma = 5/4$, by (3.44b).

It is important to remark that, since the axes are scaled by the ambient temperature T, the behaviour near $|\overline{E}|R \approx v$ is independent of T, even when the temperature is so high that the thermality dominates the overall magnitude of the detector's response. In the region $|\overline{E}|R \ll v$, the behaviour in the plots is consistent with the asymptotic formulae given above.

In Figure 3.5, we plot the ratio of detailed balance temperatures $T_{\mathrm{DB}}/T_{\mathrm{DB}}^{\mathrm{Lin}}$, with the same parameter range as in Figure 3.4. For $|\overline{E}|R \gg v$, the ratio $T_{\mathrm{DB}}/T_{\mathrm{DB}}^{\mathrm{Lin}}$ is close to unity, as one would anticipate from Figure 3.4, but it starts to deviate significantly from unity near $|\overline{E}|R \approx v$, where in some regions $T_{\mathrm{DB}}/T_{\mathrm{DB}}^{\mathrm{Lin}} \gg 1$ but in some regions $T_{\mathrm{DB}}/T_{\mathrm{DB}}^{\mathrm{Lin}} < 1$. The behaviour at $|\overline{E}|R \ll v$ is consistent with the asymptotic formulae given above.

3.5 Summary

In this Chapter, we provided the framework for describing a Unruh-DeWitt (UDW) detector probing a scalar field initially prepared in a thermal state. We allowed for the field to have a modified dispersion relation (see (3.5)), which in a fundamental relativistic spacetime setting allows for dispersion relations that might arise from Planck-scale physics [118] and within an analogue system

allows one to probe dispersive effects beyond the phononic regime.

Quantifying the detector response by the detector response function $\mathcal{F}$ and detailed balance temperature T_{DB}, we found the behaviour of $\mathcal{F}$ and T_{DB} in various asymptotic regimes and interpolated numerically between them. We found regimes in which the detailed balance temperature is lower than the ambient temperature, indicating a cooling effect. By comparing the response and detailed balance temperature of a detector undergoing circular motion with those of a detector undergoing inertial motion, whose velocity matched the orbital velocity of the detector in circular motion, we isolated the effect of acceleration. The combination of numerical and analytic evidence indicated that the contribution in detector response due to acceleration is negligible for $|\overline{E}|R \gg v$, but nontrivial behaviour due to the acceleration occurs at $|\overline{E}|R \lesssim v$.

While the interplay between the various regimes is subtle, one general feature is that a cooling effect is more likely to occur when the ambient temperature is high, which becomes clear in light of the cooling inequality, (3.11) and (3.12).

We found that acceleration effects dominate over velocity effects at energy gaps smaller than the orbital angular velocity, even when the ambient temperature is so high that the overall magnitude of the detector's transition rate is dominated by the ambient temperature.

In the next Chapter, we apply this modelling to an analogue system with an inherent sample temperature, thin-film superfluid helium-4. We close this Chapter with a summary of its findings — an ambient temperature equips the circular motion Unruh effect with the characteristic of Robin Hood [119]: *Where there is little, the Unruh effect gives; and where there is plenty, the Unruh effect takes.*

Chapter 4

Interlude — Third sound detectors in accelerated motion

"As had been foreseen when the experiments were planned, their execution bordered on the impossible."

Heike K Onnes
Nobel Lecture (1913)

In Chapter 2, we introduced analogue spacetimes and the continuous quasiparticle detector model; in Chapter 3, we investigated ambient temperature effects in analogue $(2+1)$-dimensional Minkowski spacetime. We now consider a physical example of an analogue system in which the ambient temperature should be taken into account, thin-film superfluid helium-4. In this Chapter, we demonstrate that a laser sampling fluctuations in the height of a sample of thin-film superfluid helium-4 acts as a continuous quasiparticle detector and present a proposal to explore acceleration dependence in the response of the detector. The contents of this Chapter were extracted from, or based on, the journal article "Third sound detectors in accelerated motion" [2] in collaboration with Vitor S Barroso, Steffen Biermann, August Geelmuyden, Cisco Gooding, Grégoire Ithier, Xavier Rojas, Jorma Louko, and Silke Weinfurtner.

4.1 Superfluid helium-4

Superfluidity was first understood by Kapitsa (rus. Капица, rom. Capiṭa) in 1938, who remarked that, below 2.17 K, liquid helium exhibited an *abnormally low viscosity* [120]. At this temperature, known as the λ-point, liquid helium undergoes a second-order phase transition, becoming helium-II, or superfluid

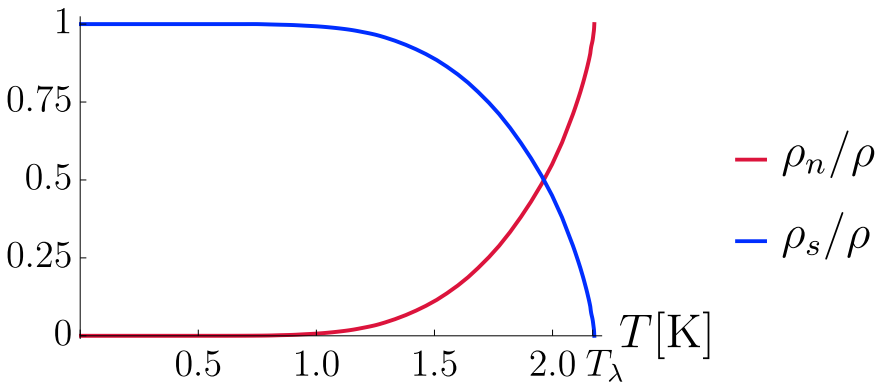

Figure 4.1: Normal component density ρ_n and superfluid component density ρ_s as ratios of the total density $\rho = \rho_s + \rho_n$, plotted as functions of sample temperature T. λ-point phase transition temperature denoted by $T_\lambda = 2.17$ K. Created with experimental data reported in [122].

helium. Landau (rus. Ландау) [121] described superfluid helium below the λ-point as a mixture of a *normal* component and a *superfluid* component, a model now known as Landau's two-fluid model.

In the two-fluid model, the normal component is characterised by its velocity field $\boldsymbol{v}_n$, pressure p_n, density ρ_n, and kinematic viscosity ν_n, whereas the superfluid component is described by only its velocity field $\boldsymbol{v}_s$, pressure p_s, and density ρ_s — the superfluid component has zero viscosity. The mass flux density is given by $\boldsymbol{j} = \rho_n \boldsymbol{v}_n + \rho_s \boldsymbol{v}_s$. In addition, the velocity field of the superfluid component is irrotational $\nabla \times \boldsymbol{v}_s = \boldsymbol{0}$ and may be written in terms of a velocity potential, $\boldsymbol{v}_s = \nabla \phi_s$. We note that the superfluid component is thus an inviscid, irrotational fluid, as described in Section 2.2.1.

The total density of the fluid is given by $\rho = \rho_n + \rho_s$ and varies little with the temperature below the λ-point; however, the individual components ρ_n and ρ_s vary greatly, as may be seen in Figure 4.1. At temperatures below 1 K, the superfluid component density comprises more than 99% of the total density, $\rho_s/\rho > 0.99$ [122, 123], with this ratio quickly tending to unity as the temperature decreases.

4.1.1 First and second sounds

Within the two-fluid model, the normal and superfluid components move independently. First, the two components can move in phase, $\boldsymbol{v}_n \approx \boldsymbol{v}_s$ [124]; the fluid in a given volume element oscillates as a whole, with the normal and superfluid components moving together. Linearising the equations of motion describing the two components, one finds oscillations in the pressure — sound waves — propagating at the speed

$$c_1 = \sqrt{\frac{\partial p}{\partial \rho}}, \tag{4.1}$$

referred to as the *first sound*.

On the other hand, one may consider when the two fluid components move with opposite phase, $\boldsymbol{v}_n \approx -\frac{\rho_s}{\rho_n}\boldsymbol{v}_s$, in which case the total mass flux density vanishes $\boldsymbol{j} \approx 0$. The normal and superfluid components move in opposition, such that the centre of mass in any given volume element remains at rest. In this case, the counterflowing normal and superfluid components enable the propagation of temperature oscillations. These oscillations in temperature propagate with a speed

$$c_2 = \sqrt{\frac{\rho_s}{\rho_n}\frac{Ts^2}{c_P}}, \tag{4.2}$$

where c_P is the specific heat capacity of helium-4, T is the temperature of the sample, and s is the entropy of the helium. In the two-fluid model, the entropy is carried entirely by the normal component; that is to say, $s_n = s$ and $s_s = 0$. The speed c_2 is referred to as the speed of *second sound*.

The second sound is a purely superfluid phenomenon: as the temperature of the sample approaches the λ-point, the density of the superfluid component tends to zero, $\rho_s \to 0$ as $T \to 2.17\ \mathrm{K}$, in which case, the second sound vanishes.

4.1.2 Third and fourth sounds

In addition to the first and second sounds, Atkins [125, 126] showed that there exists also the *third sound* and the *fourth sound*. Both the third and fourth sounds occur when the viscous normal component of the velocity field vanishes, $\boldsymbol{v}_n = \boldsymbol{0}$. In this case, the normal component of the fluid is viscously clamped to the substrate on which the sample lies, while the superfluid component is free to move [126, 127].

The fourth sound, present only in narrow channels, arises from oscillations in

the superfluid pressure and is given by

$$c_4 = \sqrt{\frac{\rho_s}{\rho} c_1}\,, \tag{4.3}$$

where c_1 is the first sound (4.1). Again, as this vanishes for $T > 2.17$ K, this phenomenon is only found in the superfluid phase.

The third sound, present only in thin films of superfluid helium, describes the speed at which surface waves propagate on the free surface of superfluid helium thin films, given by

$$c_3 = \sqrt{\frac{\rho_s}{\rho} g_{\text{eff}} h_0}\,, \tag{4.4}$$

where h_0 is the depth of the thin film and g_{eff} is the effective gravity experienced by the helium sample. Again, the ratio ρ_s/ρ informs us that this is a purely superfluid phenomenon.

We simplify the expression (4.4). First, we recall that at temperatures below 1 K, we have $\rho_s/\rho > 0.99$ with the ratio quickly tending to unity, leading to

$$c_3 = \sqrt{g_{\text{eff}} h_0}\,, \tag{4.5}$$

which is identically the propagation speed of waves in shallow water.

Second, the effect of gravity in thin films is negligible compared to the van der Waals contribution and the effective gravity is [128, 129]

$$g_{\text{eff}} = g_0 + 3\frac{\alpha_{\text{vdW}}}{h_0^4} \approx 3\frac{\alpha_{\text{vdW}}}{h_0^4}\,, \tag{4.6}$$

where g_0 is the acceleration due to gravity and α_{vdW} is the van der Waals interaction coefficient.

We can therefore write the surface-wave propagation speed as

$$c_3 = \sqrt{3\frac{\alpha_{\text{vdW}}}{h_0^3}}\,. \tag{4.7}$$

We remark that at temperatures above 1 K, the formula for the third sound speed (4.4) no longer applies and the temperature of the sample should be taken into consideration. This is explored in detail in [125].

4.2 Third sound on thin-film superfluid helium-4

In this Section, we demonstrate how waves propagating on the surface of thin films of superfluid helium-4 act as an analogue scalar field. We work under several assumptions. First, we assume a saturated thin film of helium-4, with equilibrium height $h_0 > 10$ nm, at which thickness third sound waves may form [125, 126] and the superfluid may be considered incompressible [130]. We assume a sample temperature below 500 mK, below which the normal component [122, 131] and evaporation and recondensation of the superfluid [125] are negligible. This assumption further implies that the saturated helium vapour pressure is approximately zero and the pressure gradient arising from the interaction between the thin film and helium vapour is negligible [132]. We work within the isothermal limit, in which we assume there is no heat transfer in the system from wave propagation and hence we will ignore temperature gradients. In the thin-film regime, the normal component does not contribute to the dynamics, as $\boldsymbol{v}_n = \boldsymbol{0}$; hence, we work only with the superfluid component and drop the subscript s, writing simply $\boldsymbol{v}$ and ρ. Finally, we work within the long-wavelength limit, assuming that the wavelength of any excitations on the superfluid interface satisfies $|\boldsymbol{k}|h_0 \ll 1$.

4.2.1 Thin-film superfluid helium-4

We consider a thin film of superfluid helium confined in inertial coordinates $(t, \boldsymbol{x}, z)$ between a hard surface at $z = 0$ and its free surface at $z = h(t, \boldsymbol{x})$. We assume a steady and uniform density ρ and align the z axis such that the effective gravity is given by $\boldsymbol{g} = -\nabla(g_{\text{eff}} z)$.

The substrate is considered hard, such that no fluid may flow through it. This is encompassed by the *no-penetration* boundary condition at $z = 0$,

$$\boldsymbol{v} \cdot \hat{\boldsymbol{z}}|_{z=0} \;=\; 0\,, \tag{4.8}$$

where $\hat{\boldsymbol{z}}$ is the unit vector parallel to the z-axis.

To construct the free surface, we impose that the fluid does not flow through the surface at $z = h$,

$$\frac{\mathrm{D}}{\mathrm{D}t}(z-h)\bigg|_{z=h} \;=\; 0\,, \tag{4.9a}$$

where we define the material derivative,

$$\frac{\mathrm{D}f}{\mathrm{D}t} \;\coloneqq\; \frac{\partial f}{\partial t} + \boldsymbol{v}\cdot\nabla f\,, \tag{4.9b}$$

for some function f. The boundary condition described by (4.9) is called the *kinematic condition*. Explicitly, the kinematic condition (4.9) is given by

$$v_z|_{z=h} = \frac{\partial h}{\partial t} + \boldsymbol{v}|_{z=h} \cdot \nabla h \,, \tag{4.10}$$

where $v_z \coloneqq \boldsymbol{v} \cdot \hat{\boldsymbol{z}}$.

We recall that the superfluid component of the velocity field is irrotational and may be written as the gradient of a velocity potential. As in [105], the dynamics of the superfluid can be linearised at the superfluid free surface for small perturbations both in the height $h(t, \boldsymbol{x}) = h_0 + \delta h(t, \boldsymbol{x})$ and in the velocity $\boldsymbol{v} = \nabla\varphi$, where h_0 is the equilibrium height of the thin film and we have assumed zero background flow such that $\nabla\varphi(t, \boldsymbol{x}, z)$ is the perturbation to the (vanishing) background $\boldsymbol{v}_0 = \boldsymbol{0}$.

The conservation of mass within the film-vapour system and equations of motion for the superfluid helium flow can be linearised for small perturbations in the film height [125, 126, 132],

$$\rho\frac{\partial \delta h}{\partial t} + \rho h_0 \nabla \cdot \boldsymbol{v}|_{z=h_0} + J_m^{\text{vap}} = 0 \,, \tag{4.11a}$$

$$\left.\frac{\partial \boldsymbol{v}}{\partial t}\right|_{z=h_0} + g_{\text{eff}}\nabla\delta h - \frac{\sigma}{\rho}\nabla\left(\nabla^2\delta h\right) + \frac{1}{\rho}\nabla p - s\nabla T = 0 \,, \tag{4.11b}$$

where $J_m^{\text{vap}} = \frac{\mathrm{d}m}{\mathrm{d}t}$ is the change in mass due to evaporation and recondensation, σ is the surface tension of liquid helium, s is the entropy of the fluid, and g_{eff} is the effective gravity, given for thin films by (4.6).

4.2.2 Surface wave dynamics on thin-film helium-4

In this Section, we demonstrate that the system of equations (4.11) reduces to a wave equation for the perturbations in the height δh. We began Section 4.2 with several assumptions, under which we have $J_m^{\text{vap}} \approx 0$, $\nabla p \approx 0$, and $\nabla T \approx 0$. We also note that the equations (4.11) are written in terms of the velocity field at the free surface $\boldsymbol{v}|_{z=h_0}$, hence, we define $\phi(t, \boldsymbol{x}) \coloneqq \varphi(t, \boldsymbol{x}, h_0)$ such that $\boldsymbol{v}|_{z=h_0} = \nabla\phi$. Then, the equations (4.11) then reduce to

$$\frac{\partial \delta h}{\partial t} = -h_0\nabla^2\phi \,, \tag{4.12a}$$

$$\frac{\partial \phi}{\partial t} = -g_{\text{eff}}\delta h + \frac{\sigma}{\rho}\nabla^2\delta h \,, \tag{4.12b}$$

where (4.12b) may be recognised as the linearised, time-dependent Bernoulli equation for the system.

We also linearise the kinematic condition (4.10), yielding

$$\frac{\partial \delta h}{\partial t} = \left.\frac{\partial \varphi}{\partial z}\right|_{z=h_0}, \tag{4.13}$$

where we have used $\boldsymbol{v} = \nabla\varphi$. In the long-wavelength regime, Equation 4.12a and the kinematic condition (4.13) are equivalent. We can see this as follows. It is shown in [105] that the velocity potential φ admits a decomposition into spatial eigenfunctions $\varphi = \sum_{\boldsymbol{k}} \chi_{\boldsymbol{k}}(\boldsymbol{x}) \cosh(|\boldsymbol{k}|z)$ such that $\chi_{\boldsymbol{k}}$ satisfies the Helmholtz equation $(\nabla^2 + |\boldsymbol{k}|^2)\chi_{\boldsymbol{k}} = 0$. By the long-wavelength assumption $|\boldsymbol{k}|h_0 \ll 1$, we have $\cosh(|\boldsymbol{k}|h_0) \approx 1$ and $\sinh(|\boldsymbol{k}|h_0) \approx |\boldsymbol{k}|h_0$. It then follows that

$$\left.\frac{\partial \varphi}{\partial z}\right|_{z=h_0} = -h_0 \nabla^2 \phi \,. \tag{4.14}$$

Comparing the right-hand sides of (4.12a) and (4.13), we see that (4.14) confirms their consistency.

We may rewrite the coupled system of equations as two independent equations for the motion of δh and ϕ separately. We find both δh and ϕ obey the same wave equation,

$$\frac{1}{h_0 g_{\text{eff}}} \frac{\partial^2 \delta h}{\partial t^2} = \nabla^2 \delta h - \frac{\sigma}{g_{\text{eff}} \rho} \nabla^2 (\nabla^2 \delta h) \,, \tag{4.15a}$$

$$\frac{1}{h_0 g_{\text{eff}}} \frac{\partial^2 \phi}{\partial t^2} = \nabla^2 \phi - \frac{\sigma}{g_{\text{eff}} \rho} \nabla^2 (\nabla^2 \phi) \,. \tag{4.15b}$$

The dispersion relation associated with (4.15a) is given by

$$\omega^2 = c_3^2 |\boldsymbol{k}|^2 \left(1 + \frac{\sigma}{g_{\text{eff}} \rho} |\boldsymbol{k}|^2\right) , \tag{4.16}$$

where we have identified the third sound speed c_3 (4.7).

For thin films, in which the effective gravity dominates over capillary (surface tension) effects, we have $\sigma|\boldsymbol{k}|^2 \ll g_{\text{eff}}\rho$, leading the linear, non-dispersive dispersion relation

$$\omega = c_3 |\boldsymbol{k}| \,, \tag{4.17}$$

corresponding to the Klein-Gordon (KG) equation,

$$\frac{1}{c_3^2} \frac{\partial^2 \delta h}{\partial t^2} = \nabla^2 \delta h \,. \tag{4.18}$$

We bring this Section to a close by matching the velocity potential ϕ, the analogue field, with a quantum field Φ.

The Lagrangian for the field ϕ is the KG Lagrangian

$$\mathcal{L} = \frac{1}{2}\rho h_0 \left[\left(\frac{1}{c_3}\frac{\partial \phi}{\partial t} \right)^2 - |\nabla \phi|^2 \right] . \tag{4.19}$$

The conjugate momentum π to the field ϕ is

$$\pi = \frac{\partial \mathcal{L}}{\partial(\partial_t \phi)} = \frac{\rho h_0}{c_3^2}\frac{\partial \phi}{\partial t} = -\rho \delta h \, , \tag{4.20}$$

where we have used that (4.12b) reduces to $\partial_t \phi = -g_{\text{eff}} \delta h$ under the current long-wavelength approximation and $c_3^2 = h_0 g_{\text{eff}}$.

By contrast, the Lagrangian for a quantum scalar field in an analogue spacetime setting is given by

$$\mathcal{L} = \frac{1}{2}\hbar^2 \left[\left(\frac{1}{c_{\text{eff}}}\frac{\partial \Phi}{\partial t} \right)^2 - |\nabla \Phi|^2 \right] , \tag{4.21}$$

where c_{eff} is the speed of sound in the analogue system.

Comparing the two Lagrangians (4.19) and (4.21), we can connect the hydrodynamical field ϕ of this Chapter, with the analogue quantum field Φ found in Chapter 2 and Chapter 3,

$$\phi(t, \boldsymbol{x}) = \sqrt{\frac{\hbar^2 g_{\text{eff}}}{\rho c_3^2}}\, \Phi(t, \boldsymbol{x}) \, , \tag{4.22}$$

where we have identified $c_{\text{eff}} = c_3$.

In an analogue spacetime, such as thin-film superfluid helium in a laboratory, one may directly measure the system. Methods such as multiplex digital holography [133] allow for the temporal and spatial resolution of the fluid surface. In the long-wavelength approximation, we see (4.12b) reduces to $\delta h = -g_{\text{eff}} \partial_t \phi$. As such, a time and space-resolved measurement of δh allows one to find ϕ.

4.2.3 Effective field theory description

In the long-wavelength regime, in which capillary effects may be neglected, we may equivalently describe the system (4.12) as an effective field theory with Hamiltonian density

$$\mathcal{H} = \frac{1}{2}\rho \left[h_0 (\nabla \phi)^2 + g_{\text{eff}} (\delta h)^2 \right] , \tag{4.23}$$

where the first and second terms correspond to the kinetic and potential energy densities at the surface respectively.

Varying the Hamiltonian (4.23) with respect to the fields $(-\rho\delta h)$ and ϕ, Hamilton's equations of motion give

$$\rho\frac{\partial\delta h}{\partial t} = \frac{\delta\mathcal{H}}{\delta\phi}, \qquad \Longleftrightarrow \qquad \rho\frac{\partial\delta h}{\partial t} = -\rho h_0\nabla^2\phi, \tag{4.24a}$$

$$\frac{\partial\phi}{\partial t} = -\frac{1}{\rho}\frac{\delta\mathcal{H}}{\delta(\delta h)}, \qquad \Longleftrightarrow \qquad \frac{\partial\phi}{\partial t} = -g_{\text{eff}}\delta h, \tag{4.24b}$$

which one may recognise as the equations of motion (4.12) in the long-wavelength limit.

Within the current assumptions, the height fluctuations δh behave as quantised quasiparticles (phonons), which have been well characterised [134, 135] and experimentally exploited [136]. Before finding the canonical commutation relations, we find first the leading order relation between density perturbations and height perturbations in a fluid.

We consider a fluid of constant density ρ confined between $z = 0$ and $z = h_0$. By conservation of mass, we have

$$\int_0^{h_0}\mathrm{d}z\,\rho = \frac{M}{A}, \tag{4.25}$$

where M/A is a constant with units of mass per unit area. In the present case of a fluid with constant density, the integral may be evaluated as $M/A = \rho h_0$.

If we perturb the height of the fluid, the conservation of mass requires that the density must react. In particular, we have

$$\frac{M}{A} = \int_0^{h_0+\delta h}\mathrm{d}z\,(\rho+\delta\rho) = \rho h_0 + \rho\delta h_0 + \int_0^{h_0}\mathrm{d}z\,\delta\rho + \mathcal{O}(\delta h\delta\rho). \tag{4.26}$$

Identifying $M/A = \rho h_0$, Equation 4.26 to leading order informs

$$\rho\delta h = -\int_0^{h_0}\mathrm{d}z\,\delta\rho. \tag{4.27}$$

Upon quantisation, we find the canonical commutation relations between $\hat{\phi}$ and $\delta\hat{h}$. We begin with Landau's two-fluid model [121], in which paper Landau writes the canonical commutation relation

$$[\hat{\rho}(t,\boldsymbol{r}_1),\hat{\varphi}(t,\boldsymbol{r}_2)] = \mathrm{i}\hbar\delta^{(3)}(\boldsymbol{r}_1-\boldsymbol{r}_2). \tag{4.28}$$

We evaluate $\boldsymbol{r}_2$ at $z = h_0$ and integrate the left-hand side of commutation

relation (4.28) over the bulk of the helium sample with respect to $\boldsymbol{r}_1$,

$$\int_0^{h_0} \mathrm{d}z\, [\rho + \delta\hat{\rho}(t, \boldsymbol{x}_1, z), \hat{\varphi}(t, \boldsymbol{x}_2, h_0)] \;=\; \int_0^{h_0} \mathrm{d}z \left[\delta\hat{\rho}(t, \boldsymbol{x}_1, z), \hat{\phi}(t, \boldsymbol{x}_2)\right] , \\ = \; -\left[\rho\delta\hat{h}(t, \boldsymbol{x}_1), \hat{\phi}(t, \boldsymbol{x}_2)\right] , \tag{4.29}$$

where we have written $\varphi|_{z=h_0} = \phi$ and, in the second equality, we used the relation (4.27). Integrating the right-hand side of (4.28) and combining with (4.29), we arrive at the commutation relation between height perturbations and the velocity potential,

$$\left[\hat{\phi}(t, \boldsymbol{x}_1), \rho\delta\hat{h}(t, \boldsymbol{x}_2)\right] \;=\; -\mathrm{i}\hbar\delta^{(2)}(\boldsymbol{x}_1 - \boldsymbol{x}_2)\,. \tag{4.30}$$

Writing $\hat{\pi}(t, \boldsymbol{x}_2) = -\rho\delta\hat{h}(t, \boldsymbol{x}_2)$, we see that this is equivalent to the canonical commutation relation $[\hat{\phi}(t, \boldsymbol{x}_1), \hat{\pi}(t, \boldsymbol{x}_2)] = \mathrm{i}\hbar\delta^{(2)}(\boldsymbol{x}_1 - \boldsymbol{x}_2)$.

4.3 Lasers as local detectors of interface fluctuations

In Section 2.2.3, we saw how a $(1+1)$-dimensional scalar field $\hat{\psi}$ interacting with a $(2+1)$-dimensional scalar field $\hat{\phi}$ acts as a continuous quasiparticle detector of excitations in the field $\hat{\phi}$. In this Section, we demonstrate that a laser field acts as a local detector of third sound excitations in thin-film superfluid helium-4.

4.3.1 Free laser field

The electromagnetic Lagrangian is given by

$$\mathcal{L}_{\mathrm{em}} \;=\; -\frac{1}{\mu_0} F^{\mu\nu} F_{\mu\nu}\,, \tag{4.31}$$

where μ_0 is the vacuum permeability, $F_{\mu\nu} = \partial_\mu A_\nu - \partial_\nu A_\mu$ is the Faraday tensor, and $A_\mu = (A_t, \boldsymbol{A})$ is the electromagnetic four-potential. Working in the Coulomb gauge ($A_t = 0$ and $\nabla \cdot \boldsymbol{A} = 0$) with a fixed polarisation ($\boldsymbol{A} = A(t, z)\hat{\boldsymbol{e}}$ with $\hat{\boldsymbol{z}} \cdot \hat{\boldsymbol{e}} = 0$), the electromagnetic Lagrangian (4.31) becomes

$$\mathcal{L}_{\mathrm{em}} \;=\; \frac{1}{2\mu_0}\left[\left(\frac{1}{c}\frac{\partial A(t,z)}{\partial t}\right)^2 - \left(\frac{\partial A(t,z)}{\partial z}\right)^2\right] , \tag{4.32}$$

where c is the speed of light.

We assume a perturbed Ansatz for the laser field,

$$A(t,z) \;=\; A_0 \cos(\omega_{\mathrm{L}} t - k_{\mathrm{L}} z + \psi(t,z)) \;, \tag{4.33}$$

where ω_{L} is the optical frequency of the laser, k_{L} is the wavenumber, A_0 is the amplitude, and $\psi(t,z)$ is a perturbation in the laser phase, which will act as the effective $(1+1)$-dimensional probing field.

The amplitude can be considered constant, even during the interaction with the superfluid helium described in Section 4.3.2, under the assumption that perturbations on the interface of the superfluid helium have small gradients $\nabla\delta h$ such that the beam is not deflected as it passes through the sample [137].

We substitute the Ansatz (4.33) into the free electromagnetic Lagrangian $\mathcal{L}_{\mathrm{em}}$ (4.31). We simplify this by averaging over fast oscillations as ω_{L} is large, yielding [70]

$$\mathcal{L}_{\mathrm{em}} \;=\; \frac{A_0^2}{4\mu_0}\left[\left(\frac{1}{c}\frac{\partial\psi(t,z)}{\partial t}\right)^2 - \left(\frac{\partial\psi(t,z)}{\partial z}\right)^2\right] , \tag{4.34a}$$

$$S_{\mathrm{em}} \;=\; \int \mathrm{d}t\mathrm{d}\boldsymbol{x}\mathrm{d}z\, \mathcal{L}_{\mathrm{em}} \,. \tag{4.34b}$$

4.3.2 Light-matter interaction

We consider now the light-matter interaction between the laser and the sample of thin-film superfluid helium. Physically, we transmit a focused laser beam on a trajectory through the sample, which lies on a transparent substrate.

The interaction between light and matter is described by [138]

$$\mathcal{L}_{\mathrm{int}} \;=\; \frac{1}{2}\boldsymbol{P}\cdot\boldsymbol{E} \;=\; \left(\frac{\varepsilon-\varepsilon_0}{2}\right)|\boldsymbol{E}|^2 \,, \tag{4.35}$$

where $\boldsymbol{P}$ is the polarisation in a medium, ε_0 is the vacuum permittivity, and ε is the permittivity of the medium.

Superfluid helium may be considered optomechanically as a dilute gas [137, 138] such that we have $\varepsilon \approx \varepsilon_0 + \rho_N\alpha$, where $\rho_N = \frac{\rho}{m_4}$ is the number density of helium-4, m_4 is the mass of helium-4, and α is the polarisability. As such, we rewrite the interaction Lagrangian as

$$\mathcal{L}_{\mathrm{int}} \;=\; \frac{\alpha\rho_N}{2}\left(\frac{\partial A(t,z)}{\partial t}\right)^2 . \tag{4.36}$$

Using the Ansatz (4.33) and fast-oscillation averaging, the interaction Lagrangian

is written as

$$\mathcal{L}_{\text{int}} = \mathcal{L}^{(1)}_{\text{int}} + \mathcal{L}^{(2)}_{\text{int}}\,, \tag{4.37a}$$

$$\mathcal{L}^{(1)}_{\text{int}} = \frac{1}{2}\alpha\rho_N A_0^2\omega_{\text{L}}\frac{\partial\psi(t,z)}{\partial t}\,, \tag{4.37b}$$

$$\mathcal{L}^{(2)}_{\text{int}} = \frac{1}{4}\alpha\rho_N A_0^2\left(\frac{\partial\psi(t,z)}{\partial t}\right)^2\,, \tag{4.37c}$$

where we have dropped the constant term $\frac{1}{4}\alpha\rho_N A_0^2\omega_{\text{L}}^2$ which does not contribute to the equations of motion.

The quadratic term $\mathcal{L}^{(2)}_{\text{int}}$ in (4.37) may be combined with the free electromagnetic Lagrangian $\mathcal{L}_{\text{em}}$ (4.31) to describe an effective speed of light in the medium,

$$\begin{aligned}\mathcal{L}_{\text{em}} + \mathcal{L}^{(2)}_{\text{int}} &= \frac{A_0^2}{4\mu_0}\left[\frac{1}{c^2}\left(1+\frac{\alpha\rho_N}{\varepsilon_0}\right)\left(\frac{\partial\psi(t,z)}{\partial t}\right)^2 - \left(\frac{\partial\psi(t,z)}{\partial z}\right)^2\right]\,,\\ &= \frac{A_0^2}{4\mu_0}\left[\left(\frac{1}{c_{\text{eff}}}\frac{\partial\psi(t,z)}{\partial t}\right)^2 - \left(\frac{\partial\psi(t,z)}{\partial z}\right)^2\right]\,,\end{aligned} \tag{4.38}$$

where we have used $c^2 = (\mu_0\varepsilon_0)^{-1}$ and introduced the speed of light in the medium $c^2_{\text{eff}} := c^2(1+\alpha\rho_N/\varepsilon_0)^{-1}$, which defines the index of refraction

$$n = \frac{c}{c_{\text{eff}}} = \sqrt{1+\frac{\alpha\rho_N}{\varepsilon_0}}\,. \tag{4.39}$$

We can see now that the interaction between the laser and the superfluid helium must arise from $\mathcal{L}^{(1)}_{\text{int}}$ in (4.37). The associated action is

$$S_{\text{int}} = \int \mathrm{d}t\mathrm{d}\boldsymbol{x}\int_0^{h(t,\boldsymbol{x})}\mathrm{d}z\,\mathcal{L}^{(1)}_{\text{int}} = \frac{1}{2}\alpha\rho_N A_0^2\omega_{\text{L}}\int\mathrm{d}t\mathrm{d}\boldsymbol{x}\int_0^{h(t,\boldsymbol{x})}\mathrm{d}z\,\frac{\partial\psi(t,z)}{\partial t}\,. \tag{4.40}$$

We appeal to the Leibniz integral rule to evaluate the integral over z,

$$\int_0^{h(t,\boldsymbol{x})}\mathrm{d}z\,\frac{\partial\psi(t,z)}{\partial t} = \frac{\mathrm{d}}{\mathrm{d}t}\int_0^{h(t,\boldsymbol{x})}\mathrm{d}z\,\psi(t,z) - \psi(t,h(t,\boldsymbol{x}))\frac{\partial h(t,\boldsymbol{x})}{\partial t}\,. \tag{4.41}$$

We substitute (4.41) into the action (4.40) and note that the total derivative in time will vanish as a boundary term, resulting in

$$\begin{aligned}S_{\text{int}} &= -\frac{1}{2}\alpha\rho_N A_0^2\omega_{\text{L}}\int\mathrm{d}t\mathrm{d}\boldsymbol{x}\,\frac{\partial h(t,\boldsymbol{x})}{\partial t}\psi(t,h(t,\boldsymbol{x}))\,,\\ &= -\frac{1}{2}\alpha\rho_N A_0^2\omega_{\text{L}}\int\mathrm{d}t\mathrm{d}\boldsymbol{x}\mathrm{d}z\,\frac{\partial h(t,\boldsymbol{x})}{\partial t}\psi(t,z)\delta(z-h(t,\boldsymbol{x}))\,.\end{aligned} \tag{4.42}$$

We consider perturbations in the height of the form $h(t,\boldsymbol{x}) = h_0 + \delta h(t,\boldsymbol{x})$, for

which the action (4.42) reduces to

$$S_{\text{int}} \;=\; -\frac{1}{2}\alpha\rho_N A_0^2\omega_{\text{L}}\int \mathrm{d}t\mathrm{d}\boldsymbol{x}\mathrm{d}z\,\frac{\partial\delta h(t,\boldsymbol{x})}{\partial t}\psi(t,z)\delta(z-h_0)\,. \tag{4.43}$$

Furthermore, the interaction spot is localised to a trajectory $\boldsymbol{x} = \boldsymbol{X}(t)$. We account for this by including a delta function in the action (4.42), resulting in

$$S_{\text{int}} \;=\; -\frac{1}{2}\alpha\rho_N A_0^2\omega_{\text{L}}\int \mathrm{d}t\mathrm{d}\boldsymbol{x}\mathrm{d}z\,\frac{\partial\delta h(t,\boldsymbol{x})}{\partial t}\psi(t,z)\delta(z-h_0)\delta^{(2)}(\boldsymbol{x}-\boldsymbol{X}(t))\,. \tag{4.44}$$

We vary the total action $S_{\text{em}} + S_{\text{int}}$ ((4.34) and (4.44)) with respect to the laser phase ψ to find the equation of motion

$$-\frac{1}{c_{\text{eff}}^2}\frac{\partial^2\psi(t,z)}{\partial t^2} + \frac{\partial^2\psi(t,z)}{\partial z^2} \;=\; \alpha\rho_N\omega_{\text{L}}\mu_0\frac{\partial\delta h(t,\boldsymbol{X}(t))}{\partial t}\delta(z-h_0)\,. \tag{4.45}$$

We denote the homogeneous solution of (4.45) by $\psi_0(t,z)$, whereas the inhomogeneous part can be solved using the causal Green's function for the operator $-c_{\text{eff}}^{-2}\partial_t^2 + \partial_z^2$ on an infinite domain, which is $G(t,z) = \frac{c_{\text{eff}}}{2}\Theta(t-|z|/c_{\text{eff}})$, where $\Theta(x)$ is the Heaviside function. This results in the solution

$$\psi(t,z) \;=\; \psi_0(t,z) - \frac{(n^2-1)k_{\text{L}}}{2n}\delta h(\tau,\boldsymbol{X}(\tau))\,, \tag{4.46}$$

where $k_{\text{L}} = \omega_{\text{L}}/c$ and $\tau = t-|z-h_0|/c_{\text{eff}}$, and we have written $\alpha\rho_N\mu_0 = (n^2-1)/c^2$ using (4.39). The fluctuations in the laser phase (4.46) attributable to height fluctuations read

$$\psi_{\delta h}(t,z) \;\coloneqq\; \frac{1}{2n}(n^2-1)k_{\text{L}}\delta h(\tau,\boldsymbol{X}(\tau))\,. \tag{4.47}$$

In Section 4.2, we saw that height fluctuations δh in superfluid helium-4 act as an effective $(2+1)$-dimensional scalar field. In Section 4.3.1, we introduced the dynamics of a free laser. In this Section, we considered the interaction between a laser and thin-film superfluid helium-4. We see now in (4.46) that the $(1+1)$-dimensional probing field ψ samples fluctuations in the sample height δh along the interaction trajectory $\boldsymbol{X}$.

In light of Section 2.2.3, we rewrite the interaction action (4.43), using integration by parts, as

$$S_{\text{int}} \;=\; \frac{1}{2}\alpha\rho_N A_0^2\omega_{\text{L}}\int \mathrm{d}t\mathrm{d}\boldsymbol{x}\mathrm{d}z\,\delta h(t,\boldsymbol{x})\frac{\partial\psi(t,z)}{\partial t}\delta(z-h_0)\,. \tag{4.48}$$

Upon quantisation, we read from (4.48) the effective interaction Hamiltonian

between the laser field ψ and the height fluctuations δh on the trajectory $\boldsymbol{X}(t)$,

$$\hat{H}_{\text{int}} \;=\; -\frac{1}{2}\alpha\rho_N A_0^2\omega_{\text{L}}\delta\hat{h}(t,\boldsymbol{X}(t))\otimes\frac{\partial\hat{\psi}(t,h_0)}{\partial t}\,. \tag{4.49}$$

By comparison with the continuous quasiparticle detector interaction Hamiltonian (2.84) in Section 2.2.3, one sees that the interaction Hamiltonian (4.49) also describes a field $\hat{\psi}$ acting as a continuous Unruh-DeWitt (UDW) detector for excitations in the height field $\delta\hat{h}$. Furthermore, this establishes the theoretical foundation for realising a UDW detector in a laboratory.

4.3.3 Analogue response function

In (4.22), we found a map between hydrodynamical and quantum fields. Furthermore, the Hamiltonian (4.49) demonstrates that a laser acts as a continuous quasiparticle detector of height fluctuations in thin-film superfluid helium-4. We now combine these observations with the thermal field theory modelling of Chapter 3 to encompass the non-negligible sample temperature of superfluid helium-4. We take the interaction trajectory to be uniform circular motion,

$$\boldsymbol{X}(t) \;=\; (R\cos(\Omega t), R\sin(\Omega t))\;, \tag{4.50}$$

where R is the orbital radius and $\Omega = \frac{\mathrm{d}\theta}{\mathrm{d}t}$ is the angular speed. We use the notation $\delta\hat{h}(t) \coloneqq \delta\hat{h}(t,\boldsymbol{X}(t))$ for height fluctuations, $\hat{\phi}(t) \coloneqq \hat{\phi}(t,\boldsymbol{X}(t))$ for the velocity potential, and $\hat{\Phi}(t) \coloneqq \hat{\Phi}(t,\boldsymbol{X}(t))$ for the scalar quantum field.

We consider the interaction between surface modes on superfluid helium-4 and the laser as described by the interaction Hamiltonian (4.49). The sample temperature provides a notion of thermality such that we assume that the height fluctuations $\delta\hat{h}$ to be in a thermal state in inverse temperature β and that the phase field $\hat{\psi}$ is in a coherent phase state [137].

Working to first order in perturbation theory as in Section 2.2.3 using the interaction Hamiltonian (4.49), one arrives at the response function

$$\begin{aligned}
\mathcal{F}_{\delta h}(\omega,\beta) \;&=\; \int \mathrm{d}s\,\mathrm{e}^{-\mathrm{i}\omega s}\,\langle\delta\hat{h}(s)\delta\hat{h}(0)\rangle_\beta\;, && \text{(4.51a)}\\
&=\; \frac{1}{g_{\text{eff}}^2}\int \mathrm{d}s\,\mathrm{e}^{-\mathrm{i}\omega s}\,\langle\tfrac{\mathrm{d}}{\mathrm{d}s'}\hat{\phi}(s')\Big|_{s'=s}\tfrac{\mathrm{d}}{\mathrm{d}s''}\hat{\phi}(s'')\Big|_{s''=0}\rangle_\beta\;, && \text{(4.51b)}\\
&=\; \frac{\hbar^2}{\rho g_{\text{eff}}c_3^2}\int \mathrm{d}s\,\mathrm{e}^{-\mathrm{i}\omega s}\,\langle\tfrac{\mathrm{d}}{\mathrm{d}s'}\hat{\Phi}(s')\Big|_{s'=s}\tfrac{\mathrm{d}}{\mathrm{d}s''}\hat{\Phi}(s'')\Big|_{s''=0}\rangle_\beta\;, && \text{(4.51c)}\\
&=\; \frac{\hbar^2}{\rho g_{\text{eff}}c_3^2}\mathcal{F}(\omega,\beta)\,, && \text{(4.51d)}
\end{aligned}$$

where we have used (4.24b) and (4.22) in the second and third equalities respectively and, in the fourth equality, we have identified the derivative-coupled response function $\mathcal{F}$ (3.4) for a detector probing a quantum scalar field prepared in a thermal state in inverse temperature β.

The interaction trajectory, uniform circular motion, is described by two free parameters, usually the orbital radius R and the angular speed Ω; however, using $v = \Omega R$ and $a = v^2 R^{-1}$, one can equally parameterise the orbit using the velocity v and acceleration a. Using (3.7), the response function $\mathcal{F}$ reads

$$\begin{aligned}\mathcal{F}(\omega,\beta) \;=\; & \frac{\omega^2}{2\hbar c_3^2}\sum_{m>\omega v/a} J^2_{|m|}\left(\frac{mv}{c_3}-\frac{\omega v^2}{ac_3}\right) \\ & + \frac{\omega^2}{2\hbar c_3^2}\sum_{m>\omega v/a}\frac{1}{\mathrm{e}^{\hbar(ma/v+\omega)/(k_{\mathrm{B}}T)}-1}J^2_{|m|}\left(\frac{mv}{c_3}-\frac{\omega v^2}{ac_3}\right) \\ & + \frac{\omega^2}{2\hbar c_3^2}\sum_{m>-\omega v/a}\frac{1}{\mathrm{e}^{\hbar(ma/v-\omega)/(k_{\mathrm{B}}T)}-1}J^2_{|m|}\left(\frac{mv}{c_3}+\frac{\omega v^2}{ac_3}\right) . \end{aligned} \tag{4.52}$$

As discussed in Section 3.4, the circular motion response function (4.52) encodes two distinct motion effects. The first is due to the detector's acceleration and the second is a Doppler effect, due to the detector's speed v with respect to the thermal bath. We again compare the response function $\mathcal{F}$ with the response of a detector undergoing linear motion with the same speed v, in which case only a Doppler effect is present. Restoring dimensionful units to (3.14), we have

$$\mathcal{F}_{\mathrm{Lin}}(\omega,\beta) \;=\; \frac{1}{2}\frac{\omega^2}{\hbar c_3^2}\gamma_s\Theta\left(-\frac{\omega}{c_3}\right)+\frac{\omega^2\gamma_s}{2\pi\hbar c_3^2}\int_{-\pi/2}^{\pi/2}\frac{\mathrm{d}\theta}{\mathrm{e}^{\gamma_s^2(1+\frac{v}{c_3}\sin\theta)\hbar|\omega|/(k_{\mathrm{B}}T)}-1}, \tag{4.53}$$

where $\gamma_s = (1 - v^2/c_3^2)^{-1/2}$ is the Lorentz gamma factor.

In the classical limit, $\gamma_s^2\hbar|\omega| \ll k_{\mathrm{B}}T$, the linear motion response function (4.53) reduces to (3.40a),

$$\mathcal{F}_{\mathrm{Lin}}(\omega,\beta) \;=\; \frac{1}{2}\frac{\omega^2}{\hbar c_3^2}\gamma_s\Theta\left(-\frac{\omega}{c_3}\right)+\frac{|\omega|k_{\mathrm{B}}T}{2\hbar^2c_3^2}, \tag{4.54}$$

For excitations ($\omega > 0$), only the second term in (4.54) remains, which describes the expectation value of a fluctuating hydrodynamic interface in terms of fluctuation-dissipation relation at temperature T in the long wavelength limit [137, 139, 140]. This term is linear in the energy gap $|\omega|$ and independent of the linear velocity v.

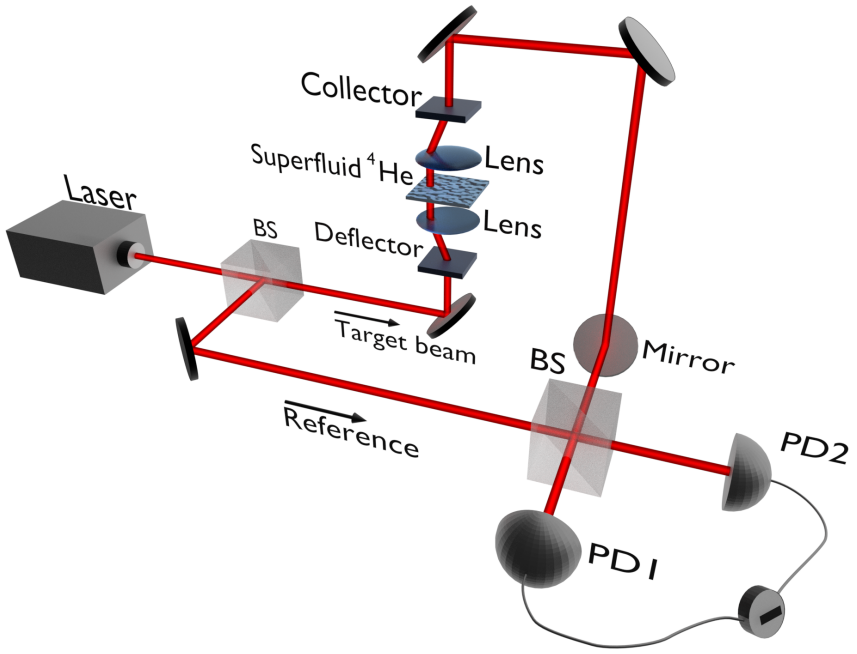

Figure 4.2: A beam splitter (BS) separates the input laser into two arms, namely a target and a reference. The target beam is focused on the sample plane to a spot, with width much smaller than the long-wavelength surface perturbations. A deflector-lens configuration moves the target beam on a circular trajectory through the superfluid helium sample with optical axis perpendicular to the fluid surface. After the sample, a lens-collector combination, followed by a series of mirrors, brings the beam back to a static path and lead it to a second beam splitter (BS), where the target and reference arms are combined. The resulting beams are detected at two photodiodes (PD1) and (PD2).

4.4 Experimental proposal

We consider now an experimental proposal for probing observer-dependence in detector response. A schematic of the experimental setup is presented in Figure 4.2. The helium sample in the schematic must be prepared within a cryostat capable of reaching temperatures below $1\ \mathrm{K}$ and, with the cryostat, a substrate is coated with a thin film of superfluid helium-4. We consider a typical saturated film thickness of $h_0 = 100\ \mathrm{nm}$, which is currently within experimental reach [135, 141]. A deflector-lens configuration moves the target beam on a circular trajectory. As such, the cryostat must have optical access, such that the laser beam may pass through the thin film of superfluid helium.

We present in Table 4.1 typical physical parameters of superfluid helium at temperature $T = 500\ \mathrm{mK}$, below which temperature the parameters vary little [122]. The third sound sound (4.5) is then given by $c_3 \approx 8.8 \times 10^{-2}\ \mathrm{m\ s^{-1}}$. To maintain the analogy with a scalar quantum field with linear dispersion relation, we operate within the long-wavelength, non dispersive regime $\omega \ll c_3\sqrt{\rho g_{\mathrm{eff}}/\sigma} \approx (2\pi)2.4\ \mathrm{kHz}$ using Table 4.1.

In this Section, we consider a detector in the near-sonic limit with speed $v = 0.95c_3$, with rotational frequencies of the order of hundreds of Hertz. To achieve this, we consider a range of trajectory radii $R = 20 - 100\ \mu\text{m}$. We assume that the profile of the laser can be focused to a spot of radius $10\ \mu\text{m}$. We assume a laser power $P = 0.5\ \text{mW}$, low enough to prevent the evaporation of the superfluid helium-4, with a wavelength in the near-infrared $\lambda_{\text{L}} = 700\ \text{nm}$. We operate with typical probing frequencies $100\ \text{Hz} - 1\ \text{kHz}$ and a sample temperature between $1\ \mu\text{K} - 1\ \text{K}$. With these operating conditions, we satisfy our modelling assumptions in Section 4.2.

4.4.1 Isolation of observer-dependence

After interacting with the superfluid helium-4, the laser beam is reflected by a series of mirrors and passes through a beam splitter, in which the laser beam is combined with a reference laser beam. Finally, the two beams are detected by two photodiodes by a suitable detection scheme, such as phase-referenced homodyne photodetection described in [137, 142]. From such a process, the autocorrelation, or the two-point, function of the phase field ψ can be extracted $\langle \psi(t), \psi(0) \rangle$. Even if all measurement noise is suppressed, there is still noise in the laser phase from quantum fluctuations, known as shot-noise [142]. As such, taking the Fourier transform of the autocorrelation function, we find the response function, which may be identified with the Power Spectral Density (PSD),

$$S_\psi(\omega) \;=\; \int \mathrm{d}s\, \mathrm{e}^{-\mathrm{i}\omega s}\, \langle \hat{\psi}_{\delta h}(t, h_0) \hat{\psi}_{\delta h}(0, h_0) \rangle + \sigma^2_{\text{sn}}\,, \tag{4.55}$$

where $\hat{\psi}_{\delta h}$ is the fluctuation in the laser phase attributable to fluctuations in the height, given by (4.47), and $\sigma^2_{\text{sn}} = \hbar\omega_{\text{L}}/P$ is the contribution due to shot-noise.

Combining (4.47), (4.51), and (4.55), we relate the PSD S_ψ (4.55) to the response function $\mathcal{F}$ (3.7),

$$S_\psi(\omega) \;=\; \kappa \mathcal{F}(\omega, \beta) + \sigma^2_{\text{sn}}\,, \tag{4.56a}$$

$$\kappa \;=\; \frac{(n^2-1)^2 \hbar^2 k_{\text{L}}^2}{4n^2 \rho g_{\text{eff}} c_3^2}\,. \tag{4.56b}$$

For the parameters stated, we have $\kappa \approx 6.3 \times 10^{-64} \text{kg m}^2\ \text{s}^2$. We can see that the signal in the laser encodes the same information as the response function of a UDW detector probing a scalar field prepared in a thermal state in $2+1$ Minkowski spacetime and will hence also exhibit trajectory-dependence, in particular acceleration-dependence.

As discussed in Section 3.4, we may isolate and identify acceleration-dependence

Table 4.1: Experimental parameters for helium-4. The van der Waals constant is given for a quartz substrate [141]; for other materials, α_{vdW} would be of the same order of magnitude.

Parameter	**Value**
Film height, h_0	$100\ \mathrm{nm}$
Mass density, ρ	$145\ \mathrm{kg\,m^{-3}}$
Surface tension, σ	$37.9 \times 10^{-5}\ \mathrm{J\,m^{-2}}$
Van der Waals const., α_{vdW}	$2.6 \times 10^{-24}\ \mathrm{m^5 s^{-2}}$
Index of refraction, n	1.025

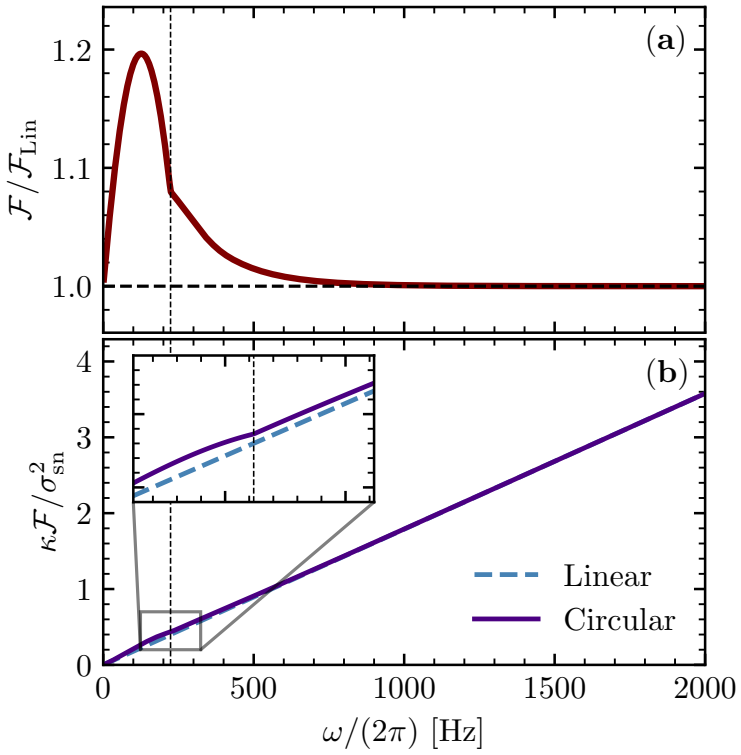

Figure 4.3: (a) Ratio of circular motion response function (4.52) to linear motion response function (4.54). **(b)** Ratio of response to shot-noise for both circular motion and linear motion. Inset shows ratio for low frequencies, at which frequencies the two responses disagree. Vertical dashed line at the angular frequency $\Omega/(2\pi)$. All plots are at temperature $T = 10\,\mathrm{mK}$ with orbital radius $R = 60\ \mu\mathrm{m}$.

in the detector response by taking the difference between the circular motion and linear motion response functions. As such, we define the difference spectrum $S_\delta(\omega)$,

$$S_\delta(\omega) \;=\; S_\psi(\omega) - \left(\kappa\mathcal{F}_{\mathrm{Lin}}(\omega,\beta) + \sigma_{\mathrm{sn}}^2\right) . \tag{4.57}$$

In Figure 4.3, we compare the circular motion and linear motion response functions over our frequency range and well within the non-dispersive regime. Both the circular motion and the inertial motion are taken at the same speed

$v = 0.95c_3$. For the temperature and range of frequencies considered, the linear approximation of the linear motion response function (4.54) is well motivated.

In line with the observations made in Section 3.4, the ratio $\mathcal{F}/\mathcal{F}_{\text{Lin}}$ demonstrates that velocity-dependent response dominates for high frequencies; whereas for lower frequencies, a response due to acceleration can be identified. Furthermore, a measurement of the response function $\mathcal{F}$ at high frequencies determines $\mathcal{F}_{\text{Lin}}$ over our full frequency range, by the linearity of (4.54). As such, the quantity $\mathcal{F}_{\text{Lin}}$ in (4.57) is operationally measurable from the circular motion response (4.52) alone. The kink visible in the ratio $\mathcal{F}/\mathcal{F}_{\text{Lin}}$ when probing at the angular frequency and originates from a discontinuity in the first derivative of the response function; the same kink may be found in Figure 3.3.

To determine the feasibility of the difference spectrum (4.57), we use the Signal-to-Noise (SNR) [70]

$$\text{SNR} = \sqrt{\frac{\mathcal{N}\mathcal{B}}{2}} \frac{S_\delta(\omega)}{\sigma_{\text{sn}}^2 \sqrt{1 + 2\frac{S_\delta(\omega)}{\sigma_{\text{sn}}^2} + 2\frac{S_\delta^2(\omega)}{\sigma_{\text{sn}}^4}}}\,, \tag{4.58}$$

where $\mathcal{N}$ is the number of realisations and $\mathcal{B}$ is the resolution bandwidth in units of the measurement bandwidth. Only when the SNR is larger than unity can the acceleration-dependent signal S_δ be observed over the shot-noise σ_{sn}^2.

We use the quantifier (4.58) to numerically explore a range of experimental parameters. We first consider in Figure 4.4i when the helium sample is fixed at $T = 10$ mK and the orbital radius is varied. With the speed v kept fixed throughout and $a = v^2 R^{-1}$, it follows that varying the orbital radius is equivalent to varying the acceleration. We see that the SNR is larger for smaller orbital radii — for larger accelerations — which encapsulates the essence of the Unruh effect. Next, in Figure 4.4ii, we fix the orbital radius $R = 60\ \mu$m and vary the sample temperature. We saw in Figure 3.4 that an acceleration-dependent signature is present independent of the ambient temperature. A remarkable feature of the SNR plotted in Figure 4.4ii is that the acceleration-dependent response increases as the sample temperature increases: acceleration-dependence is enhanced by the presence of a background temperature.

4.5 Discussion

In this Chapter, we presented a proposal for observing acceleration-dependence in the response of a continuous quasiparticle detector in a realisable analogue spacetime. In our experimental setup, a laser acts as a local detector of perturbations on the surface of superfluid helium-4. We demonstrated that these surface

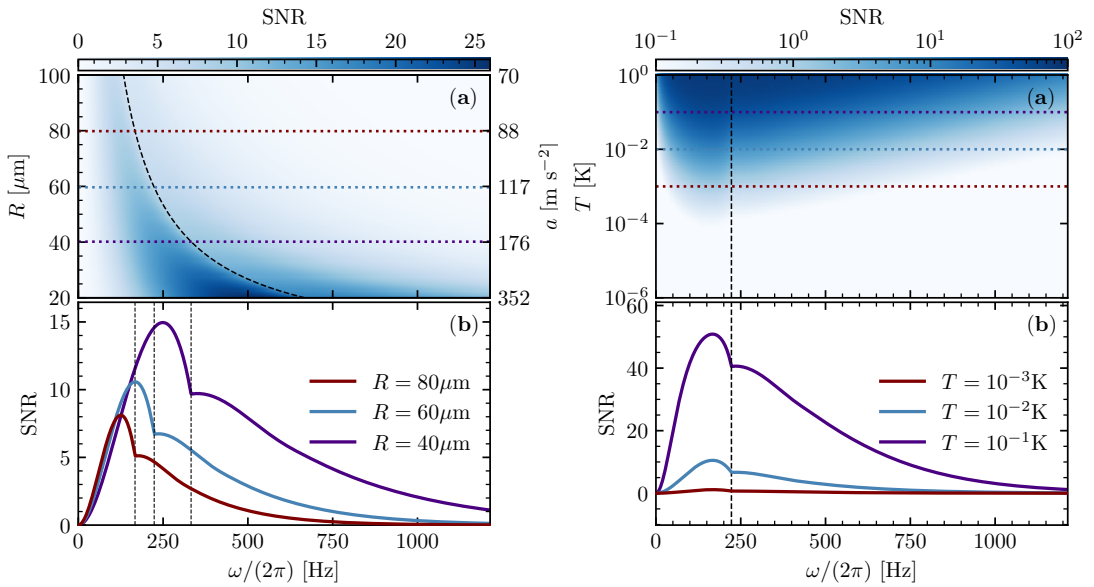

(i) **(ii)**

Figure 4.4: (i) SNR (4.58) for $\mathcal{N} = 10^5$ realisations with a bandwidth of $\mathcal{B} = 1$. Superfluid temperature $T = 10\,\mathrm{mK}$, orbital speed $v = 0.95c_3$, orbital radius R as shown; the laser trajectory angular frequency and acceleration are determined in terms of these quantities by $\Omega = v/R$ and $a = v^2/R$. The horizontal axis is the frequency. Panel (a) Heatmap of computed SNR for orbital radii $20\,\mu\mathrm{m} \leq R \leq 100\,\mu\mathrm{m}$. The horizontal colourbar indicates the magnitude of the SNR. Dashed black curve is the orbital angular frequency Ω. Purple, blue and dark red dotted lines are lines of constant radii, whose SNRs are displayed in panel (b). Panel (b) Profile of computed SNR for constant radial slices in panel (a). Vertical black dashed lines represent orbital angular frequencies for $R = 40\,\mu\mathrm{m}$ (far right), $60\,\mu\mathrm{m}$, and $80\,\mu\mathrm{m}$ (far left). **(ii)** SNR (4.58) for $\mathcal{N} = 10^5$ realisations with a bandwidth of $\mathcal{B} = 1$. Orbital radius $R = 60\,\mu\mathrm{m}$, speed $v = 0.95c_3$, frequency on the horizontal axis as in Figure 4.4i. Dashed vertical black line shows the orbital angular frequency Ω. Panel (a) Heatmap of computed SNR for superfluid at temperatures $1\,\mu\mathrm{K} \leq T \leq 1\,\mathrm{K}$. Purple, blue and dark red dotted lines are lines of constant superfluid temperature, whose SNRs are displayed in panel (b). Panel (b) Profile of computed SNR for constant temperature slices in panel (a).

perturbations admit a description as an effective field theory and found that the fluctuations in the phase of a laser due to its interaction with superfluid helium-4 encode information about the interaction trajectory. We provided a map between hydrodynamical and quantum scalar fields, enabling us to employ the theoretical framework developed in Chapter 3 to include the helium sample temperature in our modelling.

By comparing the response of a detector undergoing uniform circular motion and a detector in inertial motion, we developed a suitable SNR measure derived from the principle of extracting and isolating only acceleration-dependent effects within the detector response. We numerically evaluated this measure for a range of temperatures and orbital radii. We found two circumstances in

which the acceleration-dependent signal increased. First, when the orbital radius decreased with the speed fixed. In uniform circular motion at fixed speed, the acceleration and the orbital radius are inversely proportional. As such, decreasing the orbital radius increases the acceleration of the detector and an increase in the acceleration-dependent signal is consistent with this observation. Second, the SNR increased with an increase of the sample temperature. We have confirmed that trajectory-dependence still persists in a system with a significant ambient temperature and, furthermore, that the background temperature enhances the signature of this effect. Finally, we reiterate that the parameter regimes are all within experimental reach.

In the next Chapter, we test the robustness of Unruh-like phenomena by comparing a detector undergoing uniform circular motion in a thermal bath with a detector undergoing uniform circular motion whilst being accelerated in a direction orthogonal to the plane of rotation.

Chapter 5

Ambient temperature versus ambient acceleration in the circular motion Unruh effect

"A circle may be small, yet it may be as mathematically beautiful and perfect as a large one."

Isaac D'Israeli
Miscellanies (1796)

THE thermal aspect of the linearly accelerated Unruh effect predicts that an observer in $(3+1)$-dimensional Minkowski spacetime is unable to distinguish between being linearly accelerated with proper acceleration a through the Minkowski vacuum from being static in a thermal bath at temperature $T = a/(2\pi)$. We concern ourselves in this Chapter with the robustness of this effect and address the following question:

Does an observer in circular motion through a thermal bath of temperature T_U respond in the same way as an observer undergoing uniform acceleration as well as circular motion in the plane orthogonal to its acceleration?

The contents of this Chapter were extracted from, or based on, the journal article "Ambient temperature versus ambient acceleration in the circular motion Unruh effect" [3] in collaboration with Leo Parry, T Rick Perche, and Jorma Louko.

5.1 Spacetime, field, and detector preliminaries

We work in $(3+1)$-dimensional Minkowski spacetime in inertial coordinates (t, x, y, z) with the metric $\mathrm{d}s^2 = -\mathrm{d}t^2 + \mathrm{d}x^2 + \mathrm{d}y^2 + \mathrm{d}z^2$. We consider a quantised, real scalar field $\hat{\Phi}$ with linear dispersion relation, decomposed as in (2.30).

In this Chapter, we will address two scenarios, when the field is prepared in the Minkowski vacuum $|0_{\mathrm{M}}\rangle$ and when the field is prepared in a thermal state $|\beta\rangle$ in inverse temperature β, where the notion of thermality is with respect to the time evolution generated by ∂_t.

When the field $\hat{\Phi}$ is in the Minkowski vacuum, we will use the Unruh-DeWitt (UDW) detector formalism established in Chapter 2. In particular, we will couple the detector to the field using the interaction Hamiltonian (2.32). We will work in the long-interaction limit, except in interpreting the small-energy-gap limit in Section 5.2.2. As such, we will principally work with the stationary response function $\mathcal{F}$ (2.44).

When the field $\hat{\Phi}$ is prepared in a thermal state, we will also use a linearly coupled detector, described by interaction Hamiltonian (2.32). This is in contrast to the thermal-field-theory formalism used in Chapter 3, in which case we used a derivative-coupled interaction Hamiltonian (3.3) to sidestep the otherwise infrared-divergent thermal Wightman function $\mathcal{W}_\beta$. In $3+1$ dimensions, the thermal Wightman function (2.39) is well defined. As in Chapter 3, when Φ is prepared in a thermal state defined with respect to the time evolution generated by ∂_t, we consider only stationary trajectories whose time evolution is also generated by ∂_t. As such, this will also be a stationary situation and we work with the stationary response function $\mathcal{F}$ (2.44).

We work in a genuinely relativistic setting — rather than an analogue spacetime — with trajectories parametrised with respect to proper time τ. The detector energy gap is denoted by E. Finally, in Chapter 2, we adopted the notation $\mathcal{W}(\tau, 0) \coloneqq \mathcal{W}(\mathsf{x}(\tau), \mathsf{x}(0))$. Throughout this Chapter, we condense this notation further, writing $\mathcal{W}(\tau) \coloneqq \mathcal{W}(\tau, 0)$.

5.1.1 Finite-time interaction

Anticipating considering a finite-time interaction later in Section 5.2, we outline some preliminaries. We consider the detector interaction Hamiltonian (2.32), for which the transition probability $\mathcal{P}$ (2.37b) reads

$$\mathcal{P}(E) \;=\; \lambda^2 \int_{\mathbb{R}^2} \mathrm{d}\tau \mathrm{d}\tau' \, \chi(\tau)\chi(\tau') \mathrm{e}^{-\mathrm{i}E(\tau-\tau')} \mathcal{W}(\tau, \tau') \,, \tag{5.1}$$

where λ and χ are the coupling constant and switching function in the interaction Hamiltonian (2.32).

Example 5.1 (Gaussian Switching)**.** As an example, we consider a massless scalar field in $3+1$ Minkowski spacetime prepared in the Minkowski vacuum and a detector undergoing inertial motion. The Wightman function is given by

$$\mathcal{W}(\tau,0) \;=\; -\frac{1}{4\pi^2}\frac{1}{(\tau-\mathrm{i}\varepsilon)^2}\,. \tag{5.2}$$

We assume the temporal profile of the interaction takes the form of a Gaussian,

$$\chi_{\mathrm{G}}(\tau) \;=\; \mathrm{e}^{-\pi\tau^2/(2T^2)}\,, \tag{5.3}$$

where T is the characteristic length scale of the interaction. We remark that this switching function does not have compact support and the detector probes the field for an arbitrarily long time. However, the exponential suppression mimics that of a finite time interaction and the Gaussian switching often leads to integral expressions, which may be evaluated in terms of known functions.

Combining the Wightman function for the inertial detector (5.2) and Gaussian switching (5.3) with the transition probability (5.1) leads to [42]

$$\mathcal{P}_{\mathrm{G}}(E) \;=\; \frac{\lambda^2}{4\pi}\left(\mathrm{e}^{-E^2T^2/\pi} - ET\,\mathrm{erfc}\left(\frac{ET}{\sqrt{\pi}}\right)\right)\,, \tag{5.4}$$

where erfc denotes the complementary error function [111]. ■

This example illustrates that the transition probability $\mathcal{P}$ diverges in the long-interaction-time limit. In particular, it is clear from (5.4) that $\mathcal{P}$ diverges linearly with the interaction time T as $T\to\infty$. This motivates the definition of the response function, or transition rate,

$$\mathcal{F}(E) \;=\; \lim_{T\to\infty}\frac{1}{\lambda^2}\frac{\mathcal{P}(E)}{T}\,. \tag{5.5}$$

In the case of Gaussian switching (5.4), we have

$$\mathcal{F}(E) \;=\; \lim_{T\to\infty}\frac{1}{\lambda^2}\frac{\mathcal{P}_{\mathrm{G}}(E)}{T} \;=\; -\frac{E}{2\pi}\Theta(-E)\,, \tag{5.6}$$

which one may recognise as the response function for a detector undergoing inertial motion in $3+1$ dimensions (2.67). This result follows from $\lim_{a\to\infty}\mathrm{erfc}(ax) = 2\Theta(-x)$.

However, there is nothing fundamental about choosing Gaussian switching to obtain the response function, and any other switching function with a suitable

time parameter T may have been chosen. For a further discussion of this, see Appendix D. In particular, we demonstrate three equivalent definitions of the response function encountered in the literature (see, for example, [3, 5, 23, 71, 72, 143–146]),

$$\mathcal{F}(E) = \lim_{T\to\infty} \frac{1}{\lambda^2}\frac{\mathcal{P}(E)}{T} = \frac{1}{\lambda^2}\lim_{T\to\infty}\frac{\mathrm{d}\mathcal{P}(E)}{\mathrm{d}T} = \int_{\mathbb{R}} \mathrm{d}\tau\, \mathrm{e}^{-\mathrm{i}E\tau}\mathcal{W}(\tau)\,. \tag{5.7}$$

5.2 Hypertor motion

In this Section, we consider when the field is prepared in the Minkowski vacuum and the detector is undergoing a stationary motion known as "hypertor", or "loxodromic", motion [4, 71, 72, 91]. This motion consists of uniform circular motion in a plane and uniform linear acceleration parallel to the axis of rotation — helical motion.

Without loss of generality, we choose the frame in which the detector is linearly accelerating parallel to the z-axis and undergoing circular motion in the x-y axis in inertial coordinates. The detector's trajectory is then parameterised by its proper time τ as

$$\mathsf{x}(\tau) = \left(\frac{1}{a}\sinh(a\gamma\tau), R\cos(\Omega\gamma\tau), R\sin(\Omega\gamma\tau), \frac{1}{a}\cosh(a\gamma\tau)\right), \tag{5.8}$$

$$\gamma = \frac{1}{\sqrt{1-R^2\Omega^2}}, \tag{5.9}$$

where $a > 0$ is the proper acceleration of the centre of the circular motion, and $R > 0$ and $\Omega > 0$ are the radius and angular velocity of the circular motion, as measured in the frame of the uniformly accelerated centre. We assume $R\Omega < 1$ to ensure that the trajectory is timelike.

The trajectory (5.8) is the composition of uniform linear acceleration and uniform motion. In particular, it is the integral curve of the sum of a boost Killing vector and a (linearly independent) rotational Killing vector, resulting in a stationary trajectory. We will discuss the classification of timelike stationary trajectories using Killing vectors in Chapter 6.

The pullback of the Wightman function to the trajectory (5.8) is given by

$$\mathcal{W}_{\mathrm{H}}(\tau) = -\frac{1}{4\pi^2}\frac{1}{\frac{4}{a^2}\sinh^2(\frac{\gamma a}{2}(\tau-\mathrm{i}\varepsilon)) - 4R^2\sin^2(\frac{\gamma\Omega}{2}(\tau-\mathrm{i}\varepsilon))}, \tag{5.10}$$

where we use the subscript H to clarify the hypertor motion. The detector's

response function is then given by

$$\begin{aligned}\mathcal{F}_{\rm H}(E) &= \int_{\mathbb{R}} \mathrm{d}\tau\, \mathrm{e}^{-\mathrm{i}E\tau}\mathcal{W}_{\rm H}(\tau)\,, \\ &= -\frac{1}{4\pi^2}\int_{\mathbb{R}} \mathrm{d}\tau\, \mathrm{e}^{-\mathrm{i}E\tau}\frac{1}{\frac{4}{a^2}\sinh^2(\frac{\gamma a}{2}(\tau-\mathrm{i}\varepsilon)) - 4R^2\sin^2(\frac{\gamma\Omega}{2}(\tau-\mathrm{i}\varepsilon))}\,. \end{aligned} \tag{5.11}$$

The integral (5.11) may not be evaluated in terms of known functions. In the following Sections, we analyse the asymptotic behaviour in various limiting regimes.

5.2.1 Small-gap limit

The first asymptotic behaviour we consider is the limit of a small energy gap, $E \to 0$, with all other parameters fixed. We find a power series in E to all orders.

We begin by isolating the distributional behaviour of the Wightman function (5.10) as in [69],

$$\mathcal{W}_{\rm H}(\tau) \sim -\frac{1}{4\pi^2(\tau-\mathrm{i}\varepsilon)^2}\,. \tag{5.12}$$

Adding and subtracting the short-distance Hadamard contribution (5.12) under the integral in (5.11), we find

$$\begin{aligned}\mathcal{F}_{\rm H}(E) = &\underbrace{-\frac{1}{4\pi^2}\int_{\mathbb{R}} \mathrm{d}\tau\, \cos(E\tau)\left(\frac{1}{\frac{4}{a^2}\sinh^2(\frac{\gamma a\tau}{2}) - 4R^2\sin^2(\frac{\gamma\Omega\tau}{2})} - \frac{1}{\tau^2}\right)}_{\textbf{(a)}} \\ &\underbrace{-\frac{1}{4\pi^2}\int_{\mathbb{R}} \mathrm{d}\tau\, \mathrm{e}^{-\mathrm{i}E\tau}\frac{1}{(\tau-\mathrm{i}\varepsilon)^2}}_{\textbf{(b)}}\,. \end{aligned} \tag{5.13}$$

We make four observations. The grouping of the addition and subtraction under the integral in (5.13) separates the integral into a regular contribution **(a)** and a distributional contribution **(b)**. The small-τ behaviour in **(a)** is divergence free and the limit $\varepsilon \to 0^+$ has been taken. The integral **(a)** is even in τ and we replace $\exp(\mathrm{i}E\tau)$ by $\cos(E\tau)$. The integral **(b)** encodes the distributional behaviour of the Wightman function through its $-\mathrm{i}\varepsilon$.

We can recognise integral **(b)** as the first integral in (2.66), which we identify as the inertial response function in $3+1$ Minkowski spacetime [69]. Using the notation of (2.67), we denote this by $\mathcal{F}_0(E)$ and re-express the response function (5.13) as

$$\mathcal{F}_{\rm H}(E) = \mathcal{F}_0(E) + \mathcal{F}^{\rm corr}_{\rm H}(E)\,, \tag{5.14a}$$

$$\mathcal{F}_{\mathrm{H}}^{\mathrm{corr}}(E) \;=\; -\frac{1}{4\pi^2}\int_{\mathbb{R}} \mathrm{d}\tau\, \cos(E\tau)\left(\frac{1}{\frac{4}{a^2}\sinh^2(\frac{\gamma a\tau}{2}) - 4R^2\sin^2(\frac{\gamma\Omega\tau}{2})} - \frac{1}{\tau^2}\right). \tag{5.14b}$$

We now find a power series of the response function in powers of E. A dominated convergence theorem argument allows us to take the limit $E \to 0$ under the integral to give the leading-order contribution,

$$\Gamma_0 \;\coloneqq\; \lim_{E\to 0}\mathcal{F}_{\mathrm{H}}^{\mathrm{corr}}(E) \;=\; -\frac{1}{4\pi^2}\int_{\mathbb{R}} \mathrm{d}\tau\, \left(\frac{1}{\frac{4}{a^2}\sinh^2(\frac{\gamma a\tau}{2}) - 4R^2\sin^2(\frac{\gamma\Omega\tau}{2})} - \frac{1}{\tau^2}\right). \tag{5.15}$$

We add and subtract Γ_0 to $\mathcal{F}_{\mathrm{H}}^{\mathrm{corr}}(E)$ (5.14b) and factor out τ^{-2} yields

$$\mathcal{F}_{\mathrm{H}}(E) \;=\; \Gamma_0 - \frac{1}{4\pi^2}\int_{\mathbb{R}} \mathrm{d}\tau\, \left(\frac{\cos(E\tau)-1}{\tau^2}\right)\left(\frac{\tau^2}{\frac{4}{a^2}\sinh^2(\frac{\gamma a\tau}{2}) - 4R^2\sin^2(\frac{\gamma\Omega\tau}{2})} - 1\right). \tag{5.16}$$

Expanding the second pair of brackets in (5.16), we identify two well-defined integrals, the second of which may be evaluated after a change of variables and integration by parts, leading to a sinc integral

$$\frac{1}{4\pi^2}\int_{\mathbb{R}} \mathrm{d}\tau\, \frac{\cos(E\tau)-1}{\tau^2} \;=\; -\frac{|E|}{4\pi^2}\int_{\mathbb{R}} \mathrm{d}\sigma\, \frac{\sin(2\sigma)}{\sigma} \;=\; -\frac{|E|}{4\pi}. \tag{5.17}$$

Adding together (5.17) and $\mathcal{F}_0$ (2.67) leads to $-E/4\pi$, so that the full transition rate can now be cast as

$$\mathcal{F}_{\mathrm{H}}^{\mathrm{corr}}(E) \;=\; \Gamma_0 - \frac{E}{4\pi} - \frac{1}{4\pi^2}\int_{\mathbb{R}} \mathrm{d}\tau\, \frac{\cos(E\tau)-1}{\frac{4}{a^2}\sinh^2(\frac{\gamma a\tau}{2}) - 4R^2\sin^2(\frac{\gamma\Omega\tau}{2})}. \tag{5.18}$$

The remaining integral in (5.18) exhibits exponential decay due to the hyperbolic sine function in the denominator. We Maclaurin expand the cosine and by Fubini's theorem we interchange the sum and the integral, obtaining

$$\begin{aligned}\int_{\mathbb{R}} \mathrm{d}\tau\, &\frac{\cos(E\tau)-1}{\frac{4}{a^2}\sinh^2(\frac{\gamma a\tau}{2}) - 4R^2\sin^2(\frac{\gamma\Omega\tau}{2})} \\ &= \sum_{n=1}^{\infty}\frac{(-1)^n E^{2n}}{(2n)!}\int_{\mathbb{R}} \mathrm{d}\tau\, \frac{\tau^{2n}}{\frac{4}{a^2}\sinh^2(\frac{\gamma a\tau}{2}) - 4R^2\sin^2(\frac{\gamma\Omega\tau}{2})}.\end{aligned} \tag{5.19}$$

We define the following countable family of integrals with dimensions of E^{1-2n}:

$$\Gamma_n \;\coloneqq\; -\frac{1}{4\pi^2}\int_{\mathbb{R}} \mathrm{d}\tau\, \frac{\tau^{2n}}{\frac{4}{a^2}\sinh^2(\frac{\gamma a\tau}{2}) - 4R^2\sin^2(\frac{\gamma\Omega\tau}{2})}, \tag{5.20}$$

which gives us a series expansion for $\mathcal{F}_{\mathrm{H}}(E)$,

$$\mathcal{F}_{\mathrm{H}}(E) \;=\; \Gamma_0 - \frac{E}{4\pi} + \sum_{n=1}^{\infty} \frac{(-1)^n}{(2n)!}\Gamma_n E^{2n}\,, \tag{5.21}$$

convergent for $|E| < \gamma a$. We may see the convergence of the series as follows. By the change of variables $\tau = z/(\gamma a)$, we write Γ_n (5.20) as

$$\Gamma_n \;=\; -\frac{a^2}{8\pi}\frac{1}{(\gamma a)^{2n+1}} K_n\,, \tag{5.22a}$$

$$K_n \;=\; \int_0^\infty \mathrm{d}z\, \frac{z^{2n}}{\sinh^2\!\left(\frac{z}{2}\right) - a^2R^2\sin^2\!\left(\frac{\Omega}{2a}z\right)}\,. \tag{5.22b}$$

We note that the integral K_n and its integrand are positive. We bound the integrand as

$$\frac{z^{2n}}{\sinh^2\!\left(\frac{z}{2}\right) - a^2R^2\sin^2\!\left(\frac{\Omega}{2a}z\right)} \;\leq\; \frac{z^{2n}}{\sinh^2\!\left(\frac{z}{2}\right) - R^2\Omega^2\left(\frac{z}{2}\right)^2} \;\leq\; \frac{z^{2n}}{(1-R^2\Omega^2)\sinh^2\!\left(\frac{z}{2}\right)}\,, \tag{5.23}$$

where we have used the inequalities $\sin(z) \leq z$ and $z \leq \sinh(z)$ for $z \geq 0$. This leads to the bound

$$0 \;<\; K_n \;\leq\; \gamma^2 \int_0^\infty \mathrm{d}z\, \frac{z^{2n}}{\sinh^2\!\left(\frac{z}{2}\right)}\,, \tag{5.24}$$

where we have identified $\gamma^2 = (1-R^2\Omega^2)^{-1}$. This integral may be evaluated using [117, (3.527.1)], leading to

$$0 \;<\; K_n \;\leq\; 4\gamma^2(2n)!\zeta(2n)\,, \tag{5.25}$$

where ζ is the Riemann zeta function [111]. We note $\zeta(2n) \leq \zeta(2) = \frac{1}{6}\pi^2$ for $n \geq 1$. Combining these observations, we may bound the summand in (5.21) as

$$\left|\frac{(-1)^n}{(2n)!}\Gamma_n E^{2n}\right| \;\leq\; \frac{1}{12}a\gamma\pi\left(\frac{E}{\gamma a}\right)^{2n}\,. \tag{5.26}$$

By comparison with the geometric series, we see that the series in (5.21) is indeed convergent for $|E| < \gamma a$.

We compute the effective temperature (2.54) in this limit as

$$T_{\mathrm{H}} \;=\; 2\pi\Gamma_0 + \left(2\pi\Gamma_1 - \frac{1}{24\pi\Gamma_0}\right)E^2 + \mathcal{O}(|E|^4)\,. \tag{5.27}$$

We now interpret this result in terms of the long-interaction-time limit.

5.2.2 Interpretation: small energy gap versus long interaction time

We may also write (5.21) by means of a generating function, which is related to the case of a detector undergoing hypertor motion with Gaussian switching (see Example 5.1). The transition probability (2.37b) in this case reads

$$\begin{aligned}\mathcal{P}_{\mathrm{H}}(E) &= \lambda^2 T \int_{\mathbb{R}} \mathrm{d}\tau\, \mathrm{e}^{-\pi\tau^2/(4T^2)} \mathrm{e}^{-\mathrm{i}E\tau} \mathcal{W}_{\mathrm{H}}(\tau)\,, \\ &= -\frac{\lambda^2 T}{4\pi^2} \int_{\mathbb{R}} \mathrm{d}\tau\, \mathrm{e}^{-\pi\tau^2/(4T^2)} \mathrm{e}^{-\mathrm{i}E\tau} \frac{1}{\frac{4}{a^2}\sinh^2(\frac{\gamma a}{2}(\tau - \mathrm{i}\varepsilon)) - 4R^2 \sin^2(\frac{\gamma\Omega}{2}(\tau - \mathrm{i}\varepsilon))}\,. \end{aligned} \tag{5.28}$$

By adding and subtracting the vacuum transition rate multiplied by $\lambda^2 T$, we can separate the distributional and regular behaviours of the integral in (5.28),

$$\begin{aligned}\mathcal{P}_{\mathrm{H}}(E) &= -\frac{\lambda^2 T}{4\pi^2} \int_{\mathbb{R}} \mathrm{d}\tau\, \cos(E\tau) \left(\frac{\mathrm{e}^{-\pi\tau^2/(4T^2)}}{\frac{4}{a^2}\sinh^2(\frac{\gamma a\tau}{2}) - 4R^2 \sin^2(\frac{\gamma\Omega\tau}{2})} - \frac{1}{\tau^2} \right) \\ &\qquad - \lambda^2 T \int_{\mathbb{R}} \mathrm{d}\tau\, \frac{\mathrm{e}^{-\mathrm{i}E\tau}}{4\pi^2(\tau - \mathrm{i}\varepsilon)^2}\,, \\ &= -\frac{\lambda^2 T}{4\pi^2} \int_{\mathbb{R}} \mathrm{d}\tau\, \cos(E\tau) \left(\frac{\mathrm{e}^{-\pi\tau^2/(4T^2)}}{\frac{4}{a^2}\sinh^2(\frac{\gamma a\tau}{2}) - 4R^2 \sin^2(\frac{\gamma\Omega\tau}{2})} - \frac{1}{\tau^2} \right) \\ &\qquad - \frac{\lambda^2 E T}{2\pi}\Theta(-E)\,, \end{aligned} \tag{5.29}$$

where the first integral is regular and the second integral has been evaluated using the residue theorem.

We define $g \coloneqq \pi/(4T^2)$ and the time-dependent transition rate $F_{\mathrm{H}}(E; g)$,

$$F_{\mathrm{H}}(E; g) \coloneqq \frac{\mathcal{P}_{\mathrm{H}}(E)}{\lambda^2 T}\,, \tag{5.30a}$$

$$\begin{aligned} &= -\frac{1}{4\pi^2} \int_{\mathbb{R}} \mathrm{d}\tau\, \cos(E\tau) \left(\frac{\mathrm{e}^{-g\tau^2}}{\frac{4}{a^2}\sinh^2(\frac{\gamma a\tau}{2}) - 4R^2 \sin^2(\frac{\gamma\Omega\tau}{2})} - \frac{1}{\tau^2} \right) \\ &\quad - \frac{E}{2\pi}\Theta(-E). \end{aligned} \tag{5.30b}$$

Differentiating F_{H} with respect to g, we find

$$\begin{aligned} \left.\frac{\mathrm{d}^n F_{\mathrm{H}}}{\mathrm{d}g^n}\right|_{g=0,E=0} &= \frac{1}{4\pi^2} \int_{\mathbb{R}} \mathrm{d}\tau\, \frac{(-1)^n \tau^{2n}}{\frac{4}{a^2}\sinh^2(\frac{\gamma a\tau}{2}) - 4R^2 \sin^2(\frac{\gamma\Omega\tau}{2})} \\ &= (-1)^n \Gamma_n\,, \end{aligned} \tag{5.31}$$

for $n \geq 1$.

We remark that evaluation at $g = 0$ corresponds to the limit $T \to \infty$. Therefore, we may use the finite-time transition rate in the limit of long interactions to write $\mathcal{F}_{\mathrm{H}}(E)$ in terms of derivatives of $F_{\mathrm{H}}(E; g)$ with respect to g as

$$\mathcal{F}_{\mathrm{H}}(E) \;\sim\; F_{\mathrm{H}}(0;0) - \frac{E}{4\pi} + \sum_{n=1}^{\infty} \frac{E^{2n}}{(2n)!} F_{\mathrm{H}}^{(n)}(0;0)\,, \tag{5.32}$$

where $F_{\mathrm{H}}^{(n)}(0;0) \coloneqq \frac{\mathrm{d}^n F_{\mathrm{H}}(0;g)}{\mathrm{d}g^n}|_{g=0}$.

The expression (5.32) above is again the Taylor series (5.21), however the coefficients — which are unique whenever the Taylor series exists — are exactly given in terms of the transition probability for a detector in hypertor motion with Gaussian switching. In particular, these coefficients are given by derivatives with respect to the inverse of the interaction time, whose evaluation at $g = 0$ links the behaviours of long interaction times with that of small energy gaps, $g \to 0^+ \iff T \to \infty$.

5.2.3 Small-radius limit

The next asymptotic regime we consider is the limit of small orbital radii R, keeping all other parameters fixed. Geometrically, this corresponds to a small circular deviation from uniformly accelerated motion. As expected, we recover the Unruh effect to leading order with lower-order corrections due to circular motion.

To study the behaviour of $\mathcal{F}_{\mathrm{H}}(E)$ (5.11), it will be practical to work with the following dimensionless quantities

$$\rho \;\coloneqq\; aR\,,\; \alpha \;\coloneqq\; a/\Omega\,,\; z \;\coloneqq\; \Omega\gamma\tau/2\,,\; \varpi \;\coloneqq\; \frac{2E}{\gamma\Omega}\,, \tag{5.33}$$

so that small-radius limit is the limit of small ρ. In dimensionless variables, the timelike condition $R\Omega < 1$ corresponds to $\rho < \alpha$.

In the variables (5.33), we then define

$$\begin{aligned} w_{\mathrm{H}}(z) \;&\coloneqq \mathcal{W}_{\mathrm{H}}(2z/\gamma\Omega)\,, \\ &= \frac{\alpha^2\Omega^2}{16\pi^2(\rho^2\sin^2(z - \mathrm{i}\varepsilon) - \sinh^2(\alpha(z - \mathrm{i}\varepsilon)))}\,. \end{aligned} \tag{5.34}$$

In the dimensionless variables (5.33), the response function reads

$$\mathcal{F}_{\mathrm{H}}(E) \;=\; \frac{2}{\gamma\Omega}\int_{\mathbb{R}} \mathrm{d}z\, \mathrm{e}^{-\mathrm{i}\varpi z} w_{\mathrm{H}}(z) \tag{5.35}$$

$$= \frac{\alpha^2\Omega}{8\pi^2\gamma}\int_{\mathbb{R}} \mathrm{d}z\, \mathrm{e}^{-\mathrm{i}\varpi z}\frac{1}{\rho^2\sin^2(z-\mathrm{i}\varepsilon)-\sinh^2(\alpha(z-\mathrm{i}\varepsilon))}\,.$$

As before, we isolate the distributional behaviour of $\mathcal{F}_{\mathrm{H}}(E)$, splitting it into its inertial and correction contributions. The inertial term is again given by (2.67). The correction term is given by

$$\mathcal{F}_{\mathrm{H}}^{\mathrm{corr}}(E) \;=\; -\frac{\gamma\Omega}{4\pi^2}\int_0^\infty \mathrm{d}z\, \cos(\varpi z)\left(\frac{\alpha^2-\rho^2}{\sinh^2(\alpha z)-\rho^2\sin^2(z)}-\frac{1}{z^2}\right). \tag{5.36}$$

We consider now the leading-order behaviour in the small-radius limit, $\rho \to 0$. A dominated convergence argument allows us to take the limit under the integral, leaving the leading-order contribution

$$\lim_{\rho\to 0}\mathcal{F}_{\mathrm{H}}^{\mathrm{corr}}(E) \;=\; -\frac{\gamma\Omega}{4\pi^2}\int_0^\infty \mathrm{d}z\, \cos(\varpi z)\left(\frac{\alpha^2}{\sinh^2(\alpha z)}-\frac{1}{z^2}\right). \tag{5.37}$$

We consider now the subleading contributions, which may be written as

$$\mathcal{F}_{\mathrm{H}}^{\mathrm{corr}}(E) - \lim_{\rho\to 0}\mathcal{F}_{\mathrm{H}}^{\mathrm{corr}}(E) \;= \\ -\rho^2\frac{\gamma\Omega}{4\pi^2}\int_0^\infty \mathrm{d}z\, \underbrace{\cos(\varpi z)\frac{\left(\frac{\alpha^2\sin^2(z)}{\sinh^2(\alpha z)}-1\right)}{\sinh^2(\alpha z)}}_{\textbf{(a)}}\underbrace{\frac{1}{1-\rho^2\frac{\sin^2(z)}{\sinh^2(\alpha z)}}}_{\textbf{(b)}}. \tag{5.38}$$

Function **(a)** is a regular, integrable function of z, independent of ρ. Function **(b)** can be expanded to the first n terms as a geometric series with a remainder term. The remainder term is given by

$$\rho^2\int_0^\infty \mathrm{d}z\, \cos(\varpi z)\frac{\left(\frac{\alpha^2\sin^2(z)}{\sinh^2(\alpha z)}-1\right)}{\sinh^2(\alpha z)}\left(\rho^2\frac{\sin^2(z)}{\sinh^2(\alpha z)}\right)^{n+1}\frac{1}{1-\rho^2\frac{\sin^2(z)}{\sinh^2(\alpha z)}}\,. \tag{5.39}$$

We can bound $(1-\rho^2\sin^2(z)/\sinh^2(\alpha z))^{-1}$ above by $(1-\rho^2/\alpha^2)^{-1}$. The remaining integral in this bound then converges due to the exponential suppression at infinity and regularity at zero. Hence, the remainder term is order ρ^{2n+4}.

We are interested in the small-ρ limit. In particular, we can assume $\rho < 1$ and the remainder, therefore, tends to zero as $n \to \infty$. This justifies the following expansion in small ρ under the integral,

$$\mathcal{F}_{\mathrm{H}}^{\mathrm{corr}}(E) \;=\; -\frac{\gamma\Omega}{4\pi^2}\int_0^\infty \mathrm{d}z\, \cos(\varpi z)\left(\frac{\alpha^2}{\sinh^2(\alpha z)}-\frac{1}{z^2}\right)$$

$$+\frac{\gamma\Omega\rho^2}{4\pi^2}\int_0^\infty \mathrm{d}z\,\cos(\varpi z)\left(\frac{1}{\sinh^2(\alpha z)}-\frac{\alpha^2\sin^2(z)}{\sinh^4(\alpha z)}\right)+\mathcal{O}(\rho^4). \quad (5.40)$$

Both integrals in (5.40) may be evaluated in terms of elementary functions. Evaluating the integrals in (5.40) and using dimensionful parameters, we find the leading and subleading contributions to $\mathcal{F}$,

$$\mathcal{F}_{\mathrm{H}}(E) = \frac{E}{2\pi}\frac{1}{\mathrm{e}^{2\pi E/a}-1}+\frac{aR^2}{24\pi\gamma}\Bigg(\left[\gamma^2a^2+(E-\gamma\Omega)^2\right]g\left(\frac{2(E-\gamma\Omega)}{\gamma a}\right)$$
$$-2\left[3\gamma^2\Omega^2+\gamma a^2+E^2\right]g\left(\frac{E}{\gamma a}\right)+\left[\gamma^2a^2+(E+\gamma\Omega)^2\right]g\left(\frac{2(E+\gamma\Omega)}{\gamma a}\right)\Bigg)+\mathcal{O}(R^4)\,, \quad (5.41)$$

where $g(u)=u\coth(\pi u)$.

We identify the leading-order term in (5.41) as (2.51), the characteristic thermal response of the Unruh effect. The subleading term is more complicated; however, as $g(u)$ is even, we can identify the subleading term as an even function of E.

5.2.4 Large-gap limit

Our final asymptotic regime is the limit of a large detector gap, $E\to\infty$ with all other parameters fixed. Throughout this Section, we continue to use the dimensionless parameters (5.33).

The response function splits into a distributional (inertial) contribution given by (2.67) and a correction term given by (5.36), reading

$$\mathcal{F}^{\mathrm{corr}}_{\mathrm{H}}(E) = \frac{\Omega\gamma}{8\pi^2}\int_{\mathbb{R}}\mathrm{d}z\,\cos(\varpi z)\left(\frac{1}{z^2}+\frac{\alpha^2-\rho^2}{\rho^2\sin^2(z)-\sinh^2(\alpha z)}\right). \quad (5.42)$$

By the evenness of the integrand in (5.42), we replace $\cos(\varpi z)$ by $\exp(\mathrm{i}|\varpi|z)$ in (5.42). We then deform the integration contour from the real axis to a contour $\mathcal{C}$ that passes the pole at $z=0$ in the upper half-plane, on a semicircle so small that the contour deformation crosses no singularities. As $z=0$ is outside of the contour $\mathcal{C}$, the residue theorem informs us that the integral $\int_{\mathcal{C}}\exp(\mathrm{i}|\varpi|z)z^{-2}\,\mathrm{d}z$ vanishes, leaving us with

$$\mathcal{F}^{\mathrm{corr}}_{\mathrm{H}}(E) = \frac{\Omega\gamma}{8\pi^2}\int_{\mathcal{C}}\mathrm{d}z\,\mathrm{e}^{\mathrm{i}|\varpi|z}\frac{\alpha^2-\rho^2}{\rho^2\sin^2(z)-\sinh^2(\alpha z)}. \quad (5.43)$$

As in [23], a contour integration argument then says that the leading contribution to (5.43) at large $|\varpi|$ comes from the pole in the upper half-plane that is closest to the real axis. We identify now this pole.

We consider the zeroes of the function

$$f(z) \;=\; \rho^2 \sin^2(z) - \sinh^2(\alpha z)\,, \tag{5.44}$$

the denominator of the integrand in (5.43). We are interested in the root of $f(z)$ with the smallest positive imaginary part. We consider now two propositions to characterise this root.

Proposition 5.1. *Let $\alpha > 0$ and $\rho > 0$. There exists a positive, nonzero solution $z_0 \in (0, \frac{\pi}{\alpha})$ to*

$$\rho \sinh(z) - \sin(\alpha z) \;=\; 0\,, \tag{5.45}$$

for $\alpha > \rho$.

Proof. See Appendix E, Section E.1. □

Proposition 5.2. *Let $\alpha > \rho > 0$. The root z_0 of $f(z) = \rho^2 \sin^2(z) - \sinh^2(\alpha z)$ with the smallest, positive imaginary part is given by $z_0 = \mathrm{i}\mu$, where μ is the smallest, nonzero solution of*

$$\sin(\alpha\mu) \;=\; \rho \sinh(\mu)\,. \tag{5.46}$$

Proof. See Appendix E, Section E.2. □

We recall that the timelike condition $R\Omega < 1$ implies $0 < \rho < \alpha$. Then, by Proposition 5.1 and Proposition 5.2, the pole z_0 in the upper half-plane closest to the real axis is given by $z_0 = \mathrm{i}\mu$, where μ is the smallest, positive solution of

$$\rho \sinh(\mu) - \sin(\alpha\mu) \;=\; 0\,. \tag{5.47}$$

Having identified the pole of the integrand in (5.43) with the smallest positive imaginary part, an application of the residue theorem then gives the leading contribution to $\mathcal{F}^{\mathrm{corr}}(E)$ (5.43) in the large energy gap limit,

$$\mathcal{F}^{\mathrm{corr}}_{\mathrm{H}}(E) \;\sim\; \frac{\alpha a}{4\pi\gamma} \frac{\mathrm{e}^{-\mu|\varpi|}}{\rho^2 \sinh(2\mu) - \alpha \sin(2\alpha\mu)}\,, \text{ as } |\varpi| \to \infty. \tag{5.48}$$

A final quantity of interest is the effective temperature (2.54). Recalling from (5.33) that $|\varpi| = \frac{2}{\Omega\gamma}|E|$, we obtain

$$T_{\mathrm{H}} \;=\; \frac{\gamma\Omega}{2\mu} + o(1)\,, \text{ as } |E| \to \infty. \tag{5.49}$$

In the following Section, we perform a complementary analysis of circular motion in a $3+1$ thermal bath and in a subsequent Section, compare the results of Section 5.2 and Section 5.3.

5.3 Circular motion in a thermal bath

In this Section, we summarise our results for an analysis complementary to that of Section 5.2. We consider a massless, real, scalar field in $3+1$ Minkowski spacetime in a thermal bath. We probe the field with a UDW detector, coupled with interaction Hamiltonian (2.32). We assume the circular motion to have no drift in the rest frame of the thermal bath, that is to say time evolution is generated by ∂_t both in the thermal bath and the circular motion trajectory. In this case, the system is time-translation invariant along the circular trajectory and the whole system is stationary [1]. We analyse the same limits as in the hypertor motion, except for the small-radius limit, whose analysis we defer until Section 5.4.

In inertial coordinates, we consider circular motion in the x-y plane, parametrised by proper time τ as

$$\mathsf{x}(\tau) \;=\; (\gamma\tau, R\cos(\Omega\gamma\tau), R\sin(\Omega\gamma\tau), 0)\,, \tag{5.50}$$

where γ is given by (5.9), R represents the trajectory radius as observed by an inertial observer in the centre of the circular trajectory, and Ω is the angular velocity measured by the same observer.

We consider a particle detector undergoing circular motion (5.50) in Minkowski spacetime, probing a quantum scalar field initially prepared in a thermal state in temperature T. We define the parameter $a \coloneqq 2\pi T$, such that the pullback of the Wightman function to the circular trajectory and the associated response function are given by (see (2.46) or [23])

$$\mathcal{W}_{\text{TB}}(\tau) \;=\; -\frac{1}{4\pi^2}\frac{a\sinh(2aR\sin(\frac{\gamma\Omega}{2}\tau))}{4R\sin(\frac{\gamma\Omega}{2}\tau)\left\{\cosh(a\gamma(\tau-\mathrm{i}\varepsilon))-\cosh(2aR\sin(\frac{\gamma\Omega}{2}(\tau-\mathrm{i}\varepsilon)))\right\}}\,, \tag{5.51}$$

$$\mathcal{F}_{\text{TB}}(E) \;=\; \int_{\mathbb{R}}\mathrm{d}\tau\,\mathrm{e}^{-\mathrm{i}E\tau}\mathcal{W}_{\text{TB}}(\tau)\,, \tag{5.52}$$

where the subscript TB indicates that we are considering a Thermal Bath.

To avoid any ambiguity, we define

$$\left.\frac{\sinh\left(2aR\sin\left(\frac{\gamma\Omega}{2}\tau\right)\right)}{\sin\left(\frac{\gamma\Omega}{2}\tau\right)}\right|_{\tau=0} \coloneqq \lim_{\tau\to 0}\frac{\sinh\left(2aR\sin\left(\frac{\gamma\Omega}{2}\tau\right)\right)}{\sin\left(\frac{\gamma\Omega}{2}\tau\right)}\,, \tag{5.53}$$

rendering the Wightman function (5.51) well-defined.

The parameter a is in principle a rescaling of the ambient temperature T; however, this is chosen to agree with the temperature experienced by an observer

undergoing uniform linear acceleration with proper acceleration a.

In particular, in the absence of circular motion, we have

$$\lim_{R\to 0} \mathcal{W}_{\text{TB}}(\tau) \;=\; -\frac{1}{4\pi^2}\frac{1}{\frac{4}{a^2}\sinh^2(\frac{a}{2}(\tau-\mathrm{i}\varepsilon))}\,, \tag{5.54}$$

which one may recognise as the pullback of the Wightman function in $3+1$ dimensions to a uniformly accelerated trajectory in the Minkowski vacuum (2.50) or equivalently the pullback of the Wightman function to a static trajectory in $3+1$ dimensions in a thermal bath (2.47).

The integral in the response function (5.52) may not be evaluated in terms of known functions, as in the case of hypertor motion analysed in Section 5.2. As such, we study (5.52) in asymptotic regimes. The techniques used in this Section are either similar to those used in Section 5.2, or have already been reported in the literature [23, 69]. As such, we omit some details of the calculations. Finally, we recall that we postpone the limit of a small orbital radius to Section 5.4.

5.3.1 Small-gap limit

Thermal states are Hadamard and as such the Wightman function (5.51) has the short-distance behaviour given by

$$\mathcal{W}_{\text{TB}}(\tau) \;\sim\; -\frac{1}{4\pi^2(\tau-\mathrm{i}\varepsilon)^2}\,,\ \text{as}\ \tau\to 0\,. \tag{5.55}$$

As in Section 5.2.1, we isolate the distributional contribution arising from (5.55) and obtain a small-E expansion of the response function. We note that, the term $\cosh(a\gamma(\tau-\mathrm{i}\varepsilon))$ in the denominator in (5.51) forces exponential convergence of the integral coefficients in the obtained expansion.

We find

$$\mathcal{F}_{\text{TB}}(E) \;\sim\; \tilde{\Gamma}_0 - \frac{E}{4\pi} + \sum_{n=1}^{\infty}\frac{(-1)^n}{(2n)!}\tilde{\Gamma}_n E^{2n}\,, \tag{5.56}$$

where $\tilde{\Gamma}_0$ and $\tilde{\Gamma}_n$ are analogous to hypertor small energy gap expansion coefficients Γ_0 (5.15) and Γ_n (5.20),

$$\tilde{\Gamma}_0 \;=\; -\frac{1}{4\pi^2}\int_{\mathbb{R}}\mathrm{d}\tau\,\left(\frac{a\sinh(2aR\sin(\Omega\gamma\tau/2))}{4R\sin(\gamma\Omega\tau/2)\{\cosh(a\gamma\tau)-\cosh(2aR\sin(\gamma\Omega\tau/2))\}}-\frac{1}{\tau^2}\right)\,, \tag{5.57}$$

$$\tilde{\Gamma}_n \;=\; -\frac{1}{4\pi^2}\int_{\mathbb{R}}\mathrm{d}\tau\,\tau^{2n}\left(\frac{a\sinh(2aR\sin(\Omega\gamma\tau/2))}{4R\sin(\gamma\Omega\tau/2)\{\cosh(a\gamma\tau)-\cosh(2aR\sin(\gamma\Omega\tau/2))\}}\right)\,. \tag{5.58}$$

From this, we can immediately write down the small-gap expansion for the effective temperature (2.54) for circular motion in a thermal bath,

$$T_{\text{TB}} \;=\; 2\pi\tilde{\Gamma}_0 + \left(2\pi\tilde{\Gamma}_1 - \frac{1}{24\pi\tilde{\Gamma}_0}\right) E^2 + \mathcal{O}(|E|^4)\,. \tag{5.59}$$

5.3.2 Large-gap limit

We consider next the asymptotic regime of a large energy gap, $E \to \infty$ with all other parameters fixed. This has already been analysed in [23]; hence, we report the relevant findings briefly for later comparison. We work with the dimensionless parameters defined in (5.33).

We first define

$$\begin{aligned} w_{\text{TB}}(z) \;&:=\mathcal{W}_{\text{TB}}(2z/\gamma\Omega)\,, \\ &= \frac{\alpha^2\Omega^2\,\text{cosec}(z)\sinh(2\rho\sin z)}{16\pi^2\rho(\cosh(2\rho\sin z)-\cosh(2\alpha z))}\,. \end{aligned} \tag{5.60}$$

We split the response function (5.52) into an inertial contribution given by (2.67) and a correction term given by

$$\mathcal{F}^{\text{corr}}_{\text{TB}}(E) \;=\; \frac{\gamma\Omega}{8\pi^2}\int_{\mathbb{R}} \mathrm{d}z\;\cos(\varpi z)\left(\frac{1}{z^2} + \frac{(\alpha^2-\rho^2)\,\text{cosec}(z)\sinh(2\rho\sin z)}{\rho(\cosh(2\rho\sin z)-\cosh(2\alpha z))}\right)\,. \tag{5.61}$$

We consider now the limit $|E| \to \infty$, corresponding to $\varpi \to \infty$ in dimensionless variables, with all other parameters fixed. As detailed in [23], we extend the integral in (5.61) into the complex plane. Then, the leading contribution to the response function is given by the nonzero pole with the smallest positive imaginary part. However, the singularity structure of the Wightman function (5.60) is more complicated than in the hypertor motion. One finds a critical temperature T_{crit}, characterising a change in the position of this pole. We define the critical parameter $a_{\text{crit}} = 2\pi T_{\text{crit}}$, where a_{crit} is the solution to the transcendental equation

$$R\Omega \;=\; \frac{2Ra_{\text{crit}}}{\pi}\text{arcsinh}\left(\frac{\pi}{2Ra_{\text{crit}}}\right)\,. \tag{5.62}$$

The pole with the smallest positive imaginary part is given by $z = \mathrm{i}\mu_-$ for $a > a_{\text{crit}}$ and by $z = \mathrm{i}\mu_+$ for $a < a_{\text{crit}}$. It has been shown in [23] that $\mu_\pm$ are the solutions to the following transcendental equations

$$\frac{\mu_+}{R\Omega} \;=\; \sinh\mu_+\,, \qquad \frac{1}{2RT} \;=\; \frac{\mu_-}{R\Omega} + \sinh\mu_-\,. \tag{5.63}$$

Returning to dimensionful parameters, the leading-order contribution to the

response function correction (5.61) in the limit of large energy gaps is given by

$$\mathcal{F}^{\text{corr}}_{\text{TB}}(E) \sim \frac{1}{8\pi R\gamma}\frac{\mathrm{e}^{-2|\varpi|\mu_\pm}/(\gamma\Omega)}{\sinh\mu_\pm(R\Omega\cosh\mu_\pm \mp 1)}, \text{ as } |E|\to\infty, \tag{5.64}$$

where the choice of $\pm$ sign is determined by whether $a > a_{\text{crit}}$ ($-$ sign) or $a < a_{\text{crit}}$ ($+$ sign).

The resulting effective temperature (2.54) experienced by the detector is then given by

$$T_{\text{TB}} = \frac{\gamma\Omega}{2\mu_\pm} + o(1), \text{ as } |E|\to\infty. \tag{5.65}$$

5.4 Thermal bath versus uniform acceleration

In this Section, we compare the results of Section 5.2 and Section 5.3, contrasting the two motions in limiting regimes and provide numerical plots to cover a wider range of the parameter space. As in Section 5.3, we assume that the temperature of the thermal bath is given by $T = a/(2\pi)$, where a is the proper acceleration at the centre of the hypertor trajectory (5.8). Hence, $a = 0$ corresponds to circular motion in the x-y plane through the Minkowski vacuum in both scenarios.

5.4.1 Small-gap limit

We begin our comparison with the regime of small energy gaps, as analysed in Section 5.2.1 and Section 5.3.1. As the integral expressions for the response functions in the two cases were amenable to the same techniques, we were able to find series the expansions (5.21) and (5.56). As such, the small-energy-gap behaviour of the transition rate is determined by the behaviour of the integrals Γ_0 (5.15) and $\tilde{\Gamma}_0$ (5.57). These coefficients also determine the leading-order behaviour of the effective temperatures of the detectors (5.27) and (5.59) in this regime. Therefore, we now direct our attention towards comparing Γ_0 and $\tilde{\Gamma}_0$.

We investigate these differences numerically. In Figure 5.1i, we use the orbital radius as a characteristic length scale and plot $R\Gamma_0$ and $R\tilde{\Gamma}_0$ as functions of the dimensionless variables Ra and $R\Omega$. For trajectories with low circular motion speeds $R\Omega \ll 1$, the two coefficients match. This is expected on geometric grounds as, in this limit, the trajectories approach either a uniformly linearly accelerated detector or a static detector in a thermal bath, the known duality due to the Unruh effect. Furthermore, the two coefficients also match in the limit of small accelerations/low initial thermal state temperatures. This is also expected as both motions reduce to uniform circular motion interacting with the Minkowski vacuum in $3{+}1$ Minkowski spacetime. We find that the leading-order

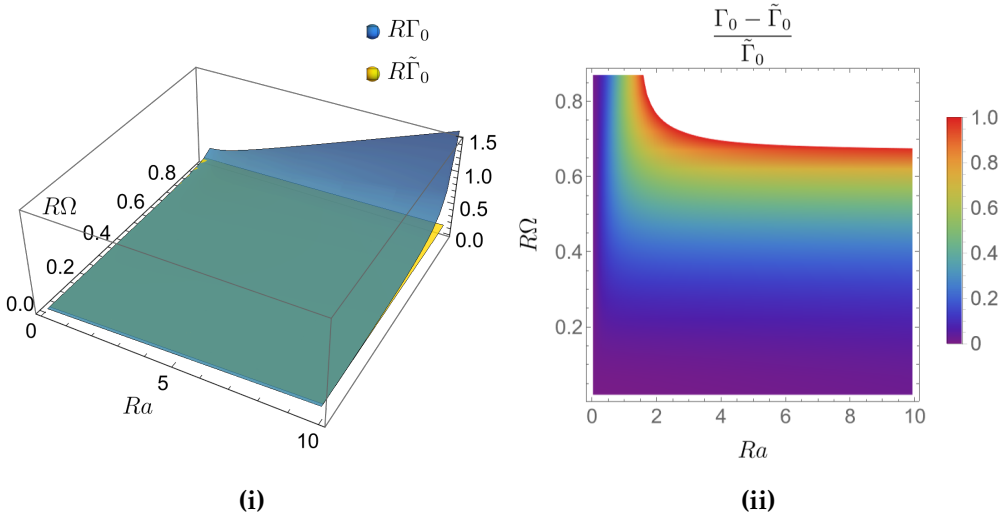

Figure 5.1: Comparison of the leading-order coefficients in the expansion of $\mathcal{F}(E)$ for detectors undergoing hypertor motion (Γ_0) and circular motion in a thermal bath of temperature $a/2\pi$ ($\tilde{\Gamma}_0$), where a is the uniform acceleration parameter of the hypertor. **(i)** $R\Gamma_0$ and $R\tilde{\Gamma}_0$ as a function of Ra and $R\Omega$ with plotting range $0 \leq R\Omega \leq 0.91$ and $0 \leq Ra \leq 10$. **(ii)** The normalised relative difference between Γ_0 and $\tilde{\Gamma}_0$ as a function of Ra and $R\Omega$ with plotting range $0 \leq R\Omega \leq 0.86$ and $0 \leq Ra \leq 10$. The white region represents when the normalised relative difference is greater than one.

contribution to $\mathcal{F}_{\text{H}}(E)$ (T_{H}) is always larger than the leading-order contribution to $\mathcal{F}_{\text{TB}}(E)$ (T_{TB}) and the discrepancy between the two cases grows as $R\Omega \to 1$.

Overall, one sees that particle detectors with small energy gaps would be able to distinguish between circular motion interacting with a field initially prepared in a thermal state at temperature $a/2\pi$ and a hypertor trajectory interacting with the Minkowski vacuum. The detectors may distinguish the two cases more clearly when the angular velocity Ω is large compared to $1/R$. In Figure 5.1ii, we plot the normalised relative difference between Γ_0 and $\tilde{\Gamma}_0$. This highlights the regions of parameter space where the two coefficients, and hence two motions, are most dissimilar. For small accelerations/low initial state temperatures, there is a region where the two coefficients differ by less than 10%. Furthermore, for low speeds $R\Omega \lesssim 0.1$, one may notice how similar the two motions are. As the ratio $(\Gamma_0 - \tilde{\Gamma}_0)/\tilde{\Gamma}_0$ is always positive, we find that the leading-order coefficient to the response function of a detector undergoing hypertor motion probing the Minkowski vacuum is larger than that of a detector undergoing circular motion probing a scalar field initially in a thermal state.

5.4.2 Small-radius limit

We now compare the experience of the detector undergoing hypertor motion and circular motion in a thermal bath in the limit of small orbital radii.

As established in Section 5.2 and Section 5.3, the Wightman function in both cases exhibits the same Hadamard short-distance distributional behaviour. As such, the difference in the two Wightman functions is itself a regular function. This is similar to the state-subtraction method when one renormalises, say, a stress-energy tensor in semiclassical gravity. Therefore, we use this to compare the transition rates of the two motions.

We write the difference in transition rates as

$$\begin{aligned}\Delta\mathcal{F}(E) &:= \mathcal{F}_{\text{H}}(E) - \mathcal{F}_{\text{TB}}(E)\,, \\ &= \int_{\mathbb{R}} \mathrm{d}\tau\, \mathrm{e}^{-\mathrm{i}E\tau}(\mathcal{W}_{\text{H}}(\tau) - \mathcal{W}_{\text{TB}}(\tau))\,. \end{aligned} \tag{5.66}$$

Should we be able to find a limiting form of $\Delta\mathcal{F}$ (5.66), we would then be able to find a limiting form of $\mathcal{F}_{\text{TB}}(E) = \mathcal{F}_{\text{H}}(E) - \Delta\mathcal{F}(E)$ in the limit of small R, using the results of (5.41).

We use the dimensionless variables defined in (5.33) to write the difference in the transition rates as

$$\begin{aligned}\Delta\mathcal{F}(E) \;=\; \frac{\gamma\Omega}{8\pi^2}\int_0^\infty \mathrm{d}z\, \cos(\varpi z)\Bigg(&\frac{\alpha^2-\rho^2}{\rho^2\sin^2(z)-\sinh^2(\alpha z)} \\ &- \frac{(\alpha^2-\rho^2)\,\mathrm{cosec}(z)\sinh(2\rho\sin z)}{\rho(\cosh(2\rho\sin z)-\cosh(2\alpha z))}\Bigg)\,. \end{aligned} \tag{5.67}$$

The two terms in the integrand in (5.67) have each a single singularity on the real line at $z = 0$, whose behaviours are given by (5.12) and (5.55), which cancel each other out, ensuring the integrand is regular in a neighbourhood around $z = 0$. Furthermore, each term exhibits exponential decay for large z due to the terms $\sinh^2(\alpha z)$ and $\cosh(2\alpha z)$, which is strong enough to bound the remainder term from Taylor's theorem as in Section 5.2.3. Hence, we perform a small-ρ expansion within the integral. Indeed, we find

$$\begin{aligned}&\frac{\alpha^2-\rho^2}{\rho^2\sin^2(z)-\sinh^2(\alpha z)} - \frac{(\alpha^2-\rho^2)\,\mathrm{cosec}(z)\sinh(2\rho\sin z)}{\rho(\cosh(2\rho\sin z)-\cosh(2\alpha z))} \\ &\qquad = \frac{2\alpha^2\rho^2}{3}\frac{\sin^2(\alpha z)}{\sinh^2(z)} + \mathcal{O}(\rho^4)\,, \end{aligned} \tag{5.68}$$

where the left-hand side is the integrand in (5.67).

Using the expansion (5.68) within the integral (5.67), the leading-order be-

haviour of $\Delta\mathcal{F}(E)$ is given by

$$\Delta\mathcal{F}(E) \;=\; \frac{\gamma\Omega\alpha^2\rho^2}{12\pi}\int_0^\infty \cos(\varpi z)\frac{\sin^2(z)}{\sinh^2(\alpha z)} + \mathcal{O}(\rho^4)\,, \tag{5.69}$$

which may be evaluated in terms of elementary functions. In dimensionful variables, the leading-order small-R asymptotic behaviour of $\Delta\mathcal{F}(E)$ (5.66) is given by

$$\Delta\mathcal{F}(E) \;=\; \frac{a^3R^2}{48\pi}\left(g\left(\frac{E+\Omega}{a}\right)+g\left(\frac{E-\Omega}{a}\right)-2g\left(\frac{E}{a}\right)\right)+\mathcal{O}(R^4)\,, \tag{5.70}$$

where $g(u) = u\coth(\pi u)$. One may show that $g(u+v)+g(u-v)-2g(u)\geq 0$ with equality if and only if $v=0$; hence, as the difference in response functions between hypertor motion and circular motion through a thermal bath is positive, it follows that the transition rate for the hypertor motion is larger than that for circular motion in a thermal bath. As expected, the order unity terms cancel each other out and are therefore given by the leading term in (5.41), which recovers the Unruh effect.

We plot in Figure 5.2 the (dimensionless) leading-order coefficient of the difference in response function (5.70). We see that a detector is only able to distinguish between hypertor motion and circular motion through a thermal bath if $|E|\lesssim\Omega$; whereas, for $|E|\gtrsim\Omega$, the difference $\Delta\mathcal{F}(E)$ (5.70) quickly decays. We recall that we found in Chapter 3 a similar behaviour, in which a detector may not distinguish between circular motion in a $2+1$ thermal bath and inertial motion when probing with an energy gap larger than the its rotational frequency, $|E|\gtrsim\Omega$.

We may use the difference in transition rates (5.66) to compute the leading-order behaviour of the difference in effective temperatures (2.54) in the small-radius limit. We note the following. Given the results of Section 5.2.3, we know that both response functions may be written as a small perturbation about the response function for a uniformly linearly accelerated observer,

$$\mathcal{F}(E) \;=\; \mathcal{F}_a(E) + R^2\delta\mathcal{F}(E)\,, \tag{5.71}$$

where $\mathcal{F}_a(E)$ is the response function for a uniformly linearly accelerated detector given by (2.51) and $\delta\mathcal{F}(E)$ is order unity as $R\to 0$. Furthermore, $\delta\mathcal{F}(E)$ is an even function of E, which follows from the evenness of $g(u)$ in (5.70) and (5.41).

The effective temperature (2.54) for a response function of the form (5.71) may

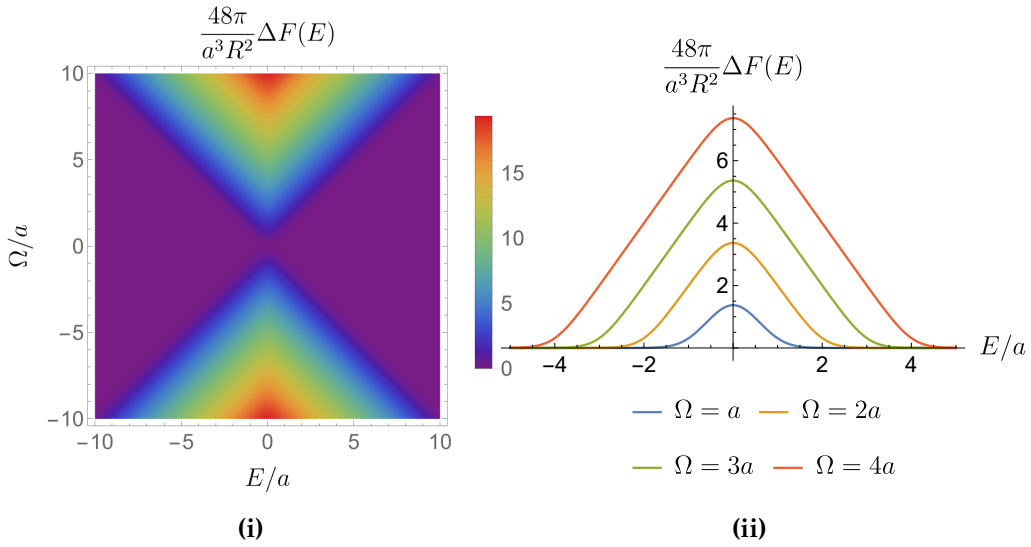

Figure 5.2: Leading-order correction coefficient to the transition rate difference in (5.70). **i)** Density plot of the leading-order coefficient with plotting ranges $-10 \leq E/a \leq 10$, $-10 \leq \Omega/a \leq 10$. **ii)** Horizontal slices from a) for fixed angular velocities with plotting range $-5 \leq E/a \leq 5$.

be expanded as a series in R as

$$T(E) \;=\; T_U + R^2\delta\mathcal{F}(E)\left(\frac{1}{\mathcal{F}_a(E)} - \frac{1}{\mathcal{F}_a(-E)}\right)\frac{T_U}{\ln\left(\frac{\mathcal{F}_a(-E)}{\mathcal{F}_a(E)}\right)} + \mathcal{O}(R^3)\,, \qquad (5.72)$$

where $T_U = a/2\pi$ is the Unruh temperature. For excitations $E > 0$, the correction to the Unruh temperature is positive, since $\mathcal{F}_a(-E) \geq \mathcal{F}(E)$ for $E > 0$.

As the factor multiplying $\delta\mathcal{F}(E)$ in (5.72) is the same for both hypertor motion and circular motion through a thermal bath, we may appeal to the difference in response functions $\Delta\mathcal{F}$ (5.70) by considering the difference in effective temperatures, $\Delta T \;=\; T_{\text{H}} - T_{\text{TB}}$,

$$\Delta T \;=\; R^2\Delta\mathcal{F}(E)\left(\frac{1}{\mathcal{F}_a(E)} - \frac{1}{\mathcal{F}_a(-E)}\right)\frac{T_U}{\ln\left(\frac{\mathcal{F}_a(-E)}{\mathcal{F}_a(E)}\right)} + \mathcal{O}(R^3)\,. \qquad (5.73)$$

We remark that the expression for ΔT (5.73) does not depend on the sign of E.

The difference in effective temperatures experienced by both detectors in the small-radius limit is proportional to both the Unruh temperature T_U and to the difference in transition rates of the detectors. Since $\Delta\mathcal{F}(E)$ is a positive function, the hypertor transition rate is always larger than the circular motion transition rate. We may, therefore, conclude that the temperature experienced by a detector undergoing hypertor motion will always be larger than that of a detector undergoing circular motion through a thermal bath for small orbital radii.

5.4.3 Large-gap limit

We now compare the two motions in the asymptotic regime of large detector energy gaps. In this Section, we consider the large-gap expansions of Section 5.2.4 and Section 5.3.2 and ask how the leading-order terms in these expansions compare in two further regimes. We show that the resulting detector responses are indistinguishable to leading order in the limits of small Ra and small $v \coloneqq R\Omega$.

The large-gap asymptotic behaviours of the transition rates for both the hypertor motion and circular motion in a thermal bath depend on the roots of transcendental equations. For completeness, we reproduce these equations in full.

In hypertor motion, we need to find the smallest, positive root of

$$\sin\left(\frac{Ra}{v}\mu\right) \;=\; Ra\sinh(\mu)\,. \tag{5.74}$$

In circular motion through a thermal bath, depending on whether $T > T_{\text{crit}}$ or $T < T_{\text{crit}}$, we need to find the smallest, positive root of

$$v \;=\; 2RT\mu_- + 2RTv\sinh(\mu_-)\,, \qquad T > T_{\text{crit}}\,, \tag{5.75a}$$

$$\mu_+ \;=\; v\sinh(\mu_+)\,, \qquad T < T_{\text{crit}}\,, \tag{5.75b}$$

where T_{crit} is the solution of

$$\frac{1}{4RT_{\text{crit}}} \;=\; \sinh\left(\frac{v}{4RT_{\text{crit}}}\right)\,. \tag{5.76}$$

We consider the limits of small acceleration/low ambient temperature and small velocity. In the former, one expects the two motions to tend to circular motion in $3+1$ Minkowski spacetime through the Minkowski vacuum. Geometrically, in the case of small velocities, hypertor motion tends to an accelerated trajectory and circular motion tends to a static trajectory. As such, the duality between an accelerated trajectory and a static trajectory in a thermal bath — the Unruh effect — appears.

5.4.3.1 Small acceleration parameter

We consider first the limit of a small acceleration, $a \to 0$ with all other parameters of motion fixed.

We consider first the hypertor motion transcendental equation (5.74). Rewriting (5.74) as

$$\frac{\sin(Rav^{-1}\mu)}{Rav^{-1}\mu} \;=\; \frac{\sinh(\mu)}{v^{-1}\mu}\,, \tag{5.77}$$

it is clear that in the limit $a \to 0$, (5.77) tends to

$$\mu \;=\; v \sinh(\mu)\,. \tag{5.78}$$

For timelike trajectories with $0 < v < 1$, Equation 5.78 has three solutions: one on the positive real line, zero, and a further solution on the negative real line — for more details, see Proposition 5.3 and its proof in Section E.3. We are only interested in the positive solution. Furthermore, (5.78) is identical to the circular motion transcendental equation for $T < T_{\text{crit}}$ (5.75b). Therefore, $\mu \to \mu_+$ as $a \to 0$.

To further compare the two scenarios, we rewrite the hypertor correction to inertial motion (5.48) using the double-angle formulae for $\sin$ and $\sinh$ as

$$\begin{aligned}\mathcal{F}_{\text{H}}^{\text{corr}}(E) \;&\sim\; \frac{a^2}{4\pi\gamma\Omega}\frac{\mathrm{e}^{-2\frac{|E|\mu}{\gamma\Omega}}}{\rho^2\sinh(2\mu)-\alpha\sin(2\alpha\mu)}\,,\\ &=\; \frac{a^2}{8\pi\gamma\Omega}\frac{\mathrm{e}^{-2\frac{|E|\mu}{\gamma\Omega}}}{\rho^2\sinh(\mu)\cosh(\mu)-\alpha\sin(\alpha\mu)\cos(\alpha\mu)}\,.\end{aligned} \tag{5.79}$$

The positive solution to (5.74) is bounded in the limit $a \to 0$, such that $a\mu \to 0$ in this limit. We can therefore use the small-angle approximation $\alpha\sin(\alpha\mu)\cos(\alpha\mu) \approx \alpha^2\mu$, which in combination with the defining equation (5.78) lead to $\alpha\sin(\alpha\mu)\cos(\alpha\mu) \approx \alpha^2 R\Omega\sinh(\mu)$. This remark along with the definition $\alpha = a/\Omega$ allow us to write the response rate (5.79) as

$$\mathcal{F}_{\text{H}}^{\text{corr}}(E) \;\sim\; \frac{1}{8\pi\gamma R}\frac{\mathrm{e}^{-2\frac{|E|\mu}{\gamma\Omega}}}{\sinh\mu(R\Omega\cosh\mu-1)}\,. \tag{5.80}$$

This is the response rate for a detector in circular motion in a $3+1$ thermal bath given by (5.64) with the identification $\mu_+ \mapsto \mu$. In addition, the effective temperatures of the two motions agree to leading order since $\mu \to \mu_+$ as $a \to 0$. Therefore, in the limit of small accelerations/low ambient temperatures, we reconcile the experience of a UDW detector undergoing hypertor motion probing a quantum scalar field in the Minkowski vacuum with that of a detector undergoing uniform circular motion probing a quantum scalar field in a thermal state in temperature $T = a/(2\pi) < T_{\text{crit}}$.

5.4.3.2 Small circular velocity

We consider now the limit of small circular velocities $v = R\Omega \to 0$ with all other parameters fixed.

We consider first the circular motion through a thermal bath. We begin first with two propositions.

Proposition 5.3. *Let* $0 < v < 1$ *and* $f_v(z) = \sinh(vz) - z$. *The equation*

$$f_v(z) \;=\; 0\,, \tag{5.81}$$

has three roots, $z = \pm z_0$ *and* 0, *where* $z_0 > 0$. *Further,* $z_0 \to \infty$ *as* $v \to 0$.

Proof. See Appendix E, Section E.3. □

Proposition 5.4. *Let* $0 < v < 1$ *and* $f_v(z) = \sinh(vz) - z$. *The leading-order behaviour of the positive root* z_0 *of the equation*

$$f_v(z) \;=\; 0\,, \tag{5.82}$$

is given by

$$z_0 \;\sim\; -\frac{1}{v} W_{-1}\Big(-\frac{v}{2}\Big)\,, \tag{5.83}$$

as $v \to 0$, *where* W_{-1} *is the lower branch of the Lambert* W *function.*

Proof. See Appendix E, Section E.4. □

We can find an estimate for the critical temperature (5.76) by noting that it is of the form $z = \sinh(z)$, where $z = (4RT_{\text{crit}})^{-1}$, and we may appeal to Proposition 5.3 and Proposition 5.4. In the limit of small velocities $v \to 0$, we have the estimate

$$T_{\text{crit}} \;\sim\; -\frac{v}{4RW_{-1}\big(-\frac{v}{2}\big)}\,. \tag{5.84}$$

By either (5.84) or Proposition 5.3, we have $T_{\text{crit}} \to 0$ as $v \to 0$. As such, for any fixed ambient temperature T as $v \to 0$, we have $T > T_{\text{crit}}$ and only the behaviour of μ_- in (5.75a) need be considered.

Considering (5.75a), we see that as $v \to 0$, the left-hand side tends to zero. As such, the right-hand side must be small. However, the right-hand side is positive for μ_-. As such μ_- must be small. We make the Ansatz $\mu_- = a_1 v + a_2 v^2 + a_3 v^3 + \mathcal{O}(v^4)$. Under this Ansatz, we find the solution

$$\mu_- \;=\; \frac{1}{2RT}(v - v^2 + v^3) + \mathcal{O}(v^4)\,. \tag{5.85}$$

For completeness, we comment on the behaviour of μ_+, the positive solution to (5.75b), in the limit $v \to 0$. Dividing by v, this equation may be written as $y = \sinh(vy)$, where $y = \mu_+/v$. As such, we may appeal to Proposition 5.3

and Proposition 5.4, leading to $y \sim -v^{-1}W_{-1}(-\frac{v}{2})$. In terms of μ_+, we have

$$\mu_+ \;\sim\; -W_{-1}\Big(-\frac{v}{2}\Big)\,. \tag{5.86}$$

We consider now the large-gap detailed balance effective temperature (5.65) for a detector in circular motion through a thermal bath and recall that, depending on the magnitude of the ambient temperature T with respect to a critical temperature T_{crit}, we have that the detailed balance temperature T_{TB} is proportional to either μ_-^{-1} ($T > T_{\text{crit}}$) or μ_+^{-1} ($T < T_{\text{crit}}$).

As $\mu_+ \to \infty$ (5.86), we have $T_{\text{TB}} \to 0$ for $T < T_{\text{crit}}$. However, using (5.85), for $T > T_{\text{crit}}$, we find

$$\begin{aligned} T_{\text{TB}} \;&=\; \frac{\gamma\Omega R T}{v(1-v+v^2)} + \mathcal{O}(v^3)\,, \\ &=\; T\Big(1+v+\frac{1}{2}v^2\Big) + \mathcal{O}(v^3)\,, \end{aligned} \tag{5.87}$$

the detector acts as a thermometer for the thermal bath.

We consider now the same limit to find an expansion for the first positive root of (5.74). For small v, we anticipate μ to be small; however, due to the oscillatory nature of the left-hand side of (5.74), we also anticipate $Rav^{-1}\mu$ to be close to π. As such, we write $z = \pi - Rav^{-1}\mu$ and (5.74) reduces to

$$\sin(z) \;=\; Ra\sinh\Big(\frac{v}{Ra}(\pi - z)\Big)\,, \tag{5.88}$$

where z is considered small. We consider an Ansatz of the form $z = a_1 v + a_2 v^2 + \mathcal{O}(v^3)$. Expanding (5.88) in small arguments, we find $z = \pi(v - v^2) + \mathcal{O}(v^3)$, such that

$$\mu \;=\; \frac{v\pi}{Ra}(1 - v + v^2) + \mathcal{O}(v^4)\,. \tag{5.89}$$

Combining this with the large-gap detailed balance effective temperature (5.49), one finds

$$\begin{aligned} T_{\text{H}} \;&=\; \frac{\gamma\Omega Ra}{2\pi v(1-v+v^2)} + \mathcal{O}(v^3)\,, \\ &=\; \frac{a}{2\pi}\Big(1+v+\frac{1}{2}v^2\Big) + \mathcal{O}(v^3)\,. \end{aligned} \tag{5.90}$$

We identify the leading-order contribution as the Unruh temperature T_U.

We unify the effective temperatures (5.87) and (5.90) through the Unruh temperature T_U: a detector with a large energy gap undergoing circular motion with a small circular velocity v through a thermal bath of temperature $T = a/(2\pi)$ perceives an effective temperature equal to that of a detector undergoing hypertor

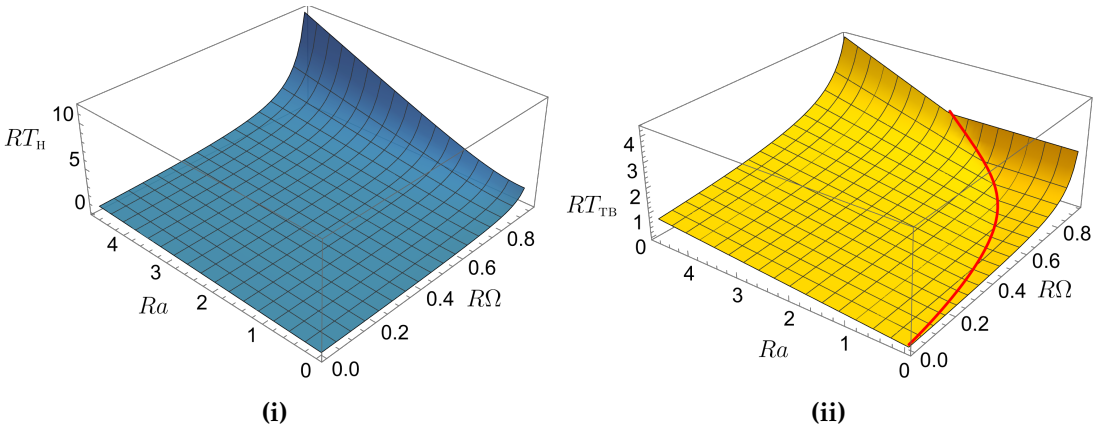

Figure 5.3: Effective temperature experienced by a detector undergoing i) hypertor motion and ii) circular motion in a $3+1$ thermal bath in the large-gap limit as functions of dimensionless variables Ra and $R\Omega$. **i)** Effective temperature experienced by a detector in hypertor motion interacting with the Minkowski vacuum. The plotting range is $0 \leq Ra \leq 4.8$, $0 \leq R\Omega \leq 0.91$. **ii)** Effective temperature experienced by a detector in circular motion interacting with a scalar field initially prepared in a thermal state. The plotting range is $0 \leq Ra \leq 4.8$, $0 \leq R\Omega \leq 0.91$. A red line is shown at parameter values satisfying $T = T_{\text{crit}}$ where $T_{\text{crit}} = a_{\text{crit}}/2\pi$.

motion with a proper acceleration at the centre of a and a small circular velocity v. Remarkably, the two agree to the first three orders.

5.4.3.3 Numerical results

In Figure 5.3, we plot the effective temperatures experienced by detectors undergoing the two motions analysed in Section 5.2, Section 5.3, and Section 5.4. The effective temperatures are plotted as functions of the dimensionless variables Ra and $R\Omega$. In Figure 5.3i, we plot the effective temperature experienced by a detector undergoing hypertor motion. In Figure 5.3ii, we plot the effective temperature experienced by a detector undergoing circular motion in a $3+1$ thermal bath at temperature $T = a/(2\pi)$, where a is the proper acceleration of an observer at the centre of the hypertor motion. A red line in Figure 5.3ii corresponds to the critical temperature (5.76), across which the leading-order behaviour of the effective temperature changes in the large-gap limit.

5.5 Discussion

In this Chapter, motivated by the duality between the experience of an observer in uniform linear acceleration with proper acceleration a and an observer at rest in a thermal bath at temperature $T = a/(2\pi)$ in $(3+1)$-dimensional Minkowski spacetime, we analysed how far this duality holds when both observers also

undergo uniform circular motion. This is described by two scenarios, first the combination of linear acceleration and circular motion in the plane orthogonal to the acceleration — a stationary motion known as hypertor motion — and second, circular motion through a thermal bath. To compare the two cases, we considered the same orbital radius R and angular speed Ω for both. Furthermore, we fixed the temperature of the thermal bath at $T = a/(2\pi)$, where a is the proper acceleration of an observer at the centre of the hypertor motion. As such, in the limit of vanishing circular velocities, one recovers the Unruh effect.

We compared the two scenarios in three analytically accessible asymptotic regimes: small energy gaps, small orbital radii, and large energy gaps. In general, we found that the addition of circular motion breaks this duality over much of the parameter space.

We were able to reconcile the two motions when the parameters of the circular motion were small, or if the acceleration parameter a was small, as expected on geometric grounds. By contrast, over much of the parameter space, the two situations exhibit stark differences. In the regimes of small energy gaps and small orbital radii, we found that the effective temperature experienced by an observer undergoing hypertor motion is always higher than that experienced by an observer undergoing circular motion in a $3+1$ thermal bath at temperature $T = a/2\pi$.

In the limit of small orbital radii, we found the detector transition rate and effective temperature to leading order and a subleading correction at order R^2. We found that the orbital frequency of the circular motion Ω plays a key role in the ability of an observer to distinguish between the two motions in this regime. In particular, for $|E| \lesssim \Omega$, a detector may distinguish between the two scenarios. However, for $|E| > \Omega$, the subleading corrections at order R^2 quickly become indistinguishable. This is reminiscent of the comparison of circular motion and inertial motion through a $2+1$ thermal bath in Chapter 3, in which, for $R|E| > R\Omega = v$, a detector may not distinguish between the two motions.

An interesting result was that in the limit of large energy gaps, if one further considers the limit of small velocities, the effective temperatures experienced by an observer in each motion agree to the first three orders.

In summary, while a particle detector interacting with a massless scalar field in $3+1$ Minkowski spacetime would be unable to distinguish between a thermal bath at temperature $T = a/2\pi$ and uniform linear acceleration with proper acceleration a, we found that the addition of circular motion breaks this duality. Any circular motion perturbation around these two motions enables a particle detector to distinguish between a thermal bath and a temperature provided by linear acceleration across most of the parameter space.

All motions considered until now, inertial motion, linear acceleration, circular motion, and hypertor motion, are all stationary trajectories in Minkowski spacetime. All stationary trajectories in $3+1$ Minkowski spacetime were found and classified by Letaw in 1980 [71]. In Chapter 6, we extend this and classify the stationary trajectories in Minkowski spacetimes of all dimensions.

Chapter 6

Interlude — Stationary trajectories in Minkowski spacetimes

"L'algèbre n'est qu'une géométrie écrite; la géométrie n'est qu'une algèbre figurée."
(Algebra is but written geometry; geometry is but figured algebra.)

Sophie Germain

At the heart of the Unruh effect, as introduced in Chapter 2, lie two trajectories, inertial motion and uniform linear acceleration. We studied two further trajectories, uniform circular motion and hypertor motion, in Chapter 3 and Chapter 5. All four trajectories have the property that the Wightman function with respect to a stationary state, pulled back to one of these trajectories, is a function of the difference in proper time along that trajectory only. As an equation, this is concisely and concretely given by (2.42).

These four trajectories are, furthermore, the integral curves of timelike Killing vectors and the solutions with constant curvature of the Lorentz-signature Frenet-Serret equations due to Letaw [71]. In $3+1$ dimensions, there are two further trajectories with these properties, the catenary and the semicubical parabola. Together, these six trajectories constitute the family of stationary trajectories in $3+1$ Minkowski spacetime. In this Chapter, we extend this classification to Minkowski spacetimes of arbitrary dimension. In line with the deep connection between algebra and geometry outlined in the quotation by Sophie Germain in this chapter's epigraph, we perform this classification both algebraically and geometrically. Algebraically, we classify the conjugacy classes of the Poincaré group, the isometry group of Minkowski spacetime, in terms of its Lie algebra

of Killing vectors and specialise to the timelike Killing vectors, which gives rise to a classification of stationary trajectories. Geometrically, we extend the Frenet-Serret formalism in $3+1$ Minkowski spacetime to $n+1$ Minkowski spacetime. We find a formula for the number of classes of timelike trajectories in $n+1$ Minkowski spacetime, as well as find an ordinary differential equation satisfied by the generalised four-velocity of the stationary trajectories.

Except Section 6.4, the contents of this Chapter were extracted from, or based on, the journal article "Stationary trajectories in Minkowski spacetimes" [4].

6.1 Curves of constant curvature

The classification of stationary trajectories in $3+1$ Minkowski spacetime originates in the work of Letaw [71], who in 1981 found that the stationary trajectories could either be defined as the timelike solutions to the Frenet-Serret equations with constant (in proper time) curvature invariants or equivalently as the orbits of timelike Killing vectors. However, the study of curves defined in terms of their curvature invariants first began with the work of Frenet [147] and Serret [148] in three-dimensional, flat, Euclidean-signature space with the standard metric. Frenet and Serret found a coupled set of differential equations for the tangent vector, normal vector, and binormal vector, which together form an orthonormal basis in $\mathbb{R}^3$. These differential equations are known as the Frenet-Serret equations and were later generalised by Jordan [149] to flat, Euclidean spaces of arbitrary dimension.

Our interest in stationary worldlines in Minkowski spacetime follows from the property that the Wightman function with respect to a stationary state, pulled back to a stationary trajectory, is a function of only the difference in proper time along that trajectory. This property has been further employed in formulating quantum energy inequalities [150–152].

We now briefly introduce the Frenet-Serret equations in three dimensions.

6.1.1 Frenet-Serret equations

In three-dimensional Euclidean space $\mathbb{R}^3$ with the standard metric $\mathrm{d}s^2 = \mathrm{d}x^2 + \mathrm{d}y^2 + \mathrm{d}z^2$, any differentiable curve $\boldsymbol{\alpha}$ may be parametrised by its arc length s. With this parametrisation, the curve $\boldsymbol{\alpha}(s)$ has a unit tangent vector,

$$||\boldsymbol{\alpha}'(s)|| \;=\; 1\,, \tag{6.1}$$

where a prime denotes differentiation with respect to the arc length s and $||\cdot||$ is the standard norm in $\mathbb{R}^3$. In spaces with Lorentzian signature, there are two natural analogous choices. First, spacelike curves x^μ may be parametrised by their proper length ℓ, in which case $u^\mu := \frac{\mathrm{d}\mathsf{x}^\mu}{\mathrm{d}\ell}$ has norm $u^\mu u_\mu = 1$. Second, timelike curves x^μ may be parametrised by their proper time τ, in which case $u^\mu := \frac{\mathrm{d}\mathsf{x}^\mu}{\mathrm{d}\tau}$ has norm $u^\mu u_\mu = -1$. In what follows, we assume that the curve $\boldsymbol{\alpha}$ is non-degenerate, $\boldsymbol{\alpha}''(s) \neq 0$ [153].

There are three vector quantities of interest that may be constructed from $\boldsymbol{\alpha}$, the tangent vector $\boldsymbol{T}$, the (unit) normal vector $\boldsymbol{N}$, and the binormal vector $\boldsymbol{B}$,

$$\boldsymbol{T}(s) := \frac{\mathrm{d}\boldsymbol{\alpha}(s)}{\mathrm{d}s}\,, \tag{6.2a}$$

$$\boldsymbol{N}(s) := \frac{1}{\left|\left|\frac{\mathrm{d}^2\boldsymbol{\alpha}(s)}{\mathrm{d}s^2}\right|\right|}\frac{\mathrm{d}^2\boldsymbol{\alpha}(s)}{\mathrm{d}s^2}\,, \tag{6.2b}$$

$$\boldsymbol{B}(s) := \boldsymbol{T}(s)\times\boldsymbol{N}(s)\,. \tag{6.2c}$$

We remark that by the assumption of non-degeneracy, $\boldsymbol{\alpha}''(s) \neq \boldsymbol{0}$ and so the unit normal is well defined.

We show now that the tangent, normal, and binormal vectors (6.2) form an orthonormal set. By (6.1), we have $||\boldsymbol{T}(s)||^2 = \boldsymbol{T}(s)\cdot\boldsymbol{T}(s) = 1$. Differentiating this relation with respect to s and using the commutativity of the dot product, we have $\boldsymbol{T}'(s)\cdot\boldsymbol{T}(s) = 0$. By (6.2), we see $\boldsymbol{N}(s) \propto \boldsymbol{T}'(s)$. Therefore, the tangent and normal vectors are orthogonal, $\boldsymbol{T}(s)\cdot\boldsymbol{N}(s) = 0$. Hence, by definition of the binormal vector (6.2), the three vectors are mutually orthogonal. By (6.1), we have $||\boldsymbol{T}(s)|| = 1$ and by definition $||\boldsymbol{N}(s)|| = 1$. As $\boldsymbol{T}$ and $\boldsymbol{N}$ are orthogonal unit vectors, it follows that $||\boldsymbol{B}(s)|| = 1$. Therefore, the three vectors (6.2) are orthonormal and form a basis in $\mathbb{R}^3$.

We now define the *curvature* of the curve $\kappa(s)$ to be the function of proportionality between the normal vector and the derivative of the tangent vector,

$$\frac{\mathrm{d}\boldsymbol{T}(s)}{\mathrm{d}s} = \kappa(s)\boldsymbol{N}(s)\,, \tag{6.3a}$$

$$\kappa(s) := \left|\left|\frac{\mathrm{d}^2\boldsymbol{\alpha}(s)}{\mathrm{d}s^2}\right|\right| = \left|\left|\frac{\mathrm{d}\boldsymbol{T}(s)}{\mathrm{d}s}\right|\right|. \tag{6.3b}$$

We consider now the definition of the binormal (6.2). Differentiating with respect to s, we have $\boldsymbol{B}'(s) = \boldsymbol{T}(s)\times\boldsymbol{N}'(s)$, since $\boldsymbol{T}'(s)\times\boldsymbol{N}(s) = 0$ by (6.3). Furthermore, it follows that $\boldsymbol{B}'(s)\cdot\boldsymbol{T}(s) = \boldsymbol{B}'(s)\cdot\boldsymbol{B}(s) = 0$. Therefore, the vector $\boldsymbol{B}'(s)$ must be proportional to the normal vector $\boldsymbol{N}(s)$ since the set $\{\boldsymbol{T}(s), \boldsymbol{N}(s), \boldsymbol{B}(s)\}$ forms an orthonormal basis. We call this function of proportionality the *torsion*

of the curve $\tau(s)$,

$$\frac{\mathrm{d}\boldsymbol{B}(s)}{\mathrm{d}s} \;=\; -\tau(s)\boldsymbol{N}(s)\,, \tag{6.4}$$

where the minus sign is by convention. We make now a few remarks. In the case $\tau(s) = 0$, we see the binormal vector is constant and the curve $\boldsymbol{\alpha}(s)$ must lie in the plane spanned by $\boldsymbol{T}(s)$ and $\boldsymbol{N}(s)$, known as the osculating plane. As such, we may interpret the torsion of a curve $\tau(s)$ as a measure of the failure of a curve to be planar.

Finally, we note that since the tangent, normal, and binormal vectors form an orthonormal basis, we have the following cyclic relations $\boldsymbol{B}(s) = \boldsymbol{T}(s) \times \boldsymbol{N}(s)$, $\boldsymbol{T}(s) = \boldsymbol{N}(s) \times \boldsymbol{B}(s)$, and $\boldsymbol{N}(s) = \boldsymbol{B}(s) \times \boldsymbol{T}(s)$. Differentiation of the final relation with respect to s, we have

$$\frac{\mathrm{d}\boldsymbol{N}(s)}{\mathrm{d}s} \;=\; \frac{\mathrm{d}\boldsymbol{B}(s)}{\mathrm{d}s} \times \boldsymbol{T}(s) + \boldsymbol{B}(s) \times \frac{\mathrm{d}\boldsymbol{T}(s)}{\mathrm{d}s}\,, \tag{6.5}$$

using (6.3) and (6.4) along with the cyclic relations, we have

$$\frac{\mathrm{d}\boldsymbol{N}(s)}{\mathrm{d}s} \;=\; -\kappa(s)\boldsymbol{T}(s) + \tau(s)\boldsymbol{B}(s)\,. \tag{6.6}$$

Together, (6.3), (6.4), and (6.6) are known as the Frenet-Serret equations,

$$\frac{\mathrm{d}\boldsymbol{T}(s)}{\mathrm{d}s} = \kappa(s)\boldsymbol{N}(s)\,, \tag{6.7a}$$

$$\frac{\mathrm{d}\boldsymbol{N}(s)}{\mathrm{d}s} = -\kappa(s)\boldsymbol{T}(s) + \tau(s)\boldsymbol{B}(s)\,, \tag{6.7b}$$

$$\frac{\mathrm{d}\boldsymbol{B}(s)}{\mathrm{d}s} = -\tau(s)\boldsymbol{N}(s)\,, \tag{6.7c}$$

which are often written in matrix form

$$\begin{pmatrix} \boldsymbol{T}' \\ \boldsymbol{N}' \\ \boldsymbol{B}' \end{pmatrix} \;=\; \begin{pmatrix} 0 & \kappa & 0 \\ -\kappa & 0 & \tau \\ 0 & -\tau & 0 \end{pmatrix} \begin{pmatrix} \boldsymbol{T} \\ \boldsymbol{N} \\ \boldsymbol{B} \end{pmatrix}\,, \tag{6.8}$$

where we have omitted the dependence on the arc length s.

A special class of solutions are the curves of constant curvature and torsion, which we demonstrate now through the following example.

Example 6.1 (Constant curvature invariants)**.** We consider now the Frenet-Serret equations (6.7) in the special case when κ and τ are constant. In this case, we may combine the Frenet-Serret equations into a single equation for the tangent $\boldsymbol{T}$,

$$\boldsymbol{T}'''(s) \;=\; -(\kappa^2 + \tau^2)\boldsymbol{T}'(s)\,. \tag{6.9}$$

The Ansatz $\boldsymbol{T}(s) = \boldsymbol{A}\mathrm{e}^{ims}$ leads to the characteristic equation

$$m^3 \;=\; (\kappa^2+\tau^2)m\,, \tag{6.10}$$

with solutions $m = 0, \pm\sqrt{\kappa^2+\tau^2}$. As such, we have

$$\boldsymbol{T}(s) \;=\; \boldsymbol{A}\cos(\sqrt{\kappa^2+\tau^2}\,s) + \boldsymbol{B}\sin(\sqrt{\kappa^2+\tau^2}\,s) + \boldsymbol{C}\,, \tag{6.11}$$

where $\boldsymbol{A}$, $\boldsymbol{B}$, and $\boldsymbol{C}$ are constant vectors. We choose initial conditions such that $\boldsymbol{T}(0) = \hat{\boldsymbol{x}}$, $\boldsymbol{N}(0) = \hat{\boldsymbol{y}}$, and $\boldsymbol{B}(0) = \hat{\boldsymbol{z}}$, which leads to

$$\boldsymbol{A} \;=\; \frac{\kappa^2}{\kappa^2+\tau^2}\hat{\boldsymbol{x}} - \frac{\kappa\tau}{\kappa^2+\tau^2}\hat{\boldsymbol{z}}\,,\quad \boldsymbol{B} \;=\; \frac{\kappa}{\sqrt{\kappa^2+\tau^2}}\hat{\boldsymbol{y}}\,,\quad \boldsymbol{C} \;=\; \frac{\tau^2}{\kappa^2+\tau^2}\hat{\boldsymbol{x}} + \frac{\tau\kappa}{\kappa^2+\tau^2}\hat{\boldsymbol{z}}\,, \tag{6.12}$$

where $\hat{\boldsymbol{x}}$, $\hat{\boldsymbol{y}}$, and $\hat{\boldsymbol{z}}$ form the standard basis in $\mathbb{R}^3$.

Applying an orthogonal transformation to the solution (6.11) and (6.12), we may consider the tangent vector in a different frame, which is equivalent to having chosen a different initial condition. We consider an orthogonal transformation of the form

$$\boldsymbol{T}(s) \;=\; \begin{pmatrix} \frac{A_x}{\alpha} & 0 & \frac{C_x}{\beta} \\ 0 & \frac{B_y}{\alpha} & 0 \\ \frac{A_z}{\alpha} & 0 & \frac{C_z}{\beta} \end{pmatrix} \begin{pmatrix} \alpha\cos(\sqrt{\kappa^2+\tau^2}\,s) \\ \alpha\sin(\sqrt{\kappa^2+\tau^2}\,s) \\ \beta \end{pmatrix}\,, \tag{6.13}$$

where α and β are real coefficients such that the matrix is an element of the orthogonal group $\mathrm{O}(3)$ and we clarify the notation $A_x \coloneqq \boldsymbol{A}\cdot\hat{\boldsymbol{x}}$, with the other matrix coefficients analogously defined. We denote by M the matrix in (6.13).

Imposing that M be orthogonal, $M \in \mathrm{O}(3)$, we find

$$\alpha \;=\; \frac{\kappa}{\sqrt{\kappa^2+\tau^2}}\,, \qquad\qquad \beta \;=\; \frac{\tau}{\sqrt{\kappa^2+\tau^2}}\,. \tag{6.14}$$

As $M \in \mathrm{O}(3)$, we have $M^{-1} = M^{\mathsf{T}} \in \mathrm{O}(3)$. From this, we can write the tangent vector $\boldsymbol{T}$ in the new frame as

$$M^{\mathsf{T}}\boldsymbol{T}(s) \;=\; \frac{1}{\sqrt{\kappa^2+\tau^2}} \begin{pmatrix} \kappa\cos(\sqrt{\kappa^2+\tau^2}\,s) \\ \kappa\sin(\sqrt{\kappa^2+\tau^2}\,s) \\ \tau \end{pmatrix}\,. \tag{6.15}$$

Finally, we recall the definition of the tangent vector (6.2). We may therefore

integrate (6.15) to find the constant curvature curve

$$\widetilde{\boldsymbol{\alpha}}(s) \;=\; \frac{1}{\kappa^2+\tau^2}\begin{pmatrix} \kappa\sin(\sqrt{\kappa^2+\tau^2}\,s) \\ -\kappa\cos(\sqrt{\kappa^2+\tau^2}\,s)+\kappa \\ \tau\sqrt{\kappa^2+\tau^2}\,s \end{pmatrix}, \tag{6.16}$$

where the notation $\widetilde{\boldsymbol{\alpha}} \coloneqq M^{\mathsf{T}}\boldsymbol{\alpha}$ emphasises that we are in a rotated frame and we have chosen the initial condition $\widetilde{\boldsymbol{\alpha}}(0) = \mathbf{0}$. In this rotated frame, it is clear that the curve has the geometry of a helix. ■

We bring this Section to a close by considering the degenerate curve, $\boldsymbol{\alpha}''(s) = \mathbf{0}$. Such a curve has vanishing curvature $\kappa(s) = 0$ and upon integration, one sees $\boldsymbol{\alpha}(s) = \boldsymbol{T}_0 s + \boldsymbol{\alpha}_0$, describing a planar curve. Hence, as torsion $\tau(s)$ is the measure of the failure of a curve to be planar, the curve must also have zero torsion. This property extends to the generalisation of the Frenet-Serret equations due to Jordan [149], in which one has generalised curvatures χ_i with $1 \leq i \leq n$ and $\chi_i = 0$ implies $\chi_j = 0$ for all $j \in \mathbb{N}$ such that $i < j \leq n$. In $\mathbb{R}^3$, we simply have $\chi_1 = \kappa$, $\chi_2 = \tau$ and $\chi_1 = 0$ implies $\chi_2 = 0$. In the following Sections, we will provide the framework for the Lorentzian-signature Frenet-Serret equations in $n+1$ dimensions.

6.2 Killing vectors in Minkowski spacetimes

Having introduced the Frenet-Serret equations in flat, Euclidean space in Section 6.1, we consider now their Lorentz-signature counterparts algebraically. The stationary trajectories are the timelike solutions to the (Lorentz-signature) Frenet-Serret equations with curvature invariants constant in proper time. Letaw [71] further demonstrated that the stationary trajectories of $3+1$ Minkowski spacetime may also be defined as the orbits of timelike Killing vectors. Due to the freedom in the choice of frame, each solution to the Frenet-Serret equations is determined only up to a Poincaré transformation of the worldline, leading to equivalence classes of trajectories. A trajectory generated by some Killing vector ξ is determined only up to conjugation of the generator of that Killing vector. In this Section, we determine the conjugacy classes of the Poincaré group, the isometry group of Minkowski spacetime, and then restrict our attention to the classes whose associated Killing vector is timelike, thereby classifying the stationary trajectories of $(n+1)$-dimensional Minkowski spacetime for $n \geq 1$.

6.2.1 Isometries of Minkowski spacetime

The isometry group of Minkowski spacetime $\mathbb{R}^{n,1}$ is the Poincaré group. We consider only the connected component of the Poincaré group, the restricted Poincaré group $\mathrm{ISO}^+(n,1)$, consisting of the connected component of the Lorentz group plus translations.

A general element of $\mathrm{ISO}^+(n,1)$ is a pair $g = (\Lambda, a)$, where Λ is an element of the restricted Lorentz group $\mathrm{SO}^+(n,1)$ and $a \in \mathbb{R}^{n,1}$. The restricted Lorentz group is the subgroup of Lorentz transformations preserving orientation and time orientation. The Poincaré group acts on $\mathbb{R}^{n,1}$ as follows. Let $g = (\Lambda, a) \in \mathrm{ISO}^+(n,1)$ and $\mathsf{x} \in \mathbb{R}^{n,1}$, then in components we have $g\,\mathsf{x}^\mu = \Lambda^\mu{}_\nu \mathsf{x}^\nu + a^\mu$. The Poincaré group is equipped with the group multiplication law $\widetilde{g} \cdot g = (\widetilde{\Lambda}, \widetilde{a}) \cdot (\Lambda, a) = (\widetilde{\Lambda}\Lambda, \widetilde{\Lambda}a + \widetilde{a})$ and inverse elements are given by $g^{-1} = (\Lambda^{-1}, -\Lambda^{-1}a)$.

The restricted Lorentz group is a subgroup of the restricted Poincaré group with elements $(\Lambda, 0)$. Pure spacetime translations $h = (\mathbb{1}, a)$ form a normal subgroup of the Poincaré group, which may be verified by explicitly computing $g \cdot h \cdot g^{-1}$. As such, this decomposes $\mathrm{ISO}^+(n,1)$ as a semidirect product, $\mathrm{ISO}^+(n,1) = \mathbb{R}^{n,1} \rtimes \mathrm{SO}^+(n,1)$. This structure as a semidirect product of Lie groups is inherited at the level of Lie algebras, $\mathfrak{iso}(n,1) = \mathbb{R}^{n,1} \rtimes \mathfrak{so}(n,1)$.

Given a Lie group G and associated Lie algebra $\mathfrak{g}$, G acts naturally on $\mathfrak{g}$ by conjugation, $G \times \mathfrak{g} \to \mathfrak{g}$, $(g, X) \mapsto gXg^{-1}$. We use a matrix group notation, anticipating its use in Section 6.2.3. We define a conjugacy class in the Lie algebra in the following sense $Y \sim X \iff \exists g \in G$ such that $Y = gXg^{-1}$.

When considering the Poincaré group acting on Minkowski spacetime, the generators of the Lie algebra $\mathfrak{iso}(n,1)$ are the Killing vector fields. A Killing vector field is the velocity vector field of a one-parameter isometry group at the identity. It is natural then to consider representations of these generators. The infinitesimal Poincaré transformation of a scalar field $\phi(\mathsf{x})$ leads to

$$\phi(\mathsf{x}) \;\to\; \phi(\mathsf{x}) - \left(a^\mu \partial_\mu + \tfrac{1}{2}\omega^{\mu\nu}(\mathsf{x}_\nu \partial_\mu - \mathsf{x}_\mu \partial_\nu)\right) \phi(\mathsf{x})\,, \tag{6.17}$$

where a^μ and $\omega^{\mu\nu}$ are constant and $\omega^{\mu\nu}$ is antisymmetric. This is the standard vector field representation and may be written as

$$\phi(\mathsf{x}) \;\to\; \left(1 - a^\mu P_\mu - \tfrac{1}{2}\omega^{\mu\nu} M_{\mu\nu}\right) \phi(\mathsf{x})\,, \tag{6.18}$$

where $P_\mu = \partial_\mu$ is the generator of spacetime translations and $M_{\mu\nu} = (\mathsf{x}_\nu \partial_\mu - \mathsf{x}_\mu \partial_\nu)$ is the generator of spacetime rotations.

Alternatively, Killing vectors $\xi = \xi^\mu \partial_\mu$ of a spacetime $\mathcal{M}$ are defined by,

$$\nabla_\mu \xi_\nu + \nabla_\nu \xi_\mu \;=\; 0\,. \tag{6.19}$$

Combining (6.19) with the Ricci identity, one may show the following identity holds [154]

$$\nabla_\mu \nabla_\nu \xi_\sigma \;=\; R^\rho{}_{\mu\nu\sigma}\xi_\rho\,. \tag{6.20}$$

In the case of Minkowski spacetime $\mathbb{R}^{n,1}$ in Minkowski coordinates, equations (6.19) and (6.20) reduce to the following,

$$\partial_\mu \xi_\nu + \partial_\nu \xi_\mu \;=\; 0\,, \tag{6.21a}$$

$$\partial_\mu \partial_\nu \xi_\sigma \;=\; 0\,. \tag{6.21b}$$

One may integrate (6.21b) and combine it with (6.21a) to write

$$\xi^\mu \;=\; c^\mu + \omega^{\mu\nu}\mathsf{x}_\nu\,, \tag{6.22}$$

where c^μ is a constant and $\omega^{\mu\nu}$ is antisymmetric, $\omega^{\mu\nu} = -\omega^{\nu\mu}$, leading to $\xi = c^\mu\partial_\mu + \frac{1}{2}\omega^{\mu\nu}(\mathsf{x}_\nu\partial_\mu - \mathsf{x}_\mu\partial_\nu)$.

With foresight, we define the following notation with $i < j$:

$$\mathrm{T}_0 \;=\; \partial_t\,, \tag{6.23a}$$

$$\mathrm{S}_i \;=\; \partial_i\,, \tag{6.23b}$$

$$\mathrm{NT}_{0i} \;=\; \partial_t - \partial_i\,, \tag{6.23c}$$

$$\mathrm{B}_{0i} \;=\; t\partial_i + x_i\partial_t\,, \tag{6.23d}$$

$$\mathrm{R}_{ij} \;=\; x_j\partial_i - x_i\partial_j\,, \tag{6.23e}$$

$$\begin{aligned}\mathrm{NR}_{0ij} \;&=\; \mathrm{B}_{0i} - \mathrm{R}_{ij}\,,\\ &=\; (t - x_j)\partial_i + x_i(\partial_t + \partial_j)\,,\end{aligned} \tag{6.23f}$$

where R_{ij} is the Killing vector associated with a rotation in the x^i–x^j plane, NR_{0ij} is the Killing vector associated with a null rotation consisting of a boost along the x^i–axis and a rotation in the x^i–x^j plane, B_{0i} is the Killing vector associated with a boost along the x^i–axis, T_0 is the Killing vector associated with a timelike translation, S_i is the Killing vector associated with a spacelike translation parallel to the x^i–axis, and NT_{0i} is the Killing vector associated with a null translation with spatial translation parallel to the x^i–axis.

Throughout this Chapter, we adopt the notation $\oplus$ to represent linear combinations of (6.23) with scalars suppressed. Explicitly, $\xi = \mathrm{T}_0 \oplus \mathrm{R}_{12}$ represents $\xi = a\partial_t + b(x_2\partial_1 - x_1\partial_2)$ with a, b both nonzero.

6.2.2 Conjugacy classes of the restricted Lorentz group

We recall that $\mathrm{ISO}^+(n,1)$ is a semidirect product of the restricted Lorentz group $\mathrm{SO}^+(n,1)$ and the group of spacetime translations $\mathbb{R}^{n,1}$. Owing to this decomposition, one may systematically approach determining the conjugacy classes of the Poincaré group by first classifying with the restricted Lorentz group and then considering the spacetime translations.

6.2.2.1 Conjugacy classes of the Möbius group

To classify the conjugacy classes of $\mathrm{SO}^+(n,1)$, we first consider the restricted Lorentz group in $3+1$ dimensions, $\mathrm{SO}^+(3,1)$, which is isomorphic to the projective special linear group in 2 dimensions with complex coefficients, $\mathrm{PSL}(2,\mathbb{C}) = \mathrm{SL}(2,\mathbb{C})/\{\mathbb{1},-\mathbb{1}\}$, known as the Möbius group [155]. To see this, one notes that there is a homomorphism between $\mathbb{R}^{3,1}$ and anti-hermitian matrices by the map

$$\mathsf{x}^\mu \;\to\; \mathrm{i}\big(\mathsf{x}^0\mathbb{1} + \boldsymbol{x}\cdot\boldsymbol{\sigma}\big)\;, \tag{6.24}$$

where $\boldsymbol{\sigma} = (\sigma_x,\sigma_y,\sigma_z)$ are the Pauli matrices. The determinant of the resulting matrix is the Minkowski squared distance from the origin, $\mathsf{x}^\mu\mathsf{x}_\mu$. The special linear group $\mathrm{SL}(2,\mathbb{C})$ acts naturally on the set of anti-hermitian matrices by conjugation, which preserves the determinant and hence preserves the Minkowski squared distance. This implies a (surjective) homomorphism $\mathrm{SL}(2,\mathbb{C}) \to \mathrm{SO}^+(3,1)$. The kernel of this map is $\{\mathbb{1},-\mathbb{1}\}$. Therefore, by the first isomorphism theorem, $\mathrm{PSL}(2,\mathbb{C}) = \mathrm{SL}(2,\mathbb{C})/\{\mathbb{1},-\mathbb{1}\} \cong \mathrm{SO}^+(3,1)$.

The Möbius group is well studied with well-known conjugacy classes [156]. There are five conjugacy classes: identity, elliptic, parabolic, hyperbolic and loxodromic. In the context of the restricted Lorentz group, these correspond to the identity, spatial rotations, null rotations, boosts, and boosts combined with rotations. Without loss of generality, the elliptic conjugacy class is generated by R_{12}, the parabolic conjugacy class by NR_{012}, the hyperbolic conjugacy class by B_{01}, and the loxodromic conjugacy class by $\mathrm{B}_{01}\bigoplus\mathrm{R}_{23}$.

6.2.2.2 Conjugacy classes of the restricted Lorentz group

We are now in a position to classify the conjugacy classes of $\mathrm{SO}^+(n,1)$. First, we note the conjugacy classes of $\mathrm{SO}^+(n,1)$ for $n<3$: $\mathrm{SO}^+(1,1)$ contains only the identity and hyperbolic classes, whereas $\mathrm{SO}^+(2,1)$ contains the identity, elliptic, parabolic, and hyperbolic conjugacy classes. Both follow from reducing the available dimensions in the $\mathrm{SO}^+(3,1)$ case.

For $n>3$, it has been demonstrated that elements of $\mathrm{SO}^+(n,1)$ are conjugate

to one of three canonical forms depending on the eigenvalues of the element [157, 158]. In particular, any element of $\mathrm{SO}^+(n,1)$ can be reduced to the form $\xi_0 \oplus \eta \oplus \mathbb{1}$, where $\xi_0 \in \mathrm{SO}^+(3,1)$ or $\mathrm{SO}^+(2,1)$, $\eta \in \mathrm{SO}(m)$, $\mathbb{1}$ is the $(n-m-3)$ or $(n-m-2)$-dimensional identity matrix respectively, and $\oplus$ is the direct sum of matrices. Furthermore, elements of $\mathrm{SO}(m)$ can be reduced to a canonical form [158]: for m even, $\eta = \oplus_{i=1}^{m/2} \eta_i$ and for m odd, $\eta = \oplus_{i=1}^{\lfloor m/2 \rfloor} \eta_i \oplus 1$, where $\eta_i \in \mathrm{SO}(2)$.

6.2.2.3 Summary

We write down the non-identity conjugation classes for $n \geq 3$ (cf. classification of the orthochronous components of $\mathrm{O}(n,1)$ [159, 160]),

$$\xi_{\mathrm{E}}^k = \begin{cases} \mathrm{R}_{12} & k = 1\,, \\ \mathrm{R}_{12} \bigoplus_{i=2}^{k} \mathrm{R}_{2i-1\,2i} & k \geq 2\,, \end{cases} \tag{6.25a}$$

$$\xi_{\mathrm{P}}^k = \begin{cases} \mathrm{NR}_{012} & k = 1\,, \\ \mathrm{NR}_{012} \bigoplus_{i=2}^{k} \mathrm{R}_{2i-1\,2i} & k \geq 2\,, \end{cases} \tag{6.25b}$$

$$\xi_{\mathrm{L}}^l = \begin{cases} \mathrm{B}_{01} & l = 1\,, \\ \mathrm{B}_{01} \bigoplus_{i=2}^{l} \mathrm{R}_{2i-2\,2i-1} & l \geq 2\,, \end{cases} \tag{6.25c}$$

for $1 \leq k \leq \lfloor \frac{n}{2} \rfloor$, $1 \leq l \leq \lceil \frac{n}{2} \rceil$, where $n+1$ is the spacetime dimension and $\lfloor \cdot \rfloor$ and $\lceil \cdot \rceil$ are the floor and ceiling functions respectively. We will refer to ξ_{E}^k as the elliptic conjugacy class, ξ_{P}^k as the parabolic conjugacy class, and ξ_{L}^l as the loxodromic conjugacy class. It is important to note that the boosts and rotations appearing in (6.25) are considered to have non-zero rotation angles, that is to say the scalar coefficients are non-zero. The set of non-identity conjugacy classes of $\mathrm{SO}^+(n,1)$ are then given by $\{\xi_{\mathrm{E}}^k, \xi_{\mathrm{P}}^k, \xi_{\mathrm{L}}^l : 1 \leq k \leq \lfloor \frac{n}{2} \rfloor, 1 \leq l \leq \lceil \frac{n}{2} \rceil\}$ for $n \geq 2$. We remark that, using the terminology of the conjugacy classes of the Möbius group, ξ_{L}^1 is the hyperbolic conjugacy class. We denote the identity conjugacy class by $\mathbb{1}$.

As a consistency check, we consider $n = 3$, consisting of the Killing vector $\{\mathbb{1}, \xi_E^1, \xi_{\mathrm{P}}^1, \xi_{\mathrm{L}}^1, \xi_{\mathrm{L}}^2\}$, which we may recognise as the identity, elliptic, parabolic, hyperbolic, and loxodromic conjugacy classes that we reported earlier.

6.2.3 Conjugacy classes of the restricted Poincaré group

We now extend the classification to the restricted Poincaré group. We represent elements of $\mathrm{ISO}^+(n,1)$ as

$$g = \begin{pmatrix} \Lambda & a \\ 0^{\intercal} & 1 \end{pmatrix}, \tag{6.26}$$

where $\Lambda \in \mathrm{SO}^+(n,1)$, $1 \in \mathbb{R}$, and $a,\ 0 \in \mathbb{R}^{n,1}$ and are viewed as column vectors . In terms of matrices, $\mathrm{ISO}^+(n,1)$ acts on $\mathbb{R}^{n,1}$ by

$$g \cdot \mathsf{x} \;=\; \begin{pmatrix} \Lambda & a \\ 0^\intercal & 1 \end{pmatrix} \begin{pmatrix} \mathsf{x} \\ 1 \end{pmatrix} \;=\; \begin{pmatrix} \Lambda \mathsf{x} + a \\ 1 \end{pmatrix} . \tag{6.27}$$

We return to the generators of the Poincaré Lie algebra (6.18), one may perform an infinitesimal transformation directly on the coordinates x^α to find a matrix representation. The Lorentz generators $(M_{\mu\nu})^A{}_B$ and translation generators $(P_\mu)^A{}_B$ are given by

$$(M_{\mu\nu})^A{}_B \;=\; \delta^A_\mu \eta_{\nu B} - \delta^A_\nu \eta_{\mu B}\,, \tag{6.28a}$$

$$(P_\mu)^A{}_B \;=\; \delta^A_\mu \delta^{n+1}_B\,, \tag{6.28b}$$

where $A,\, B = 0,\, 1,\, \ldots,\, n+1$. In this notation, the spacetime rotation generators are given in matrix form by $\mathrm{R}_{ij} = M_{ij}$, $\mathrm{B}_{0i} = M_{0i}$, $\mathrm{NR}_{0ij} = M_{0i} - M_{ij}$.

We consider a linear combination of Killing vectors. This will have a matrix (Lorentz group) component N and a vector (translation) component K. Under conjugation by $g = (\Lambda, a)$, we have

$$g \cdot \begin{pmatrix} N & K \\ 0^\intercal & 0 \end{pmatrix} \cdot g^{-1} \;=\; \begin{pmatrix} \Lambda N \Lambda^{-1} & -\Lambda N \Lambda^{-1} a + \Lambda K \\ 0^\intercal & 0 \end{pmatrix} . \tag{6.29}$$

We are now in a position to find the conjugacy classes. We consider first the purely timelike and purely spacelike translations before considering a combination of timelike and spacelike translations.

6.2.3.1 Temporal translation

We consider first the timelike translations $\mathrm{T}_0 = P_0$. One may add a timelike translation to the identity conjugacy class, resulting in the class of inertial trajectories T_0.

Adding a timelike translation to the loxodromic conjugacy class (6.25c) results in

$$\mathrm{T}_0 \oplus \xi^l_{\mathrm{L}} \;=\; \alpha \partial_t + (t\partial_1 + x^1 \partial_t) + \sum_{i=2}^{l} b_i (x^{2i-1} \partial_{2i-2} - x^{2i-2} \partial_{2i-1})\,. \tag{6.30}$$

This linear combination has the matrix part

$$N^\mu{}_\nu \;=\; (\,\delta^\mu_0 \eta_{1\nu} - \delta^\mu_1 \eta_{0\nu}) + \sum_{i=2}^{l} b_i (\delta^\mu_{2i-2} \eta_{2i-1\,\nu} - \delta^\mu_{2i-1} \eta_{2i-2\,\nu})\,, \tag{6.31}$$

and a vector part $K^\mu = \alpha\delta^\mu_0$. The matrix part of the loxodromic conjugacy class ξ^l_{L} is also given by (6.30) and has no vector contribution. Comparing with the general form of conjugation given by (6.29), we may force $(-\Lambda N\Lambda^{-1}a + \Lambda K)$, the vector part of $\mathrm{T}_0 \oplus \xi^l_{\mathrm{L}}$, to vanish by choosing $a^\mu = \alpha\eta^{\mu\beta}(\Lambda^{-1})^1{}_\beta$. Therefore, with this choice of a,

$$\begin{aligned} g\cdot\left(\mathrm{T}_0\bigoplus\xi^l_{\mathrm{L}}\right)\cdot g^{-1} &= (\Lambda,a)\cdot(N,K)\cdot(\Lambda,a)^{-1}\,,\\ &= (\Lambda N\Lambda^{-1},0)\,,\\ &= (\Lambda,0)\cdot(N,0)\cdot(\Lambda,0)^{-1}\,,\\ &\sim \xi^l_{\mathrm{L}}\,. \end{aligned} \tag{6.32}$$

As such, there exists an element $g = (\Lambda, a)$ with a as above, such that $\mathrm{T}_0\oplus\xi^l_{\mathrm{L}} \sim \xi^l_{\mathrm{L}}$.

We consider now the elliptic ξ^k_{E} (6.25a) and parabolic ξ^k_{P} (6.25b) generators. Neither of these can be timelike anywhere. However, both $\mathrm{T}_0 \oplus \xi^k_{\mathrm{E}}$ and $\mathrm{T}_0 \oplus \xi^k_{\mathrm{P}}$ can be timelike somewhere. Since conjugation does not change the timelike/null/spacelike nature of a Killing vector, we conclude that $\mathrm{T}_0\oplus\xi^k_{\mathrm{E(P)}} \not\sim \xi^k_{\mathrm{E(P)}}$.

6.2.3.2 Spatial translation

We consider now the spacelike translations $\mathrm{S}_m = P_m$ with $1 \le m \le n$ fixed. A spacelike translation added to the identity conjugacy class results in a spatial curve. Consider now the loxodromic conjugacy class, $\mathrm{S}_m \oplus \xi^l_{\mathrm{L}}$. This can be written in terms of Killing vectors as

$$\mathrm{S}_m \oplus \xi^l_{\mathrm{L}} = \alpha\partial_m + (x^1\partial_t + t\partial_t) + \sum_{i=2}^{l} b_i(x^{2i-1}\partial_{2i-2} - x^{2i-2}\partial_{2i-1})\,. \tag{6.33}$$

The vector part of the conjugation $(\Lambda, a)\cdot(\mathrm{S}_m \oplus \xi^l_{\mathrm{L}})\cdot(\Lambda, a)^{-1}$ reads

$$\begin{aligned} 0 = {} & -\Lambda^\mu{}_0(\Lambda^{-1})^1{}_\beta a^\beta - \Lambda^\mu{}_1(\Lambda^{-1})^0{}_\beta a^\beta + \alpha\Lambda^\mu{}_m \\ & + \sum_{i=2}^{l} b_i\left(\Lambda^\mu{}_{2i-2}(\Lambda^{-1})^{2i-1}{}_\beta - \Lambda^\mu{}_{2i-1}(\Lambda^{-1})^{2i-2}{}_\beta\right)a^\beta\,. \end{aligned} \tag{6.34}$$

In the case $m = 1$, this translation is parallel to the boost. By choosing $a^\beta = \alpha\eta^{\beta\rho}(\Lambda^{-1})^0{}_\rho$, one may force the vector contribution (6.34) vanish. We recall that $1 \le l \le \lceil\frac{n}{2}\rceil$. In the case $1 < m \le 2l-1$, this translation is parallel to an axis of rotation and can be conjugated away. For m even, $a^\beta = -\alpha/(b_{(m+2)/2})\eta^{\beta\rho}(\Lambda^{-1})^{m+1}{}_\rho$ and for m odd, $a^\beta = \alpha/(b_{(m+1)/2})\eta^{\beta\rho}(\Lambda^{-1})^{m-1}{}_\rho$ will make (6.34) vanish. However, for $2l-1 < m \le n$ with $l < \lceil\frac{n}{2}\rceil$, one is unable to conjugate away S_m. If $l = \lceil\frac{n}{2}\rceil$,

then the result depends on the parity of n. If n is odd, then all available spatial dimensions are filled by the boost along x^1 and rotations in the remaining $(n-1)/2$ independent planes. By contrast, if n is even, there is then one free axis, parallel to which one may perform a spatial translation.

To summarise, $\mathrm{S}_m \oplus \xi^l_{\mathrm{L}} \sim \xi^l_{\mathrm{L}}$ for $1 \leq m \leq 2l-1$ and $1 \leq l < \lceil \frac{n}{2} \rceil$. Whereas, for $2l-1 < m \leq n$ and $1 \leq l \leq \lceil \frac{n}{2} \rceil$, $\mathrm{S}_m \oplus \xi^l_{\mathrm{L}}$ forms a new conjugacy class.

The analyses for $\mathrm{S}_m \oplus \xi^k_{\mathrm{E}}$ and $\mathrm{S}_m \oplus \xi^k_{\mathrm{P}}$ are characteristically and computationally similar to the loxodromic case. We summarise the results now. For $1 \leq m \leq 2k$ and $1 \leq k \leq \lfloor \frac{n}{2} \rfloor$, one may choose a translation a suitably to conjugate away the translation S_m. However, for $2k < m \leq n$ with $1 \leq k \leq \lfloor \frac{n}{2} \rfloor$, there is a free axis, parallel to which one may perform a spatial translation, producing two more sets of conjugacy classes, $\mathrm{S}_m \oplus \xi^k_{\mathrm{E(P)}}$ for $2k < m \leq n$.

We remark that in all cases where one may add a spatial translation, it is parallel to an axis, along which and parallel to which there are no other motions. As such, if one were to add multiple spatial translations, each along axes independent of the other motions, one could choose a Λ to align all translations along one axis. This is possible since, in each conjugacy class, Λ was hitherto arbitrary. Hence, we need only consider one spatial translation.

6.2.3.3 Temporal and spatial translation

We consider now the case of spatial and temporal translations, $\mathrm{T}_0 \oplus \xi \bigoplus_i \mathrm{S}_i$. If the translations T_0 or S_i are parallel to a plane of boost or plane of rotation, they can be conjugated away as seen in Sections 6.2.3.1 and 6.2.3.2. We first consider the loxodromic conjugacy class $\xi = \xi^l_{\mathrm{L}}$ (6.25c). The timelike translation T_0 can be conjugated away so we have $\xi^l_{\mathrm{L}} \bigoplus_i \mathrm{S}_i$. Any S_i parallel to the rotations or the boost can be conjugated away. This will either conjugate away all S_i or we are left with $\xi^l_{\mathrm{L}} \bigoplus_{i \geq 2l} \mathrm{S}_i$. Finally, one can perform rotations in the hyperplanes containing the S_i to align them along one axis, leaving $\xi^l_{\mathrm{L}} \oplus \mathrm{S}_{2l}$.

We consider now the parabolic and elliptic conjugacy classes (6.25a) and (6.25b). Once again, we can conjugate away any translations parallel to a plane of rotation and then rotate in the planes containing the remaining spatial translations, leaving $\mathrm{T}_0 \oplus \xi^k_{\mathrm{E(P)}} \oplus \mathrm{S}_{2k+1}$. In this case, we consider the relative magnitudes of the translations T_0 and S_{2k+1}. Let $\mathrm{T}_0 \oplus \mathrm{S}_{2k+1} = \alpha\partial_t - \beta\partial_{2k+1}$, then: if $|\alpha| > |\beta|$, this is conjugate to T_0; if $|\alpha| < |\beta|$, this is conjugate to S_{2k+1}; and if $|\alpha| = |\beta|$, this is a null translation $\mathrm{NT}_{0,2k+1}$.

Finally, we consider the identity conjugacy class $\mathbb{1}$. We can perform temporal and spatial translations $\mathrm{T}_0 \oplus \mathbb{1} \bigoplus_i \mathrm{S}_i$. Depending on whether $\mathrm{T}_0 \bigoplus_i \mathrm{S}_i$ is timelike, spacelike, or null, this is conjugate to T_0, S_1, or NT_{01}.

6.2.3.4 Summary of conjugacy classes

Just as we listed the conjugacy classes of $\mathrm{SO}^+(n,1)$ for small n, we note that the conjugacy classes of $\mathrm{ISO}^+(0,1)$ consist of $\{\mathbb{1},\ \mathrm{T}_0\}$, and the conjugacy classes of $\mathrm{ISO}^+(1,1)$ are $\{\mathbb{1},\ \mathrm{T}_0,\ \mathrm{B}_{01},\ \mathrm{S}_1,\ \mathrm{NT}_{01}\}$. We can now list the conjugacy classes of the Poincaré group, $\mathrm{ISO}^+(n,1)$. We first have the conjugacy classes of $\mathrm{SO}^+(n,1)$,

$$\{\mathbb{1}, \xi^k_{\mathrm{E}},\ \xi^k_{\mathrm{P}},\ \xi^l_{\mathrm{L}} : 1 \leq k \leq \lfloor \tfrac{n}{2} \rfloor,\ 1 \leq l \leq \lceil \tfrac{n}{2} \rceil\}\,. \tag{6.35}$$

In addition, we have those with a time translation,

$$\{\mathrm{T}_0,\ \mathrm{T}_0 \oplus \xi^k_{\mathrm{E}},\ \mathrm{T}_0 \oplus \xi^k_{\mathrm{P}} : 1 \leq k \leq \lfloor \tfrac{n}{2} \rfloor\}\,. \tag{6.36}$$

We also have those with a spatial translation, which we may align along the x^n–axis without loss of generality,

$$\{\mathrm{S}_n\,, \xi^k_{\mathrm{E}} \oplus \mathrm{S}_n,\ \xi^k_{\mathrm{P}} \oplus \mathrm{S}_n,\ \xi^l_{\mathrm{L}} \oplus \mathrm{S}_n : 1 \leq k \leq \lfloor \tfrac{n}{2} \rfloor,\ 1 \leq l \leq \lceil \tfrac{n}{2} \rceil\}\,, \tag{6.37}$$

with the following caveats: $\xi^k_{\mathrm{E(P)}} \oplus \mathrm{S}_n \sim \xi^k_{\mathrm{E(P)}}$ if n is even and $k = \lfloor \frac{n}{2} \rfloor$; and $\xi^k_{\mathrm{L}} \oplus \mathrm{S}_n \sim \xi^k_{\mathrm{L}}$ if n is odd and $l = \lceil \frac{n}{2} \rceil$. Finally, we have the conjugacy classes with a null translation, which again may be confined to the x^0–x^n plane without loss of generality,

$$\{\mathrm{NT}_{0n},\ \mathrm{NT}_{0n} \oplus \xi^k_{\mathrm{E}},\ \mathrm{NT}_{0n} \oplus \xi^k_{\mathrm{P}} : 1 \leq k \leq \lfloor \tfrac{n}{2} \rfloor\}\,, \tag{6.38}$$

with the caveat that $\mathrm{NT}_{0n} \oplus \xi^k_{\mathrm{E(P)}} \sim \mathrm{T}_0 \oplus \xi^k_{\mathrm{E(P)}}$ if n is even and $k = \lfloor \frac{n}{2} \rfloor$.

6.2.4 Stationary trajectories in Minkowski spacetimes

The conjugacy classes of $\mathrm{ISO}^+(n,1)$ which correspond to a stationary trajectory in $\mathbb{R}^{n,1}$ are those whose associated Killing vector is timelike somewhere. For $n \geq 3$, we list them:

$$\xi_0 \equiv \mathrm{T}_0 \qquad \textit{inertial motions,} \tag{6.39a}$$

$$\xi^l_{\mathrm{LM}} \equiv \xi^l_L \qquad \textit{loxodromic motions } 1 \leq l \leq \lceil \tfrac{n}{2} \rceil, \tag{6.39b}$$

$$\xi^l_{\mathrm{dL}} \equiv \xi^l_L \oplus \mathrm{S}_n \qquad \textit{drifted loxodromic motions} \begin{cases} 1 \leq l \leq \lceil \frac{n}{2} \rceil & n \text{ even}, \\ 1 \leq l < \lceil \frac{n}{2} \rceil & n \text{ odd}, \end{cases} \tag{6.39c}$$

$$\xi^k_{\mathrm{SP}} \equiv \mathrm{T}_0 \oplus \xi^k_{\mathrm{P}} \qquad \textit{semicubical parabolic motions,} \tag{6.39d}$$

$$\xi^k_{\mathrm{CM}} \equiv \mathrm{T}_0 \oplus \xi^k_{\mathrm{E}} \qquad \textit{circular motions,} \tag{6.39e}$$

for $1 \leq k \leq \lfloor \frac{n}{2} \rfloor$. The names of the conjugacy classes originate from the classification due to Letaw [71, 91]. We remark two special cases: ξ^1_{LM} is accelerated (Rindler) motion parallel to the x^1–axis and ξ^1_{dL} is drifted Rindler motion [72]. The semicubical parabolic motions have the spatial projection of a semicubical parabola in the x^1–x^2 plane with circular motions in the remaining independent planes. The circular motions exhibit circular motion in each independent plane.

Let $\mathrm{TKV}(n)$ denote the set of conjugacy classes of timelike Killing vectors of $\mathbb{R}^{n,1}$,

$$\mathrm{TKV}(n) \;=\; \{\xi_0,\, \xi^l_{\mathrm{LM}},\, \xi^l_{\mathrm{dL}},\, \xi^k_{\mathrm{SP}},\, \xi^k_{\mathrm{CM}} : 1 \leq l \leq \lceil \tfrac{n}{2} \rceil,\, 1 \leq k \leq \lfloor \tfrac{n}{2} \rfloor \}\,, \tag{6.40}$$

then the number of classes of timelike trajectories is given by

$$\#\mathrm{TKV}(n) \;=\; 1 + 3 \left\lfloor \frac{n}{2} \right\rfloor + \left\lceil \frac{n}{2} \right\rceil\,. \tag{6.41}$$

Considering now the case $n = 4$,

$$\mathrm{TKV}(4) \;=\; \{\xi_0,\, \xi^1_{\mathrm{LM}},\, \xi^2_{\mathrm{LM}},\, \xi^1_{\mathrm{dL}},\, \xi^2_{\mathrm{dL}},\, \xi^1_{\mathrm{SP}},\, \xi^2_{\mathrm{SP}}\,, \xi^1_{\mathrm{CM}}\,, \xi^2_{\mathrm{CM}}\}\,, \tag{6.42}$$

with $\#\mathrm{TKV}(4) = 9$. We will exhibit and classify these trajectories explicitly in the following Section.

6.3 Vielbein formulation

We move now to the geometric side of the stationary trajectories, from which point of view, the stationary trajectories are defined as the timelike solutions to the Frenet-Serret equations with proper-time-independent curvature invariants. In this Section, we extend the vierbein (tetrad) formalism of Letaw [71] to a vielbein formulation, applicable to Minkowski spacetime of dimension $n + 1$ with $n \geq 1$. We also present explicitly the stationary trajectories in $\mathbb{R}^{4,1}$.

6.3.1 Frenet-Serret equations in Minkowski spacetimes

We begin by constructing an orthonormal vielbein $V^\mu_a(\tau)$ for a worldline $\mathsf{x}^\mu(\tau)$ parametrised by proper time τ in $n + 1$ Minkowski spacetime. These are constructed out of derivatives of the worldline with respect to proper time. We assume that the first $n+1$ derivatives are linearly independent and none of the first $n-1$ derivatives are vanishing or null i.e. $\mathsf{x}^{\mu(k)}(\tau)\,\mathsf{x}^{(k)}_\mu(\tau) \neq 0$ for $k = 1, \ldots, n-1$.

Orthonormality is imposed by the relation

$$V_{a\mu}(\tau)V_b^{\mu}(\tau) \;=\; \eta_{ab}\,. \tag{6.43}$$

The first component of the vielbein is simply the four-velocity, $V_0^{\mu}(\tau) = \dot{\mathsf{x}}^{\mu}(\tau)$. We remark that since the first component of the vielbein $V_0^{\mu}(\tau)$ is timelike, all other components must necessarily be spacelike. One may construct a family of orthogonal vielbeins $\widetilde{V}_a^{\mu}(\tau)$ by the Gram-Schmidt process such that

$$\widetilde{V}_k^{\mu}(\tau) \;=\; \mathsf{x}^{(k+1)\mu}(\tau) - \sum_{j=1}^{k} \frac{\mathsf{x}^{(k+1)\rho}(\tau)\mathsf{x}_{\rho}^{(j)}(\tau)}{\mathsf{x}^{(j)\sigma}(\tau)\mathsf{x}_{\sigma}^{(j)}(\tau)}\mathsf{x}^{(j)\mu}(\tau)\,. \tag{6.44}$$

The orthonormal vielbeins $V_a^{\mu}(\tau)$ are then constructed by the normalisation of $\widetilde{V}_a^{\mu}(\tau)$. The final vielbein is given by

$$V_n^{\mu}(\tau) \;=\; \frac{1}{\sqrt{n!}}\varepsilon^{\rho_0\rho_1\ldots\rho_{n-1}\mu}V_{0\rho_0}(\tau)V_{1\rho_1}(\tau)\ldots V_{n-1\,\rho_{n-1}}(\tau)\,. \tag{6.45}$$

Differentiation of the orthonormality condition (6.43) yields

$$\dot{V}_{a\mu}(\tau)V_b^{\mu}(\tau) + V_{a\mu}(\tau)\dot{V}_b^{\mu}(\tau) \;=\; 0. \tag{6.46}$$

Since the vielbeins form a basis, one may write the proper time derivatives in the basis of vielbeins,

$$\dot{V}_a^{\mu}(\tau) \;=\; K_a{}^b(\tau)V_b^{\mu}(\tau)\,. \tag{6.47}$$

Combining equations (6.46) and (6.47) informs us that the matrix K_{ab} is antisymmetric. Furthermore, since each V_b^{μ} is constructed out of the first $b+1$ derivatives of the worldline, whereas $\dot{V}_a^{\mu}$ is constructed out of the first $a+2$ derivatives, we have that $K_a{}^b$ vanishes for $b > a+1$. This tells us that the only non-vanishing components are those immediately above and below the diagonal and one may write this matrix as

$$K_{ab}(\tau) \;=\; \chi_a(\tau)\delta_{a,b-1} - \chi_b(\tau)\delta_{b,a-1}\,, \tag{6.48}$$

where δ_{ab} is the Kronecker delta. We remark that (6.47) and (6.48) form the higher-dimensional, Lorentz-signature equivalent of the Frenet-Serret equations (6.8).

We consider only case when V_0^{μ} is future direct and when χ_a are constant in proper time; as such, we suppress the dependence on τ in our notation. These χ_a are then referred to as the curvature invariants.

The explicit form of the matrix of curvature invariants (6.48) enables us to

rewrite the Frenet-Serret equations as

$$V_1^\mu = \frac{1}{\chi_0}\dot{V}_0^\mu \,, \tag{6.49a}$$

$$V_2^\mu = \frac{1}{\chi_0\chi_1}\left(\ddot{V}_0^\mu - \chi_0^2 V_0^\mu\right) \,, \tag{6.49b}$$

$$V_a^\mu = \frac{1}{\chi_{a-1}}\left(\dot{V}_{a-1}^\mu + \chi_{a-2}V_{a-2}^\mu\right) \,, \quad a = 3, \ldots, n \,, \tag{6.49c}$$

$$\dot{V}_n^\mu = -\chi_{n-1}V_{n-1}^\mu \,. \tag{6.49d}$$

Note that setting any $\chi_a = 0$ renders the Frenet-Serret equations ill defined. We discuss this further in Appendix G. The Frenet-Serret equations (6.49) enable one to write each component of the vielbein in terms of derivatives of V_0^μ. One sees that these differential equations can be written down explicitly in the general case,

$$V_a^\mu = \frac{1}{\prod_{i=0}^{a-1}\chi_i}\sum_{q=0}^{\lfloor \frac{a}{2} \rfloor} b_{2q}^a \frac{\mathrm{d}^{a-2q}}{\mathrm{d}\tau^{a-2q}}V_0^\mu \,, \quad a = 3, \ldots, n \,, \tag{6.50}$$

where the coefficients b_{2q}^a are defined as follows,

$$b_0^a = 1 \,, \tag{6.51a}$$

$$b_2^a = \sum_{i,j=0}^{a-2}\eta_{ij}\chi_i\chi_j \,, \tag{6.51b}$$

$$b_{2q}^a = \sum_{p_1=2q-2}^{a-2}\chi_{p_1}^2\sum_{p_2=2q-4}^{p_1-2}\chi_{p_2}^2\cdots\sum_{i,j=0}^{p_{q-1}-2}\eta_{ij}\chi_i\chi_j \,, \tag{6.51c}$$

where the dots in (6.51c) represent successive insertions of terms of the form $\sum_{p_k=2q-2k}^{p_{k-1}-2}\chi_{p_k}^2$. For example,

$$b_8^a = \sum_{p_1=6}^{a-2}\chi_{p_1}^2\sum_{p_2=4}^{p_1-2}\chi_{p_2}^2\sum_{p_3=2}^{p_2-2}\chi_{p_3}^2\sum_{i,j=0}^{p_3-2}\eta_{ij}\chi_i\chi_j \,. \tag{6.52}$$

One may prove (6.50) using strong induction and the relation

$$b_{2q}^m + \chi_{m-1}^2 b_{2(q-1)}^{m-1} = b_{2q}^{m+1} \,, \tag{6.53}$$

which may be derived by expanding (6.51).

In Appendix F, we simplify the Frenet-Serret equations and find the ordinary differential equation satisfied by V_0^μ. The generalised Frenet-Serret equations in

$n+1$ Minkowski spacetime are therefore given by

$$V_1^\mu = \frac{1}{\chi_0}\dot{V}_0^\mu \,, \tag{6.54a}$$

$$V_2^\mu = \frac{1}{\chi_0\chi_1}\left(\ddot{V}_0^\mu - \chi_0^2 V_0^\mu\right) \,, \tag{6.54b}$$

$$V_a^\mu = \frac{1}{\chi_{a-1}}\left(\dot{V}_{a-1}^\mu + \chi_{a-2}V_{a-2}^\mu\right) \,, \quad a = 3,\,\ldots\,,\,n \,, \tag{6.54c}$$

$$V_{n+1}^\mu = 0 \,, \tag{6.54d}$$

with V_a^μ given by (6.50) for $a = 3,\,\ldots\,,\,n+1$. Equation 6.54d then constitutes an ordinary differential equation for V_0^μ, just as we found an ordinary differential equation for the tangent vector $\boldsymbol{T}$ in Example 6.1. Solving this for V_0^μ, one may then the other components of the vielbein (6.54).

Using terminology from differential equations, the characteristic equation of (6.54d) is then

$$\sum_{q=0}^{\left\lfloor\frac{n+1}{2}\right\rfloor} b_{2q}^{n+1} m^{n+1-2q} = 0 \,, \tag{6.55}$$

which has definite parity. The coefficients of the general solution can then be fixed by an initial condition, for which we may adopt

$$V_a^\mu(\tau)\big|_{\tau=0} = \delta_a^\mu \,. \tag{6.56}$$

One may remark that under a Poincaré transformation of the worldline

$$\mathsf{x}^\mu \;\to\; \mathsf{x}'^\mu = \Lambda^\mu{}_\nu \mathsf{x}^\nu + c^\nu \,, \tag{6.57}$$

the vielbeins transform as

$$V_a^\mu \;\to\; V'^\mu_{\ a} = \Lambda^\mu{}_\nu V_a^\nu \,. \tag{6.58}$$

The transformed vielbeins $V'^\mu_{\ a}$ also form an orthonormal basis, obeying the orthonormality condition (6.43) $V'_{a\mu}V'^\mu_{\ b} = \eta_{ab}$. The choice of the direction of the tangent vector at $\tau = 0$ (6.56) determines which orthonormal basis one uses. This is the geometric counterpart of Killing vectors belonging to the same conjugacy class in Section 6.2.4.

A priori, one is able to express solutions to (6.55) in terms of radicals only for $n \leq 8$ [161]. We demonstrate this extended formalism in the following Section to explicitly calculate and classify the stationary trajectories in $4+1$ Minkowski spacetime.

6.3.2 Example: $4+1$ Minkowski spacetime

In this Section, we use the formalism of Section 6.3.1 to present the stationary trajectories in $4+1$ Minkowski spacetime. We demonstrate the equivalence between solutions to the Frenet-Serret equations with constant curvature invariants and the integral curves of timelike Killing vectors in $4+1$ dimensions. We classify the resulting trajectories into nine equivalence classes.

The characteristic equation (6.55) in $4+1$ dimensions reads

$$0 \;=\; m(m^4 - 2am^2 - b)\,, \tag{6.59}$$

where $2a = -b_2^5$ and $b = -b_4^5$, each given by (6.51c). This has the solutions $m = 0$ and $m^2 = a \pm \sqrt{a^2+b}$, which we write as $m^2 = \sqrt{a^2+b} + a$ or $m^2 = -(\sqrt{a^2+b} - a)$. Hence, $m = 0,\ \pm R_+,\ \pm \mathrm{i}R_-$, where $R_\pm^2 = \sqrt{a^2+b} \pm a$. The general solution for V_0^μ is then

$$V_0^\mu \;=\; A^\mu + B^\mu \cosh(R_+\tau) + C^\mu \sinh(R_+\tau) + D^\mu \cos(R_-\tau) + E^\mu \sin(R_-\tau)\,. \tag{6.60}$$

Using the initial conditions (6.56), the coefficients are found to be

$$A^\mu \;=\; \left(1 - \frac{\chi_0^2}{b}(\chi_2^3 + \chi_3^2), 0, -\frac{\chi_0\chi_1\chi_3^2}{b}, 0, -\frac{\chi_0\chi_1\chi_2\chi_3}{b}\right)\,, \tag{6.61a}$$

$$B^\mu \;=\; \frac{1}{R^2}\left(\frac{\chi_0^2}{R_+^2}(\chi_0^2 - \chi_1^2 + R_-^2), 0, \frac{\chi_0\chi_1}{R_+^2}(\chi_0^2 - \chi_1^2 - \chi_2^2 + R_-^2), 0, \frac{\chi_0\chi_1\chi_2\chi_3}{R_+^2}\right)\,, \tag{6.61b}$$

$$C^\mu \;=\; \frac{1}{R^2}\left(0, \frac{\chi_0}{R_+}(\chi_0^2 - \chi_1^2 + R_-^2), 0, \frac{\chi_0\chi_1\chi_2}{R_+}, 0\right)\,, \tag{6.61c}$$

$$D^\mu \;=\; \frac{1}{R^2}\left(\frac{\chi_0^2}{R_-^2}(\chi_0^2 - \chi_1^2 - R_+^2), 0, \frac{\chi_0\chi_1}{R_-^2}(\chi_0^2 - \chi_1^2 - \chi_2^2 - R_+^2), 0, \frac{\chi_0\chi_1\chi_2\chi_3}{R_-^2}\right)\,, \tag{6.61d}$$

$$E^\mu \;=\; \frac{1}{R^2}\left(0, -\frac{\chi_0}{R_-}(\chi_0^2 - \chi_1^2 - R_+^2), 0, -\frac{\chi_0\chi_1\chi_2}{R_-}, 0\right)\,, \tag{6.61e}$$

where $R^2 = R_+^2 + R_-^2$.

We explicitly calculate the stationary trajectories in $4+1$ Minkowski spacetime in Appendix G. We report the results case-by-case. For $m \leq n$, the stationary trajectories of $\mathbb{R}^{m,1}$ are embedded in $\mathbb{R}^{n,1}$. Hence to find all stationary trajectories in $\mathbb{R}^{n,1}$, one solves the Frenet-Serret equations (6.54) for each $m = 0,\ 1,\ \ldots,\ n$.

The stationary trajectories of $4+1$ Minkowski spacetime are as follows: Case 0: the class of inertial trajectories (G.2). Case I: the class of Rindler trajectories (G.3). Case IIa: the class of drifted Rindler motions (G.4). Case IIb: the class of motions

with semicubical parabolic spatial projection (G.5). Case IIc: the class of circular motions (G.6). Case III: the class of loxodromic motions (G.9). Case IVa: the class of drifted loxodromic motions in the x^1–x^2 plane with circular motion in the x^3–x^4 plane (G.14). Case IVb: the class of motions with semicubical parabolic spatial projection in the x^1–x^2 plane with circular motion in the x^3–x^4 plane (G.16). Case IVc: the class of circular motions in the x^1–x^2 plane with circular motion in the x^3–x^4 plane (G.18).

As expected from the previous calculation of $\#\mathrm{TKV}(4)$ (6.42), there are nine classes of stationary trajectory. In agreement with [71, 91], we recover the six classes of stationary trajectory in $3+1$ Minkowski spacetime.

Since stationary trajectories of Minkowski spacetime are both timelike solutions to the Frenet-Serret equations and the integral curves of timelike Killing vectors, we finish this Section by unifying the two frameworks and present the stationary trajectories with their respective timelike Killing vector according to the classification (6.39),

$$\text{Case } 0\text{: Inertial (G.2) } \xi_0 = \mathrm{T}_0\,, \tag{6.62a}$$

$$\text{Case I: Rindler (G.3) } \xi^1_{\mathrm{RM}} = \mathrm{B}_{01}\,, \tag{6.62b}$$

$$\text{Case IIa: Drifted Rindler (G.4) } \xi^1_{\mathrm{dR}} = \mathrm{B}_{01} \oplus \mathrm{S}_2\,, \tag{6.62c}$$

$$\text{Case IIb: Semicubical parabolic (G.5) } \xi^1_{\mathrm{SP}} = \mathrm{T}_0 \oplus \mathrm{NR}_{012}\,, \tag{6.62d}$$

$$\text{Case IIc: Circular (G.6) } \xi^1_{\mathrm{CM}} = \mathrm{T}_0 \oplus \mathrm{R}_{12}\,, \tag{6.62e}$$

$$\text{Case III: Loxodromic (G.9) } \xi^2_{\mathrm{RM}} = \mathrm{B}_{01} \oplus \mathrm{R}_{23}\,, \tag{6.62f}$$

$$\text{Case IVa: Drifted loxodromic with circular (G.14) } \xi^2_{\mathrm{dR}} = \mathrm{B}_{01} \oplus \mathrm{S}_2 \oplus \mathrm{R}_{34}\,, \tag{6.62g}$$

$$\text{Case IVb: Semicubical parabolic with circular (G.16) } \xi^2_{\mathrm{SP}} = \mathrm{T}_0 \oplus \mathrm{NR}_{012} \oplus \mathrm{R}_{34}\,, \tag{6.62h}$$

$$\text{Case IVc: Double circular motion (G.18) } \xi^2_{\mathrm{CM}} = \mathrm{T}_0 \oplus \mathrm{R}_{12} \oplus \mathrm{R}_{34}\,. \tag{6.62i}$$

6.4 Stationary trajectories in de Sitter spacetimes

In this Section, we give an application of the formalism developed in this Chapter to a curved spacetime. In particular, the maximally symmetric spacetime of constant positive curvature, de Sitter (dS) spacetime. We may view n-dimensional dS as embedded in $n+1$ Minkowski spacetime [84] with the embedding equation

$$\eta_{AB} X^A X^B = \alpha^2\,, \tag{6.63}$$

where $X^A = (X^0, X^1, \ldots, X^n)$ are coordinates in $\mathbb{R}^{n,1}$, $\eta_{AB} = \mathrm{diag}(-1, 1, \ldots, 1)$ is the Minkowski metric in $n+1$ dimensions, and $\alpha > 0$ is the de Sitter radius of curvature.

The isometry group of dS is then inherited from its embedding space $\mathbb{R}^{n,1}$, subject to leaving the embedding equation (6.63) invariant. By definition, the action of the indefinite orthogonal group $\mathrm{O}(n,1)$ on $X^A \in \mathbb{R}^{n,1}$ leaves the quadratic form $\eta_{AB}X^AX^B$ invariant. We restrict our attention to the transformations that are continuously connected to the identity and preserve time and space orientation, the restricted Lorentz group $\mathrm{SO}^+(n,1)$, which is indeed a subgroup of the isometry group of $\mathbb{R}^{n,1}$. Given the classification of the restricted Lorentz group in Section 6.2.2, we see that only the loxodromic Killing vectors ξ^l_{L} (6.25c) give rise to timelike Killing vectors.

We remark that dS is not a globally static spacetime. Later, in Chapter 8, we will consider the static patch of dS, described by the coordinates

$$X^0 = \sqrt{\alpha^2 - r^2}\sinh(t/\alpha)\,, \tag{6.64a}$$
$$X^1 = \sqrt{\alpha^2 - r^2}\cosh(t/\alpha)\,, \tag{6.64b}$$
$$X^i = r x_i\,, \tag{6.64c}$$

where $2 \leq i \leq n$ and x_i are the embedding coordinates of the $(n-2)$-dimensional unit sphere $\mathbb{S}^{n-2}$ in $\mathbb{R}^{n-1}$. The metric of the static patch is

$$\mathrm{d}s^2 = -\left(1 - \frac{r^2}{\alpha^2}\right)\mathrm{d}t^2 + \frac{\mathrm{d}r^2}{1 - \frac{r^2}{\alpha^2}} + r^2\mathrm{d}\Omega^2_{n-2}\,, \tag{6.65}$$

where $\mathrm{d}\Omega^2_{n-2}$ is the metric on $\mathbb{S}^{n-2}$. We note the presence of a cosmological horizon at $r = \alpha$.

Example 6.2 ($2+1$ static patch)**.** We consider the case $n = 3$, describing $(2+1)$-dimensional dS. The geometry of the static patch is described by the metric

$$\mathrm{d}s^2 = -\left(1 - \frac{r^2}{\alpha^2}\right)\mathrm{d}t^2 + \frac{\mathrm{d}r^2}{1 - \frac{r^2}{\alpha^2}} + r^2\mathrm{d}\theta^2\,, \tag{6.66}$$

where dS has been embedded in $\mathbb{R}^{3,1}$ via

$$X^0 = \sqrt{\alpha^2 - r^2}\sinh(t/\alpha)\,, \tag{6.67a}$$
$$X^1 = \sqrt{\alpha^2 - r^2}\cosh(t/\alpha)\,, \tag{6.67b}$$
$$X^2 = r\cos(\theta)\,, \tag{6.67c}$$
$$X^3 = r\sin(\theta)\,. \tag{6.67d}$$

The two conjugacy classes of timelike Killing vectors of $\mathrm{SO}^+(3,1)$ inherited from $\mathbb{R}^{3,1}$ are ξ^1_{L} and ξ^2_{L}. Let $f : \mathrm{dS} \hookrightarrow \mathbb{R}^{3,1}$ be the inclusion map given by the embedding (6.67). Then, by direct calculation, the pullback of these two timelike Killing vectors to the static patch is given by

$$f^*(\xi^1_{\mathrm{L}}) = \partial_t \,, \tag{6.68a}$$

$$f^*(\xi^2_{\mathrm{L}}) = \partial_t \oplus \partial_\theta \,. \tag{6.68b}$$

We see that B_{01} in $\mathbb{R}^{n,1}$ generates inertial motion ∂_t in the static patch. Furthermore, the hypertor motion of Chapter 5 generated by ξ^2_{L} corresponds to circular motion in the static patch. ■

We can now classify the stationary trajectories in the static patch. In Example 6.2, we saw that a boost in Minkowski spacetime corresponds to inertial motion in the static patch generated by ∂_t and that the Killing vector corresponding to a rotation in the x^1–x^2 plane again corresponds to a rotation. In general, due to the spherical symmetry of the static patch in (6.64) and (6.65), the family of loxodromic Killing vectors ξ^l_{L}, when pulled back to the static patch, correspond to a linear combination of inertial motion generated by ∂_t and circular motions in the independent planes of rotation.

The family of elliptic Killing vectors ξ^k_{E} again correspond to rotations in independent planes. As such, it would be tempting to write that the isometry group $\mathrm{SO}^+(n,1)$ reduces to $\mathbb{R} \times \mathrm{SO}(n-1)$ in the static patch. However, the null rotations do not admit a simple interpretation and may not be characterised as elements of $\mathbb{R} \times \mathrm{SO}(n-1)$.

Notwithstanding the null rotations, for the purposes of classifying stationary trajectories as the orbits of timelike Killing vectors, it is sufficient to work with the isometry group $\mathbb{R} \times \mathrm{SO}(n-1)$. We remark that this is also the isometry group of n-dimensional Schwarzschild spacetime. It then follows that the stationary trajectories in the static patch of dS are

$$\partial_t \qquad\qquad \textit{inertial motions,} \tag{6.69a}$$

$$\partial_t + \sum_{i=1}^{l} a_i \partial_{\theta_{2i-1}} \qquad \textit{circular motions } 1 \leq l \leq \lfloor \tfrac{n-1}{2} \rfloor \,, \tag{6.69b}$$

where $a_i \in \mathbb{R}$ and each ∂_{θ_i} corresponds to a rotation in an independent plane. We remark that in the context of the Myers-Perry black hole solution [162–164], a generalisation of the Kerr metric to higher dimensions, the Killing vectors ∂_{θ_i} correspond to the independent rotations of the black hole.

We bring this Section to a close by remarking that further techniques would

be required to extend this classification to the maximally symmetric spacetime of constant negative curvature, Anti-de Sitter (AdS) spacetime, since, owing to its negative curvature, n-dimensional AdS must be embedded in $\mathbb{R}^{n-1,2}$; hence, its isometry group inherited from $\mathbb{R}^{n-1,2}$ is $\mathrm{SO}^+(n-1,2)$. A classification of the conjugacy classes of the split signature restricted special orthogonal group $\mathrm{SO}^+(n-1,2)$ is therefore needed. To this end, classifications of the conjugacy classes have been given for $\mathrm{SO}^+(2,2)$ and $\mathrm{SO}^+(3,2)$ in [165] and [166], respectively.

6.5 Summary

In this Chapter, we introduced the Frenet-Serret equations, as studied by Frenet [147] and Serret [148], which provide a framework for describing curves in three dimensions in terms of their curvature and torsion. The Frenet-Serret equations were later generalised to n dimensions by Jordan [149], in which work the concepts of curvature and torsion are replaced by generalised curvatures. A particular class of curves for which the Frenet-Serret equations may be solved are the curves of constant generalised curvature. We solved the Frenet-Serret equations explicitly in three spatial dimensions, finding the curve of constant nonzero curvature and torsion, the helix.

Later, the Frenet-Serret equations were generalised from curves in flat Euclidean space $\mathbb{R}^3$ to curves in Minkowski spacetime $\mathbb{R}^{3,1}$ by Letaw [71], allowing for the computation and classification of stationary trajectories in $\mathbb{R}^{3,1}$. In this work, Letaw further found that these trajectories correspond also to the integral curves of timelike Killing vectors.

Building on these works, we extended the classification of stationary curves in $(3+1)$-dimensional Minkowski spacetime to $(n+1)$-dimensional Minkowski spacetime. Due to the insight of Letaw, we classified the stationary trajectories both algebraically and geometrically. Algebraically, we classified the conjugacy classes of the isometry group of $\mathbb{R}^{n,1}$ and identified the timelike Killing vectors within this classification. Geometrically, we derived the Frenet-Serret equations in $n+1$ Minkowski spacetime, employing a basis of vielbeins, and we found an ordinary differential equation satisfied by the generalised four-velocity of the stationary trajectory. To demonstrate the equivalence of these two classifications, we considered a concrete example in $4+1$ Minkowski spacetime. In the general setting, we found five types of trajectories: the inertial motions, the loxodromic motions, the drifted loxodromic motions, the semicubical parabolic motions, and the circular motions, with each type consisting of conjugacy classes with

qualitatively similar motions.

Finally, we brought the Chapter to a close through a new application of the framework, classifying the stationary trajectories of the static patch of dS spacetime. This application is possible as one may embed dS in Minkowski spacetime of one higher spatial dimension. Therefore, dS inherits the isometry group of the embedding space, subject to leaving the embedding equation invariant, and is as such a subgroup of the isometry group of Minkowski spacetime. We found that the loxodromic Killing vectors in Minkowski spacetime are the only timelike Killing vectors that leave the embedding equation invariant. In preparation for Chapter 8, we considered a specific coordinate chart, the static patch. We found that the pullback to the static patch of the loxodromic Killing vectors in the embedding space leads to circular motions.

In the next Chapter, we consider circular motion in Minkowski spacetime with a cylindrical boundary to see the effect of finite size in the response of a detector. However, in Chapter 8, we will return to the spacetimes of constant curvature and combine the insights of finite size and an ambient temperature to consider circular motion in both dS and AdS.

Chapter 7

Circular motion in Minkowski spacetime: thermality versus finite size

"Discworld is real. It's the way worlds should work."

Terry Pratchet
The Science of Discworld III: Darwin's Watch

THE Unruh effect, both linear and circular, as introduced in Chapter 2 rests on several assumptions, which may not be reproducible in an experimental realisation of the effect. We mention now four assumptions. First, the choice of dispersion relation; in the analogue spacetimes provided by condensed-matter systems such as the surface of superfluid helium or in a Bose-Einstein condensate (BEC), the dispersion relation is approximately linear only for small momenta. Second, the choice of field modes. In the discussion of the Unruh effect in Chapter 2, we considered a field in (spatially infinite) Minkowski spacetime; however, any experimental realisation will take place in a spatially finite laboratory. Third, the choice of initial state. Fourth, the choice of interaction time. In Chapter 2, we worked in the long-interaction-time regime; however, any experiment must run for a finite time.

In Chapter 3, we relaxed two of these assumptions; we found the response function of a detector probing a scalar field with a modified dispersion relation prepared in a thermal, rather than vacuum, state in (3.5).

Motivated by the inherent finite size of any experiment, such as the superfluid helium sample volume in Chapter 4 , the focus of this Chapter is the effect of a cylindrical boundary on the experience of an Unruh-DeWitt (UDW) detector. We

consider both when the field is prepared in its vacuum state and when the field is prepared in a thermal state at a fixed temperature. We allow for a modified dispersion relation and briefly discuss the inclusion of a finite-time interaction, touching upon all four of the above assumptions. The contents of this Chapter are based on an article in preparation in collaboration with Jorma Louko [73].

7.1 Spacetime, field, and detector preliminaries

As in Chapter 3, we work in $(2+1)$-dimensional analogue Minkowski spacetime in inertial coordinates (t, x, y) with the metric

$$\mathrm{d}s^2 \;=\; -\mathrm{d}t^2 + \mathrm{d}x^2 + \mathrm{d}y^2 \,. \tag{7.1}$$

We consider a quantised, real scalar field $\hat{\Phi}$ with a dispersion relation that is isotropic in (x, y) and subject to mild monotonicity conditions, which we will specify in Section 7.1.1. We do not assume the dispersion relation to be Lorentz invariant. We denote by $\mathcal{H}_\Phi$ the standard Fock space in which positive frequencies are defined with respect to the timelike Killing vector ∂_t.

To model a cylindrical cavity, we assume the field obeys Dirichlet boundary conditions [167] at some fixed radius $r = a > 0$, $\hat{\Phi}(\mathsf{x})|_{r=a} = 0$. In polar coordinates (t, r, θ), where $(x, y) = (r\cos\theta, r\sin\theta)$, we decompose the field as

$$\hat{\Phi}(\mathsf{x}) \;=\; \sum_{m\in\mathbb{Z}}\sum_{n\in\mathbb{N}} \phi_{mn}(\mathsf{x})\hat{a}_{mn} + \mathrm{Hc}\,, \tag{7.2a}$$

$$\phi_{mn}(\mathsf{x}) \;=\; \frac{1}{\sqrt{2\pi a^2\omega_{mn}}\,|J_{|m|+1}(q_{|m|n})|} J_{|m|}\left(\frac{r}{a}q_{|m|n}\right) \mathrm{e}^{-\mathrm{i}\omega_{mn}t+\mathrm{i}m\theta}\,, \tag{7.2b}$$

where ω_{mn} is the (modified) dispersion relation and $q_{|m|n}$ is the n^{th} zero of the Bessel function of the first kind $J_{|m|}$.

We probe the field by a pointlike detector undergoing uniform circular motion parametrised by Minkowski time t, described by the worldline

$$\mathsf{x}(t) \;=\; (t, R\cos(\Omega t), R\sin(\Omega t))\,, \tag{7.3}$$

where $0 < R < a$ and $\Omega > 0$ are the orbital radius and angular frequency respectively. The orbital speed is $v = R\Omega$ and we assume the trajectory is timelike $v < 1$.

7.1.1 Response function mode sum

We consider two cases. We address first when the field is prepared in the Minkowski vacuum $|0_{\mathrm{M}}\rangle$. We probe the field by a UDW, as detector described in Chapter 3 by the interaction Hamiltonian (2.32). We recall that we are working in an analogue spacetime setting and we denote the detector energy gap by $\overline{E}$. As the inertial response function in $2+1$ dimensions (2.79) is discontinuous at $\overline{E}=0$, we assume $\overline{E}\neq 0$.

In the Minkowski vacuum, the response function $\mathcal{F}$ of a detector probing a scalar field with Dirichlet boundary conditions (7.2) is may be calculated using (7.2) as

$$\mathcal{F}(\overline{E},a) \;=\; \frac{1}{a^2}\sum_{m\in\mathbb{Z}}\sum_{n\in\mathbb{N}}\frac{J^2_{|m|}\big(\frac{R}{a}q_{|m|n}\big)}{\omega_{mn}J^2_{|m|+1}(q_{|m|n})}\delta\big(\omega_{mn}-m\Omega+\overline{E}\big)\;. \tag{7.4}$$

In the case of a massless Klein-Gordon (KG) field, we have $\omega_{mn}=q_{|m|n}/a$ and we may find a condition on the boundary a such that the detector may register excitations $\overline{E}>0$. The response function (7.4) is nonzero when the argument of the delta function vanishes. We have $\omega_{mn}=q_{|m|n}/a>0$ and by assumption, $\Omega>0$. As such, the argument of the delta function in (7.4) may only vanish for $m>0$. The Bessel function zeros $q_{|m|n}$ obey the inequality $m<q_{|m|n}$ [111]. As such, we have

$$0\;<\;\overline{E}\;=\;m\Omega-\frac{q_{|m|n}}{a}\;<\;\frac{m}{a}(a\Omega-1)\;. \tag{7.5}$$

We therefore require $a\Omega>1$, corresponding physically to a point on the boundary $r=a$ co-rotating faster than the speed of light. For de-excitations $\overline{E}<0$, we find no such restrictions.

We address second when the field has been prepared in a thermal state $|\beta\rangle$ in inverse temperature $\beta>0$, where the notion of thermality is with respect to the time evolution generated by ∂_t.

In Chapter 3, we introduced the derivative-coupled interaction Hamiltonian (3.3) to sidestep the otherwise infrared-divergent thermal Wightman function. In a finite-size system with Dirichlet boundary conditions, $\omega_{mn}>0$ is discrete and we do not formally require a derivative coupling between the field and the detector; however, in the large-boundary limit $a\to\infty$, we expect to recover the Minkowski spacetime thermal response function (3.5), which does require a derivative-coupled interaction. For a well-defined continuum limit $a\to\infty$, we use the derivative-coupled interaction Hamiltonian (3.3) and impose the mild monotonicity conditions of Section 3.1.1 on the dispersion relation ω in the large-boundary limit. In particular, we assume that ω is spatially isotropic

such that $\omega = \omega(|\boldsymbol{k}|)$, where $\omega(K)$ is a function of a non-negative argument and ω is positive everywhere except possibly at $K = 0$. We write $\omega'(K) = \mathrm{d}\omega(K)/\mathrm{d}K$ and assume that $\omega'(K) > 0$ for $K > 0$. If $\omega(0) = 0$, we assume that $\omega'(0) > 0$.

With these restrictions on the dispersion relation made, the response function of a detector probing a scalar field with Dirichlet boundary conditions (7.2) prepared in a thermal state is given by

$$\mathcal{F}(\overline{E}, \beta, a) = \mathcal{F}_\infty(\overline{E}, a) + \Delta\mathcal{F}_\beta(\overline{E}, a)\,, \tag{7.6a}$$

$$\mathcal{F}_\infty(\overline{E}, a) = \frac{\overline{E}^2}{a^2} \sum_{m\in\mathbb{Z}} \sum_{n\in\mathbb{N}} \frac{J^2_{|m|}\left(\frac{R}{a} q_{|m|n}\right)}{\omega_{mn} J^2_{|m|+1}(q_{|m|n})} \delta\left(\omega_{mn} - m\Omega + \overline{E}\right)\,, \tag{7.6b}$$

$$\begin{aligned}\Delta\mathcal{F}_\beta(\overline{E}, a) = \frac{\overline{E}^2}{a^2} \sum_{m\in\mathbb{Z}} \sum_{n\in\mathbb{N}} n(\beta\omega_{mn}) \frac{J^2_{|m|}\left(\frac{R}{a} q_{|m|n}\right)}{\omega_{mn} J^2_{|m|+1}(q_{|m|n})} \big(&\delta\left(\omega_{mn} - m\Omega + |\overline{E}|\right) \\ &+ \delta\left(\omega_{mn} - m\Omega - |\overline{E}|\right)\big)\,,\end{aligned} \tag{7.6c}$$

where $\mathcal{F}_\infty$ is the vacuum contribution, independent of β, while $\Delta\mathcal{F}_\beta$ is the additional contribution due to the ambient temperature and $n(x)$ is the Bose thermal factor (2.40). The notation $\mathcal{F}_\infty$ indicates the contribution remaining in the limit $\beta \to \infty$. We also note that $\Delta\mathcal{F}_\beta$ is even in $\overline{E}$ and we have written (7.6) in a way that makes this manifest.

We remark that $\mathcal{F}_\infty$ is related to the vacuum response function (7.4) by

$$\mathcal{F}_\infty(\overline{E}, a) = \overline{E}^2 \mathcal{F}(\overline{E}, a)\,. \tag{7.7}$$

As the thermal response function (7.6) is well defined both for a linear-coupled and derivative-coupled detector model, the relation (7.7) follows by integration by parts within the transition probability [168].

7.1.2 Finite interaction time

In Appendix D and in [3, 90], it was shown that the detector transition rate may be written as

$$\mathcal{P}(\overline{E}) = \frac{\lambda^2}{2\pi} \int_{\mathbb{R}} \mathrm{d}\omega\, \widehat{\mathcal{W}}(\omega) |\widehat{\chi}(\overline{E} - \omega)|^2\,, \tag{7.8}$$

where λ is the coupling constant and $\widehat{\mathcal{W}}$ and $\widehat{\chi}$ are the Fourier transforms of the Wightman function and switching functions respectively. The Fourier transform of the Wightman function, however, is the stationary response function. The response function in the long-time limit may be recovered by considering a switching function such that $|\widehat{\chi}(\omega)|^2 = \delta(\omega)$ is the Dirac delta.

As such, we may take the stationary response function (7.6) and find the finite-time response function, $\mathcal{F}_\chi(\overline{E}) \coloneqq \mathcal{P}(\overline{E})/\lambda^2$,

$$\begin{aligned}\mathcal{F}_\chi(\overline{E},a,\beta) \;=\; & \frac{1}{2\pi a^2}\sum_{m\in\mathbb{Z}}\sum_{n\in\mathbb{N}}\frac{J^2_{|m|}\left(\frac{R}{a}q_{|m|n}\right)}{\omega_{mn}J^2_{|m|+1}(q_{|m|n})}|\widehat{\chi}(\overline{E}+\omega_{mn}-m\Omega)|^2 \\ & +\frac{1}{2\pi a^2}\sum_{m\in\mathbb{Z}}\sum_{n\in\mathbb{N}}n(\beta\omega_{mn})\frac{J^2_{|m|}\left(\frac{R}{a}q_{|m|n}\right)}{\omega_{mn}J^2_{|m|+1}(q_{|m|n})}|\widehat{\chi}(\overline{E}+\omega_{mn}-m\Omega)|^2 \\ & +\frac{1}{2\pi a^2}\sum_{m\in\mathbb{Z}}\sum_{n\in\mathbb{N}}n(\beta\omega_{mn})\frac{J^2_{|m|}\left(\frac{R}{a}q_{|m|n}\right)}{\omega_{mn}J^2_{|m|+1}(q_{|m|n})}|\widehat{\chi}(\overline{E}-\omega_{mn}+m\Omega)|^2\,.\end{aligned} \tag{7.9}$$

The finite-time response function (7.9) incorporates several experimentally relevant features including finite-size and finite-interaction-time effects. In particular, (7.9) is the response of a detector in $(2+1)$-dimensional analogue Minkowski spacetime with a cylindrical boundary, undergoing uniform circular motion, probing a scalar field with dispersion relation ω_{mn}, with Dirichlet boundary conditions at $r=a$, initially prepared in a thermal state in inverse temperature β, with an interaction time described by switching function χ.

In the following Sections, we will specialise to a UDW detector probing a massless field with KG dispersion relation for an infinite amount of time. In particular, we will consider the large-boundary limit $a\to\infty$.

7.2 Large-boundary limit: Vacuum contribution

In this Section, we find the leading and subleading contributions to the vacuum response function $\mathcal{F}$ (7.4) in the large-boundary limit $a\to\infty$ with all other parameters fixed. We specialise to a KG field, such that the response function is given by

$$\mathcal{F}(\overline{E},a) \;=\; \frac{1}{a}\sum_{m\in\mathbb{Z}}\sum_{n\in\mathbb{N}}\frac{J^2_{|m|}\left(\frac{R}{a}q_{|m|n}\right)}{q_{|m|n}J^2_{|m|+1}(q_{|m|n})}\delta(\omega_{mn}-m\Omega+\overline{E})\,, \tag{7.10}$$

where $\omega_{mn}=q_{|m|n}/a$.

Given the distributional nature of the response function (7.10), we introduce the integrated response

$$\mathcal{G}(a) \;=\; \int_{\mathbb{R}}\mathrm{d}\overline{E}\,\sigma(\overline{E})\mathcal{F}(\overline{E},a)\,, \tag{7.11}$$

where $\sigma\in C^\infty_0(\mathbb{R})$ is a real-valued function of compact support such that $0\notin$

$\mathrm{supp}\{\sigma\}$ and either $\mathrm{supp}\{\sigma\} \subset \mathbb{R}_{>0}$ or $\mathrm{supp}\{\sigma\} \subset \mathbb{R}_{<0}$.

For the response function (7.10), the integrated response reads

$$\mathcal{G}(a) \;=\; \frac{1}{a}\sum_{m\in\mathbb{Z}}\sum_{n\in\mathbb{N}} \frac{J^2_{|m|}\big(\frac{R}{a}q_{|m|n}\big)}{q_{|m|n}J^2_{|m|+1}(q_{|m|n})}\sigma(m\Omega-\omega_{mn})\,. \tag{7.12}$$

In Appendix H, we show that

$$\begin{aligned}\mathcal{G}(a) \;=\; &\int_{\mathbb{R}} \mathrm{d}\overline{E}\,\sigma(E)\Bigg(\frac{1}{2}\sum_{m>\overline{E}/\Omega} J^2_{|m|}(mv-\overline{E}R)\\ &-\frac{R^2}{4a^3}\Bigg(\sum_{n=1}^{\infty}\Bigg[\frac{\pi^3}{2}(n+\tfrac{1}{4})^2-\frac{3\pi}{16}-\frac{q^2_{1n}}{q_{1n}J^2_2(q_{1n})}\Bigg]+\frac{\pi(5\pi^2-18)}{128}\Bigg)\delta(|\overline{E}|-\Omega)+o(a^{-3})\Bigg)\,,\end{aligned} \tag{7.13}$$

where $\delta(|\overline{E}|-\Omega)=\delta(\overline{E}-\Omega)+\delta(\overline{E}+\Omega)$.

By comparison with (7.11), we read off the response function as

$$\begin{aligned}\mathcal{F}(\overline{E},a) \;=\; &\frac{1}{2}\sum_{m>\overline{E}/\Omega} J^2_{|m|}(mv-\overline{E}R)\\ &-\frac{R^2}{4a^3}\Bigg(\sum_{n=1}^{\infty}\Bigg[\frac{\pi^3}{2}(n+\tfrac{1}{4})^2-\frac{3\pi}{16}-\frac{q^2_{1n}}{q_{1n}J^2_2(q_{1n})}\Bigg]+\frac{\pi(5\pi^2-18)}{128}\Bigg)\delta(|\overline{E}|-\Omega)+o(a^{-3})\,,\end{aligned} \tag{7.14}$$

where the o-notation is used in a distributional sense.

The leading-order contribution to (7.14) is the mode-sum representation of the response of a detector undergoing uniform circular motion in (unbounded) Minkowski spacetime [169]. The subleading term, at order a^{-3}, contributes only for detectors whose angular frequency is equal to their energy gap. We remark that numerical evidence suggests that the overall coefficient is negative, as one might expect on physical grounds; a boundary reduces the density of states.

As a mathematical side outcome of this asymptotic analysis, we find an asymptotic expansion of the normalisation factor in (7.12) in terms of the McMahon expansion for large zeros of the Bessel function, $q_{|m|n}$ as $n\to\infty$ [111], which we have not encountered in the existing literature,

$$\frac{1}{q_{|m|n}J^2_{|m|+1}(q_{|m|n})} \;\sim\; \frac{\pi}{2}X'_{|m|}(\pi\alpha_{|m|n})\,, \tag{7.15}$$

as $n\to\infty$, where $\alpha_{|m|n}\coloneqq n+\frac{1}{2}|m|-\frac{1}{4}$ and $X_{|m|}$ is given by (H.7). The McMahon expansion reads $q_{|m|n}\;\sim X_{|m|}(\pi\alpha_{|m|n})$. The proof of this asymptotic behaviour

was provided by Gergő Nemes (Tokyo Metropolitan University) [170] and is given in Appendix H.

7.2.1 Static observers

In the static observer limit, $\Omega \to 0$ with R fixed, we note that the subleading term in (7.14) is proportional to $\delta(\overline{E})$. We do not consider detectors with an energy gap of zero, hence this correction term vanishes in the limit $\Omega \to 0$.

The behaviour of the leading-order term depends on the sign of the energy gap. For $\overline{E} > 0$, the summation in the leading contribution vanishes. For $\overline{E} < 0$, the summation becomes

$$\lim_{\Omega\to 0} \frac{1}{2} \sum_{m>\overline{E}/\Omega} J^2_{|m|}(mv - \overline{E}R) \;=\; \frac{1}{2}\sum_{m\in\mathbb{Z}} J^2_{|m|}(\overline{E}R) \;=\; \frac{1}{2}\,, \tag{7.16}$$

where we have used Neumann's addition formula [111], $\sum_{m\in\mathbb{Z}} J^2_{|m|}(x) = 1$. This may be summarised as

$$\lim_{\Omega\to 0} \mathcal{F}(\overline{E}, a) \;=\; \frac{1}{2}\Theta(-\overline{E}) + o(a^{-3})\,, \tag{7.17}$$

which we recognise as the response function for a detector undergoing inertial motion in unbounded Minkowski spacetime (2.79).

7.3 Large-boundary limit: Thermal contribution

In this Section, we find the leading and subleading contributions to the thermal response function $\mathcal{F}(\overline{E}, a, \beta)$ in the large-boundary limit $a \to \infty$ with all other parameters fixed. We specialise to a KG field, such that the response function is given by

$$\mathcal{F}(\overline{E}, \beta, a) \;=\; \mathcal{F}_\infty(\overline{E}, a) + \Delta\mathcal{F}_\beta(\overline{E}, a)\,, \tag{7.18a}$$

$$\mathcal{F}_\infty(\overline{E}, a) \;=\; \frac{\overline{E}^2}{a}\sum_{m\in\mathbb{Z}}\sum_{n\in\mathbb{N}} \frac{J^2_{|m|}\big(\frac{R}{a}q_{|m|n}\big)}{q_{|m|n}J^2_{|m|+1}(q_{|m|n})}\delta\big(\omega_{mn} - m\Omega + \overline{E}\big)\,, \tag{7.18b}$$

$$\Delta\mathcal{F}_\beta(\overline{E}, a) \;=\; \frac{\overline{E}^2}{a}\sum_{m\in\mathbb{Z}}\sum_{n\in\mathbb{N}} n(\beta\omega_{mn}) \frac{J^2_{|m|}\big(\frac{R}{a}q_{|m|n}\big)}{q_{|m|n}J^2_{|m|+1}(q_{|m|n})}\big(\delta\big(\omega_{mn} - m\Omega + |\overline{E}|\big) + \delta\big(\omega_{mn} - m\Omega - |\overline{E}|\big)\big)\,, \tag{7.18c}$$

where $\omega_{mn} = q_{|m|n}/a$ and n is the Bose thermal factor (2.40).

To address $\mathcal{F}_\infty$, we recall the relation $\mathcal{F}_\infty(\overline{E},a) = \overline{E}^2\mathcal{F}(\overline{E},a)$ (7.7). As such, the asymptotic behaviour of $\mathcal{F}_\infty$ is given by (7.14) multiplied by $\overline{E}^2$.

We address now the thermal contribution to the response function $\Delta\mathcal{F}_\beta$. Given the distributional nature of $\Delta\mathcal{F}_\beta$, we introduce the integrated response function contribution due to finite temperature

$$\Delta\mathcal{G}_\beta(a) \;=\; \int_{\mathbb{R}} \mathrm{d}\overline{E}\,\overline{E}^{-2}\,\sigma(\overline{E})\Delta\mathcal{F}_\beta(\overline{E})\,, \tag{7.19}$$

where $\sigma \in C_0^\infty(\mathbb{R})$ is a real-valued function of compact support such that $0 \notin \mathrm{supp}\{\sigma\}$ and either $\mathrm{supp}\{\sigma\} \subset \mathbb{R}_{>0}$ or $\mathrm{supp}\{\sigma\} \subset \mathbb{R}_{<0}$.

For the thermal contribution to the response function $\Delta\mathcal{F}_\beta$ (7.18c), the integrated response due to finite temperature reads

$$\Delta\mathcal{G}_\beta(a) \;=\; \frac{1}{a}\sum_{m\in\mathbb{Z}}\sum_{n\in\mathbb{Z}} n(\beta\omega_{mn})\frac{J^2_{|m|}\left(\frac{R}{a}q_{|m|n}\right)}{q_{|m|n}J^2_{|m|+1}(q_{|m|n})}\big(\sigma(m\Omega-\omega_{mn}) + \sigma(-(m\Omega-\omega_{mn}))\big)\,. \tag{7.20}$$

In Appendix I, we show that

$$\begin{aligned}\Delta\mathcal{G}_\beta(a) \;=\; & \\ \int_{\mathbb{R}} \mathrm{d}\overline{E}\,\overline{E}^{-2}\sigma(\overline{E})\Bigg(&\frac{\overline{E}^2}{2}\sum_{m>|\overline{E}|/\Omega} n(\beta\omega_+)J^2_{|m|}(\omega_+R) + \frac{\overline{E}^2}{2}\sum_{m>-|\overline{E}|/\Omega} n(\beta\omega_-)J^2_{|m|}(\omega_-R) \\ &- \frac{R^2\overline{E}^2}{2\beta a^2}\left[\sum_{n=1}^{\infty}\left(\frac{\pi^2}{2}(n+\tfrac{1}{4}) - \frac{q_{1n}}{q_{1n}J_2^2(q_{1n})}\right) + \frac{(23\pi^2-36)}{192}\right]\delta(|\overline{E}|-\Omega) + o(a^{-2})\Bigg)\,,\end{aligned} \tag{7.21}$$

where $\omega_\pm = m\Omega \mp |\overline{E}|$ and $\delta(|\overline{E}|-\Omega) = \delta(\overline{E}-\Omega) = \delta(\overline{E}+\Omega)$. By comparison with (7.19), we read off the thermal contribution to the response function $\Delta\mathcal{F}_\beta$ as

$$\begin{aligned}\Delta\mathcal{F}_\beta(\overline{E},a) \;=\; & \frac{\overline{E}^2}{2}\sum_{m>|\overline{E}|/\Omega} n(\beta\omega_+)J^2_{|m|}(\omega_+R) + \frac{\overline{E}^2}{2}\sum_{m>-|\overline{E}|/\Omega} n(\beta\omega_-)J^2_{|m|}(\omega_-R) \\ &- \frac{R^2\overline{E}^2}{2\beta a^2}\left[\sum_{n=1}^{\infty}\left(\frac{\pi^2}{2}(n+\tfrac{1}{4}) - \frac{q_{1n}}{q_{1n}J_2^2(q_{1n})}\right) + \frac{(23\pi^2-36)}{192}\right]\delta(|\overline{E}|-\Omega) + o(a^{-2})\,.\end{aligned} \tag{7.22}$$

The leading-order contribution to (7.22) is the mode-sum representation of the thermal contribution to the response function of a detector undergoing uniform circular motion in (unbounded) Minkowski spacetime [1]. The subleading term,

at order a^{-2}, contributes only for detectors whose angular frequency is equal to their energy gap. As for the vacuum contribution, numerical evidence suggests that the overall coefficient is negative, as expected. We remark that the presence of an ambient temperature means that a detector is more sensitive to a boundary.

7.3.1 Static observers

In the static observer limit, $\Omega \to 0$ with R fixed, (7.22) reduces to

$$\lim_{\Omega\to 0} \Delta\mathcal{F}_\beta(\overline{E}, a) = \frac{1}{2} n(\beta|\overline{E}|)\overline{E}^2 \sum_{m\in\mathbb{Z}} J^2_{|m|}(|\overline{E}|R)\,, \tag{7.23a}$$

$$= \frac{1}{2}\overline{E}^2 n(\beta|\overline{E}|)\,, \tag{7.23b}$$

using Neumann's addition formula [111].

The static observer in a thermal bath therefore registers the response function given by (7.17) and (7.23b),

$$\mathcal{F}_{\text{static}}(\overline{E}, a, \beta) = \frac{\overline{E}^2}{2}\Theta(-\overline{E}) + \frac{\overline{E}^2}{2} n(\beta|\overline{E}|)\,. \tag{7.24}$$

We recall that the overall factor of $\overline{E}^2$ arises from the derivative coupling, ensuring that (7.24) remains finite in the limit $\overline{E} \to 0$. We may calculated the detailed balance temperature (3.9) experienced by the static detector,

$$T_{\text{DB}} = \frac{1}{\beta}\,. \tag{7.25}$$

As expected, static observers in a thermal bath register a response function with the characteristics of a thermometer [26].

7.4 Summary

In this Chapter, motivated by the experimental modelling of Chapter 4, we addressed the effect of thermality and finite size on the experience of a UDW detector. Initially allowing for full generality, we included a modified dispersion relation, an initial thermal state, boundary conditions, and a finite-time interaction, resulting in the response function (7.9). We then specialised to a KG field probed by a detector for an infinite amount of time.

In the large-boundary limit $a \to \infty$, we found the leading and subleading contributions to the response function both when the field was prepared in its vacuum state and when the field was prepared in a thermal state in a fixed

temperature. In both cases, we recovered at leading order the response function for a detector in unbounded Minkowski spacetime. At subleading order, we found resonance peaks in the detector's response, more significant when the field has an ambient temperature. The overall sign of the resonance peaks is negative, representing the reduction in the density of states in the system due to the presence of a boundary. These peaks are only present for detectors whose angular frequency matches their energy gap.

In Chapter 3 and Chapter 5, we found that a detector with $\overline{E} > \Omega$ is unable to distinguish between linear motion through a thermal bath and circular motion through a thermal bath at the same speed. In this Chapter, we see that the interplay between the angular frequency Ω and detector energy gap $\overline{E}$ again plays a role — resonant detectors with $\overline{E} = \Omega$ are more sensitive to a cylindrical boundary. Furthermore, resonant detectors probing a field in a thermal state are yet more responsive to a cylindrical boundary.

In this Chapter, we did not discuss the detailed balance temperature as a measure of detector response; the definition of the effective, detailed balance temperature (3.9) involves the natural logarithm of the ratio of response functions. The response functions (7.10) and (7.18) and their asymptotic expansions (7.14) and (7.22) contain contributions from Dirac deltas and hence their natural logarithms are not well defined. We may observe from (7.9) that the Dirac deltas arise from the long-interaction-time limit. As such, a detector interacting for a strictly finite amount of time will register a well-defined effective temperature. We leave the analysis of finite-time effects to future work.

In the next Chapter, we consider the spacetimes of constant positive and negative curvature, de Sitter (dS) and Anti-de Sitter (AdS), in which a positive curvature provides a notion of an ambient temperature, via the Euclidean vacuum, whereas negative curvature provides a notion of spatial confinement. Using the results of this Chapter and Chapter 3, we analyse how closely dS and AdS may be considered curved-spacetime analogues of finite temperature and finite size.

Chapter 8

Interlude — Circular motion in (anti-)de Sitter spacetime: thermality versus finite size

> *"The field equations, in their most general form, contain a term multiplied by a constant, which is denoted by the Greek letter Λ... sometimes called the "cosmical constant." This is a name without any meaning."*
>
> Willem de Sitter
> *Kosmos* (1932)

MINKOWSKI spacetime is the spacetime of constant vanishing curvature; it is an exact vacuum solution of Einstein's field equations with vanishing cosmological constant Λ. If one allows the inclusion of a nonzero cosmological constant, one may find two further exact vacuum solutions of constant positive curvature and constant negative curvature, de Sitter (dS) and Anti-de Sitter (AdS), respectively [171–173]. These solutions may be viewed as one-parameter extensions of Minkowski spacetime, as both spacetimes reduce to Minkowski spacetime in the limit of vanishing cosmological constant.

In our presentation of the Unruh effect in Chapter 2, there were two key ingredients: that the underlying spacetime be Minkowski and that the trajectory be linearly accelerated. Throughout this Thesis, we explored other Unruh-like phenomena [71, 72, 91], such as circular motion and hypertor motion, giving a classification of all such uniformly accelerated trajectories in Chapter 6. Now, instead of changing the trajectory, one may consider changing the underlying

spacetime; the two natural candidates are dS and AdS.

The dS and AdS spacetimes of $n+1$ dimensions may be embedded in $\mathbb{R}^{n+1,1}$ and $\mathbb{R}^{n,2}$ respectively. In 1997, Deser and Levin [174, 175] demonstrated that the Unruh effect in the embedding spacetime descends into the embedded spacetimes. In AdS, however, there is a critical acceleration [144], below which a detector may not excite and no thermality may be registered. This approach, investigating a spacetime through its embedding space, has become known as the Global Embedding Minkowski Spacetime (GEMS) approach. Finally, in the domain of the AdS/CFT correspondence, there is an exact solution to the geometry describing a string accelerating through AdS [176], in which geometry, due to the acceleration, a horizon forms, splitting the string into two causally disconnected pieces; hence, a Gibbons-Hawking temperature [50] may be associated with the horizon, the Unruh temperature.

In this Chapter, we investigate the circular motion Unruh effect in a genuinely relativistic but curved-spacetime setting, in $2+1$ dS and $2+1$ AdS spacetimes, where positive curvature provides a notion of an ambient temperature, via the Euclidean vacuum, whereas negative curvature provides a notion of spatial confinement. For AdS, the role of a boundary is played by the asymptotically AdS infinity, where a boundary condition is needed to make the quantum dynamics unitary [177], as information may reach spatial infinity in finite coordinate time. For the static patch of dS, to which we refer as Rindler-de Sitter (RdS) spacetime, the restriction of the Euclidean vacuum is a thermal state [178–180] in a temperature proportional to the square root of the cosmological constant.

In the limit of a small cosmological constant, the ambient temperature of RdS tends to zero and the time for information to reach spatial infinity in AdS tends to infinite. By comparison with the results of Chapter 3 and Chapter 7, we investigate how closely RdS and AdS may be considered as curved-spacetime analogues of a low ambient temperature and a large cylindrical boundary. The contents of this Chapter were extracted from, or based on, the preprint "Circular motion in (anti-)de Sitter spacetime: thermality versus finite size" [5] in collaboration with Jorma Louko.

8.1 Anti-de Sitter spacetime

In this Section, we consider the spacetime of constant negative curvature, AdS spacetime [84]. AdS is not globally hyperbolic owing to its timelike boundary at spatial infinity, through which information can propagate [177]. However, by imposing boundary conditions at spatial infinity, one can employ a consistent

quantisation scheme for a quantum field [177, 181–187]. We adopt the Dirichlet boundary condition at spatial infinity and consider the response of the detector in the small cosmological constant limit, with the field in its global vacuum. Thermal states will be considered in Section 8.2.

8.1.1 Spacetime, field, and detector preliminaries

Anti-de Sitter spacetime in $2+1$ dimensions can be embedded in $\mathbb{R}^{2,2}$ with the embedding equation

$$\eta^{2,2}_{AB} X^A X^B \;=\; -\alpha^2 \,, \tag{8.1}$$

where $\alpha > 0$ is the radius of curvature [84], $X^A = (T^0, T^1, X^1, X^2)$ are the coordinates on $\mathbb{R}^{2,2}$, and $\eta^{2,2}_{AB} = \mathrm{diag}(-1,-1,1,1)$. The cosmological constant Λ is related to α by $\Lambda = -1/\alpha^2$. The Ricci scalar of AdS_3 is $\mathcal{R} = -6/\alpha^2$. We have adopted the notation $\eta^{p,q}$ to emphasise the signature of the embedding space.

In this Chapter, we work in the Universal Covering Space of Anti-de Sitter (CAdS), which contains no closed timelike curves. Points on CAdS are denoted by x. We use the global coordinates (t, r, θ) in which the metric on AdS_3 is given by

$$\mathrm{d}s^2 \;=\; -\left(1 + \frac{r^2}{\alpha^2}\right)\mathrm{d}t^2 + \frac{\mathrm{d}r^2}{1+\frac{r^2}{\alpha^2}} + r^2 \mathrm{d}\theta^2 \,, \tag{8.2}$$

where $-\infty < t < \infty$, $0 \le r < \infty$, and $0 \le \theta < 2\pi$, with the usual coordinate singularity at $r = 0$ and θ periodicially identified with period 2π. The embedding in the embedding space $\mathbb{R}^{2,2}$ is given by

$$T^0 \;=\; \sqrt{r^2+\alpha^2}\cos(t/\alpha) \,, \tag{8.3a}$$
$$T^1 \;=\; \sqrt{r^2+\alpha^2}\sin(t/\alpha) \,, \tag{8.3b}$$
$$X^1 \;=\; r\cos\theta \,, \tag{8.3c}$$
$$X^2 \;=\; r\sin\theta \,. \tag{8.3d}$$

The small cosmological constant limit $\Lambda \to 0^-$ is given by the limit $\alpha \to \infty$, which recovers Minkowski spacetime $\mathbb{R}^{2,1}$, as can be seen by the form of the metric (8.2).

We consider a quantised, real, massless, conformally coupled scalar field $\hat{\Phi}$ and we probe the field with a pointlike detector in uniform circular motion,

$$(t, r, \theta) \;=\; (\gamma\tau, R, \Omega\gamma\tau) \,, \tag{8.4}$$

where τ is proper time, $R > 0$ is the radius, $\Omega = \frac{\mathrm{d}\theta}{\mathrm{d}t} > 0$ is the angular velocity,

and

$$\gamma \;=\; \frac{1}{\sqrt{1-R^2\Omega^2+\frac{R^2}{\alpha^2}}}\,, \tag{8.5}$$

to which we refer as the Lorentz factor for circular motion in AdS. We assume that the worldline is timelike, $R\Omega < \sqrt{1+R^2/\alpha^2}$.

In the large-boundary limit, we have $\lim_{\alpha\to\infty}\gamma = \frac{1}{\sqrt{1-R^2\Omega^2}} = \Gamma$, where Γ is the Lorentz factor associated with circular motion in Minkowski spacetime $\mathbb{R}^{2,1}$.

The detector-field interaction is described by the interaction Hamiltonian (2.32). The detector energy gap is denoted $E \in \mathbb{R}\setminus\{0\}$ and the Hamiltonian of the detector $H_{\rm D}$ generates dynamics with respect to the proper time τ.

In this Section, we will consider first a finite-time interaction, working with the response function

$$\mathcal{F}(E) \;=\; \int \mathrm{d}\tau'\mathrm{d}\tau''\chi(\tau')\chi(\tau'')\mathrm{e}^{-\mathrm{i}E(\tau'-\tau'')}\mathcal{W}(\tau',\tau'')\,, \tag{8.6}$$

where $\mathcal{W}(\tau',\tau'')$ is the pullback of the Wightman function $\mathcal{W}(\mathsf{x}',\mathsf{x}'') = \langle\hat{\Phi}(\mathsf{x}')\hat{\Phi}(\mathsf{x}'')\rangle$ to the circular trajectory.

We prepare the field Φ in the global vacuum state, defined with respect to the global timelike Killing vector ∂_t in coordinates (8.2). Then, the Wightman function for a scalar field in AdS_3 is given by [34, 188]

$$\mathcal{W}(\mathsf{x}',\mathsf{x}'') \;=\; \frac{1}{4\pi}\left(\frac{1}{\sqrt{\sigma(\mathsf{x}',\mathsf{x}'')}}+\frac{\zeta}{\sqrt{\sigma(\mathsf{x}',\mathsf{x}'')+4\alpha^2}}\right)\,, \tag{8.7a}$$

$$\sigma(\mathsf{x}',\mathsf{x}'') \;=\; \eta^{2,2}_{AB}\Big(X'^A-X''^A\Big)\Big(X'^B-X''^B\Big)\,, \tag{8.7b}$$

where $\zeta \in \{-1,0,1\}$ corresponding to Dirichlet, transparent, or Neumann boundary conditions at spatial infinity and σ is the geodesic squared distance in the embedding space.

We will only consider Dirichlet boundary conditions, $\zeta = -1$. We adopt the notation $\mathcal{W}(\tau',\tau'') = \mathcal{W}(\mathsf{x}(\tau'),\mathsf{x}(\tau''))$ and $\sigma(\tau',\tau'') = \sigma(\mathsf{x}(\tau'),\mathsf{x}(\tau''))$ for the pullback of the Wightman function (8.7a) and geodesic squared distance (8.7b) to a trajectory $\mathsf{x}(\tau)$ parametrised by its proper time. Along a stationary trajectory [4, 71, 91], such as uniform circular motion, the Wightman function (8.7a) is stationary in the sense of (2.42). The Wightman function should be understood in the distributional sense as $\lim_{\varepsilon\to0^+}\mathcal{W}(\tau'-\tau''-\mathrm{i}\varepsilon,0)$. Then, in (8.7a), the branch of the square root is taken such that the limit $\varepsilon\to0^+$ of the square root is positive when $\sigma(\mathsf{x}',\mathsf{x}'')>0$ [34].

The geodesic squared distance in global coordinates along the circular trajec-

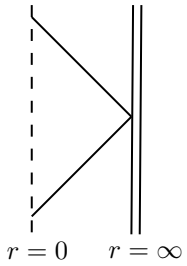

Figure 8.1: Conformal diagram of CAdS.

tory is given by

$$\sigma(s,0) \;=\; -4\alpha^2 \sin^2\Big(\frac{\gamma s}{2\alpha}\Big) - 2R^2\Big(\cos(\Omega\gamma s) - \cos\Big(\frac{\gamma s}{\alpha}\Big)\Big)\;. \tag{8.8}$$

The Wightman function associated with (8.8) has a pole at $s = 0$ and two infinite families of branch points. In the large-boundary limit, these branch points lie around $s = \frac{2\alpha}{\gamma}\pi n$ and $s = \frac{2\alpha}{\gamma}\frac{(2k+1)}{2}\pi$ with $n,\ k \in \mathbb{Z}$. As such, the singularity structure of the Wightman function in CAdS_3 is fundamentally different from the Wightman function of the Minkowski vacuum in $\mathbb{R}^{2,1}$, which has a single pole at $s = 0$.

8.1.2 Finite-time interaction

To sidestep the technical challenge of handling the branch points directly, we use a switching function χ of compact support. For α sufficiently large, the only singularity in the domain of the integral is the pole at $s = 0$. Keeping the support of the switching function fixed, we perform a large-α expansion under the integral by a dominated-convergence argument. After this, we take the long-interaction-time limit.

Using the time-translation of the Wightman function (8.7a) along the circular trajectory, we rewrite the response function (8.6) as

$$\mathcal{F}(E) \;=\; \int \mathrm{d}s\, X(s) \mathrm{e}^{-\mathrm{i}Es} \mathcal{W}(s,0)\,, \tag{8.9}$$

where X is the self-convolution of χ,

$$X(s) \;=\; \int \mathrm{d}\tau'\, \chi(\tau' + \tfrac{1}{2}s)\chi(\tau' - \tfrac{1}{2}s)\,. \tag{8.10}$$

We assume χ to be smooth and of compact support. X is then also smooth and of compact support. In the long-interaction-time limit, one usually lets $\chi \to 1$ and divides by the total interaction time because the response function (8.6) diverges linearly with the interaction time. In terms of X (8.10), this process amounts to

the limit $X \to 1$.

In $\mathcal{F}(E)$ (8.9), we first handle the singular behaviour at $s = 0$ coming from the term $1/(4\pi\sqrt{\sigma(s,0)}\,)$ in (8.7a), understood again in the distributional sense $\lim_{\varepsilon\to 0^+} 1/(4\pi\sqrt{\sigma(s-\mathrm{i}\varepsilon,0)}\,)$, where the square root in the denominator is positive imaginary for $s > 0$ and negative imaginary for $s < 0$.

Around $s = 0$, we have the expansion

$$\mathcal{W}(s-\mathrm{i}\varepsilon,0) \sim \frac{1}{4\pi\mathrm{i}(s-\mathrm{i}\varepsilon)}\,. \tag{8.11}$$

As in Chapter 5, we may isolate the singular contribution to the Wightman function by adding and subtracting (8.11) under the integral [3, 69],

$$\mathcal{F}(E) \;=\; \int \mathrm{d}s\, X(s)\mathrm{e}^{-\mathrm{i}Es}\left(\mathcal{W}(s-\mathrm{i}\varepsilon,0) - \frac{1}{4\pi\mathrm{i}(s-\mathrm{i}\varepsilon)} + \frac{1}{4\pi\mathrm{i}(s-\mathrm{i}\varepsilon)}\right). \tag{8.12}$$

In the first two terms in (8.12), the singularities at $s = 0$ cancel, and the $\varepsilon \to 0^+$ limit may be taken under the integral. We may hence split the integral as

$$\mathcal{F}(E) \;= \mathcal{F}_0(E) + \mathcal{F}_{\text{corr}}(E)\,, \tag{8.13a}$$

$$\mathcal{F}_0(E) \;=\; \int \mathrm{d}s\, \frac{X(s)\mathrm{e}^{-\mathrm{i}Es}}{4\pi\mathrm{i}(s-\mathrm{i}\varepsilon)}\,, \tag{8.13b}$$

$$\mathcal{F}_{\text{corr}}(E) \;=\; \int \mathrm{d}s\, X(s)\mathrm{e}^{-\mathrm{i}Es}\left(\mathcal{W}(s,0) - \frac{1}{4\pi\mathrm{i}s}\right). \tag{8.13c}$$

To address (8.13b), we appeal to the Sokhotski-Plemelj (pol. Sochocki, rus. Сохоцкий) theorem [189],

$$\lim_{\varepsilon\to 0^+} \int_a^b \mathrm{d}x\, \frac{f(x)}{x-\mathrm{i}\varepsilon} = \mathrm{i}\pi f(0) + \mathcal{P}\int_a^b \mathrm{d}x\, \frac{f(x)}{x}\,, \tag{8.14}$$

where $\mathcal{P}$ indicates the Cauchy principal value. An application of (8.14) to (8.13b) leads to

$$\mathcal{F}_0(E) \;=\; \frac{1}{4}X(0) - \frac{1}{2\pi}\int_0^\infty \mathrm{d}s\, \frac{X(s)\sin(Es)}{s}\,, \tag{8.15a}$$

where we have used that $X(s)$ is even.

Owing to the compact support of X, we may express the integrand of $\mathcal{F}_{\text{corr}}$ (8.13c) as an asymptotic power series in α, where, for sufficiently large α, the singularities of the Wightman function are outside of the support of X and the error term is uniform in s.

Using the Wightman function (8.7a) with Dirichlet boundary conditions $\zeta = -1$, $\mathcal{F}_{\text{corr}}$ (8.13c) may be written as

$$\mathcal{F}_{\text{corr}}(E) \;=\; \frac{1}{4\pi\mathrm{i}}\int \mathrm{d}s\, X(s)\mathrm{e}^{-\mathrm{i}Es}\left(\frac{1}{\sqrt{-\sigma(s,0)}}-\frac{1}{s}\right)-\frac{1}{8\pi\alpha}\int \mathrm{d}s\,\frac{X(s)\mathrm{e}^{-\mathrm{i}Es}}{\sqrt{1+\frac{\sigma(s,0)}{4\alpha^2}}}\,. \tag{8.16}$$

We recall that $\sqrt{-\sigma(s,0)}$ is positive for $s > 0$ and negative for $s < 0$, the integrand in the first term in (8.16) is nonsingular at $s = 0$, $\sigma(s,0)$ (8.8) for fixed $s \neq 0$ has a large-α expansion in integer powers of α^{-2}, and X has compact support. It then follows that the large-α expansion of (8.16) proceeds in integer powers of α^{-1}. The even powers will come from the first term and the odd powers will come from the second term. Note that the first term is independent of the boundary condition at infinity in (8.7a) and so contains only curvature corrections, whereas the second term is responsible for both boundary effects and curvature corrections.

8.1.3 Large-α limit

In this Section, we calculate the first four terms in the large-α expansion of the response function (8.13). We interpret each term in the long-interaction-time limit and compare these terms with the large-boundary limit in $2+1$ Minkowski spacetime with a cylindrical boundary [73] of Chapter 7.

We begin with the terms of order unity. The first is given by $\mathcal{F}_0$ (8.15) and the second is found by a large-α expansion under the first integral in (8.16),

$$\mathcal{F}^{(0)}_{\text{corr}}(E) \;=\; \lim_{\alpha\to\infty}\mathcal{F}_{\text{corr}}(E)\,, \tag{8.17a}$$

$$=\frac{1}{2\pi}\int_0^\infty \mathrm{d}s\, X(s)\frac{\sin(Es)}{s}\left(1-\frac{1}{\sqrt{\Gamma^2-4R^2\sin^2\left(\frac{\Gamma\Omega}{2}s\right)/s^2}}\right)\,, \tag{8.17b}$$

where $\Gamma \coloneqq (1-R^2\Omega^2)^{-1/2}$ is the Lorentz factor associated with circular motion in Minkowski spacetime. We are able to take the limit under the integral by the dominated convergence theorem owing to the compact support of X. Since the integrand of (8.17b) is even, we have combined the $s < 0$ and $s > 0$ contributions to write the integral over $s > 0$.

We find the order-α^{-1} contribution by a large-α expansion under the second integral in (8.16), leading to

$$\mathcal{F}^{(1)}_{\text{corr}} \;=\; -\frac{1}{8\pi\alpha}\int \mathrm{d}s\, X(s)\mathrm{e}^{-\mathrm{i}Es}\,. \tag{8.18}$$

The order-α^{-2} contribution comes from the large-α under the first integral

in (8.16)

$$\mathcal{F}^{(2)}_{\text{corr}}(E) \;=\; -\frac{1}{8\pi \mathrm{i}\alpha^2}\int \mathrm{d}s\, X(s)\mathrm{e}^{-\mathrm{i}Es}\frac{\left(-\frac{1}{12}\Gamma^4 s + R^4\Omega\Gamma^3\frac{\sin(\Omega\Gamma s)-\Omega\Gamma s}{s^2}\right)}{\left(\Gamma^2 - 4R^2\sin^2\left(\frac{\Gamma\Omega}{2}s\right)/s^2\right)^{3/2}}\,. \tag{8.19}$$

The integrand is nonsingular at $s = 0$.

The order-α^{-3} contribution arises from the large-α expansion under the second integral in (8.16),

$$\mathcal{F}^{(3)}_{\text{corr}}(E) \;=\; -\frac{1}{64\pi\alpha^3}\int \mathrm{d}s\, X(s)\mathrm{e}^{-\mathrm{i}Es}\left(\Gamma^2 s^2 - 4R^2\sin^2\left(\tfrac{\Gamma\Omega}{2}s\right)\right)\,. \tag{8.20}$$

8.1.3.1 Long-interaction-time limit

We consider now the long-interaction-time limit $X(s) \to 1$ of the terms in the asymptotic expansion. The leading-order contributions are the limiting forms of (8.15) and (8.17b),

$$\mathcal{F}_0(E) \;=\; \frac{1}{2}\Theta(-E)\,, \tag{8.21a}$$

$$\mathcal{F}^{(0)}_{\text{corr}}(E) \;=\; \frac{1}{2\pi}\int_0^\infty \mathrm{d}s\,\frac{\sin(Es)}{s}\left(1 - \frac{1}{\sqrt{\Gamma^2 - 4R^2\sin^2\left(\frac{\Gamma\Omega}{2}s\right)/s^2}}\right)\,. \tag{8.21b}$$

The first term (8.21a) is the response of an inertial detector in $2+1$ Minkowski spacetime (2.79), whereas both terms combined are the response function of a detector in uniform circular motion in $2+1$ Minkowski spacetime, given by (2.80b).

The order-α^{-1} term (8.18) in the long-interaction-time limit is

$$\mathcal{F}^{(1)}_{\text{corr}}(E) \;=\; -\frac{1}{4\alpha}\delta(E)\,, \tag{8.22}$$

which vanishes as $E \neq 0$ by assumption.

The order-α^{-2} term (8.19) is

$$\mathcal{F}^{(2)}_{\text{corr}}(E) \;=\; -\frac{1}{4\pi\alpha^2}\int_0^\infty \mathrm{d}s\,\sin(Es)\frac{\left(-\frac{1}{12}\Gamma^4 s + R^4\Omega\Gamma^3\frac{\sin(\Omega\Gamma s)-\Omega\Gamma s}{s^2}\right)}{\left(\Gamma^2 - 4R^2\sin^2\left(\frac{\Gamma\Omega}{2}s\right)/s^2\right)^{3/2}}\,. \tag{8.23}$$

We shall return to the interpretation of this term at the end of this Section.

The order-α^{-3} term (8.20) can be expressed as

$$\mathcal{F}^{(3)}_{\text{corr}}(E) = \frac{1}{64\pi\alpha^3}\left(2R^2+\Gamma^2\frac{\partial^2}{\partial E^2}\right)\int \mathrm{d}s\, X(s)\mathrm{e}^{-\mathrm{i}Es} - \frac{R^2}{64\pi\alpha^3}\int \mathrm{d}s\, X(s)\left(\mathrm{e}^{-\mathrm{i}(E-\Gamma\Omega)s}+\mathrm{e}^{-\mathrm{i}(E+\Gamma\Omega)s}\right) . \quad (8.24)$$

In the long-interaction-time limit, (8.24) has the distributional limit

$$\mathcal{F}^{(3)}_{\text{corr}}(E) = \frac{1}{32\alpha^3}\left(2R^2+\Gamma^2\frac{\partial^2}{\partial E^2}\right)\delta(E) - \frac{R^2}{32\alpha^3}(\delta(E-\Gamma\Omega)+\delta(E+\Gamma\Omega)) . \quad (8.25)$$

The first term in (8.25) vanishes since $E \neq 0$ by assumption, resulting in

$$\mathcal{F}^{(3)}_{\text{corr}}(E) = -\frac{R^2}{32\alpha^3}(\delta(E-\Gamma\Omega)+\delta(E+\Gamma\Omega)) . \quad (8.26)$$

The deltas in (8.20) are resonance peaks at the detector's angular frequency.

Recall that we introduced the AdS length scale α as a model of the finite-size cylindrical boundary in Minkowski spacetime investigated in Chapter 7. We may now compare our expansion (8.21)- (8.26) to that found in Section 7.2. Our order-α^0 contribution (8.21) is equal to the Minkowski spacetime response function (2.80b). Our next contribution (8.23) is order α^{-2} and the response in Minkowski spacetime with cylindrical boundary has no corresponding term. This term must hence be interpreted as a curvature correction. Indeed, the Ricci scalar of CAdS_3 is proportional to α^{-2}. Our next contribution (8.26) is order α^{-3}, coming from the boundary contribution to the Wightman function (8.7a), and we find that this term does agree, in its falloff and its resonance structure, with the corresponding term in Minkowski spacetime with a cylindrical boundary, given by (7.14).

8.1.4 Static observers

In this Section, we consider the term-wise behaviour of the response function for a static observer, obtained by setting $\Omega = 0$. The proper acceleration of a static observer is given by

$$A = \frac{1}{\alpha}\frac{\left(\frac{R}{\alpha}\right)}{\sqrt{1+\left(\frac{R}{\alpha}\right)^2}} , \quad (8.27)$$

which is bounded above by α^{-1} and reduces to 0 for the geodesic observer at $R = 0$. The limit $\lim_{\Omega\to 0}\mathcal{F}(E)$ is well defined both at the level of the full response function and also at the level of the asymptotic expansion in α (8.17b)-(8.20);

hence, we simply evaluate the terms in this expansion at $\Omega = 0$, obtaining

$$\mathcal{F}_0(E)|_{\Omega=0} = \mathcal{F}_0(E)\,, \tag{8.28a}$$
$$\mathcal{F}^{(0)}_{\text{corr}}(E)\big|_{\Omega=0} = 0\,, \tag{8.28b}$$
$$\mathcal{F}^{(1)}_{\text{corr}}(E)\big|_{\Omega=0} = -\frac{1}{8\pi\alpha}\int \mathrm{d}s\, X(s)\cos(Es)\,, \tag{8.28c}$$
$$\mathcal{F}^{(2)}_{\text{corr}}(E)\big|_{\Omega=0} = -\frac{1}{96\pi\alpha^2}\int \mathrm{d}s\, sX(s)\sin(Es)\,, \tag{8.28d}$$
$$\mathcal{F}^{(3)}_{\text{corr}}(E)\big|_{\Omega=0} = -\frac{1}{64\pi\alpha^3}\int \mathrm{d}s\, s^2X(s)\cos(Es)\,, \tag{8.28e}$$

where we have used the evenness of $X(s)$. None of the above terms depend on R; however, it can be shown that the order-α^{-4} contribution $\mathcal{F}^{(4)}_{\text{corr}}(E)$, not displayed here, does.

In the long-interaction-time limit, $X(s) \to 1$, Eqs. (8.28) reduce to

$$\mathcal{F}_0(E)|_{\Omega=0} = \mathcal{F}_0(E)\,, \tag{8.29a}$$
$$\mathcal{F}^{(0)}_{\text{corr}}(E)\big|_{\Omega=0} = 0\,, \tag{8.29b}$$
$$\mathcal{F}^{(1)}_{\text{corr}}(E)\big|_{\Omega=0} = -\frac{1}{4\alpha}\delta(E)\,, \tag{8.29c}$$
$$\mathcal{F}^{(2)}_{\text{corr}}(E)\big|_{\Omega=0} = \frac{1}{24\alpha^2}\frac{\partial}{\partial E}\delta(E)\,, \tag{8.29d}$$
$$\mathcal{F}^{(3)}_{\text{corr}}(E)\big|_{\Omega=0} = \frac{1}{16\alpha^3}\frac{\partial^2}{\partial E^2}\delta(E)\,, \tag{8.29e}$$

obtained by writing the powers of s under the integral in (8.28) as derivatives with respect to E outside the integral. Since we have assumed $E \neq 0$, the correction terms (8.29c)-(8.29e) vanish. Proceeding to higher orders in α, all correction terms in this limit are derivatives of $\delta(E)$ and vanish. This is consistent with the expectation from the GEMS paradigm [174, 175] that a detector on the static worldline, with acceleration less than α^{-1}, should not see thermality, and with the static detector analysis in [144].

8.2 Thermal states in CAdS

In this Section, we generalise the AdS analysis of Section 8.1 from the global vacuum to a thermal state in inverse temperature β. We first consider thermal states in a general static spacetime and then specialise to CAdS. We calculate the leading corrections to the response function in the large-α limit.

8.2.1 Thermal states in static spacetimes

We consider a quantised, conformally coupled, massless, real, scalar field $\hat{\Phi}$ prepared in a thermal state in an $(n+1)$-dimensional static spacetime $(\mathcal{M}, g_{\mu\nu})$. Such a spacetime admits a coordinate system in which the metric is given by

$$\mathrm{d}s^2 \;=\; -g_{00}(\boldsymbol{x})\mathrm{d}t^2 + h_{ij}(\boldsymbol{x})\mathrm{d}x^i\mathrm{d}x^j\,. \tag{8.30}$$

The conformally coupled, massless, Klein-Gordon (KG) equation is given by

$$0 \;=\; (\Box - \xi R)\,\hat{\Phi}(\mathsf{x})\,, \tag{8.31a}$$

$$\;=\; \left(g^{00}(\boldsymbol{x})\partial_0\partial_0 + \frac{1}{\sqrt{-g(\boldsymbol{x})}}\partial_i\sqrt{-g(\boldsymbol{x})}h^{ij}(\boldsymbol{x})\partial_j - \xi(n)\mathcal{R}\right)\hat{\Phi}(\mathsf{x})\,, \tag{8.31b}$$

where $g(\boldsymbol{x}) = \det(g_{\mu\nu})$, $\mathcal{R}$ is the Ricci scalar curvature, and $\xi(n) = (n-1)/(4n)$ is the conformal coupling. If we consider the mode decomposition

$$\hat{\Phi}(\mathsf{x}) \;=\; \sum_k \phi_k(\mathsf{x})\hat{a}_k + \mathrm{Hc}\,, \tag{8.32}$$

then the field modes ϕ_k are also solutions to (8.31b). We will specify the momenta k in more detail later. Due to the separation of time and space in (8.31b), the equation admits a separable solution. The positive-frequency field modes with respect to the Killing vector ∂_t are of the form

$$\phi_k(\mathsf{x}) \;=\; \frac{1}{\sqrt{2\omega_k}} f_k(\boldsymbol{x})\mathrm{e}^{-\mathrm{i}\omega_k t}\,. \tag{8.33}$$

In static spacetimes, in coordinates adapted to the staticity (8.30), the KG norm is given by

$$(\phi_1, \phi_2) = \mathrm{i}\int_\Sigma \mathrm{d}^n\boldsymbol{x}\,\sqrt{-g(\boldsymbol{x})}g^{00}(\boldsymbol{x})(\phi_1\partial_0\phi_2^* - \phi_2^*\partial_0\phi_1)\,, \tag{8.34}$$

where Σ is any Cauchy surface. We assume that $\{\phi_k\}$ forms a complete set, which we normalise with respect to the KG norm (8.34),

$$(\phi_k(\mathsf{x}), \phi_{k'}(\mathsf{x})) \;=\; \delta_{kk'} \;=\; -(\phi_k^*(\mathsf{x}), \phi_{k'}^*(\mathsf{x}))\,, \tag{8.35}$$

$$(\phi_k(\mathsf{x}), \phi_{k'}^*(\mathsf{x})) \;=\; 0\,. \tag{8.36}$$

As a consequence of this normalisation (8.35), the completeness relation of the spatial modes f_k is

$$-\int \mathrm{d}^n\boldsymbol{x}\,\sqrt{-g(\boldsymbol{x})}g^{00}(\boldsymbol{x})f_k(\boldsymbol{x})f^*_{k'}(\boldsymbol{x}) \;=\; \delta_{kk'}\,. \tag{8.37}$$

By restricting to a static spacetime, the field Hamiltonian $\hat{H}$ is time independent and, for field modes (8.30), $\hat{H}$ is given by [190–193]

$$\hat{H} \;=\; \frac{1}{2}\sum_k \omega_k\Big(\hat{a}_k\hat{a}^\dagger_k + \hat{a}^\dagger_k\hat{a}_k\Big)\,. \tag{8.38}$$

Due to the time independence of the Hamiltonian (8.38), conventional concepts about thermal averaging are still valid in this spacetime [190]. The thermal expectation value of an operator $\hat{A}$ at inverse temperature $\beta = 1/T$ is given by the statistical average over a canonical ensemble,

$$\langle\hat{A}\rangle_\beta \;=\; \frac{\mathrm{Tr}\Big(\mathrm{e}^{-\beta\hat{H}}\hat{A}\Big)}{\mathrm{Tr}\Big(\mathrm{e}^{-\beta\hat{H}}\Big)}\,, \tag{8.39}$$

and the local temperature observed by a static observer on a (static) curved spacetime is given by Tolman's law [194–196],

$$T_{\mathrm{obs}}(\boldsymbol{x}) \;=\; \frac{T}{\sqrt{-g_{00}(\boldsymbol{x})}}\,. \tag{8.40}$$

In AdS in the coordinates (8.3), we have $-g_{00}(\boldsymbol{x}) = 1$ at the origin, giving a distinguished reference point. In the RdS spacetime of Section 8.3, we will use the coordinates (8.56), in which the origin is similarly distinguished. In writing $\exp(-\beta\hat{H})$ in (8.39), we consider β as measured by a static observer at the origin.

The operator in whose thermal expectation value we are interested is $\hat{\Phi}(\mathsf{x})\hat{\Phi}(\mathsf{x}')$. This operator-valued distribution is well defined and requires no renormalisation. It follows from (8.39) that the thermal expectation value is given by

$$\langle\hat{\Phi}(\mathsf{x})\hat{\Phi}(\mathsf{x}')\rangle_\beta \;=\; \sum_k (1+n(\beta\omega_k))\phi_k(\mathsf{x})\phi^*_k(\mathsf{x}') + n(\beta\omega_k)\phi^*_k(\mathsf{x})\phi_k(\mathsf{x}')\,, \tag{8.41}$$

where $n(x)$ is the Bose thermal factor (2.40). The distributional character of $\langle\hat{\Phi}(\mathsf{x})\hat{\Phi}(\mathsf{x}')\rangle_\beta$ can be encoded by the insertion of suitable $\mathrm{i}\varepsilon$ convergence factors in (8.41). We note that this is the same expression (2.39b) as in our earlier discussion of thermal states in Minkowski spacetime in Chapter 2.

8.2.2 Field and detector preliminaries

Specialising now to CAdS, we consider a quantised, conformally coupled, massless scalar field $\hat{\Phi}$,

$$\hat{\Phi}(t,r,\theta) \;=\; \sum_k \phi_k(t,r,\theta)\hat{a}_k + \mathrm{Hc}\,, \tag{8.42}$$

where the annihilation $\hat{a}_k$ and creation $\hat{a}_k^\dagger$ operators obey the commutation relation $[\hat{a}_k, \hat{a}_{k'}^\dagger] = \delta_{k,k'}$. The Hilbert space is a Fock space with a Fock vacuum $|0\rangle$ satisfying $\hat{a}_k\,|0\rangle$ for all k.

We prepare the field in a thermal state in inverse temperature β. In place of the interaction Hamiltonian (2.32), we use a derivative-coupled interaction Hamiltonian [1, 73],

$$\hat{H}_\mathrm{I} \;=\; \lambda\chi(\tau)\hat{\mu}(\tau)\otimes\frac{\mathrm{d}}{\mathrm{d}\tau}\hat{\Phi}(\mathsf{x}(\tau))\,. \tag{8.43}$$

Note that the derivative is with respect to proper time τ, rather than Minkowski time t as in (3.3). The derivative in (8.43) cures the infrared divergence that occurs in the finite temperature Wightman function in $2+1$ dimensions in the $\alpha\to\infty$ limit [1, 73].

Working again to first order in perturbation theory in λ, the thermal response function is given by

$$\mathcal{F}(E,\beta) = \int \mathrm{d}\tau'\mathrm{d}\tau''\,\chi(\tau')\chi(\tau'')\mathrm{e}^{-\mathrm{i}E(\tau'-\tau'')}\mathcal{W}_\beta(\tau',\tau'')\,, \tag{8.44}$$

where $\mathcal{W}_\beta(\tau',\tau'') = \langle \frac{\mathrm{d}}{\mathrm{d}\tau'}\hat{\Phi}(\mathsf{x}(\tau'))\frac{\mathrm{d}}{\mathrm{d}\tau''}\hat{\Phi}(\mathsf{x}(\tau''))\rangle_\beta$ is the thermal Wightman function.

We can calculate the thermal Wightman function in the same way as the vacuum Wightman function construction in [188] by utilising that CAdS is conformal to half of Einstein Static Universe (ESU) [177]. Then, the field modes in CAdS, normalised with respect to the KG norm (8.34), are given by

$$\phi_{lm}(t,r,\theta) \;=\; \frac{1}{\left(1+\frac{r^2}{\alpha^2}\right)^{1/4}}\sqrt{\frac{1}{4\pi\alpha}\frac{(l-m)!}{(l+m)!}}\mathrm{P}_l^m\left(\frac{1}{\sqrt{1+\frac{r^2}{\alpha^2}}}\right)\mathrm{e}^{\mathrm{i}m\theta-\mathrm{i}\omega_l t}\,, \tag{8.45}$$

where $l\in\mathbb{N}_0=\{0,1,2,\dots\}$, $|m|\le l$, $\omega_l=\frac{1}{\alpha}(l+\frac{1}{2})$, and P_l^m is the associated Legendre function of degree l and order m, with argument taking values between -1 and $+1$, also known as Ferrers' functions or associated Legendre functions *on the cut* [111]. Appropriate boundary conditions are required to ensure the well-posedness of the Cauchy problem [177, 181]. We adopt Dirichlet boundary conditions. As in [188], we do this by subtracting the antipodal Wightman

function in ESU from the Wightman function; we may cover ESU by coordinates (σ, ρ, θ), where $-\infty < \sigma < \infty$, $0 \leq \rho < \pi$, and $0 \leq \theta < 2\pi$, then the Wightman function antipodal to $\mathcal{W}(\mathsf{x}, \mathsf{x}')$ is $\mathcal{W}(\mathsf{x}_A, \mathsf{x}')$, where $\mathsf{x} = (\sigma, \rho, \theta)$ and $\mathsf{x}_A = (\sigma, \pi - \rho, \theta)$. After pulling back to the circular trajectory (8.4), the thermal, derivative-coupled, Wightman function also enjoys the time-translation symmetry of the linearly coupled Wightman function (8.7a).

The thermal Wightman function (8.41) and response function split into vacuum and thermal contributions respectively,

$$\mathcal{W}_\beta(s,0) \;=\; \mathcal{W}_\infty(s,0) + \Delta\mathcal{W}_\beta(s,0)\,, \tag{8.46a}$$

$$\mathcal{F}(E,\beta) \;=\; \mathcal{F}_\infty(E) + \Delta\mathcal{F}_\beta(E)\,. \tag{8.46b}$$

The vacuum contribution $\mathcal{F}_\infty$ is equal to E^2 times the result from Section 8.1.3. We now focus on the contribution due to the ambient temperature, $\Delta\mathcal{F}_\beta$.

In the long-interaction-time limit, $X \to 1$, $\Delta\mathcal{F}_\beta$ is given by

$$\Delta\mathcal{F}_\beta(E) \;=\; \int \mathrm{d}s\, \mathrm{e}^{-\mathrm{i}Es}\Delta\mathcal{W}_\beta(s,0)\,, \tag{8.47}$$

where

$$\begin{aligned}\Delta\mathcal{W}_\beta(s,0) \;=\; \frac{\gamma^2}{4\pi\alpha}\frac{1}{\sqrt{1+\frac{R^2}{\alpha^2}}}\sum_{l=0}^{\infty}\sum_{m=-l}^{l}(\omega_l - m\Omega)^2\frac{(l+|m|)!}{(l-|m|)!}(1-(-1)^l)n(\beta\omega_l) \\ \times\left[\mathrm{P}_l^{-|m|}\left(\frac{1}{\sqrt{1+\frac{R^2}{\alpha^2}}}\right)\right]^2 2\cos((\omega_l - m\Omega)\gamma s)\,.\end{aligned} \tag{8.48}$$

γ is given by (8.5), the factor $(\omega_l - m\Omega)^2$ comes from the derivative coupling, the ratio of factorials is due to Rodrigues' formula for the associated Legendre polynomials [111], the factor $(1-(-1)^l)$ comes from the Dirichlet boundary conditions, and n is the Bose thermal factor. Due to the Dirichlet boundary conditions, only odd l contribute to $\Delta\mathcal{W}_\beta$ and we change summation variable to $l = 2k+1$, $k \in \mathbb{N}_0$. Finally, we introduce the Heaviside theta [111] $\Theta(l+\frac{1}{2}-|m|) = \Theta(\alpha\omega_l - |m|)$ to extend the summation in m to the integers $\mathbb{Z}$ and exchange the summation order.

$$\Delta\mathcal{W}_\beta(s,0) \;=\; \frac{\gamma^2}{2\pi\alpha}\frac{1}{\sqrt{1+\frac{R^2}{\alpha^2}}}\sum_{m=-\infty}^{\infty}\sum_{k=0}^{\infty}(\omega_k - m\Omega)^2\Theta(\alpha\omega_k - |m|)\frac{(2k+1+|m|)!}{(2k+1-|m|)!}$$

$$\times\, n(\beta\omega_k)\left[\mathrm{P}^{-|m|}_{2k+1}\left(\frac{1}{\sqrt{1+\frac{R^2}{\alpha^2}}}\right)\right]^2 2\cos((\omega_k - m\Omega)\gamma s)\,, \quad (8.49)$$

where now $\omega_k = \frac{1}{\alpha}(2k+\frac{3}{2})$. The thermal contribution to the response function is then

$$\Delta\mathcal{F}_\beta(E) \;=\; \frac{1}{\alpha}\frac{E^2}{\sqrt{1+\frac{R^2}{\alpha^2}}}\sum_{m=-\infty}^{\infty}\sum_{k=0}^{\infty}\Theta(\alpha\omega_k - |m|)n(\beta\omega_k)\frac{(2k+1+|m|)!}{(2k+1-|m|)!}$$
$$\times\left[\mathrm{P}^{-|m|}_{2k+1}\left(\frac{1}{\sqrt{1+\frac{R^2}{\alpha^2}}}\right)\right]^2\Big(\delta(E-\gamma(\omega_k - m\Omega)) + \delta(E+\gamma(\omega_k - m\Omega))\Big)\,. \quad (8.50)$$

The Dirac deltas in (8.50) show that $\Delta\mathcal{F}_\beta(E)$ is a distribution in E.

8.2.3 Large-α limit

In this Section, we consider the large-α asymptotic behaviour of the contribution to the response function due to the ambient temperature $\Delta\mathcal{F}_\beta$ (8.50).

Both in Minkowski spacetime with a boundary and CAdS, the thermal contribution to the response function $\Delta\mathcal{F}_\beta$ ((7.18c) and (8.50)) is distributional in nature. We consider again the integrated response contribution due to finite temperature,

$$\Delta\mathcal{G}_\beta(\alpha) \;=\; \int_{\mathbb{R}} \mathrm{d}E\, E^{-2}\sigma(E)\Delta\mathcal{F}_\beta(E)\,, \quad (8.51)$$

where $\sigma \in C_0^\infty(\mathbb{R})$ is a real-valued function of compact support such that $0 \notin \mathrm{supp}\{\sigma\}$ and either $\mathrm{supp}\{\sigma\} \subset \mathbb{R}_{>0}$ or $\mathrm{supp}\{\sigma\} \subset \mathbb{R}_{<0}$. In Appendix J, we show that

$$\Delta\mathcal{G}_\beta(\alpha) \;=\; \int_{\mathbb{R}} \mathrm{d}E\,\sigma(E)\Bigg[\frac{1}{2\Gamma}\sum_{m>\frac{|E|}{\Gamma\Omega}} n(\beta\omega_+)J^2_{|m|}(\omega_+ R) + \frac{1}{2\Gamma}\sum_{m>-\frac{|E|}{\Gamma\Omega}} n(\beta\omega_-)J^2_{|m|}(\omega_- R)$$
$$- \frac{R^2}{16\beta\alpha^2}\ln\Big(\frac{\alpha}{R}\Big)\,\delta(|E| - \Gamma\Omega) + \mathcal{O}(\alpha^{-2})\Bigg]\,, \quad (8.52)$$

where $\omega_\pm = m\Omega \mp |E|/\Gamma$. By comparison with (8.51), we read off the thermal contribution to the response function $\Delta\mathcal{F}_\beta$ as

$$\Delta\mathcal{F}_\beta(E) \;=\; \frac{E^2}{2\Gamma}\sum_{m>\frac{|E|}{\Gamma\Omega}} n(\beta\omega_+)J^2_{|m|}(\omega_+ R) + \frac{E^2}{2\Gamma}\sum_{m>-\frac{|E|}{\Gamma\Omega}} n(\beta\omega_+)J^2_{|m|}(\omega_+ R)$$
$$- \frac{R^2E^2}{16\beta\alpha^2}\ln\Big(\frac{\alpha}{R}\Big)\,\delta(|E| - \Omega\Gamma) + \mathcal{O}(\alpha^{-2})\,, \quad (8.53)$$

where the $\mathcal{O}$-notation is used in a distributional sense.

We may compare this result to the corresponding expansion in Minkowski spacetime with a cylindrical boundary in Section 7.3. Up to conversion between an analogue spacetime setting and a genuinely relativistic setting, we see the leading order terms in (7.22) and (8.53) agree. However, the leading correction to (8.53) is order $\alpha^{-2}\ln\alpha$ and the subleading corrections are order α^{-2}. There is no counterpart to this term in the expansion (7.22).

8.2.4 Static observers

In the static observer limit, $\Omega \to 0$, (8.53) reduces to

$$\begin{aligned}\lim_{\Omega\to 0}\Delta\mathcal{F}_\beta(E) &= \frac{1}{2}n(\beta|E|)E^2\sum_{m\in\mathbb{Z}}J_{|m|}(ER/\Gamma)\,,\\ &= \frac{1}{2}E^2 n(\beta|E|)\,,\end{aligned} \tag{8.54a}$$

using Neumann's addition formula [111], $\sum_{m\in\mathbb{Z}}J^2_{|m|}(x)=1$. As with the analysis of a static observer in Minkowski spacetime, a static detector in CAdS acts as a thermometer (see (7.24)).

8.3 de Sitter spacetime

In this Section, we consider the spacetime of constant positive curvature, dS spacetime. Specifically, we consider the static patch of dS, to which we refer as RdS spacetime, a static, globally hyperbolic spacetime of physical and cosmological interest [197]. The name RdS is due to the fact that the restriction of the de Sitter vacuum, the Euclidean (or Bunch-Davies [179] or Chernikov-Tagirov [178] (rus. Черников-Тагиров)) vacuum, to the static patch is thermal [50, 180] in temperature $1/(2\pi\alpha)$, where α is the dS radius — akin to the restriction of the Minkowski vacuum to the Rindler patch [21, 74, 75]. We first consider a field prepared in a thermal state with arbitrary temperature and then specialise to the Euclidean vacuum.

8.3.1 Spacetime, field, and detector preliminaries

We consider $(2+1)$-dimensional dS spacetime as embedded in $3+1$ Minkowski spacetime $\mathbb{R}^{3,1}$ with the embedding equation

$$\eta^{3,1}_{AB}X^A X^B = \alpha^2\,, \tag{8.55}$$

where $X^A = (X^0, X^1, X^2, X^3)$ are the coordinates on $\mathbb{R}^{3,1}$, $\eta^{3,1} = \mathrm{diag}(-1,1,1,1)$ and $\alpha > 0$ is the de Sitter radius. The cosmological constant Λ is related to α by $\Lambda = 1/\alpha^2$. The Ricci scalar of dS_3 is $\mathcal{R} = 6/\alpha^2$.

We use coordinates (t, r, θ) in which the metric on RdS is given by

$$\mathrm{d}s^2 = -\left(1 - \frac{r^2}{\alpha^2}\right)\mathrm{d}t^2 + \frac{\mathrm{d}r^2}{1 - \frac{r^2}{\alpha^2}} + r^2\mathrm{d}\theta^2 \,, \tag{8.56}$$

where $-\infty < t < \infty$, $0 \leq r < \alpha$, and $0 \leq \theta < 2\pi$, with the usual coordinate singularity at $r = 0$ and θ periodically identified with period 2π. Note the presence of a cosmological horizon at $r = \alpha$. The embedding in the embedding space $\mathbb{R}^{3,1}$ is given by

$$X^0 = \sqrt{\alpha^2 - r^2}\sinh(t/\alpha) \,, \tag{8.57a}$$
$$X^1 = \sqrt{\alpha^2 - r^2}\cosh(t/\alpha) \,, \tag{8.57b}$$
$$X^2 = r\cos\theta \,, \tag{8.57c}$$
$$X^3 = r\sin\theta \,. \tag{8.57d}$$

The small cosmological constant limit $\Lambda \to 0^+$ is $\alpha \to \infty$, which recovers Minkowski spacetime $\mathbb{R}^{2,1}$. This can be seen immediately from the form of the metric (8.56).

We consider a quantised, conformally coupled, massless, real scalar field Φ. The field obeys the KG equation (8.31b) and we look for separable solutions of the form $\phi_{\omega m} = g_{\omega m}(r)\mathrm{e}^{\mathrm{i}m\theta - \mathrm{i}\omega t}$ with $\omega > 0$ and $m \in \mathbb{Z}$. The radial factor obeys then the equation

$$0 = \left(\frac{\omega^2}{1 - \frac{r^2}{\alpha^2}} - \frac{m^2}{r^2} - \frac{3}{4\alpha^2}\right) g_{\omega m}(r) + \frac{1}{r}\frac{\partial}{\partial r}\left(r\left(1 - \frac{r^2}{\alpha^2}\right)\frac{\partial}{\partial r} g_{\omega m}(r)\right) \,. \tag{8.58}$$

The positive-frequency modes with respect to ∂_t that are regular at $r = 0$ are then given by

$$\begin{aligned}
\phi_{\omega m}(t, r, \theta) &= \mathcal{A}_{\omega m}\left(\frac{r}{\alpha}\right)^{|m|}\left(1 - \frac{r^2}{\alpha^2}\right)^{-\frac{1}{2}\mathrm{i}\alpha\omega} \mathrm{e}^{\mathrm{i}m\theta - \mathrm{i}\omega t} \\
&\quad \times {}_2F_1\left(\tfrac{1}{2}\left(|m| + \tfrac{1}{2} - \mathrm{i}\alpha\omega\right), \tfrac{1}{2}\left(|m| + \tfrac{3}{2} - \mathrm{i}\alpha\omega\right); |m| + 1; \tfrac{r^2}{\alpha^2}\right) \,, \qquad (8.59a) \\
\mathcal{A}_{\omega m} &= \frac{\sqrt{\sinh(\pi\alpha\omega)}}{2\sqrt{2}\pi^{3/2}(|m|)!}\Gamma\left(\tfrac{1}{2}\left(|m| + \tfrac{1}{2} + \mathrm{i}\alpha\omega\right)\right)\Gamma\left(\tfrac{1}{2}\left(|m| + \tfrac{3}{2} + \mathrm{i}\alpha\omega\right)\right) \,,
\end{aligned}$$

where $\omega > 0$, $m \in \mathbb{Z}$, and ${}_2F_1$ is the hypergeometric function [111]. The field

modes (8.59) are normalised with respect to the Klein-Gordon norm (8.34) with a Kronecker delta in m and Dirac delta in ω. The normalisation factor can be read off by considering the asymptotic form near $r = \alpha$ [198] and using [111, (5.4.3)]. For comparison, the field modes for a scalar field in $1+1$ RdS and $3+1$ RdS are given in [197] and [198] respectively.

We expand the field in the field modes (8.59) as

$$\hat{\Phi}(t,r,\theta) \;=\; \int \mathrm{d}\omega \sum_{m\in\mathbb{Z}} \phi_{\omega m}(t,r,\theta)\hat{a}_{\omega m} + \mathrm{Hc}\,, \tag{8.60}$$

where the annihilation $\hat{a}_{\omega m}$ and creation $\hat{a}^\dagger_{\omega m}$ operators obey the commutation relation $[\hat{a}_{\omega m}, \hat{a}^\dagger_{\omega' m'}] = \delta(\omega-\omega')\delta_{m,m'}$. The Hilbert space is a Fock space with a Fock vacuum $|0\rangle$ satisfying $\hat{a}_{\omega m}|0\rangle$ for all ω and m. We shall consider the Fock vacuum, a thermal state in a general inverse temperature β, defined as in (8.41), and the Euclidean vacuum, in which $\beta = 2\pi\alpha$.

We probe the field with a pointlike detector in uniform circular motion,

$$(t,r,\theta) \;=\; (\gamma\tau, R, \Omega\gamma\tau)\,, \tag{8.61a}$$

$$\gamma \;=\; \frac{1}{\sqrt{1-R^2\Omega^2-\frac{R^2}{\alpha^2}}}\,, \tag{8.61b}$$

where τ is proper time, $R>0$ is the value of the radial coordinate, and $\Omega = \frac{\mathrm{d}\theta}{\mathrm{d}t} > 0$ is the angular velocity with respect to time t in (8.56). We assume that the worldline is timelike, $R\Omega < \sqrt{1-R^2/\alpha^2}$. In the large-$\alpha$ limit, we have $\lim_{\alpha\to\infty}\gamma = (1-R^2\Omega^2)^{-1/2} =: \Gamma$, where Γ is the Lorentz factor associated with circular motion in Minkowski spacetime $\mathbb{R}^{2,1}$. We couple the detector to the field Φ with the derivative-coupled interaction Hamiltonian (8.43), as described in Section 8.2.2, in the long-interaction-time limit $\chi \to 1$.

In the thermal state in inverse temperature β, the Wightman function in the derivative-coupled detector response in RdS, pulled back to the circular trajectory (8.61), is given by

$$\begin{aligned}\mathcal{W}_\beta(s,0) \;=\; &\sum_{m\in\mathbb{Z}} \int_0^\infty \mathrm{d}\omega\, |\mathcal{A}_{\omega m}|^2 \gamma^2(\omega-m\Omega)^2 \left(\frac{R}{\alpha}\right)^{2|m|} \\ &\times \left((1+n(\beta\omega))\mathrm{e}^{\mathrm{i}(m\Omega-\omega)\gamma s} + n(\beta\omega)\mathrm{e}^{-\mathrm{i}(m\Omega-\omega)\gamma s}\right) \\ &\times \left|{}_2F_1\left(\tfrac{1}{2}\{|m|+\tfrac{1}{2}-\mathrm{i}\alpha\omega\}, \tfrac{1}{2}\{|m|+\tfrac{3}{2}-\mathrm{i}\alpha\omega\}; |m|+1; \tfrac{R^2}{\alpha^2}\right)\right|^2\,,\end{aligned} \tag{8.62}$$

where $n(x)$ is the Bose thermal factor (2.40).

The response function (8.44) (in the long-time limit) is calculated from (8.62)

by first integrating over s and then integrating over ω, leading to

$$\mathcal{F}(E,\beta) = \mathcal{F}_\infty(E) + \Delta\mathcal{F}_\beta(E)\,, \tag{8.63a}$$

$$\mathcal{F}_\infty(E) = \frac{2\pi E^2}{\gamma}\sum_{m>E/(\gamma\Omega)}\left(\frac{R}{\alpha}\right)^{2|m|}|\mathcal{A}_{\varpi_m m}|^2 \times\left|{}_2F_1\left(\tfrac{1}{2}\{|m|+\tfrac{1}{2}-\mathrm{i}\alpha\varpi_m\},\tfrac{1}{2}\{|m|+\tfrac{3}{2}-\mathrm{i}\alpha\varpi_m\};|m|+1;\tfrac{R^2}{\alpha^2}\right)\right|^2\,, \tag{8.63b}$$

$$\begin{aligned}\Delta\mathcal{F}_\beta(E) = {}&\frac{2\pi E^2}{\gamma}\sum_{m>|E|/(\gamma\Omega)} n(\beta\omega_m^+)\left(\frac{R}{\alpha}\right)^{2|m|}|\mathcal{A}_{\omega_m^+ m}|^2 \\ &\times\left|{}_2F_1\left(\tfrac{1}{2}\{|m|+\tfrac{1}{2}-\mathrm{i}\alpha\omega_m^+\},\tfrac{1}{2}\{|m|+\tfrac{3}{2}-\mathrm{i}\alpha\omega_m^+\};|m|+1;\tfrac{R^2}{\alpha^2}\right)\right|^2 \\ &+\frac{2\pi E^2}{\gamma}\sum_{m>-|E|/(\gamma\Omega)} n(\beta\omega_m^-)\left(\frac{R}{\alpha}\right)^{2|m|}|\mathcal{A}_{\omega_m^- m}|^2 \\ &\times\left|{}_2F_1\left(\tfrac{1}{2}\{|m|+\tfrac{1}{2}-\mathrm{i}\alpha\omega_m^-\},\tfrac{1}{2}\{|m|+\tfrac{3}{2}-\mathrm{i}\alpha\omega_m^-\};|m|+1;\tfrac{R^2}{\alpha^2}\right)\right|^2\,,\end{aligned} \tag{8.63c}$$

where $\varpi_m = m\Omega - E/\gamma$ and $\omega_m^\pm = m\Omega \mp |E|/\gamma$. The response function (8.63) naturally decomposes into a contribution from the static vacuum $\mathcal{F}_\infty$ and a contribution due to the ambient temperature $\Delta\mathcal{F}_\beta$. It is clear that $\Delta\mathcal{F}_\beta$ is an even function of the energy gap E.

8.3.2 Large-α limit

In this Section, we consider the large-α limit of the detector response (8.63) when the field is prepared in the Euclidean vacuum. When restricted to the static patch, this is a thermal state in inverse temperature $\beta = 2\pi\alpha$, in which case the Wightman function is dS invariant [197, 199].

8.3.2.1 Thermal contribution

We first consider the thermal contribution $\Delta\mathcal{F}_\beta$ to the response function (8.63). By a simple bounding argument, we demonstrate that $\Delta\mathcal{F}_\beta$ is exponentially suppressed compared to the static vacuum contribution $\mathcal{F}_\infty$.

Let $m^\pm = 1 + \lfloor \pm|E|/(\gamma\Omega)\rfloor$, the first value of m in each summand in (8.63c), where the notation suppresses the E-dependence of $m^\pm$. It follows that

$$0 < \omega_{m^\pm}^\pm = m^\pm\Omega \mp |E|/\gamma \leq \Omega\,. \tag{8.64}$$

As $n(x)$ is decreasing in x, we have $n(\beta\omega_m^{\pm}) \leq n(\beta\omega_{m^{\pm}}^{\pm})$. Each of the two sums in $\Delta\mathcal{F}_\beta$ (8.63c) can hence be bounded above by a replacing $n(\beta\omega_m^{\pm})$ by $n(\beta\omega_{m^{\pm}}^{\pm})$, giving the bound

$$\Delta\mathcal{F}_\beta(E) \leq n(\beta\omega_{m^+}^{+})\mathcal{F}_\infty(|E|) + n(\beta\omega_{m^-}^{-})\mathcal{F}_\infty(-|E|)\,, \tag{8.65}$$

where we have used (8.63b).

As $\beta = 2\pi\alpha$, the thermal factors $n(\beta\omega_{m^{\pm}}^{\pm}) \sim \exp(-2\pi\alpha\omega_{m^{\pm}}^{\pm})$ in (8.65) are exponentially suppressed for large α, as follows from (8.64). The static vacuum factors $\mathcal{F}_\infty$ in (8.65) have the large-α limit given by

$$\lim_{\alpha\to\infty}\mathcal{F}_\infty(E) \;=\; \frac{E^2}{2\Gamma}\sum_{m>E/(\Omega\Gamma)} J^2_{|m|}(mv - ER/\Gamma)\,, \tag{8.66}$$

which is the response function for a detector undergoing uniform circular motion in $2+1$ Minkowski spacetime [169]. We see that $\Delta\mathcal{F}_\beta$ is exponentially suppressed in the large-α limit, thus any corrections that are polynomial in inverse powers of α must be interpreted as curvature corrections. We recall from Chapter 3 that the thermal corrections in Minkowski spacetime are also exponentially suppressed in the large-β (low temperature) limit. We note, however, that the coefficient of α in the exponent is not continuous in E and the parameters of the motion, and this coefficient can take arbitrarily small positive values.

8.3.2.2 Full Euclidean vacuum

We now consider the full response in the Euclidean vacuum. The Wightman function is expressible in terms of the hypergeometric function, derivable by exploiting the symmetries of de Sitter spacetime [199, 200]. In our case of a conformally coupled, massless scalar field, the Wightman function is

$$\mathcal{W}_{\text{Euc}}(\mathsf{x},\mathsf{x}') \;=\; \frac{1}{4\pi}\frac{1}{\sqrt{\sigma(\mathsf{x},\mathsf{x}')}}\,, \tag{8.67a}$$

$$\sigma(\mathsf{x},\mathsf{x}') \;=\; \eta^{3,1}_{AB}\Big(X^A - X'^A\Big)\Big(X^B - X'^B\Big)\,, \tag{8.67b}$$

where σ is the geodesic squared distance in the embedding space and we momentarily suppress the distributional character.

Pulled back to the circular trajectory (8.61), the Wightman function $\mathcal{W}_{\text{Euc}}$ is again time-translation invariant. The geodesic squared distance is given by

$$\sigma(s,0) \;=\; -4\big(\alpha^2 - R^2\big)\sinh^2\!\left(\frac{\gamma s}{2\alpha}\right) + 4R^2\sin^2\!\left(\frac{\Omega\gamma s}{2}\right)\,, \tag{8.68}$$

and the pullback of $\mathcal{W}_{\text{Euc}}$ to the circular trajectory is

$$\mathcal{W}_{\text{Euc}}(s,0) \;=\; \frac{1}{4\pi}\frac{1}{\sqrt{\sigma(s-\mathrm{i}\varepsilon,0)}}\,, \tag{8.69}$$

where the distributional character has been restored and encoded as the limit $\varepsilon \to 0^+$. As in the Minkowski vacuum, the square root in the denominator is positive imaginary for positive s and negative imaginary for negative s [69, 201].

The only distributional contribution to the response function $\mathcal{F}_{\text{Euc}}$ is at $s = 0$. Isolating this, we find [69, 201]

$$\begin{aligned}\mathcal{F}_{\text{Euc}}(E) \;&=\; \frac{E^2}{4\pi}\int_{\mathbb{R}} \mathrm{d}s\, \frac{\mathrm{e}^{-\mathrm{i}Es}}{\sqrt{\sigma(s-\mathrm{i}\varepsilon,0)}} \\ &=\; \frac{E^2}{4} - \frac{E^2}{2\pi}\int_0^\infty \mathrm{d}s\, \frac{\sin(Es)}{\sqrt{-\sigma(s,0)}}\,.\end{aligned} \tag{8.70}$$

We note that this splits the odd and even contributions to the response function as in (2.77).

It is convenient to parametrise the circular trajectory in terms of R and V, where

$$V \;\coloneqq\; \frac{R\Omega}{\sqrt{1-\frac{R^2}{\alpha^2}}}\,. \tag{8.71}$$

Geometrically, V is the velocity of the detector as seen by a static observer at $r = R$. Changing the integration variable to $z = \gamma s(2\alpha)^{-1}$, $\mathcal{F}_{\text{Euc}}$ (8.70) reads

$$\mathcal{F}_{\text{Euc}}(E) \;=\; \frac{E^2}{4} - \frac{E^2}{2\pi\Gamma_V}\int_0^\infty \mathrm{d}z\, \frac{\sin\left(\frac{2ER}{\Gamma_V V}z\right)}{z}\frac{1}{\sqrt{\sinh^2(\eta z)/(\eta z)^2 - V^2\sin^2(z)/z^2}}\,, \tag{8.72}$$

where we have written $\Gamma_V \coloneqq (1-V^2)^{-1/2}$ and $\eta \coloneqq (\Omega\alpha)^{-1} = V^{-1}(\alpha^2/R^2-1)^{-1/2}$.

We show in Appendix K that the asymptotic behaviour of (8.72) as $\eta \to 0$ with E, R, and V fixed, is given by

$$\begin{aligned}\mathcal{F}_{\text{Euc}}(E) \;&=\; \frac{E^2}{4} - \frac{E^2}{2\pi\Gamma_V}\int_0^\infty \mathrm{d}z\, \frac{\sin\left(\frac{2ER}{\Gamma_V V}z\right)}{z}\frac{1}{\sqrt{1-V^2\sin(z)^2/z^2}} \\ &\quad + \frac{E^2}{12\pi\Gamma_V}\eta^2\int_0^\infty \mathrm{d}z\, z\sin\left(\tfrac{2ER}{\Gamma_V V}z\right)\left(\frac{1}{(1-V^2\sin^2(z)/z^2)^{3/2}} - 1\right) + o(\eta^2)\,,\end{aligned} \tag{8.73}$$

where $\eta^2 = V^{-2}(\alpha^2/R^2-1)^{-1} = R^2(V\alpha)^{-2} + o(\alpha^{-2})$ in terms of the de Sitter radius of curvature as $\alpha \to \infty$.

The leading term in (8.73) is the response of a detector undergoing uniform

circular motion in $(2+1)$-dimensional Minkowski spacetime with orbital speed V and angular velocity V/R [69]. The next-to-leading term in (8.73) is proportional to α^{-2}. As this term is larger than the exponentially small thermal corrections found in Section 8.3.2.1, we may interpret this term as a curvature correction.

8.4 Discussion

Motivated by the experimentally relevant notions of an ambient temperature and spatial confinement, we investigated a detector undergoing uniform circular motion in RdS and CAdS spacetimes, the spacetimes of constant positive and negative curvature respectively. The introduction of the cosmological constant $|\Lambda| = \alpha^{-2}$ allows one to interpret RdS and CAdS as one-parameter extensions of Minkowski spacetime, which is recovered in the limit of a small cosmological constant. In this limit, the ambient temperature in RdS tends to zero and the time for information to reach spatial infinity in CAdS tends to infinity. In this Chapter, we hence investigated how closely these spacetimes may be considered as curved-spacetime analogues of a low ambient temperature or large cylindrical boundary in $2+1$ Minkowski spacetime.

In RdS, splitting the response function into its contributions from the static vacuum and thermal corrections, we found that the thermal corrections are exponentially suppressed in the limit of a small cosmological constant. This parallels a low ambient temperature in Minkowski spacetime, analysed in Section 3.2.2, in which spacetime the thermal corrections are also exponentially suppressed. We may therefore conclude that any corrections that are polynomial in inverse powers of α must be attributable to curvature corrections. We then considered the Wightman function of the full Euclidean vacuum, finding the leading and subleading contributions. To leading order, we recovered the response function of a detector probing a scalar field in the Minkowski vacuum in $2+1$ Minkowski spacetime. The subleading correction was found to be proportional to α^{-2} and we interpreted this as a curvature correction. This interpretation is further strengthened by the recollection that the Ricci scalar curvature of RdS_3 is proportional to α^{-2}.

In Chapter 6, we classified the stationary trajectories of RdS, finding two classes, the inertial motions and the circular motions. This classification descended from the embedding space. In this Chapter, we focused on circular motion in $2+1$ dimensions. We may take a GEMS approach and consider the motion in the embedding space $\mathbb{R}^{3,1}$. The Killing vector generating the circular motion pushed forward into the embedding space generates the hypertor

motion analysed in Chapter 5.

In CAdS, we considered both when the field was prepared in the global vacuum and when the field was prepared in a thermal state in an arbitrary fixed temperature. In the global vacuum, we found the first four terms in the series expansion of the response function and only three of these were nonzero in the long-interaction-time limit. To leading order, we recovered the response function of a detector probing a scalar field in the Minkowski vacuum in $2+1$ Minkowski spacetime. The first nonzero subleading correction was proportional to α^{-2} and hence proportional to the Ricci scalar curvature, which we interpreted as a curvature correction as in RdS. At order α^{-3}, we found that the detector reacts to the boundary with resonance peaks closely matching those of a detector in Minkowski spacetime with a cylindrical boundary in Chapter 7.

When the field was prepared in a thermal state, we found the first two terms in the series expansion of the response function. To leading order, we recovered the response function of a detector probing a scalar field in a thermal state in $2+1$ Minkowski spacetime. However, we found an additional resonance peak at order $\alpha^{-2}\ln(\alpha)$ with no corresponding term in the response of a detector in Minkowski spacetime with a cylindrical boundary probing a scalar field prepared in a thermal state. We may conclude, therefore, that CAdS is a curved-spacetime analogue of Minkowski spacetime with a cylindrical boundary only when the field is prepared in its global vacuum. We leave the explanation and analysis of this additional resonance peak to further study.

Chapter 9

Conclusions

In this Thesis, we have analysed and extended the framework of the circular motion Unruh effect both in spacetime and in the laboratory, bridging the gap between theory and experiment. Beginning with the circular motion Unruh effect in Minkowski spacetime, we considered the assumptions which are not reproducible in an analogue spacetime implementation of the effect, principally the assumptions of an initial vacuum state and a spatially infinite spacetime. We found that when an initial vacuum state is replaced by a thermal state, acceleration dependence is still present and identifiable in the system. We applied the formalism of thermal field theory to thin films of superfluid helium, leading to a concrete and feasible experimental proposal of the circular motion Unruh effect.

In Chapter 2, we presented three derivations of the Unruh effect, each of which highlighting a different perspective. First, geometrically: the Unruh effect may be understood through the formation of Rindler horizons due to an accelerating observer, to which a temperature may be associated, the Unruh temperature. Second, quantum field theoretically: the Minkowski vacuum is a thermal state in the Fock space adapted to the boost Killing vector. Finally, the Unruh-DeWitt (UDW) detector model: the response of a detector undergoing uniform linear acceleration is equivalent to the response of a static detector in a thermal bath at a temperature proportional to the detector's proper acceleration.

Central to the UDW approach is the response function, a measure of detector excitation and de-excitation. A detector probing the Minkowski vacuum undergoing non-inertial motion, such as uniform circular motion, will excite. However, the spectrum of the excitations is only thermal when the detector undergoes uniform linear acceleration, highlighting the uniqueness of linear acceleration amongst the stationary trajectories.

We then introduced the analogue spacetime provided by hydrodynamical systems, where small perturbations in a fluid may be viewed as waves propagating

through an effective spacetime, in which the speed of light is replaced by the speed of sound. The UDW model may be adapted to an analogue spacetime setting, in which trajectories are parametrised by coordinate (rather than proper) time and the detector energy gap is measured with respect to the coordinate time. We reproduced some key results from the analysis of the circular motion Unruh effect in $2+1$ and $3+1$ dimensions in [69]. Finally, we introduced the continuous quasiparticle detector model [70], in which the two-level UDW detector is replaced by a continuous probing field, such as a continuous laser beam, recovering the response function and thus demonstrating the equivalence between the UDW detector and a continuous quasiparticle detector.

Motivated by the inherent nonzero temperature of any experimental realisation of the circular motion Unruh effect, we considered in Chapter 3 a UDW detector probing a field prepared in a thermal state at a fixed temperature. An ambient temperature breaks Lorentz invariance and a detector will respond both to its speed and acceleration. Uniform circular motion may be characterised by two parameters, such as the orbital velocity v and acceleration a. Fixing the orbital velocity, we may consider the limit of vanishing acceleration and the resulting trajectory is inertial motion with velocity v. Therefore, to isolate acceleration-dependence, one may compare the response of a detector undergoing uniform circular motion with the response of a detector undergoing inertial motion. When the field is prepared in the Minkowski vacuum, the latter is equivalent to a detector at rest due to the Lorentz-invariance of the Minkowski vacuum. However, when the field is prepared in a thermal state, broken Lorentz invariance requires one to compare uniform circular motion with inertial motion at the same speed v. Using this observation, we found a quantifier for measuring acceleration-dependence in the response of a detector.

The key discovery of Chapter 3 is that, independent of the ambient temperature, acceleration-dependence may be identified in some range of the parameter space in the response of a UDW detector, even when the ambient temperature is so high that the detector's response function is dominated by thermal effects. We found that the angular frequency of the detector plays a role in identifying this parameter space. The response of detectors with energy gaps much larger than their orbit's angular frequency is dominated by velocity contributions. Across the parameter space, we found that the effective temperature perceived by the detector may be higher or lower than the ambient temperature. We summarise the findings of this Chapter — an ambient temperature equips the circular motion Unruh effect with the characteristic of Robin Hood [119]: *Where there is little, the Unruh effect gives; and where there is plenty, the Unruh effect takes.*

In Chapter 4, we developed an experimental proposal for the observation of

acceleration-dependent response in thin-film superfluid helium-4. Superfluid helium exists at very low but nonzero temperatures and thin films of superfluid helium exhibit a phenomenon known as third sound, the propagation of surface waves on the free surface of superfluid helium, akin to shallow-water surface waves in a classical fluid. Within experimentally implementable assumptions, small perturbations in the height of the superfluid sample may be modelled as a scalar field as per the analogue spacetime formalism in Chapter 2. Using the thermal field theory in Chapter 3, we incorporated the sample temperature in our modelling and demonstrated that a laser beam may act as a local continuous detector of interface fluctuations. Through an experimentally accessible measure, we have confirmed that trajectory-dependence still persists in a system with a significant ambient temperature and, furthermore, that the background temperature enhances the signature of this effect. These results represent the first step towards the realisation of a UDW in a laboratory.

The Unruh effect is fundamentally a duality between an accelerated observer and an observer at rest in a thermal bath. Motivated by the robustness of this equivalence, we considered in Chapter 5 how far this duality holds with the addition of circular motion. Specifically, we compared the experience of a detector undergoing uniform circular motion through a thermal bath in $3+1$ Minkowski spacetime with the experience of a detector undergoing uniform circular motion whilst uniformly accelerating orthogonal to the plane of rotation, a stationary motion known as hypertor motion. We compared the two motions in a range of asymptotic regimes, finding that the addition of circular motion in general breaks the duality. As in $2+1$ dimensions, we found that again the angular frequency plays a role in distinguishing the two motions; in the regime of small orbital radii, detectors with energy gaps much larger than the angular frequency of their orbit are unable to distinguish between the two motions. In summary, while a particle detector interacting with a massless scalar field in $3+1$ Minkowski spacetime would be unable to distinguish between a thermal bath at temperature $T = a/2\pi$ and uniform linear acceleration with proper acceleration a, we found that the addition of circular motion breaks this duality. Any circular motion perturbation around these two motions would enable a particle detector to distinguish between a thermal bath and a temperature provided by linear acceleration across most of the parameter space.

In Chapter 2, Chapter 3, Chapter 4, and Chapter 5, we saw examples of stationary trajectories: inertial motion, linear acceleration, circular motion, and hypertor motion. In $3+1$ dimensions, it was shown in [71] that there are six such motions. The remaining two are linear acceleration with a constant drift velocity and a cusped motion with the spatial projection of a semicubical

parabola. One may then ask how many stationary trajectories there are in $n+1$ Minkowski spacetime. In Chapter 6, we classified the stationary trajectories both algebraically, in terms of the conjugacy classes of the Poincaré group, and geometrically, in terms of the solutions to the Frenet-Serret equations, giving an explicit example of the classification in $4+1$ Minkowski spacetime, in which dimensions there exist nine stationary trajectories. As a further example of this classification, we classified the stationary trajectories in the static patch of de Sitter (dS) spacetime.

Motivated by the finite size of the analogue spacetimes provided by condensed matter systems such as thin-film superfluid helium discussed in Chapter 4, we considered in Chapter 7 a detector undergoing uniform circular motion in analogue $2+1$ Minkowski spacetime with a cylindrical boundary, probing a scalar field prepared in either the Minkowski vacuum or a thermal state in a fixed temperature. We also modelled the effect of a finite-time interaction and considered a field with a modified dispersion relation but we leave the study of this general response function to further study, with parameters such as temporal interaction profile informed by experimental implementations of the circular motion Unruh effect. Specialising to a Klein-Gordon (KG) field and an infinite interaction time, we considered the asymptotic behaviour of the response function in the limit of a large cylindrical boundary, both when the field was prepared in the Minkowski vacuum and when the field was prepared in a thermal state. We found the leading and subleading corrections to the response function. At leading order, we recovered the corresponding (unbounded) Minkowski spacetime results. At subleading order, we found in both cases resonance peaks between the detector's energy gap and angular frequency, indicating that resonant detectors are more sensitive to a cylindrical boundary.

Having analysed an ambient temperature in Chapter 3 and a cylindrical boundary in Chapter 7, we investigated in Chapter 8 to what extent dS and Anti-de Sitter (AdS), the spacetimes of constant positive and negative curvature respectively, may be considered curved-spacetime analogues of thermality and finite size. Positive curvature provides a notion of an ambient temperature, via the Euclidean vacuum, whereas negative curvature provides a notion of spatial confinement.

First, we considered a UDW detector undergoing uniform circular motion in the static patch of dS, to which we refer as Rindler-de Sitter (RdS). In the limit of a small cosmological constant, we found that the thermal contributions to the detector response function are exponentially suppressed as in Minkowski spacetime in Chapter 3. We then found the leading and subleading contributions to the response function. At leading order, we recovered the response of a

detector probing the Minkowski vacuum in $2+1$ Minkowski spacetime. At subleading order, we found a curvature correction, proportional to the Ricci scalar curvature of dS_3.

Next, we considered a UDW detector undergoing uniform circular motion in the Universal Covering Space of Anti-de Sitter (CAdS). We considered both when the field was prepared in the static vacuum and when the field was prepared in a thermal state at a fixed temperature. In the limit of a small cosmological constant in the static vacuum, we found the first three terms in the asymptotic expansion of the response function in the long-interaction-time limit. At leading order, we recovered the response of a detector probing the Minkowski vacuum in $2+1$ Minkowski spacetime. At subleading order, we found a curvature correction, proportional to the Ricci scalar curvature of AdS_3. At the next order, we found that the detector reacts to the boundary with resonance peaks closely matching those of a detector in Minkowski spacetime with a cylindrical boundary in Chapter 7, again highlighting the significance of the angular frequency in the detector's response.

When the field was prepared in a thermal state, we found the first two terms in the asymptotic expansion of the response function. At leading order, we recovered the response of a detector in a $2+1$ thermal bath in Minkowski spacetime. However, at subleading order, we found an additional resonance peak with no corresponding term in the response of a detector in Minkowski spacetime with a cylindrical boundary probing a scalar field prepared in a thermal state. We may conclude, therefore, that CAdS is a curved-spacetime analogue of Minkowski spacetime with a cylindrical boundary only when the field is prepared in its global vacuum and that thermal states in CAdS show richer features than their Minkowski spacetime counterparts.

We found throughout this Thesis that the angular frequency of the circular motion plays a special role in the response of the detector. In a thermal bath in unbounded Minkowski spacetime, the angular frequency acts as an energy-gap threshold, above which a detector's response is dominated by velocity contributions. By contrast, in spacetimes with spatial confinement, resonant detectors — those whose energy gap matches their angular frequency — are more sensitive to the boundary.

As a mathematical side outcome, we found in Chapter 3 and Chapter 7 two results concerning Bessel functions, which we have not encountered in the existing literature. In the former Chapter, we evaluated in closed form an infinite series involving squared Bessel functions. In the latter Chapter, we found an asymptotic expansion of the Bessel function normalisation factor in a finite domain in terms of the McMahon expansion, a classical expansion in the theory

of Bessel functions. The Bessel functions, their zeros, and the asymptotics thereof have been central to this work. As we bring this Thesis to a close, we recall from the preface of the second edition of Watson's *A Treatise on the Theory of Bessel Functions* [202], "to incorporate in this work the discoveries of the last twenty years would necessitate the rewriting of at least Chapters XII — XIX; my interest in Bessel functions, however, has waned since 1922, and I am consequently not prepared to undertake such a task to the detriment of my other activities."

As we investigate the most extreme corners of the Universe, the time between theoretical prediction and experimental verification ever increases. Forty-eight years passed between the prediction of the Higgs particle and its discovery. At the time of writing this Thesis, forty-eight years have also passed since the prediction of the Unruh effect. In this work, we have seen that the Unruh effect, both linear and circular, has many faces, and new avenues are emerging through analogue spacetimes. We have extended the existing theory and pushed it closer to a realistic experimental environment by including the effects of thermality and spatial confinement. This Thesis, therefore, paves the way towards the experimental confirmation of acceleration-dependence and offers a concrete system in which to test this phenomenon, bringing even the remote predictions of Quantum Field Theory (QFT) within our grasp.

Appendix A

Dominated convergence theorem

In this Appendix, we provide a typical dominated convergence theorem argument to find the small-gap limit of the response function (2.69).

A.1 Lebesgue's dominated convergence theorem

Lebesgue's dominated convergence theorem provides a sufficient condition under which a limit and an integral may be interchanged [203].

Theorem A.1 (Dominated convergence theorem)**.** *Let $(f_n)_{n\in\mathbb{N}}$ be a sequence of continuous functions and $\lim_{n\to\infty} f_n(x) = f(x)$ for each x. Assume there exists some g such that $\int_{\mathbb{R}} \mathrm{d}x\, g(x) < \infty$ (g is integrable) and $|f_n(x)| \leq g(x)$ for all n (g dominates f_n). Then, f_n and f are integrable and*

$$\lim_{n\to\infty} \int_{\mathbb{R}} \mathrm{d}x\, f_n(x) \;=\; \int_{\mathbb{R}} \mathrm{d}x\, \lim_{n\to\infty} f_n(x) \;=\; \int_{\mathbb{R}} \mathrm{d}x\, f(x)\,. \tag{A.1}$$

We are often interested in the limit of a continuous parameter $\lim_{\beta\to b} f(x,\beta)$, rather than the limit of a discrete parameter $n \in \mathbb{N}$, as in Theorem A.1. We may reconcile the two as follows. We recall that $\lim_{y\to b} h(y) = L$ if and only if $\lim_{n\to\infty} h(b_n) = L$ for any sequence $(b_n)_{n\in\mathbb{N}}$ with $b_n \neq b$ and $\lim_{n\to\infty} b_n = b$. We may therefore write $\lim_{\beta\to b} f(x,\beta) = \lim_{n\to\infty} f_n(x)$, where $f_n(x) \coloneqq f(x,\beta_n)$ and $(\beta_n)_{n\in\mathbb{N}}$ is any sequence such that $(\beta_n)_{n\in\mathbb{N}} \neq b$ and $\lim_{n\to\infty} \beta_n = b$. As such, we may appeal to Theorem A.1 for limits of both continuous and discrete parameters.

We note that in the context of measure theory, one may state a stronger version of Theorem A.1, in which the sequence of functions $(f_n)_{n\in\mathbb{N}}$ need only be measurable rather than continuous.

A.2 Small-gap limit

We consider now the small-gap limit $E \to 0$ of the response function (2.69),

$$\mathcal{F}(E) \;=\; -\frac{E}{2\pi}\Theta(-E) + \frac{v}{4\pi^2\gamma R}\int_0^\infty \mathrm{d}z\, \cos\!\left(\frac{2ER}{\gamma v}z\right)\left(\frac{\gamma^2}{z^2} - \frac{1}{z^2 - v^2\sin^2 z}\right). \tag{A.2}$$

We note that the integral is even in E and we define

$$I(E) \;=\; \int_0^\infty \mathrm{d}z\, \cos\!\left(\frac{2|E|R}{\gamma v} z\right)\left(\frac{\gamma^2}{z^2} - \frac{1}{z^2 - v^2 \sin^2 z}\right) . \tag{A.3}$$

The integrand $f(z, E)$ may be written as

$$f(z, E) \;\coloneqq\; \cos\!\left(\frac{2|E|R}{\gamma v} z\right) g(z)\,, \tag{A.4}$$

$$g(z) \;=\; \frac{\gamma^2}{z^2} - \frac{1}{z^2 - v^2 \sin^2 z}\,. \tag{A.5}$$

An elementary proof by contradiction shows $g(z) > 0$ for $z \geq 0$. Hence, $g(z)$ dominates $f(z, E)$, $|f(z, E)| \leq g(z)$ and we may take the limit $E \to 0$ under the integral to recover the leading-order behaviour of (A.3),

$$\lim_{E\to 0} I(E) \;=\; \int_0^\infty \mathrm{d}z \left(\frac{\gamma^2}{z^2} - \frac{1}{z^2 - v^2 \sin^2 z}\right) \;=:\; \Gamma_0\,. \tag{A.6}$$

We re-express $I(E)$ (A.3) by adding and subtracting Γ_0,

$$I(E) \;=\; \Gamma_0 + \int_0^\infty \mathrm{d}z \left(\cos\!\left(\frac{2|E|R}{\gamma v} z\right) - 1\right)\left(\frac{\gamma^2}{z^2} - \frac{1}{z^2 - v^2 \sin^2 z}\right) . \tag{A.7}$$

Expanding the second bracket under the integral, we note the standard integral

$$\int_0^\infty \mathrm{d}z\, \frac{\cos(az) - 1}{(az)^2} \;=\; -\frac{\pi}{2|a|}\,, \tag{A.8}$$

As such, we have

$$I(E) \;=\; \Gamma_0 - \frac{\pi\gamma R}{v}|E| - \int_0^\infty \mathrm{d}z\, \frac{\cos\!\left(\frac{2|E|R}{\gamma v} z\right) - 1}{z^2} \frac{1}{1 - v^2 \sin^2(z)/z^2}\,. \tag{A.9}$$

We consider the integral

$$J(b) \;=\; \int_0^\infty \mathrm{d}z\, \frac{\cos(bz) - 1}{(bz)^2} \frac{1}{1 - v^2 \sin^2(z)/z^2}\,, \tag{A.10}$$

in the limit $b \to 0^+$. The factor $(\cos(bz) - 1)/(bz)^2$ is bounded in absolute value by 1. However, the factor $1/(1 - v^2 \sin^2(z)/z^2)$ is not integrable since $1/(1 - v^2 \sin^2(z)/z^2) \sim 1$ as $z \to \infty$. Adding and subtracting this large-z behaviour, we have

$$J(b) \;=\; \int_0^\infty \mathrm{d}z\, \frac{\cos(bz) - 1}{(bz)^2}\left(\frac{1}{1 - v^2 \sin^2(z)/z^2} - 1\right) + \int_0^\infty \mathrm{d}z\, \frac{\cos(bz) - 1}{(bz)^2}\,. \tag{A.11}$$

As the factor $(\cos(bz) - 1)/(bz)^2$ is bounded in absolute value, we may appeal to the dominated convergence theorem to take the $b \to 0^+$ limit and evaluate the

second integral using (A.8),

$$J(b) \;=\; -\frac{\pi}{2|b|} + \mathcal{O}(1)\,, \tag{A.12}$$

as $b \to 0^+$. Returning to $I(E)$, we have

$$I(E) \;=\; \Gamma_0 - \frac{\pi\gamma R}{v}|E| - \left(\frac{2|E|R}{\gamma v}\right)^2 \int_0^\infty \mathrm{d}z\, \frac{\cos\left(\frac{2|E|R}{\gamma v}z\right) - 1}{\left(\frac{2|E|R}{\gamma v}z\right)^2} \frac{1}{1 - v^2\sin^2(z)/z^2}\,. \tag{A.13}$$

We may identify the integral in (A.13) as $J(b)$ (A.10) with $b = 2|E|R/(\gamma v)$. Appealing to (A.12) and combining the two terms at order $|E|$, we have

$$I(E) \;=\; \Gamma_0 - \pi R\gamma v|E| + \mathcal{O}(E^2)\,, \tag{A.14}$$

as $E \to 0$. The response function may therefore be written as

$$\mathcal{F}(E) \;=\; \frac{v}{4\pi^2\gamma R}\int_0^\infty \mathrm{d}z \left(\frac{\gamma^2}{z^2} - \frac{1}{z^2 - v^2\sin^2(z)}\right) - \frac{1}{4\pi}\left(1 - \frac{1}{\gamma^2}\mathrm{sgn}(E)\right) E + \mathcal{O}(E^2)\,, \tag{A.15}$$

as $E \to 0$, where $\mathrm{sgn}(E) = E/|E|$ is the signum function.

Appendix B

$2+1$ thermal response function mode sum

In this Appendix, we find the mode sum expression (3.5) for the response function. The notation and the assumptions are as in Section 3.1.1.

The positive Minkowski frequency mode functions of the massless KG field are

$$u_{\boldsymbol{k}}(\mathsf{x}) = \frac{1}{2\pi\sqrt{2\omega}} \mathrm{e}^{-\mathrm{i}\omega t + \mathrm{i}\boldsymbol{k}\cdot\boldsymbol{x}} \,, \tag{B.1}$$

where $\boldsymbol{k}$ is the spatial momentum and the dispersion relation specifies ω as a function of $|\boldsymbol{k}|$. The normalisation is $(u_{\boldsymbol{k}}, u_{\boldsymbol{k}'}) = \delta_{\boldsymbol{k},\boldsymbol{k}'}$, where $(\cdot,\cdot)$ is the Klein-Gordon inner product and δ is the Dirac delta. It follows as in [26] that the derivative correlation function $\mathcal{W}_\beta$ (3.4) has the mode sum expression

$$\begin{aligned}\mathcal{W}_\beta(t,t') \;=\; \int d^2\boldsymbol{k} \Big[\big(1+n(\beta\omega)\big) \frac{\mathrm{d}}{\mathrm{d}t} u_{\boldsymbol{k}}\big(\mathsf{x}(t)\big) \frac{\mathrm{d}}{\mathrm{d}t'} u^*_{\boldsymbol{k}}\big(\mathsf{x}(t')\big) \\ + n(\beta\omega) \frac{\mathrm{d}}{\mathrm{d}t} u^*_{\boldsymbol{k}}\big(\mathsf{x}(t)\big) \frac{\mathrm{d}}{\mathrm{d}t'} u_{\boldsymbol{k}}\big(\mathsf{x}(t')\big) \Big] \,,\end{aligned} \tag{B.2}$$

where $\mathsf{x}(t)$ is the circular motion worldline (3.2) and n is the Bose factor (2.40).

We substitute in (B.2) the mode functions (B.1) and the trajectory (3.2), perform the differentiations, and change the integration variables from (k_x, k_y) to (k, l) by the time-dependent rotation in the $\boldsymbol{k}$ plane,

$$(k,l) \;=\; \Big(k_y \cos\Big(\tfrac{\Omega(t+t')}{2}\Big) - k_x \sin\Big(\tfrac{\Omega(t+t')}{2}\Big) \,, k_y \sin\Big(\tfrac{\Omega(t+t')}{2}\Big) + k_x \cos\Big(\tfrac{\Omega(t+t')}{2}\Big) \Big) \,, \tag{B.3}$$

obtaining

$$\begin{aligned}\mathcal{W}_\beta(t,t') \;=\; \frac{1}{8\pi^2} \int \frac{\mathrm{d}k\,\mathrm{d}l}{\omega} \Big[\big(\omega - \Omega R k \cos(\Omega s/2)\big)^2 - \Omega^2 R^2 l^2 \sin^2(\Omega s/2) \Big] \\ \times \Big[\big(1+n(\beta\omega)\big) \mathrm{e}^{-\mathrm{i}\omega s + 2\mathrm{i}Rk\sin(\Omega s/2)} + n(\beta\omega) \mathrm{e}^{\mathrm{i}\omega s - 2\mathrm{i}Rk\sin(\Omega s/2)} \Big] \,,\end{aligned} \tag{B.4}$$

where $s = t - t'$ and ω is now a function of $|\boldsymbol{k}| = \sqrt{k^2+l^2}$. An equivalent

expression is

$$\begin{aligned}\mathcal{W}_\beta(t,t') \;=\; & \frac{1}{8\pi^2}\int \frac{\mathrm{d}k\,\mathrm{d}l}{\omega}\Big\{\big(1+n(\beta\omega)\big)\\ & \times\Big[\big(\omega-\Omega Rk\cos(\Omega s/2)\big)^2+\tfrac{1}{2}\mathrm{i}\Omega^2 Rk\sin(\Omega s/2)\Big]\,\mathrm{e}^{-\mathrm{i}\omega s+2\mathrm{i}Rk\sin(\Omega s/2)}\\ & +n(\beta\omega)\Big[\big(\omega-\Omega Rk\cos(\Omega s/2)\big)^2-\tfrac{1}{2}\mathrm{i}\Omega^2 Rk\sin(\Omega s/2)\Big]\,\mathrm{e}^{\mathrm{i}\omega s-2\mathrm{i}Rk\sin(\Omega s/2)}\Big\}\,, \end{aligned}\tag{B.5}$$

as can be seen by considering the difference of (B.4) and (B.5) and noting that the integral over the angle in the (k,l) plane produces a sum of J_0, J_0' and J_0'' that vanishes after an application of Bessel's differential equation [111]. Note that the integrals in (B.4) and (B.5) are free of infrared divergences when $\omega(0)=0$, which follows from the assumption $\omega'(0)>0$.

We now appeal to the following identity, also known as the Jacobi-Anger expansion

$$\mathrm{e}^{\pm 2\mathrm{i}Rk\sin(\Omega s/2)} \;=\; \sum_{n\in\mathbb{Z}} \mathrm{e}^{\pm \mathrm{i}n\Omega s/2} J_n(2Rk)\,, \tag{B.6}$$

which follows from 10.12.1 in [111]. We then regroup the sum so that all the s-dependence is in factors of the form $\mathrm{e}^{\mp\mathrm{i}\omega s\pm \mathrm{i}n\Omega s/2}$, multiplied by Bessel functions of order n, $n\pm1$ and $n\pm2$. We then convert the integral over k and l to polar coordinates by $(k,l)=(K\sin\theta, K\cos\theta)$, so that $\mathrm{d}k\,\mathrm{d}l = K\mathrm{d}K\,\mathrm{d}\theta$. The odd n terms are odd in θ and vanish on integration over θ. We relabel the even n terms by $n=2m$ with $m\in\mathbb{Z}$, substitute in (3.4), and perform the integral over t in terms of delta-functions, which collapse the integral over K, with the outcome

$$\begin{aligned}\mathcal{F}(\overline{E},\beta) \;=\; & \frac{1}{4\pi}\int_0^{2\pi}\mathrm{d}\theta\Bigg\{\sum_{m>(\overline{E}+\omega(0))/\Omega}\frac{K_m^+}{\omega'(K_m^+)\omega(K_m^+)}\Big(1+n\big(\beta\omega(K^+)\big)\Big)\\ & \times\Big[\Big(\big(\omega(K_m^+)\big)^2+\tfrac{1}{2}\Omega^2R^2(K_m^+)^2\sin^2\theta\Big)J_{2m}(2RK_m^+\sin\theta)\\ & \quad-\Omega RK_m^+\big(\omega(K_m^+)+\tfrac{1}{4}\Omega\big)\sin\theta J_{2m+1}(2RK_m^+\sin\theta)\\ & \quad-\Omega RK_m^+\big(\omega(K_m^+)-\tfrac{1}{4}\Omega\big)\sin\theta J_{2m-1}(2RK_m^+\sin\theta)\\ & \quad+\tfrac{1}{4}\Omega^2R^2(K_m^+)^2\sin^2\theta\big(J_{2m+2}(2RK_m^+\sin\theta)+J_{2m-2}(2RK_m^+\sin\theta)\big)\Big]\\ & +\sum_{m>(-\overline{E}+\omega(0))/\Omega}\frac{K_m^-}{\omega'(K_m^-)\omega(K_m^-)}\,n\big(\beta\omega(K^-)\big)\\ & \times\Big[\Big(\big(\omega(K_m^-)\big)^2+\tfrac{1}{2}\Omega^2R^2(K_m^-)^2\sin^2\theta\Big)J_{2m}(2RK_m^-\sin\theta)\\ & \quad-\Omega RK_m^-\big(\omega(K_m^-)+\tfrac{1}{4}\Omega\big)\sin\theta J_{2m+1}(2RK_m^-\sin\theta)\\ & \quad-\Omega RK_m^-\big(\omega(K_m^-)-\tfrac{1}{4}\Omega\big)\sin\theta J_{2m-1}(2RK_m^-\sin\theta)\\ & \quad+\tfrac{1}{4}\Omega^2R^2(K_m^-)^2\sin^2\theta\big(J_{2m+2}(2RK_m^-\sin\theta)+J_{2m-2}(2RK_m^-\sin\theta)\big)\Big]\Bigg\}\,, \end{aligned}\tag{B.7}$$

where $K_m^{\pm}$ are as defined in Section 3.1.1, and the notation suppresses their $\overline{E}$-dependence.

The integrals in (B.7) can be evaluated using the identities

$$\int_0^{2\pi} J_{2m}(2a\sin\theta)\,\mathrm{d}\theta \;=\; 2\pi J_m^2(a)\,, \tag{B.8a}$$

$$\int_0^{2\pi} \sin\theta J_{2m\pm1}(2a\sin\theta)\,\mathrm{d}\theta \;=\; 2\pi J_{m\pm1}(a)J_m(a)\,, \tag{B.8b}$$

$$\int_0^{2\pi} \sin^2\theta J_{2m}(2a\sin\theta)\,\mathrm{d}\theta \;=\; \pi\big(J_m^2(a)+J_{m-1}(a)J_{m+1}(a)\big)\,, \tag{B.8c}$$

where $m\in\mathbb{Z}$; these identities follow from $6.681.1$ in [117] by setting respectively $\mu=0$, $\mu=\frac{1}{2}$ and $\mu=1$. Further use of the Bessel function identities 10.6.1 and 10.6.2 in [111] then gives formula (3.5) in the main text.

We end this Appendix with two comments on the role of the time derivatives in (3.5).

First, in the case of a massive field $\omega(0)>0$, the response function (3.5) can be obtained in a more direct way: the property $\omega(0)>0$ implies that the non-derivative correlation function $\widetilde{\mathcal{W}}_\beta$ (3.1) is well defined and hence $\mathcal{W}_\beta(t',t'')=\partial_{t'}\partial_{t''}\widetilde{\mathcal{W}}_\beta\big(\mathsf{x}(t'),\mathsf{x}(t'')\big)$. Using the time translation invariance of $\mathcal{W}_\beta$ and $\widetilde{\mathcal{W}}_\beta$, we then have

$$\mathcal{F}(\overline{E},\beta) \;=\; \overline{E}^2\int_{-\infty}^{\infty}\mathrm{d}t\,\mathrm{e}^{-\mathrm{i}\overline{E}t}\,\widetilde{\mathcal{W}}_\beta\big(\mathsf{x}(t),\mathsf{x}(0)\big)\,, \tag{B.9}$$

where the $\overline{E}^2$ factor comes from integration by parts. The right-hand side of (B.9) is recognised as $\overline{E}^2$ times the response function of a detector without a derivative in the coupling as seen in Section 2.1.3. We can now apply the methods of this Appendix directly to the right-hand side of (B.9), arriving at (3.5) through significantly fewer steps: the overall $\overline{E}^2$ factor in (3.5) is exactly the overall $\overline{E}^2$ factor in (B.9).

Second, when $\omega(0)=0$, the non-derivative Wightman function $\widetilde{\mathcal{W}}_\beta$ is infrared divergent and so (B.9) is not well defined. If we, however, ignore this infrared divergence in the mode sum expression for $\widetilde{\mathcal{W}}_\beta$, and informally apply the integral interchange manipulations of this Appendix to (B.9), we find once again (3.5): the informal integral interchanges can be interpreted as a regularisation of the infrared divergence in the transition rate. This regularisation of the transition rate can be applied even when the detector's coupling does not involve a time derivative [204].

Appendix C

Bessel function identity

In this Appendix we verify the identity

$$\sum_{m=1}^{\infty}\big(J_{m-1}^2(mv)+J_{m+1}^2(mv)\big) \;=\; \frac{1}{\sqrt{1-v^2}}\,, \tag{C.1}$$

where $0\le v<1$.

Proof. The case $v=0$ is trivial as the only nonvanishing term on the left-hand side is $J_0^2(0)=1$. We henceforth assume $0<v<1$.

Using the integral representation [111, (10.9.26)],

$$J_n^2(z) \;=\; \frac{2}{\pi}\int_0^{\frac{\pi}{2}} J_{2n}(2z\cos\theta)\,\mathrm{d}\theta\,, \tag{C.2}$$

we have

$$\begin{aligned}\sum_{m=1}^{\infty}\big(J_{m-1}^2(mv)+J_{m+1}^2(mv)\big) \;&=\; \frac{2}{\pi}\sum_{m=1}^{\infty}\int_0^{\frac{\pi}{2}}\mathrm{d}\theta\,\Big(J_{2m-2}(2mv\cos\theta)\\ &\qquad\qquad + J_{2m+2}(2mv\cos\theta)\Big)\\ &=\; \frac{2}{\pi}\int_0^{\frac{\pi}{2}}\mathrm{d}\theta\sum_{m=1}^{\infty}\Big(J_{2m-2}(2mv\cos\theta)\\ &\qquad\qquad + J_{2m+2}(2mv\cos\theta)\Big)\,,\end{aligned} \tag{C.3}$$

where the interchange of the sum and the integral is justified because the summands fall off exponentially in m, uniformly in θ, as seen from [111, (10.20.4)], recalling that $0\le v\cos\theta\le v<1$.

For $0\le\theta<\pi/2$, we use Bessel function identities to rewrite the summands in (C.3) as

$$J_{2m-2}(2mv\cos\theta)+J_{2m+2}(2mv\cos\theta) \;=\; J_{2m}(2mv\cos\theta)\left(\frac{4}{v^2\cos^2\theta}-2\right)$$

$$- \frac{4}{v\cos\theta}\frac{J'_{2m}(2mv\cos\theta)}{2m}\,, \tag{C.4}$$

and we then evaluate the sum over m by the identities

$$\sum_{m=1}^{\infty} J_{2m}(2mt) = \frac{t^2}{2(1-t^2)}\,, \tag{C.5a}$$

$$\begin{aligned}\sum_{m=1}^{\infty}\frac{J'_{2m}(2mt)}{2m} &= \frac{1}{2}\left(\sum_{k=1}^{\infty}\frac{J'_k(kt)}{k} - \sum_{k=1}\frac{J'_k(kt)}{k}(-1)^{k-1}\right)\\ &= \frac{1}{2}\left[\frac{1}{2}+\frac{t}{4}-\left(\frac{1}{2}-\frac{t}{4}\right)\right]\\ &= \frac{t}{4}\,,\end{aligned} \tag{C.5b}$$

valid for $0 \le t < 1$, using [117, (8.517.3, 8.518.1, 8.518.2)]. Hence

$$\begin{aligned}\sum_{m=1}^{\infty}\left(J^2_{m-1}(mv)+J^2_{m+1}(mv)\right) &= \frac{2}{\pi}\int_0^{\frac{\pi}{2}}\mathrm{d}\theta\left[\left(\frac{4}{v^2\cos^2\theta}-2\right)\frac{v^2\cos^2\theta}{2(1-v^2\cos^2\theta)}\right.\\ &\qquad\left. - \frac{4}{v\cos\theta}\frac{v\cos\theta}{4}\right]\\ &= \frac{2}{\pi}\int_0^{\frac{\pi}{2}}\frac{\mathrm{d}\theta}{1-v^2\cos^2\theta}\\ &= \frac{1}{\sqrt{1-v^2}}\,,\end{aligned} \tag{C.6}$$

where the last integral is elementary. □

Appendix D

Transition rates and probabilities

In this Appendix, we discuss the relationship between the response function (transition rate) and the transition probability of a UDW detector interacting with a scalar field. We use the UDW detector model from Section 2.1.3 and Section 5.1.1. In particular, we demonstrate three equivalent definitions of the response function found in the literature (see, for example, [3, 5, 23, 71, 72, 143–146]),

$$\mathcal{F}_1(E) \;=\; \int_{\mathbb{R}} \mathrm{d}\tau\, \mathrm{e}^{-\mathrm{i}E\tau}\mathcal{W}(\tau)\,,\;\; \mathcal{F}_2(E) \;=\; \lim_{T\to\infty}\frac{1}{\lambda^2}\frac{\mathcal{P}(E)}{T}\,,\;\; \mathcal{F}_3(E) \;=\; \frac{1}{\lambda^2}\lim_{T\to\infty}\frac{\mathrm{d}\mathcal{P}(E)}{\mathrm{d}T}\,, \tag{D.1}$$

where $\mathcal{W}(\tau) \coloneqq \langle\hat{\Phi}(\mathsf{x}(\tau)), \hat{\Phi}(\mathsf{x}(0))\rangle$ is the pullback of the Wightman function to a stationary trajectory (2.39), $\mathcal{P}(E)$ is the transition probability (2.37b), and T is a parameter controlling the total interaction time.

We work with the interaction Hamiltonian (2.32) with switching function $\chi(\tau)$, which we assume may be written as

$$\chi(\tau) \;=\; \beta(\tau/T)\,, \tag{D.2}$$

where $\beta(u)$ is a real function determining the temporal profile of field-detector interaction. We, furthermore, assume that $\beta(0) = 1$ so that in the limit of long interaction times $T \to \infty$, we recover the infinite-time switching function $\chi(\tau) = 1$.

We focus our attention to the case of a detector coupled to a quantum scalar field in an arbitrary, static spacetime. The key assumption for the following results is that the state of the field is stationary with respect to time translations along the detector trajectory, so that the Wightman function is also stationary in the sense of (2.42). We further assume that the Wightman function decays at infinity sufficiently quickly such that its Fourier transform is once differentiable. Under these assumptions, the transition probability is given by

$$\mathcal{P}(E) \;=\; \lambda^2 \int_{\mathbb{R}^2} \mathrm{d}\tau\mathrm{d}\tau'\, \chi(\tau)\chi(\tau')\mathrm{e}^{-\mathrm{i}E(\tau-\tau')}\mathcal{W}(\tau-\tau')\,. \tag{D.3}$$

The pullback of the Wightman function may be expressed in terms of its Fourier

transform as

$$\mathcal{W}(\tau-\tau') \;=\; \frac{1}{2\pi}\int_{\mathbb{R}} \mathrm{d}\omega\, \mathrm{e}^{\mathrm{i}\omega(\tau-\tau')}\widehat{\mathcal{W}}(\omega)\,. \tag{D.4}$$

We note that due to the singular behaviour of the Wightman function at $\tau = 0$, the Fourier transform should be understood in a distributional sense. We rewrite the transition probability (D.3) as

$$\mathcal{P}(E) \;=\; \frac{\lambda^2}{2\pi}\int_{\mathbb{R}} \mathrm{d}\omega\, \widehat{\mathcal{W}}(\omega)\left(\int_{\mathbb{R}} \mathrm{d}\tau\, \mathrm{e}^{-\mathrm{i}(E-\omega)\tau}\chi(\tau)\right)\left(\int_{\mathbb{R}} \mathrm{d}\tau'\, \mathrm{e}^{\mathrm{i}(E-\omega)\tau'}\chi(\tau')\right)\,, \tag{D.5}$$

$$\;=\; \frac{\lambda^2}{2\pi}\int_{\mathbb{R}} \mathrm{d}\omega\, \widehat{\mathcal{W}}(\omega)|\widehat{\chi}(E-\omega)|^2\,, \tag{D.6}$$

where $\widehat{\chi}(\omega)$ is the Fourier transform of $\chi(\tau)$, which may also be rewritten as

$$\widehat{\chi}(\omega) \;=\; \int_{\mathbb{R}} \mathrm{d}\tau\, \mathrm{e}^{-\mathrm{i}\omega\tau}\chi(\tau) \;=\; T\int_{\mathbb{R}} \mathrm{d}u\, \mathrm{e}^{-\mathrm{i}\omega T u}\beta(u) \;=\; T\widehat{\beta}(\omega T)\,. \tag{D.7}$$

We perform the change of integration variable $v = (E-\omega)T$ in (D.6) and employ (D.7), such that

$$\mathcal{P}(E) \;=\; \frac{\lambda^2}{2\pi}T\int_{\mathbb{R}} \mathrm{d}v\, \widehat{\mathcal{W}}(E-v/T)|\widehat{\beta}(v)|^2. \tag{D.8}$$

We consider the definition $\mathcal{F}_2(E)$ in (D.1). We have

$$\mathcal{F}(E) \;=\; \lim_{T\to\infty}\frac{\mathcal{P}(E)}{\lambda^2 T} \;=\; \widehat{\mathcal{W}}(E)\times\frac{1}{2\pi}\int_{\mathbb{R}} \mathrm{d}v|\widehat{\beta}(v)|^2\,. \tag{D.9}$$

On the other hand, a second common notion of transition rate is given by $\mathcal{F}_3(E)$ in (D.1), where a derivative is taken with respect to the time parameter T. We compute this directly using (D.8), giving

$$\frac{\mathrm{d}\mathcal{P}(E)}{\mathrm{d}T} \;=\; \frac{\lambda^2}{2\pi}\int_{\mathbb{R}} \mathrm{d}v\, \widehat{\mathcal{W}}(E-v/T)|\widehat{\beta}(v)|^2 + \frac{1}{T}\frac{\lambda^2}{2\pi}\int_{\mathbb{R}} \mathrm{d}v\, \widehat{\mathcal{W}}'(E-v/T)|\widehat{\beta}(v)|^2\,. \tag{D.10}$$

Under the assumption that the derivative of $\widehat{\mathcal{W}}(\omega)$ is sufficiently regular, as is the case for the Wightman functions considered in this thesis, we take the limit $T\to\infty$ to recover

$$\mathcal{F}_3(E) \;=\; \frac{1}{\lambda^2}\lim_{T\to\infty}\frac{\mathrm{d}\mathcal{P}(E)}{\mathrm{d}T} \;=\; \widehat{\mathcal{W}}(E)\times\frac{1}{2\pi}\int_{\mathbb{R}} \mathrm{d}v\,|\widehat{\beta}(v)|^2. \tag{D.11}$$

Comparing (D.9) and (D.11), we see the equivalence of $\mathcal{F}_2(E)$ and $\mathcal{F}_3(E)$ in (D.1).

Finally, an alternative way of writing $\mathcal{F}_1$ is

$$\mathcal{F}_1(E) \;=\; \widehat{\mathcal{W}}(E)\,. \tag{D.12}$$

By normalising the switching function such that

$$\int_{\mathbb{R}} \mathrm{d}v \, |\widehat{\beta}(v)|^2 \;=\; 2\pi \,, \tag{D.13}$$

we see that all three definitions (D.9), (D.11), and (D.12), of the transition rate agree.

We finally remark that this motivates the choice of Gaussian switching function in Example 5.1, which satisfies both the normalisation condition (D.13) and $\lim_{T\to\infty} \chi(\tau; T) = 1$.

Appendix E

Propositions and proofs

In this Appendix, we provide proofs of statements made within the main body of the thesis.

E.1 Proof of Proposition 5.1

Proposition. *Let $\alpha > 0$ and $\rho > 0$. There exists a positive, nonzero solution $z_0 \in (0, \frac{\pi}{\alpha})$ to*

$$\rho \sinh(z) - \sin(\alpha z) \;=\; 0\,, \tag{E.1}$$

for $\alpha > \rho$.

Proof. Let $f(z) = \rho \sinh(z)$ and $g(z) = \sin(\alpha z)$. We note that $f(z)$ is an unbounded, strictly increasing function. We remark $f(0) = g(0) = 0$ and $f'(0) = \rho$ and $g'(0) = \alpha$. As such, if $\rho \geq \alpha > 0$, then $f'(z) > g'(z)$ for all $z > 0$; therefore, $f(z)$ and $g(z)$ never intersect.

However, for $0 < \rho < \alpha$, we have $g'(z) > f'(z)$ for all $z > 0$ that satisfy $\rho \cosh(z) < \alpha \cos(\alpha z)$. For all such z, we also have $g(z) > f(z)$.

The first positive root of $g(z)$ is at $z = \frac{\pi}{\alpha}$. As $f(z)$ is a strictly increasing function, we have $f(\frac{\pi}{\alpha}) > g(\frac{\pi}{\alpha})$.

As such, the function $f(z) - g(z) = \rho \sinh(z) - \sin(\alpha z)$ undergoes a sign change on the interval $(0, \frac{\pi}{\alpha})$. Hence, by the intermediate value theorem, it follows that there is a root z_0 on the interval $(0, \frac{\pi}{\alpha})$. □

E.2 Proof of Proposition 5.2

Proposition. *Let $\alpha > \rho > 0$. The root z_0 of $f(z) = \rho^2 \sin^2(z) - \sinh^2(\alpha z)$ with the smallest, positive imaginary part is given by $z_0 = \mathrm{i}\mu$, where μ is the smallest, nonzero solution of*

$$\sin(\alpha\mu) \;=\; \rho \sinh(\mu)\,. \tag{E.2}$$

Proof. We consider the complex function $f(z) = \rho^2 \sin^2(z) - \sinh^2(\alpha z)$, which we write as

$$f(z) \;=\; f_+(z) f_-(z)\,, \tag{E.3a}$$

$$f_\pm(z) \;=\; \rho \sin(z) \pm \sinh(\alpha z)\,, \tag{E.3b}$$

where $\alpha > \rho > 0$. We investigate first the real roots of $f_\pm$, $x \in \mathbb{R}$. Each $f_\pm(x)$ has a simple zero at $x = 0$ and no other real zeros. We can see this by observing $f_\pm(0) = 0$ and $f'_\pm(x) = \alpha\big(\frac{\rho}{\alpha}\cos(x) \pm \cosh(\alpha x)\big)$. We note that $|\cosh(\alpha x)| > 1$ and, since $\alpha > \rho$, we have $|\frac{\rho}{\alpha}\cos(x)| < 1$. Therefore, $f_+(x)$ is a strictly increasing function and $f_-(x)$ is a strictly decreasing function. Hence, the only real zero of f is a double zero at $x = 0$.

We consider now the complex roots of the equations $f_\pm(z) = 0$ of the form $z_0 = x + \mathrm{i}Y$, where $Y > 0$. We express the equations $f_\pm(z) = 0$ in terms of their real and imaginary parts

$$\mathfrak{Re}\{f_\pm(x + \mathrm{i}Y)\} \;=\; \rho\sin(x)\cosh(Y) \pm \sinh(\alpha x)\cos(\alpha Y) \;=\; 0\,, \tag{E.4a}$$
$$\mathfrak{Im}\{f_\pm(x + \mathrm{i}Y)\} \;=\; \rho\cos(x)\sinh(Y) \pm \cosh(\alpha x)\sin(\alpha Y) \;=\; 0\,. \tag{E.4b}$$

We consider first the roots of the equation $f_-(z) = 0$. These are the solutions to the system of equations

$$\rho\sin(x)\cosh(Y) - \sinh(\alpha x)\cos(\alpha Y) \;=\; 0\,, \tag{E.5a}$$
$$\rho\cos(x)\sinh(Y) - \cosh(\alpha x)\sin(\alpha Y) \;=\; 0\,. \tag{E.5b}$$

To begin, we consider the first imaginary root of $f_-(z)$ with positive imaginary part, $z_0 = \mathrm{i}\mu$ with $\mu > 0$. The equation for the real part of f_- (E.5a) is trivially satisfied. The equation for the imaginary part of the root is given by

$$\rho\sinh(\mu) \;=\; \sin(\alpha\mu)\,. \tag{E.6}$$

By Proposition 5.1, there exists a positive solution to this equation. We therefore define μ to be the smallest, positive solution to (E.6).

As $z_0 = \mathrm{i}\mu$ is the smallest, imaginary root of $f_-(z)$ with positive imaginary part, we inspect whether there exist roots of $f_-(z)$ with nonzero real part, roots of the form $z_0 = x + \mathrm{i}Y$ with $x \neq 0$ and $0 < Y \leq \mu$.

First, we consider whether there exist roots z_0 of $f_-(z)$ with positive imaginary part less than μ, $z_0 = x + \mathrm{i}Y$ with $x \neq 0$ and $0 < Y < \mu$. On the domain $x \in (0, \mu)$, the functions $\sin(\alpha x)$ and $\rho\sinh(x)$ are positive. As $0 < \rho < \alpha$, we also have

$$\rho\sinh(x) \;<\; \sin(\alpha x)\,. \tag{E.7}$$

Using the inequality (E.7) on (E.5b), we have

$$\cosh(\alpha x)\sin(\alpha Y) \;=\; \rho\cos(x)\sinh(Y) \;<\; \cos(x)\sin(\alpha Y)\,, \tag{E.8}$$

which does not hold for $x \neq 0$. By assumption $x \neq 0$ and so there does not exist a root of the equation $f_-(z) = 0$ with a positive imaginary part smaller than μ.

Next, we address whether there exist roots with nonzero real part and positive imaginary part equal to μ, $z_0 = x + \mathrm{i}\mu$ with $x \neq 0$. Setting $Y = \mu$ in (E.5b), we have

$$\rho\cos(x)\sinh(\mu) \;=\; \cosh(\alpha x)\sin(\alpha\mu)\,. \tag{E.9}$$

Using (E.6), (E.9) reduces to $\cos(x) = \cosh(\alpha x)$ which has no solutions for $x \neq 0$.

Therefore, the root of $f_-(z)$ with smallest, positive imaginary part is given by $z_0 = \mathrm{i}\mu$, where μ is the smallest, positive solution to (E.6).

Before we address the roots of $f_+(z)$, we make three observations.

1. The solution μ to (E.6) lies within the range $0 < \mu < \frac{\pi}{\alpha}$.

2. The function $\sin(\alpha Y)/\sinh(Y)$ is a decreasing function on $0 < \alpha Y < \pi$.

3. If $0 < Y < \mu$, then $\frac{\sin(\alpha Y)}{\sinh(Y)} > \frac{\sin(\alpha\mu)}{\sinh(\mu)} = \rho$.

Observation 1 follows from Proposition 5.1.

To prove Observation 2, we note that $\sin(\alpha Y)$ is a decreasing function $\frac{\pi}{2} \leq \alpha Y < \pi$, whereas $\sinh(Y)$ is an increasing function on this domain. As such, their ratio is a decreasing function on this domain. Now we consider $0 < \alpha Y < \frac{\pi}{2}$. The derivative of the function may be written as

$$\frac{\mathrm{d}}{\mathrm{d}Y}\frac{\sin(\alpha Y)}{\sinh(Y)} = \frac{\alpha\cos(\alpha Y)\cosh(Y)}{\sinh^2(Y)} \underbrace{\left(\tanh(Y) - \frac{1}{\alpha}\tan(\alpha Y)\right)}_{\textbf{(a)}}, \tag{E.10}$$

where we note the coefficient is positive for $0 < \alpha Y < \frac{\pi}{2}$. However, the function **(a)** is negative,

$$\tanh(Y) - \frac{1}{\alpha}\tan(\alpha Y) \overset{(1)}{<} Y - \frac{1}{\alpha}\tan(\alpha Y) \overset{(2)}{<} 0\,, \tag{E.11}$$

where in inequality (1) we have used that $Y > \tanh(Y)$ for all $Y > 0$ and in inequality (2) we have used $\tan(Y) > Y$ for $0 < Y < \frac{\pi}{2}$. Hence, we have proven Observation 2.

To prove Observation 3, we consider the definition of μ (E.6), expressing this as

$$\rho = \frac{\sin(\alpha\mu)}{\sinh(\mu)}\,. \tag{E.12}$$

By Observation 2, the right-hand side is a decreasing function. As such, any $Y < \mu$ must increase the right-hand side of (E.12). It then follows that $Y < \mu$ is equivalent to

$$\frac{\sin(\alpha Y)}{\sinh(Y)} > \frac{\sin(\alpha\mu)}{\sinh(\mu)} = \rho\,. \tag{E.13}$$

With these observations made, we now address whether there exists a root of $f_+(z)$ of the form $z_0 = x + \mathrm{i}Y$ with $0 < Y < \mu$. In the case $x = 0$, we require Y to satisfy

$$\rho\sinh(Y) = -\sin(\alpha Y)\,. \tag{E.14}$$

As $Y > 0$, the left-hand side of (E.14) is positive, where we have used Observation 1 above. However, the right-hand side is first positive for $Y > \frac{\pi}{\alpha} > \mu$. Therefore, any root of $f_+(z)$ with an imaginary part smaller than μ must have a nonzero real part.

We consider now roots of the form $z = x + \mathrm{i}Y$ with $x \neq 0$ and $0 < Y < \mu$. Such a root is the solution of the system of equations

$$\rho\sin(x)\cosh(Y) + \sinh(\alpha x)\cos(\alpha Y) = 0\,, \tag{E.15a}$$
$$\rho\cos(x)\sinh(Y) + \cosh(\alpha x)\sin(\alpha Y) = 0\,. \tag{E.15b}$$

We note that the system of equations (E.15) is invariant under $x \mapsto -x$. As such, we need only consider $x > 0$.

Equation (E.15b) may be rewritten as

$$\frac{\sin(\alpha Y)}{\sinh(Y)} \;=\; -\rho\frac{\cos(x)}{\cosh(\alpha x)}\,. \tag{E.16}$$

As $\rho > 0$, we have $-\rho\cos(x) < \rho$ and as $x \neq 0$, we have $\cosh(\alpha x) > 1$. As such, we may bound (E.16) by

$$\frac{\sin(\alpha Y)}{\sinh(Y)} \;=\; -\rho\frac{\cos(x)}{\cosh(\alpha x)} \;<\; \rho\,. \tag{E.17}$$

However, by Observation 3, this implies that $Y > \mu$. As such, there exist no pairs (x, Y) with $0 < Y < \mu$ such that $z_0 = x + \mathrm{i}Y$ is a root of of $f(z)$. □

E.3 Proof of Proposition 5.3

Proposition. *Let* $0 < v < 1$ *and* $f_v(z) = \sinh(vz) - z$. *The equation*

$$f_v(z) \;=\; 0\,, \tag{E.18}$$

has three roots $z = \pm z_0$ *and* 0, $z_0 > 0$. *Further,* $z_0 \to \infty$ *as* $v \to 0$.

Proof. By direct substitution, we have $f_v(0) = 0$.

By the parity of $\sinh(vz)$ and z, we have $f_v(-z) = -f_v(z)$. As such, $f_v(z) = 0 \iff f_v(-z) = 0$. Hence, a positive root at $z = z_0$ implies the existence of a second root at $z = -z_0$. Therefore, without loss of generality, we consider only positive values of z.

We note that

$$f_v'(z) \;=\; v\cosh(vz) - 1\,. \tag{E.19}$$

It is clear that $f_v(z)$ has a turning point at $z = v^{-1}\operatorname{arccosh}(v^{-1}) > 0$. As $\cosh$ is an unbounded, strictly increasing function, we see that f_v' is an unbounded, strictly increasing function.

We recall that $f_v(0) = 0$. As $f_v'(0) = -(1 - v) < 0$, where we have used $0 < v < 1$, it follows that $f_v(z) < 0$ for $z \in (0, v^{-1}\operatorname{arccosh}(v^{-1})]$.

For $z > v^{-1}\operatorname{arccosh}(v^{-1})$, $f_v'(z) > 0$ and increases without bound. Therefore, for $z > v^{-1}\operatorname{arccosh}(v^{-1})$, $f_v(z)$ is an unbounded, strictly increasing function. Therefore, as $f_v(v^{-1}\operatorname{arccosh}(v^{-1})) < 0$, it follows that there exists a point $z = z_0 > v^{-1}\operatorname{arccosh}(v^{-1})$ such that $f_v(z_0) = 0$. Because f_v' is a strictly increasing function, there exists only one such point.

We have therefore proven that the only roots to the equation (E.18) are given by $z = \pm z_0$ and 0.

Finally, we note that as $v \to 0$, $v^{-1} \to \infty$ and, for large arguments, we have $\operatorname{arccosh}(z) \sim \ln(2z)$ [111]. Hence, as $v \to 0$, we have

$$v^{-1}\operatorname{arccosh}(v^{-1}) \;\sim\; v^{-1}\ln(2v^{-1}) \to \infty\,. \tag{E.20}$$

Therefore, as $z_0 > v^{-1}\operatorname{arccosh}(v^{-1})$, we have $z_0 \to \infty$ as $v \to 0$. □

E.4 Proof of Proposition 5.4

Proposition. *Let $0 < v < 1$ and $f_v(z) = \sinh(vz) - z$. The leading-order behaviour of the positive root z_0 of the equation*

$$f_v(z) \;=\; 0\,, \tag{E.21}$$

is given by

$$z_0 \;\sim\; -\frac{1}{v}W_{-1}\Big(-\frac{v}{2}\Big)\;, \tag{E.22}$$

as $v \to 0$, where W_{-1} is the lower branch of the Lambert W function.

Proof. By Proposition 5.3, there exists a unique positive root z_0 of the equation $f_v(z) = 0$. Furthermore, z_0 is bounded below by $v^{-1}\operatorname{arccosh}(v^{-1}) \sim v^{-1}\ln(2v^{-1})$ as $v \to 0$, which further implies that $vz_0 \to \infty$ as $v \to 0$. As such, the leading-order behaviour of the positive root z_0 is governed by

$$z_0 \;=\; \frac{1}{2}\mathrm{e}^{vz_0}\,, \tag{E.23}$$

which we may be rewritten as

$$y\mathrm{e}^{y} \;=\; -\frac{v}{2}\,, \tag{E.24}$$

where $y = -vz_0$.

The equation (E.24) may be solved in terms of the Lambert W function for $v/2 < \mathrm{e}^{-1}$ [111], which we may assume without loss of generality as (E.24) holds only as $v \to 0$.

Using $y = -vz$, the leading-order solution to (E.24) is given by

$$vz_0 \;\sim\; -W_k\Big(-\frac{v}{2}\Big)\;, \tag{E.25}$$

where $k = 0,\ -1$ determines the branch of the Lambert W function.

For small arguments, the two branches behave characteristically differently. On the principal branch, we have $-W_0(-v/2) \to 0^+$ as $v \to 0$, whereas on the lower branch, $-W_{-1}(-v/2) \to \infty$ as $v \to 0$. Recalling the observation $vz \to \infty$ as $v \to 0$, we must take the solution on the lower branch W_{-1}. Therefore, the leading-order behaviour of z_0 is given by

$$z_0 \;\sim\; -\frac{1}{v}W_{-1}\Big(-\frac{v}{2}\Big)\;, \tag{E.26}$$

as $v \to 0$.

□

Appendix F

Generalised Frenet-Serret equations

In this Appendix, we simplify the generalised Frenet-Serret equations (6.49). We begin with the equations (6.49d) and the general ordinary differential equation defining V_a^μ in terms of V_0^μ (6.50). We insert (6.50) into (6.49d), resulting in an ordinary differential equation for V_0^μ,

$$0 \;=\; \frac{1}{\prod_{i=0}^{n-1}\chi_i}\left(\sum_{q=0}^{\lfloor\frac{n}{2}\rfloor} b_{2q}^n \frac{\mathrm{d}^{n+1-2q}}{\mathrm{d}\tau^{n+1-2q}}V_0^\mu + \sum_{q=0}^{\lfloor\frac{n-1}{2}\rfloor}\chi_{n-1}^2 b_{2q}^{n-1}\frac{\mathrm{d}^{n-1-2q}}{\mathrm{d}\tau^{n-1-2q}}V_0^\mu\right). \tag{F.1}$$

This can brought into a more familiar form,

$$\begin{aligned}
0 \;&=\; \frac{1}{\prod_{i=0}^{n-1}\chi_i}\left(\sum_{q=0}^{\lfloor\frac{n}{2}\rfloor} b_{2q}^n \frac{\mathrm{d}^{n+1-2q}}{\mathrm{d}\tau^{n+1-2q}}V_0^\mu + \sum_{q=0}^{\lfloor\frac{n-1}{2}\rfloor}\chi_{n-1}^2 b_{2q}^{n-1}\frac{\mathrm{d}^{n-1-2q}}{\mathrm{d}\tau^{n-1-2q}}V_0^\mu\right),\\
&\overset{\text{(a)}}{=}\; \frac{1}{\prod_{i=0}^{n-1}\chi_i}\left(\sum_{q=0}^{\lfloor\frac{n}{2}\rfloor} b_{2q}^n \frac{\mathrm{d}^{n+1-2q}}{\mathrm{d}\tau^{n+1-2q}}V_0^\mu + \sum_{q=1}^{\lfloor\frac{n+1}{2}\rfloor}\chi_{n-1}^2 b_{2(q-1)}^{n-1}\frac{\mathrm{d}^{n+1-2q}}{\mathrm{d}\tau^{n+1-2q}}V_0^\mu\right),\\
&\overset{\text{(b)}}{=}\; \frac{1}{\prod_{i=0}^{n-1}\chi_i}\left(\frac{\mathrm{d}^{n+1}}{\mathrm{d}\tau^{n+1}}V_0^\mu + \sum_{q=1}^{\lfloor\frac{n+1}{2}\rfloor}\left[b_{2q}^n + \chi_{n-1}^2 b_{2(q-1)}^{n-1}\right]\frac{\mathrm{d}^{n+1-2q}}{\mathrm{d}\tau^{n+1-2q}}V_0^\mu\right),\\
&\overset{\text{(c)}}{=}\; \frac{\chi_n}{\prod_{i=0}^{n}\chi_i}\sum_{q=0}^{\lfloor\frac{n+1}{2}\rfloor} b_{2q}^{n+1}\frac{\mathrm{d}^{n+1-2q}}{\mathrm{d}\tau^{n+1-2q}}V_0^\mu,\\
&\overset{\text{(d)}}{=}\; \chi_n V_{n+1}^\mu\,.
\end{aligned} \tag{F.2}$$

In equality **(a)**, we changed summation variable $q \mapsto q+1$ in the second summation. In equality **(b)**, we isolated the $q=0$ term and used that for odd integers $\lfloor\frac{n}{2}\rfloor = \lfloor\frac{n+1}{2}\rfloor$. For odd integers, consider the effect of replacing $\lfloor\frac{n}{2}\rfloor$ by $\lfloor\frac{n+1}{2}\rfloor$. Let $n = 2m-1$, an odd integer. Then $\lfloor\frac{n+1}{2}\rfloor = m$. Hence, the coefficient of this term would be b_{2m}^{2m-1}. Calculating this using (6.51c), one finds that the first summation is over $\sum_{2m-2}^{2m-3}$, which identically vanishes. Hence, one may replace $\lfloor\frac{n}{2}\rfloor$ by $\lfloor\frac{n+1}{2}\rfloor$

in the first sum. In equality **(c)**, we used the relation $b^m_{2q} + \chi^2_{m-1} b^{m-1}_{2(q-1)} = b^{m+1}_{2q}$ and then combined the two terms under one summation and finally multiplied by χ_n/χ_n. In equality **(d)**, we recognised that the resulting summation was (6.50) in the case $a = n + 1$.

Therefore, one may find the ordinary differential equation for V^μ_0 (and hence the four-velocity) by forcing V^μ_{n+1} to vanish. This fully determines the Frenet-Serret equations.

Appendix G

Stationary trajectories in $4+1$ Minkowski spacetime

In this Appendix, we present the stationary trajectories in $4+1$ Minkowski spacetime. One first solves the ordinary differential equation for V_0^μ, then calculates the constants of integration using (6.56) and finally brings the motion into a more familiar form by a suitable Lorentz transformation.

If one sets $\chi_a = 0$, then the Frenet-Serret equations (6.54) are no longer well defined. The geometric effect of setting $\chi_a = 0$ is to confine the motion to $\mathbb{R}^{a+1,1}$. Note, however, that the stationary trajectories of $\mathbb{R}^{m,1}$ are also present in $\mathbb{R}^{n,1}$ for $m \leq n$. Therefore, to calculate the stationary trajectories present in $\mathbb{R}^{n,1}$, one solves the Frenet-Serret equations (6.54) for each $m \leq n$. The trajectories are then written via the inclusion map,

$$\mathbb{R}^{m,1} \hookrightarrow \mathbb{R}^{n,1}\,, \tag{G.1a}$$

$$(\mathsf{x}^0, \ldots, \mathsf{x}^m) \mapsto (\mathsf{x}^0, \ldots, \mathsf{x}^m, 0, \ldots, 0)\,, \tag{G.1b}$$

where $(0, \ldots, 0)$ represents $(n-m)$–many zeros (in the case $m = n$, then there are no zeros present).

We present the stationary trajectory in cases. **Case** m gives the solution(s) to the Frenet-Serret equations (6.54) in $\mathbb{R}^{m,1}$.

Case 0 **—** The class of inertial trajectories,

$$V_0^\mu \;=\; \dot{\mathsf{x}}^\mu = (1,0,0,0,0)\,. \tag{G.2}$$

Case I — $\chi_0 > 0$. Rindler motion,

$$V_0^\mu \;=\; (\cosh(\chi_0\tau), \sinh(\chi_0\tau), 0, 0, 0)\,. \tag{G.3}$$

Case II — The solutions to the Frenet-Serret equations in $2+1$ have two free parameters, the curvature invariants χ_0 and χ_1. The classification of the stationary trajectory depends on their relation.

Case IIa — $\chi_0 > |\chi_1| > 0$. After a suitable Lorentz transformation, this is drifted Rindler motion [72],

$$V_0^\mu = \frac{1}{\sqrt{\chi_0^2-\chi_1^2}}\left(\chi_0\cosh(\sqrt{\chi_0^2-\chi_1^2}\,\tau),\chi_0\sinh(\sqrt{\chi_0^2-\chi_1^2}\,\tau),\chi_1,0,0\right). \quad \text{(G.4)}$$

Case IIb — $|\chi_0| = |\chi_1| \neq 0$,

$$V_0^\mu = \left(1+\tfrac{1}{2}\chi_0^2\tau^2,\chi_0\tau,\tfrac{1}{2}\chi_0^2\tau^2,0,0\right), \quad \text{(G.5)}$$

whose spatial profile is that of the semicubical parabola $y^2 = \frac{2}{9}\chi_0 x^3$.

Case IIc — $\chi_1 > |\chi_0| > 0$. After a suitable Lorentz transformation, this is circular motion in the x^1–x^2 plane.

$$V_0^\mu = \frac{1}{\sqrt{\chi_1^2-\chi_0^2}}\left(\chi_1,-\chi_0\sin(\sqrt{\chi_1^2-\chi_0^2}\,\tau),\chi_0\cos(\sqrt{\chi_1^2-\chi_0^2}\,\tau),0,0\right). \quad \text{(G.6)}$$

In the following cases, we give the Lorentz transformation explicitly owing to their more involved calculations.

Case III — The general solution to (6.54d) is

$$V_0^\mu = B^\mu\cosh(R_+\tau)+C^\mu\sinh(R_+\tau)+D^\mu\cos(R_-\tau)+E^\mu\sin(R_-\tau), \quad \text{(G.7a)}$$

$$B^\mu = \frac{1}{R^2}\left(R_-^2+\chi_0^2,0,\chi_0\chi_1,0,0\right), \quad \text{(G.7b)}$$

$$C^\mu = \frac{1}{R^2}\left(0,\frac{\chi_0}{R_+}(\chi_0^2-\chi_1^2+R_-^2),0,\frac{\chi_0\chi_1\chi_2}{R_+},0\right), \quad \text{(G.7c)}$$

$$D^\mu = \frac{1}{R^2}\left(R_+^2-\chi_0^2,0,-\chi_0\chi_1,0,0\right), \quad \text{(G.7d)}$$

$$E^\mu = \frac{1}{R^2}\left(0,-\frac{\chi_0}{R_-}(\chi_0^2-\chi_1^2-R_+^2),0,-\frac{\chi_0\chi_1\chi_2}{R_-},0\right). \quad \text{(G.7e)}$$

This is loxodromic motion, which may more clearly be seen by the following Lorentz transformation,

$$\Lambda^\mu{}_\nu = \begin{pmatrix}\alpha & 0 & \beta & 0 & 0\\ 0 & \gamma & 0 & \delta & 0\\ 0 & C & 0 & D & 0\\ A & 0 & B & 0 & 0\\ 0 & 0 & 0 & 0 & 1\end{pmatrix}, \quad \text{(G.8a)}$$

$$\alpha = \frac{\Delta}{R},\quad \beta = \frac{\Delta(R_+^2-\chi_0^2)}{\chi_0\chi_1 R},\quad \gamma = \frac{\Delta R_+}{\chi_0 R},\delta = -\frac{\Delta R_+(\chi_0^2-\chi_1^2-R_+^2)}{\chi_0\chi_1\chi_2 R},$$
$$A = \frac{\chi_0\chi_1}{\Delta R},\quad B = -\frac{\Delta}{R},\quad C = -\frac{\chi_1 R_-}{\Delta R},\quad D = \frac{R_-(\chi_0^2-\chi_1^2+R_-^2)}{\chi_2\Delta R},\quad \Delta^2 = R_-^2+\chi_0^2, \quad \text{(G.8b)}$$

$$\Lambda^{\mu}{}_{\nu}V_0^{\nu} \;=\; \frac{1}{R}\left(\Delta\cosh(R_+\tau), \Delta\sinh(R_+\tau), -\frac{\chi_0\chi_1}{\Delta}\sin(R_-\tau), \frac{\chi_0\chi_1}{\Delta}\cos(R_-\tau), 0\right) . \tag{G.9}$$

Case IV — The classification of the solutions to the Frenet-Serret equations in $4+1$ Minkowski spacetime depends on the relationship between the four curvature invariants. In particular, on the sign of b (6.59).

Case IVa — $b = \chi_2^2\chi_0^2 + \chi_3^2(\chi_0^2 - \chi_1^2) > 0$. The four-velocity is given by

$$V_0^{\mu} \;=\; A^{\mu} + B^{\mu}\cosh(R_+\tau) + C^{\mu}\sinh(R_+\tau) + D^{\mu}\cos(R_-\tau) + E^{\mu}\sin(R_-\tau)\,, \tag{G.10}$$

where

$$A^{\mu} \;=\; \left(1 - \frac{\chi_0^2}{b}(\chi_2^3 + \chi_3^2), 0, -\frac{\chi_0\chi_1\chi_3^2}{b}, 0, -\frac{\chi_0\chi_1\chi_2\chi_3}{b}\right) , \tag{G.11a}$$

$$B^{\mu} \;=\; \frac{1}{R^2}\left(\frac{\chi_0^2}{R_+^2}(\chi_0^2 - \chi_1^2 + R_-^2), 0, \frac{\chi_0\chi_1}{R_+^2}(\chi_0^2 - \chi_1^2 - \chi_2^2 + R_-^2), 0, \frac{\chi_0\chi_1\chi_2\chi_3}{R_+^2}\right) , \tag{G.11b}$$

$$C^{\mu} \;=\; \frac{1}{R^2}\left(0, \frac{\chi_0}{R_+}(\chi_0^2 - \chi_1^2 + R_-^2), 0, \frac{\chi_0\chi_1\chi_2}{R_+}, 0\right) , \tag{G.11c}$$

$$D^{\mu} \;=\; \frac{1}{R^2}\left(\frac{\chi_0^2}{R_-^2}(\chi_0^2 - \chi_1^2 - R_+^2), 0, \frac{\chi_0\chi_1}{R_-^2}(\chi_0^2 - \chi_1^2 - \chi_2^2 - R_+^2), 0, \frac{\chi_0\chi_1\chi_2\chi_3}{R_-^2}\right) , \tag{G.11d}$$

$$E^{\mu} \;=\; \frac{1}{R^2}\left(0, -\frac{\chi_0}{R_-}(\chi_0^2 - \chi_1^2 - R_+^2), 0, -\frac{\chi_0\chi_1\chi_2}{R_-}, 0\right) . \tag{G.11e}$$

Given the classifications in Section 6.2.4, one may hope to identify this motion as a boost, combined with a drift and circular motion. We make an ansatz of the desired form of the four-velocity and find the appropriate Lorentz transformation,

$$V_0^{\mu} \;=\; \Lambda^{\mu}{}_{\nu}\widetilde{V}_0^{\nu} \;=\; \begin{pmatrix} \frac{B^0}{\alpha} & 0 & \frac{A^0}{\beta} & 0 & \frac{D^0}{\gamma} \\ 0 & \frac{C^1}{\alpha} & 0 & -\frac{E^1}{\gamma} & 0 \\ \frac{B^2}{\alpha} & 0 & \frac{A^2}{\beta} & 0 & \frac{D^2}{\gamma} \\ 0 & \frac{C^3}{\alpha} & 0 & -\frac{E^3}{\gamma} & 0 \\ \frac{B^4}{\alpha} & 0 & \frac{A^4}{\beta} & 0 & \frac{D^4}{\gamma} \end{pmatrix} \begin{pmatrix} \alpha\cosh(R_+\tau) \\ \alpha\sinh(R_+\tau) \\ \beta \\ -\gamma\sin(R_-\tau) \\ \gamma\cos(R_-\tau) \end{pmatrix} . \tag{G.12}$$

By imposing that Λ is a Lorentz transformation, one may identify the coefficients α, β, and γ as

$$\alpha \;=\; \sqrt{-B^{\mu}B_{\mu}} \;=\; \sqrt{C^{\mu}C_{\mu}}\,, \tag{G.13a}$$

$$\beta \;=\; \sqrt{A^{\mu}A_{\mu}}\,, \tag{G.13b}$$

$$\gamma \;=\; \sqrt{D^{\mu}D_{\mu}} \;=\; \sqrt{E^{\mu}E_{\mu}}\,. \tag{G.13c}$$

Intermediate steps include the verification that $A^{\mu}D_{\mu} = C^{\mu}E_{\mu} = A^{\mu}B_{\mu} = B^{\mu}D_{\mu} = 0$. This brings the four-velocity into the more recognisable form

$$V_0^\mu = \Big(\sqrt{-B^\mu B_\mu}\cosh(R_+\tau), \sqrt{-B^\mu B_\mu}\sinh(R_+\tau), \sqrt{A^\mu A_\mu}, -\sqrt{D^\mu D_\mu}\sin(R_-\tau), \sqrt{D^\mu D_\mu}\cos(R_-\tau)\Big)\,, \quad \text{(G.14)}$$

corresponding to a boost along the x^1–axis, a drift in the x^2–axis and circular motion in the x^3–x^4 plane.

Case IVb — $b = 0 \iff \chi_0^2 = \frac{\chi_1\chi_3}{\chi_2^2+\chi_3^2}$. In this case, one finds $2a = \chi_0^2 - \chi_1^2 - \chi_2^2 - \chi_3^2 = -\frac{(\chi_2^2+\chi_3^2)^2+\chi_1^2\chi_2^2}{\chi_2^2+\chi_3^2} < 0$, leading to $R_+^2 = 0$ and $R_-^2 = -2a > 0$. The four-velocity reads

$$V_0^\mu = \widetilde{A}^\mu + \tfrac{1}{2}\widetilde{B}^\mu\tau^2 + \widetilde{C}^\mu\tau + \widetilde{D}^\mu\cos(R_-\tau) + \widetilde{E}^\mu\sin(R_-\tau)\,, \quad \text{(G.15a)}$$

$$\widetilde{A}^\mu = \left(1 - \frac{\chi_0^2}{R_-^4}(\chi_0^2-\chi_1^2), 0, -\frac{\chi_0\chi_1}{R_-^4}(\chi_0^2-\chi_1^2-\chi_2^2), 0, -\frac{\chi_0\chi_1\chi_2\chi_3}{R_-^4}\right)\,, \quad \text{(G.15b)}$$

$$\widetilde{B}^\mu = \left(\frac{\chi_0^2}{R_-^2}(\chi_0^2-\chi_1^2+R_-^2), 0, \frac{\chi_0\chi_1}{R_-^2}(\chi_0^2-\chi_1^2-\chi_2^2+R_-^2), 0, \frac{\chi_0\chi_1\chi_2\chi_3}{R_-^2}\right)\,, \quad \text{(G.15c)}$$

$$\widetilde{C}^\mu = \left(0, \frac{\chi_0}{R_-^2}(\chi_0^2-\chi_1^2+R_-^2), 0, \frac{\chi_0\chi_1\chi_2}{R_-^2}, 0\right)\,, \quad \text{(G.15d)}$$

$$\widetilde{D}^\mu = \left(\frac{\chi_0^2}{R_-^4}(\chi_0^2-\chi_1^2), 0, \frac{\chi_0\chi_1}{R_-^4}(\chi_0^2-\chi_1^2-\chi_2^2), 0, \frac{\chi_0\chi_1\chi_2\chi_3}{R_-^4}\right)\,, \quad \text{(G.15e)}$$

$$\widetilde{E}^\mu = \left(0, -\frac{\chi_0}{R_-^3}(\chi_0^2-\chi_1^2), 0, -\frac{\chi_0\chi_1\chi_2}{R_-^3}, 0\right)\,. \quad \text{(G.15f)}$$

We proceed as in (G.12) to find

$$V_0^\mu = \left(\sqrt{-\widetilde{A}^\mu\widetilde{A}_\mu} - \frac{1}{2}\frac{\widetilde{A}^\mu\widetilde{B}_\mu}{\sqrt{-\widetilde{A}^\mu\widetilde{A}_\mu}}\tau^2, \sqrt{\widetilde{C}^\mu\widetilde{C}_\mu}\tau, -\frac{1}{2}\frac{\widetilde{A}^\mu\widetilde{B}_\mu}{\sqrt{-\widetilde{A}^\mu\widetilde{A}_\mu}}\tau^2, -\sqrt{\widetilde{D}^\mu\widetilde{D}_\mu}\sin(R_-\tau), \sqrt{\widetilde{D}^\mu\widetilde{D}_\mu}\cos(R_-\tau)\right)\,, \quad \text{(G.16)}$$

whose spatial profile is the semicubical parabola $y^2 = \frac{2}{9}\frac{(\widetilde{A}^\mu\widetilde{B}_\mu)^2}{(-\widetilde{A}^\nu\widetilde{A}_\nu)(\widetilde{C}^\rho\widetilde{C}_\rho)^3}x^3$ in the x–y plane, combined with circular motion in the x^3–x^4 plane. We use (x, y) in place of (x^1, x^2) for clarity.

Case IVc — $b = \chi_2^2\chi_0^2 + \chi_3^2(\chi_0^2 - \chi_1^2) < 0$. In this case, we have both $a < 0$ and $b < 0$. Hence, $R_+^2 = \sqrt{a^2+b} + a < 0$, yet $R_-^2 = \sqrt{a^2+b} - a > 0$. We then write $a = -\alpha$, $b = -\beta$ such that $R_+^2 = -(\alpha - \sqrt{\alpha^2-\beta}) = -\rho_-^2$. The four-velocity reads

$$V_0^\mu = A^\mu + B^\mu\cos(\rho_-\tau) + C^\mu\sin(\rho_-\tau) + D^\mu\cos(R_-\tau) + E^\mu\sin(R_-\tau)\,, \quad \text{(G.17a)}$$

$$A^\mu = \left(1 - \frac{\chi_0^2}{b}(\chi_2^3+\chi_3^2), 0, -\frac{\chi_0\chi_1\chi_3^2}{b}, 0, -\frac{\chi_0\chi_1\chi_2\chi_3}{b}\right)\,, \quad \text{(G.17b)}$$

$$B^\mu = \frac{1}{R^2}\left(-\frac{\chi_0^2}{\rho_-^2}(\chi_0^2-\chi_1^2+R_-^2),0,-\frac{\chi_0\chi_1}{\rho_-^2}(\chi_0^2-\chi_1^2-\chi_2^2+R_-^2),0,-\frac{\chi_0\chi_1\chi_2\chi_3}{\rho_-^2}\right), \tag{G.17c}$$

$$C^\mu = \frac{1}{R^2}\left(0,\frac{\chi_0}{\rho_-}(\chi_0^2-\chi_1^2+R_-^2),0,\frac{\chi_0\chi_1\chi_2}{\rho_-},0\right), \tag{G.17d}$$

$$D^\mu = \frac{1}{R^2}\left(\frac{\chi_0^2}{R_-^2}(\chi_0^2-\chi_1^2+\rho_-^2),0,\frac{\chi_0\chi_1}{R_-^2}(\chi_0^2-\chi_1^2-\chi_2^2+\rho_-^2),0,\frac{\chi_0\chi_1\chi_2\chi_3}{R_-^2}\right), \tag{G.17e}$$

$$E^\mu = \frac{1}{R^2}\left(0,-\frac{\chi_0}{R_-}(\chi_0^2-\chi_1^2+\rho_-^2),0,-\frac{\chi_0\chi_1\chi_2}{R_-},0\right), \tag{G.17f}$$

where $R^2 = R_-^2 - \rho_-^2$. Proceeding once more as in (G.12), one may rewrite this four-velocity as

$$V_0^\mu = \Big(\sqrt{-A^\mu A_\mu},-\sqrt{B^\mu B_\mu}\sin(\rho_-\tau),\sqrt{B^\mu B_\mu}\cos(\rho_-\tau), \\ -\sqrt{D^\mu D_\mu}\sin(R_-\tau),\sqrt{D^\mu D_\mu}\cos(R_-\tau)\Big), \tag{G.18}$$

identifying the trajectory as independent circular motions in the x^1–x^2 and x^3–x^4 planes.

Appendix H

Large-a asymptotics in Minkowski spacetime: Vacuum contribution

In this Appendix, we demonstrate the asymptotic behaviour of the integrated response (7.12) in the large-a regime, leading to the results of Section 7.2.

H.1 Decomposition of integrated response

The integrated response function reads

$$\mathcal{G}(a) \;=\; \frac{1}{a}\sum_{m\in\mathbb{Z}}\sum_{n\in\mathbb{N}}\frac{J^2_{|m|}\left(\frac{R}{a}q_{|m|n}\right)}{q_{|m|n}J^2_{|m|+1}(q_{|m|n})}\sigma(m\Omega-\omega_{mn})\,, \tag{H.1}$$

where $\omega_{mn}=q_{|m|n}/a$.

We recall that $\sigma\in C_0^\infty$. Let $\sigma_I \coloneqq \inf\mathrm{supp}\{\sigma\}$ and $\sigma_S \coloneqq \sup\mathrm{supp}\{\sigma\}$. We assume that the support of σ is chosen such that either $\mathrm{supp}\{\sigma\}\subset\mathbb{R}_{>0}$ with $0<\sigma_I<\Omega<\sigma_S$ or $\mathrm{supp}\{\sigma\}\subset\mathbb{R}_{<0}$ with $\sigma_I<-\Omega<\sigma_S<0$. In particular, $0\notin\mathrm{supp}\{\sigma\}$. This restriction is imposed as the inertial contribution to the response function in unbounded $2+1$ Minkowski spacetime is discontinuous at $\overline{E}=0$ (2.79).

The non-zero contributions to the integrated response function (H.1) satisfy

$$\sigma_I \;<\; m\Omega-\frac{q_{|m|n}}{a} \;<\; \sigma_S\,, \tag{H.2}$$

which may be rewritten as

$$a(m\Omega-\sigma_S) \;<\; q_{|m|n} \;<\; a(m\Omega-\sigma_I)\,. \tag{H.3}$$

Depending on the value of m, the condition (H.3) falls into three different cases. For sufficiently large a, with the other parameters fixed, these cases are as follows.

- For $m\leq\frac{\sigma_I}{\Omega}$, no n satisfy (H.3).
- For $\frac{\sigma_I}{\Omega}<m\leq\frac{\sigma_S}{\Omega}$, n satisfies $1\leq n\leq N_{\text{max}}$. We denote the set of these m by $\mathcal{C}^1$.

- For $\frac{\sigma_S}{\Omega} < m$, n satisfies $N_{\min} \leq n \leq N_{\max}$. We denote the set of these m by $\mathcal{C}^2$.

We note that $N_{\min}$, $N_{\max}$ depend on m and are respectively the least and greatest values of n satisfying (H.3) and we remark that $\mathcal{C}^1$ is a finite set containing ± 1.

With this notation, we may split $\mathcal{G}$ as

$$\mathcal{G}(a) = \mathcal{G}^1(a) + \mathcal{G}^2(a)\,, \tag{H.4a}$$

$$\mathcal{G}^1(a) = \frac{1}{a}\sum_{m\in\mathcal{C}^1}\sum_{n=1}^{N_{\max}} \frac{J_{|m|}^2\left(\frac{R}{a}q_{|m|n}\right)}{q_{|m|n}J_{|m|+1}^2(q_{|m|n})}\sigma(m\Omega-\omega_{mn})\,, \tag{H.4b}$$

$$\mathcal{G}^2(a) = \frac{1}{a}\sum_{m\in\mathcal{C}^2}\sum_{n=N_{\min}}^{N_{\max}} \frac{J_{|m|}^2\left(\frac{R}{a}q_{|m|n}\right)}{q_{|m|n}J_{|m|+1}^2(q_{|m|n})}\sigma(m\Omega-\omega_{mn})\,. \tag{H.4c}$$

H.2 $\mathcal{G}^1(a)$

We consider first $\mathcal{G}^1$ (H.4b). To further decompose the sum over n, we fix a constant $p \in (0, \frac{1}{3})$ and set $N := \lfloor \left(\frac{a}{R}\right)^p \rfloor$, where $\lfloor\cdot\rfloor$ is the floor function. For sufficiently large a, we then have $N < N_{\max}$, and we may write

$$\mathcal{G}^1(a) = \mathcal{G}^1_<(a) + \mathcal{G}^1_>(a) \tag{H.5a}$$

$$\mathcal{G}^1_<(a) = \frac{1}{a}\sum_{m\in\mathcal{C}^1}\sum_{n=1}^{N-1} \frac{J_{|m|}^2\left(\frac{R}{a}q_{|m|n}\right)}{q_{|m|n}J_{|m|+1}^2(q_{|m|n})}\sigma(m\Omega-\omega_{mn})\,, \tag{H.5b}$$

$$\mathcal{G}^1_>(a) = \frac{1}{a}\sum_{m\in\mathcal{C}^1}\sum_{n=N}^{N_{\max}} \frac{J_{|m|}^2\left(\frac{R}{a}q_{|m|n}\right)}{q_{|m|n}J_{|m|+1}^2(q_{|m|n})}\sigma(m\Omega-\omega_{mn})\,. \tag{H.5c}$$

To address $\mathcal{G}^1_<$ (H.5b), we recall that $\mathcal{C}^1$ has finitely many elements. As such, $q_{|m|n}$ may be approximated by the McMahon expansion [111] for fixed m and large n, which we write in two ways

$$q_{|m|n} \sim \pi\alpha_{|m|n} + f_{|m|}(\pi\alpha_{|m|n})\,, \tag{H.6a}$$

$$q_{|m|n} \sim X_{|m|}(\pi\alpha_{|m|n})\,, \tag{H.6b}$$

where

$$\alpha_{|m|n} := n + \frac{1}{2}|m| - \frac{1}{4}\,, \tag{H.7a}$$

$$f_{|m|}(z) := \sum_{k=1}^{\infty}\frac{c_k(|m|)}{z^{2k-1}} = -\frac{4|m|^2-1}{8z} + \dots\,, \tag{H.7b}$$

$$X_{|m|}(z) := z + f_{|m|}(z)\,, \tag{H.7c}$$

where the coefficients $c_k(|m|)$ are polynomials in $|m|^2$ of degree k and a recurrence relation for their calculation is given in [205].

As m is bounded and $n < N$, the McMahon expansion (H.6) informs us that $q_{|m|n} \sim \pi n + \mathcal{O}(1)$, which is at most $q_{|m|N} = \mathcal{O}(a^p)$. As such for $n < N$, we have $\omega_{mn} = q_{|m|n}/a = o(1)$ as $a \to \infty$. Then, elementary estimates, using the

Maclaurin expansion [111]

$$J^2_{|m|}(z) \;\sim\; \frac{1}{4}z^2\delta_{|m|1} + \mathcal{O}(z^4)\,, \tag{H.8}$$

as $z \to 0$ for $m \neq 0$ and $0 < p < \frac{1}{3}$, show

$$\mathcal{G}^1_<(a) \;=\; \frac{R^2}{4a}\sum_{m\in\mathcal{C}^1}\sum_{n=1}^{N-1}\frac{1}{q_{1n}J^2_2(q_{1n})}\delta_{1|m|}\left(\left(\frac{q_{1n}}{a}\right)^2\sigma(m\Omega) - \left(\frac{q_{1n}}{a}\right)^3\sigma'(m\Omega)\right) + o(a^{-3})\,, \tag{H.9}$$

where $\sigma'(m\Omega) = \frac{\mathrm{d}}{\mathrm{d}z}\sigma(z)|_{z=m\Omega}$.

To address $\mathcal{G}^1_>$ (H.5c), we note that n may be considered large throughout the range of summation and m is bounded. We may therefore employ the McMahon expansion (H.6). In addition, we found the following asymptotic behaviour of the denominator in (H.4b), related to the McMahon expansion, which we have not encountered in the existing literature,

$$\frac{1}{q_{|m|n}J^2_{|m|+1}(q_{|m|n})} \;\sim\; \frac{\pi}{2}X'_{|m|}(\pi\alpha_{|m|n})\,. \tag{H.10}$$

$X_{|m|}$ and $\alpha_{|m|n}$ are given in (H.7). The following proof was provided by Gergő Nemes (Tokyo Metropolitan University) [170].

Proof. Let $\rho_{|m|}(t)$ be a zero of the function $C_{|m|}(z) \coloneqq J_{|m|}(z)\cos(\pi t) + Y_{|m|}(z)\sin(\pi t)$, where $Y_{|m|}$ are the Bessel functions of the second kind [111]. Then, $q_{|m|n} = \rho_{|m|}(n)$.

Using the recurrence relation [111, (10.6.2)], we have $J'_{|m|}(q_{|m|n}) = -J_{|m|+1}(q_{|m|n})$. As such, we may write

$$q_{|m|n}J^2_{|m|+1}(q_{|m|n}) \;=\; \left[\rho_{|m|}(t)\big(J'_{|m|}(\rho_{|m|}(t))\big)^2\right]\Big|_{t=n}\,. \tag{H.11}$$

By [111, (10.21.10)], we have

$$J_{|m|}(\rho_{|m|}(t)) \;=\; \left[\frac{1}{2}\rho_{|m|}(t)\frac{\mathrm{d}\rho_{|m|}(t)}{\mathrm{d}t}\right]^{-\frac{1}{2}}\,. \tag{H.12}$$

Combining (H.11) and (H.12), we find

$$\frac{1}{q_{|m|n}J^2_{|m|+1}(q_{|m|n})} \;=\; \frac{1}{\rho_{|m|}(t)\Big(J'_{|m|}\big(\rho_{|m|}(t)\big)\Big)^2}\Bigg|_{t=n} \;=\; \frac{1}{2}\frac{\mathrm{d}\rho_{|m|}(t)}{\mathrm{d}t}\Bigg|_{t=n}\,. \tag{H.13}$$

Recalling the McMahon expansion for large n, we have $\rho_{|m|}(t) \sim X_{|m|}(\pi\alpha_{|m|t})$, where $\alpha_{|m|t} \coloneqq t + \frac{1}{2}|m| - \frac{1}{4}$. Combining this with (H.13), we arrive at the desired result

$$\frac{1}{q_{|m|n}J^2_{|m|+1}(q_{|m|n})} \;\sim\; \frac{\pi}{2}X'_{|m|}(\pi\alpha_{|m|n})\,. \tag{H.14}$$

□

Using the McMahon expansion (H.6) and asymptotic behaviour (H.10), we may write $\mathcal{G}^1_>(a)$ as

$$\mathcal{G}^1_>(a) \;=\; \frac{\pi}{2a}\sum_{m\in\mathcal{C}^1}\sum_{n=N}^{N_{\max}} J^2_{|m|}\big(\tfrac{R}{a}X_{|m|}(\pi\alpha_{|m|n})\big)\,X'_{|m|}(\pi\alpha_{|m|n})\sigma\big(m\Omega-\tfrac{1}{a}X_{|m|}(\pi\alpha_{|m|n})\big)\;. \tag{H.15}$$

The summand in (H.15) vanishes for $n > N_{\max}$ by definition. As such, we may extend the range of summation to infinity and we appeal to the Euler-Maclaurin formula [206],

$$\sum_{n=p}^{q} g(n) \;=\; \int_p^q \mathrm{d}x\, g(x) + \frac{1}{2}(g(p)+g(q)) + \sum_{i=2}^{l}\frac{b_i}{i!}\big(g^{(i-1)}(q)-g^{(i-1)}(p)\big) + \int_p^q \mathrm{d}x\,\frac{\widetilde{B}_l(1-x)}{l!}g^{(l)}x\,, \tag{H.16}$$

where l is any positive integer and $\widetilde{B}_j$ and b_j are the periodic Bernoulli polynomials and Bernoulli numbers respectively [111].

Employing the Euler-Maclaurin formula (H.16) with $l = 3$, we have

$$\mathcal{G}^1_>(a) \;=\; I_1+I_2+I_3+I_4\,, \tag{H.17a}$$

$$I_1 \;=\; \frac{\pi}{2a}\sum_{m\in\mathcal{C}^1}\int_N^\infty \mathrm{d}x\, J^2_{|m|}\big(\tfrac{R}{a}X_{|m|}(\pi\alpha_{|m|x})\big)\,X'_{|m|}(\pi\alpha_{|m|x}) \times\sigma\big(m\Omega-\tfrac{1}{a}X_{|m|}(\pi\alpha_{|m|x})\big)\;, \tag{H.17b}$$

$$I_2 \;=\; \frac{\pi}{2a}\sum_{m\in\mathcal{C}^1} J^2_{|m|}\big(\tfrac{R}{a}X_{|m|}(\pi\alpha_{|m|N})\big)\,X'_{|m|}(\pi\alpha_{|m|N})\sigma\big(m\Omega-\tfrac{1}{a}X_{|m|}(\pi\alpha_{|m|N})\big)\;, \tag{H.17c}$$

$$I_3 \;=\; -\frac{\pi}{24a}\sum_{m\in\mathcal{C}^1}\frac{\mathrm{d}}{\mathrm{d}x}\bigg(J^2_{|m|}\big(\tfrac{R}{a}X_{|m|}(\pi\alpha_{|m|x})\big)\,X'_{|m|}(\pi\alpha_{|m|x}) \times\sigma\big(m\Omega-\tfrac{1}{a}X_{|m|}(\pi\alpha_{|m|x})\big)\bigg)\bigg|_{x=N}\,, \tag{H.17d}$$

$$I_4 \;=\; \frac{\pi}{12a}\int_N^\infty \mathrm{d}x\,\widetilde{B}_3(1-x)\frac{\mathrm{d}^3}{\mathrm{d}x^3}\bigg(J^2_{|m|}\big(\tfrac{R}{a}X_{|m|}(\pi\alpha_{|m|x})\big)\,X'_{|m|}(\pi\alpha_{|m|x}) \times\sigma\big(m\Omega-\tfrac{1}{a}X_{|m|}(\pi\alpha_{|m|x})\big)\bigg)\,. \tag{H.17e}$$

Elementary estimates, using (H.7) and $0 < p < \frac{1}{3}$, give

$$I_1 \;= I_0+\Delta I_1\,, \tag{H.18a}$$

$$I_0 \;=\; \sum_{m\in\mathcal{C}^1}\int_0^\infty \mathrm{d}z\,\frac{1}{2}J^2_{|m|}(Rz)\sigma(m\Omega-z)\,, \tag{H.18b}$$

$$\Delta I_1 \;=\; -\frac{R^2}{24a^3}\sum_{m\in\mathcal{C}^1}\Big(\pi^3\big(N+\tfrac{1}{4}\big)^3-\tfrac{9}{8}\pi\big(N+\tfrac{1}{4}\big)\Big)\,\sigma(m\Omega)\delta_{|m|1}$$

$$+\frac{R^2}{32a^4}\sum_{m\in\mathcal{C}^1}\pi^4N^4\sigma'(m\Omega)\delta_{|m|1}+o(a^{-3})\,, \tag{H.18c}$$

$$I_2 \;=\frac{R^2}{16a^3}\sum_{m\in\mathcal{C}^1}\Big(\pi^3\big(N+\tfrac{1}{4}\big)^2-\tfrac{3}{8}\pi\Big)\,\sigma(m\Omega)\delta_{|m|1}+o(a^{-3})\,, \tag{H.18d}$$

$$I_3 \;=\;-\frac{R^2}{48a^3}\sum_{m\in\mathcal{C}^1}\pi^3\big(N+\tfrac{1}{4}\big)\,\sigma(m\Omega)\delta_{|m|1}+o(a^{-3})\,. \tag{H.18e}$$

We note that in addressing I_1 (H.17b), we used the change of variables $z=\frac{1}{a}X_{|m|}(\pi\alpha_{|m|x})$.

We address next I_4 (H.17e). We recall from (H.7) that $X_{|m|}(\pi\alpha_{|m|x})=\pi\alpha_{|m|n}+f_{|m|}(\pi\alpha_{|m|x})$ and that for $x>N$, $|f_{|m|}(\pi\alpha_{|m|x})|\ll 1$. Then, elementary estimates and the change of variable $s=\pi\alpha_{|m|x}$ give

$$I_4\;\sim\;\frac{1}{12}\Big(\frac{\pi}{a}\Big)^3\sum_{m\in\mathcal{C}^1}\int_0^\infty \mathrm{d}s\,\widetilde{B}_3(\tfrac{a}{\pi}s-\alpha_{|m|0})\frac{\mathrm{d}^3}{\mathrm{d}s^3}\big(J^2_{|m|}(Rs)\sigma(m\Omega-s)\big)\;. \tag{H.19}$$

As $\frac{\mathrm{d}^3}{\mathrm{d}s^3}J^2_{|m|}(Rs)\sigma(m\Omega-s)$ is a bounded function of compact support, a generalisation of the Riemann-Lebesgue lemma [207, (Theorem 4)] gives

$$\int_0^\infty \mathrm{d}s\,\widetilde{B}_3(\tfrac{a}{\pi}s-\alpha_{|m|0})\frac{\mathrm{d}^3}{\mathrm{d}s^3}\big(J^2_{|m|}(Rs)\sigma(m\Omega-s)\big)\;=\;o(1)\;\Longrightarrow\;I_4\;=\;o(a^{-3})\,, \tag{H.20}$$

as $a\to\infty$.

Collecting the results of (H.18) and (H.20), we find

$$\begin{aligned}\mathcal{G}^1_>(a)\;=\;&\sum_{m\in\mathcal{C}^1}\int_0^\infty \mathrm{d}z\,\frac{1}{2}J^2_{|m|}(Rz)\sigma(m\Omega-z)+\frac{R^2}{32a^4}\sum_{m\in\mathcal{C}^1}\pi^4N^4\sigma'(m\Omega)\delta_{|m|1}\\&-\frac{R^2}{4a^3}\sum_{m\in\mathcal{C}^1}\left(\sum_{n=1}^{N-1}\Big[\frac{\pi^3}{2}\big(n+\tfrac{1}{4}\big)^2-\frac{3\pi}{16}\Big]+\frac{\pi(5\pi^2-18)}{128}\right)\sigma(m\Omega)\delta_{|m|1}+o(a^{-3})\,,\end{aligned} \tag{H.21}$$

where we have rewritten terms involving powers of N as a sum over n.

Combining $\mathcal{G}^1_<$ (H.9) and $\mathcal{G}^1_>$ (H.21), we have

$$\begin{aligned}\mathcal{G}^1(a)\;=\;&\sum_{m\in\mathcal{C}^1}\int_0^\infty \mathrm{d}z\,\frac{1}{2}J^2_{|m|}(Rz)\sigma(m\Omega-z)\\&-\frac{R^2}{4a^4}\sum_{m\in\mathcal{C}^1}\left(\sum_{n=1}^{N-1}\frac{q_{1n}^3}{q_{1n}J_2^2(q_{1n})}-\frac{\pi^4}{8}N^4\right)\sigma'(m\Omega)\delta_{|m|1}\\&-\frac{R^2}{4a^3}\sum_{m\in\mathcal{C}^1}\left(\sum_{n=1}^{N-1}\Big[\frac{\pi^3}{2}\big(n+\tfrac{1}{4}\big)^2-\frac{3\pi}{16}-\frac{q_{1n}^2}{q_{1n}J_2^2(q_{1n})}\Big]+\frac{\pi(5\pi^2-18)}{128}\right)\sigma(m\Omega)\delta_{|m|1}\\&+o(a^{-3})\,.\end{aligned} \tag{H.22}$$

The expansion (H.22), however, depends on the auxiliary function N.

To address the N-dependence of (H.22), we first fix a constant $q\in(0,\frac{1}{4})$ and

set $\widetilde{N} \coloneqq \lfloor \left(\frac{a}{R}\right)^q \rfloor$ and we write

$$\frac{1}{a^4}\sum_{n=1}^{N-1}\frac{q_{1n}^3}{q_{1n}J_2^2(q_{1n})} = \frac{1}{a^4}\sum_{n=1}^{\widetilde{N}-1}\frac{q_{1n}^3}{q_{1n}J_2^2(q_{1n})} + \frac{\pi}{2a^4}\sum_{n=\widetilde{N}}^{N-1} X_{|m|}^3(\pi\alpha_{|m|n})X'_{|m|}(\pi\alpha_{|m|n}) \,, \tag{H.23}$$

Then, elementary estimates using (H.6) give

$$\frac{1}{a^4}\sum_{n=1}^{N-1}\frac{q_{1n}^3}{q_{1n}J_2^2(q_{1n})} = \frac{\pi^4}{8a^4}N^4 + o\big(a^{-3}\big) \,. \tag{H.24}$$

Substituting this result into (H.22), the coefficient of $\sigma'(m\Omega)$ vanishes.

We write the coefficient of $\sigma(m\Omega)$ in (H.22) as

$$\begin{aligned}\sum_{n=1}^{N-1}\left[\frac{\pi^3}{2}\big(n+\tfrac{1}{4}\big)^2 - \frac{3\pi}{16} - \frac{q_{1n}^2}{q_{1n}J_2^2(q_{1n})}\right] &= \sum_{n=1}^{\infty}\left[\frac{\pi^3}{2}\big(n+\tfrac{1}{4}\big)^2 - \frac{3\pi}{16} - \frac{q_{1n}^2}{q_{1n}J_2^2(q_{1n})}\right] \\ &\quad - \sum_{n=N}^{\infty}\left[\frac{\pi^3}{2}\big(n+\tfrac{1}{4}\big)^2 - \frac{3\pi}{16} - \frac{q_{1n}^2}{q_{1n}J_2^2(q_{1n})}\right] .\end{aligned} \tag{H.25}$$

The McMahon expansion (H.6) and (H.10) show that

$$\frac{q_{1n}^2}{q_{1n}J_2^2(q_{1n})} = \frac{\pi^3}{2}\big(n+\tfrac{1}{4}\big)^2 - \frac{3\pi}{16} + \mathcal{O}(n^{-2}) \,, \tag{H.26}$$

as $n \to \infty$. As such, we see that the second term in (H.25) is $\mathcal{O}(N^{-1})$.

The leading and subleading contributions to $\mathcal{G}^1$ (H.4b) are given by

$$\begin{aligned}\mathcal{G}^1(a) &= \sum_{m\in\mathcal{C}^1}\int_0^\infty \mathrm{d}z\,\frac{1}{2}J_{|m|}^2(Rz)\sigma(m\Omega - z) \\ &\quad - \frac{R^2}{4a^3}\sum_{m\in\mathcal{C}^1}\left(\sum_{n=1}^{\infty}\left[\frac{\pi^3}{2}\big(n+\tfrac{1}{4}\big)^2 - \frac{3\pi}{16} - \frac{q_{1n}^2}{q_{1n}J_2^2(q_{1n})}\right] + \frac{\pi(5\pi^2-18)}{128}\right)\sigma(m\Omega)\delta_{|m|1} \\ &\quad + o(a^{-3}) \,.\end{aligned} \tag{H.27}$$

Note that whilst $\mathcal{G}^1_<$ (H.9) and $\mathcal{G}^1_>$ (H.21) individually depend on the auxiliary function N, the N-dependence has cancelled out in $\mathcal{G}^1$ (H.27).

H.3 $\mathcal{G}^2(a)$

We consider next $\mathcal{G}^2$ (H.4c). To decompose the sum over m, we fix a constant $q \in (0,1)$ and set $M \coloneqq \lfloor \left(\frac{a}{R}\right)^q \rfloor$. We write

$$\mathcal{G}^2(a) = \mathcal{G}^2_<(a) + \mathcal{G}^2_>(a) \,, \tag{H.28a}$$

$$\mathcal{G}^2_<(a) \;=\; \frac{1}{a}\sum_{\substack{m\in\mathcal{C}^2,\\ m\le M-1}}\sum_{n=N_{\min}}^{N_{\max}} \frac{J^2_{|m|}\left(\frac{R}{a}q_{|m|n}\right)}{q_{|m|n}J^2_{|m|+1}(q_{|m|n})}\sigma(m\Omega-\omega_{mn})\,, \tag{H.28b}$$

$$\mathcal{G}^2_>(a) \;=\; \frac{1}{a}\sum_{m=M}^{\infty}\sum_{n=N_{\min}}^{N_{\max}} \frac{J^2_{|m|}\left(\frac{R}{a}q_{|m|n}\right)}{q_{|m|n}J^2_{|m|+1}(q_{|m|n})}\sigma(m\Omega-\omega_{mn})\,. \tag{H.28c}$$

To address $\mathcal{G}^2_>$ (H.28b), we make four observations.

- First, we employ the uniform asymptotic expansion of $q_{|m|n}$ as $n\to\infty$, $q_{|m|n}\sim mz(\zeta)$ [111, (10.21.41)], where $z(\zeta)$ is the inverse of

$$\frac{2}{3}(-\zeta)^{\frac{3}{2}} \;=\; \sqrt{z^2-1}-\operatorname{arcsec}(z)\,, \tag{H.29}$$

  $\zeta=a_nm^{-2/3}$, and a_n is the n^{th} zero of the Airy function. We note $a_n<0$.

- Second, we recall that $m>M=\mathcal{O}(a^q)$. Observing the inequality (H.3), we see that $mz(\zeta)=\mathcal{O}(am)$. As such, z must be large, for which values the right-hand side of (H.29) reduces to z; hence $z\sim\frac{2}{3}(-\zeta)^{-3/2}$. In turn, this implies $\zeta=a_nm^{-2/3}\to-\infty$.

- Third, for large values of n, we have the asymptotic expansion $(-a_n)^{3/2}\sim\frac{3}{2}\pi n$ and we arrive at $z\sim\pi\frac{n}{m}$ and $q_{|m|n}\sim\pi n$. Combining this with the inequality (H.3), we find $N_{\min}$, $N_{\max}=\mathcal{O}(ma)$.

- Finally, we observe that the inequality (H.3) implies

$$m\Omega R-\sigma_SR \;<\; \frac{R}{a}q_{|m|n} \;<\; m\Omega R-\sigma_IR\,. \tag{H.30}$$

  For large m, we see $\frac{R}{a}q_{|m|n}\sim m\Omega R$.

Having made these observations, we may address $\mathcal{G}^2_>$ (H.28b). We recall from (H.13) that

$$\frac{1}{q_{|m|n}J^2_{|m|+1}(q_{|m|n})} \;=\; \frac{1}{2}\frac{\mathrm{d}\rho_{|m|}(t)}{\mathrm{d}t}\bigg|_{t=n}\,. \tag{H.31}$$

In our third observation, we found $q_{|m|n}\sim\pi n$ and so $\rho_{|m|}(t)\sim\pi t$ and we see that denominator may be approximated by $\frac{\pi}{2}$.

Then, we have

$$\mathcal{G}^2_>(a) \;\sim\; \frac{\pi}{2a}\sum_{m=M}^{\infty}\sum_{n=N_{\min}}^{N_{\max}} J^2_{|m|}\left(\frac{R}{a}q_{|m|n}\right)\sigma(m\Omega-\omega_{mn})\,. \tag{H.32}$$

By our fourth observation, we see that the argument of the Bessel function is asymptotically equal to $m\Omega R$,

$$\mathcal{G}^2_>(a) \;\sim\; \frac{\pi}{2a}\sum_{m=M}^{\infty}\sum_{n=N_{\min}}^{N_{\max}} J^2_{|m|}(mv)\,\sigma(m\Omega-\omega_{mn})\,, \tag{H.33}$$

where $v \coloneqq \Omega R < 1$ is the (fixed) speed of the timelike circular trajectory. As $m > M$ is large, we may employ the uniform asymptotic expansion of the Bessel function [111, (10.20.4)],

$$J^2_{|m|}(mv) \;\sim\; \frac{1}{2\pi\sqrt{1-v^2}}\frac{\mathrm{e}^{-2m\xi(v)}}{m}\,, \tag{H.34}$$

as $m \to \infty$, where $\xi(v) \coloneqq \ln(1+\sqrt{1-v^2}) - \ln(v) - \sqrt{1-v^2} > 0$.

As σ is a smooth function of compact support, it may be bounded above by some constant A. Then, we have

$$\mathcal{G}^2_{>}(a) \;<\; \frac{A}{4a\sqrt{1-v^2}} \sum_{m=M}^{\infty} \sum_{n=N_{\min}}^{N_{\max}} \frac{\mathrm{e}^{-2m\xi(v)}}{m} \tag{H.35}$$

Performing the summation over n yields a factor of $N_{\max} - N_{\min} + 1$. By observation three, this is of the order ma and $(N_{\max} - N_{\min} + 1)/(am)$ may then be bounded above by a constant B,

$$\mathcal{G}^2_{>}(a) \;<\; \frac{AB}{4\sqrt{1-v^2}} \sum_{m=M}^{\infty} \mathrm{e}^{-2m\xi(v)}\,. \tag{H.36}$$

Summing over m, we find

$$\mathcal{G}^2_{>}(a) \;<\; \frac{AB}{4\sqrt{1-v^2}} \sum_{m=M}^{\infty} \mathrm{e}^{-2m\xi(v)} \;=\; \frac{AB}{4\sqrt{1-v^2}} \frac{\mathrm{e}^{-2M\xi(v)}}{1-\mathrm{e}^{-2\xi(v)}} \;=\; \mathcal{O}\big(\mathrm{e}^{-2M\xi(v)}\big)\,. \tag{H.37}$$

In particular, $\mathcal{G}^2_{>}(a) = o(a^3)$ for all $q \in (0,1)$.

To address $\mathcal{G}^2_{<}$ (H.28b), we note that n is large relative to m and we use the McMahon expansion (H.6) and the asymptotic behaviour (H.10). By the support of σ, we may extend the range of summation to $N_{\min} - 1 \leq n \leq N_{\max} + 1$. Then, the Euler-Maclaurin formula (H.16) gives

$$\mathcal{G}^2_{<}(a) \;=\; J_1 + J_2\,, \tag{H.38a}$$

$$J_1 \;=\; \frac{\pi}{a} \sum_{\substack{m\in\mathcal{C}^2_{\mathrm{r}}\\ m\leq M-1}} \int_{N_{\min}-1}^{N_{\max}+1} \mathrm{d}x\, \frac{1}{2} J^2_{|m|}\big(\tfrac{R}{a} X_{|m|}(\pi\alpha_{|m|x})\big)\, X'_{|m|}(\pi\alpha_{|m|x}) \times \sigma\big(m\Omega - \tfrac{1}{a}X_{|m|}(\pi\alpha_{|m|x})\big)\,, \tag{H.38b}$$

$$J_2 \;=\; \frac{\pi}{2a(l!)} \sum_{\substack{m\in\mathcal{C}^2_{\mathrm{r}}\\ m\leq M-1}} \int_{N_{\min}-1}^{N_{\max}+1} \mathrm{d}x\, \widetilde{B}_l(1-x) \frac{\mathrm{d}^l}{\mathrm{d}x^l} \frac{1}{2} J^2_{|m|}\big(\tfrac{R}{a} X_{|m|}(\pi\alpha_{|m|x})\big) \times X'_{|m|}(\pi\alpha_{|m|x}) \sigma\big(m\Omega - \tfrac{1}{a}X_{|m|}(\pi\alpha_{|m|x})\big)\,, \tag{H.38c}$$

where we note that the other terms in (H.16) vanish as they are evaluated outside the support of the summand.

To address J_2 (H.38c), we recall $X_{|m|}(\pi\alpha_{|m|x}) = \pi\alpha_{|m|x} + f_{|m|}(\pi\alpha_{|m|x})$ (H.7). For $x \in (N_{\min} - 1, N_{\max} + 1)$, we have $|f_{|m|}(\pi\alpha_{|m|x})| \ll 1$. To leading order, we

consider $X_{|m|}(\pi\alpha_{|m|x}) \sim \pi\alpha_{|m|x}$. We perform the change of variables $s = \frac{\pi}{a}\alpha_{|m|x}$,

$$J_2 \sim \frac{1}{2(l!)}\Big(\frac{\pi}{a}\Big)^l \sum_{\substack{m\in\mathcal{C}^2,\\ m\le M-1}} \int_{\frac{\pi}{a}\alpha_{mN_{\min}-1}}^{\frac{\pi}{a}\alpha_{mN_{\max}-1}} \mathrm{d}s\, \widetilde{B}_l\big(\tfrac{a}{\pi}s - \alpha_{|m|0}\big)\, \frac{\mathrm{d}^l}{\mathrm{d}s^l}\frac{1}{2}J^2_{|m|}(Rs)\,\sigma(m\Omega - s)\,. \tag{H.39}$$

We recall from earlier observations that $n = \mathcal{O}(ma)$ for large m. As such, the upper and lower limits of integration are order m. Elementary estimates then give $J_2 = \mathcal{O}(a^{2q-l})$. By employing the Euler-Maclaurin formula (H.16) with $l \ge 5$, we find $J_2 = o(a^{-3})$.

To address J_1 (H.38b), we extend the range of integration to the positive real line by the support of σ and perform the change of variables $z = \frac{1}{a}X_{|m|}(\pi\alpha_{|m|x})$. Elementary estimates then give

$$J_1 = \sum_{\substack{m\in\mathcal{C}^2,\\ m\le M-1}} \int_0^\infty \mathrm{d}z\, \frac{1}{2}J^2_{|m|}(Rz)\sigma(m\Omega - z)\,. \tag{H.40}$$

By the estimation of $\mathcal{G}^2_>$, we see that the summation of the integral over $m \ge M$ is exponentially small. We therefore extend the range of summation over m to the full set $\mathcal{C}^2$,

$$J_1 = \sum_{m\in\mathcal{C}^2} \int_0^\infty \mathrm{d}z\, \frac{1}{2}J^2_{|m|}(Rz)\sigma(m\Omega - z) + o(a^{-3}). \tag{H.41}$$

The asymptotic expansion of $\mathcal{G}^2$ (H.4c) is given by

$$\mathcal{G}^2(a) = \sum_{m\in\mathcal{C}^2} \int_0^\infty \mathrm{d}z\, \frac{1}{2}J^2_{|m|}(Rz)\sigma(m\Omega - z) + o(a^{-3}). \tag{H.42}$$

H.4 Combining $\mathcal{G}^1$ and $\mathcal{G}^2$

The full expression for the leading and next-to-leading terms for $\mathcal{G}(a)$ is now obtained by combining $\mathcal{G}^1$ (H.27) and $\mathcal{G}^2$ (H.42), with the result

$$\begin{aligned}\mathcal{G}(a) &= \sum_{m\in\mathbb{Z}} \int_0^\infty \mathrm{d}z\, \frac{1}{2}J^2_{|m|}(Rz)\sigma(m\Omega - z)\\ &- \frac{R^2}{4a^3}\sum_{m\in\mathcal{C}^1}\left(\sum_{n=1}^\infty\left[\frac{\pi^3}{2}\big(n+\tfrac{1}{4}\big)^2 - \frac{3\pi}{16} - \frac{q_{1n}^2}{q_{1n}J_2^2(q_{1n})}\right] + \frac{\pi(5\pi^2-18)}{128}\right)\sigma(m\Omega)\delta_{|m|1}\\ &+ o(a^{-3})\,.\end{aligned} \tag{H.43}$$

To extract the response function from (H.43), rewrite the limits of the integral and the summation, perform a change of variables, and take the subleading term under the integral. This gives

$$\mathcal{G}(a) \;=\; \int_{\mathbb{R}} \mathrm{d}\overline{E}\,\sigma(E)\Bigg(\frac{1}{2}\sum_{m>\overline{E}/\Omega} J^2_{|m|}(mv-\overline{E}R)$$
$$-\frac{R^2}{4a^3}\left(\sum_{n=1}^{\infty}\left[\frac{\pi^3}{2}(n+\tfrac{1}{4})^2-\frac{3\pi}{16}-\frac{q_{1n}^2}{q_{1n}J_2^2(q_{1n})}\right]+\frac{\pi(5\pi^2-18)}{128}\right)\delta(|\overline{E}|-\Omega)+o(a^{-3})\Bigg)\,, \tag{H.44}$$

where $\delta(|\overline{E}|-\Omega)=\delta(\overline{E}-\Omega)+\delta(\overline{E}+\Omega)$.

Appendix I

Large-a asymptotics in Minkowski spacetime: Thermal contribution

In this Appendix, we demonstrate the asymptotic behaviour of the integrated response contribution due to finite temperature $\Delta\mathcal{G}_\beta$ (7.19).

I.1 Decomposition of integrated response due to finite temperature

The integrated response contribution due to finite temperature $\Delta\mathcal{G}_\beta$ (7.20) reads

$$\Delta\mathcal{G}_\beta(a) \;=\; \mathcal{G}^+(a) + \mathcal{G}^-(a)\,, \tag{I.1a}$$

$$\mathcal{G}^+(a) \;=\; \frac{1}{a}\sum_{m\in\mathbb{Z}}\sum_{n\in\mathbb{Z}} n(\beta\omega_{mn})\frac{J^2_{|m|}\big(\frac{R}{a}q_{|m|n}\big)}{q_{|m|n}J^2_{|m|+1}(q_{|m|n})}\sigma(m\Omega-\omega_{mn})\,, \tag{I.1b}$$

$$\mathcal{G}^-(a) \;=\; \frac{1}{a}\sum_{m\in\mathbb{Z}}\sum_{n\in\mathbb{Z}} n(\beta\omega_{mn})\frac{J^2_{|m|}\big(\frac{R}{a}q_{|m|n}\big)}{q_{|m|n}J^2_{|m|+1}(q_{|m|n})}\sigma(-(m\Omega-\omega_{mn}))\,, \tag{I.1c}$$

where $\omega_{mn} = q_{|m|n}/a$.

We recall that $\sigma \in C_0^\infty$. Let $\sigma_I \coloneqq \inf\operatorname{supp}\{\sigma\}$ and $\sigma_S \coloneqq \sup\operatorname{supp}\{\sigma\}$. We assume that the support of σ is chosen such that either $\operatorname{supp}\{\sigma\} \subset \mathbb{R}_{>0}$ with $0 < \sigma_I < \Omega < \sigma_S$ or $\operatorname{supp}\{\sigma\} \subset \mathbb{R}_{<0}$ with $\sigma_I < -\Omega < \sigma_S < 0$. Since $\Delta\mathcal{F}_\beta$ is even in $\overline{E}$, we shall for now assume that $\operatorname{supp}\{\sigma\} \subset \mathbb{R}_{>0}$ and relax this assumption in (I.23).

We recall that $\operatorname{supp}\{\sigma\} \subset [\sigma_I, \sigma_S]$. For fixed m in (I.1b) and (I.1c), the values of n in the sums over n are hence restricted by

$$a(m\Omega-\sigma_S) \;<q_{|m|n}\;<\; a(m\Omega-\sigma_I) \qquad \text{in } \mathcal{G}^+\,, \tag{I.2a}$$

$$a(m\Omega+\sigma_I) \;<q_{|m|n}\;<\; a(m\Omega+\sigma_S) \qquad \text{in } \mathcal{G}^-\,. \tag{I.2b}$$

Depending on the value of m, the conditions (I.2) fall into three different cases. For sufficiently large a, with the other parameters fixed, these cases are as follows.

In $\mathcal{G}^+$:

- For $m \leq \frac{\sigma_I}{\Omega}$, no n satisfy (H.3).

- For $\frac{\sigma_I}{\Omega} < m \leq \frac{\sigma_S}{\Omega}$, n satisfies $1 \leq n \leq N^+_{\text{max}}$. We denote the set of these m by $\mathcal{C}^{1+}$.

- For $\frac{\sigma_S}{\Omega} < m$, n satisfies $N^+_{\text{min}} \leq n \leq N^+_{\text{max}}$. We denote the set of these m by $\mathcal{C}^{2+}$.

In $\mathcal{G}^-$:

- For $m \leq -\frac{\sigma_S}{\Omega}$, no n satisfy (H.3).

- For $-\frac{\sigma_S}{\Omega} < m \leq -\frac{\sigma_I}{\Omega}$, n satisfies $1 \leq n \leq N^-_{\text{max}}$. We denote the set of these m by $\mathcal{C}^{1-}$.

- For $-\frac{\sigma_I}{\Omega} < m$, n satisfies $N^-_{\text{min}} \leq n \leq N^-_{\text{max}}$. We denote the set of these m by $\mathcal{C}^{2-}$.

We note that the sets $\mathcal{C}^{1\pm}$ are finite and $\pm 1 \in \mathcal{C}^{1\pm}$. Note also that the notation suppresses the dependence of $N^\pm_{\text{max}}$ and $N^\pm_{\text{min}}$ on a and m.

With this notation, we may split $\mathcal{G}^\pm$ as

$$\mathcal{G}^\pm(a) \;=\; \mathcal{G}^{1\pm}(a) + \mathcal{G}^{2\pm}(a)\,, \tag{I.3a}$$

$$\mathcal{G}^{1\pm}(a) \;=\; \frac{1}{a}\sum_{m\in\mathcal{C}^{1\pm}}\sum_{n=1}^{N^\pm_{\text{max}}} n(\beta\omega_{mn})\frac{J^2_{|m|}\left(\frac{R}{a}q_{|m|n}\right)}{q_{|m|n}J^2_{|m|+1}(q_{|m|n})}\sigma(\pm(m\Omega-\omega_{mn}))\;, \tag{I.3b}$$

$$\mathcal{G}^{2\pm}(a) \;=\; \frac{1}{a}\sum_{m\in\mathcal{C}^{2\pm}}\sum_{n=N^\pm_{\text{min}}}^{N^\pm_{\text{max}}} n(\beta\omega_{mn})\frac{J^2_{|m|}\left(\frac{R}{a}q_{|m|n}\right)}{q_{|m|n}J^2_{|m|+1}(q_{|m|n})}\sigma(\pm(m\Omega-\omega_{mn}))\;. \tag{I.3c}$$

I.2 $\mathcal{G}^{1\pm}$

We consider first $\mathcal{G}^{1\pm}$ (I.3b). To further decompose the sum over n, we fix a constant $p \in (0, \frac{1}{3})$ and set $N := \lfloor \left(\frac{a}{R}\right)^p \rfloor$, where $\lfloor\cdot\rfloor$ is the floor function. For sufficiently large a, we then have $N < N^\pm_{\text{max}}$, and we may write

$$\mathcal{G}^{1\pm}(a) \;=\; \mathcal{G}^{1\pm}_<(a) + \mathcal{G}^{1\pm}_>(a)\,, \tag{I.4a}$$

$$\mathcal{G}^{1\pm}_<(a) \;=\; \frac{1}{a}\sum_{m\in\mathcal{C}^{1\pm}}\sum_{n=1}^{N-1} n(\beta\omega_{mn})\frac{J^2_{|m|}\left(\frac{R}{a}q_{|m|n}\right)}{q_{|m|n}J^2_{|m|+1}(q_{|m|n})}\sigma(\pm(m\Omega-\omega_{mn}))\;, \tag{I.4b}$$

$$\mathcal{G}^{1\pm}_>(a) \;=\; \frac{1}{a}\sum_{m\in\mathcal{C}^{1\pm}}\sum_{n=N}^{N^\pm_{\text{max}}} n(\beta\omega_{mn})\frac{J^2_{|m|}\left(\frac{R}{a}q_{|m|n}\right)}{q_{|m|n}J^2_{|m|+1}(q_{|m|n})}\sigma(\pm(m\Omega-\omega_{mn}))\;. \tag{I.4c}$$

To address $\mathcal{G}^{1\pm}_<$ (I.4b), we recall that there are only finitely many elements of $\mathcal{C}^{1\pm}$ and for $n < N$, we have $q_{|m|n}/a = o(1)$ as $a \to \infty$. Elementary estimates, using (H.8) and $0 < p < \frac{1}{3}$, give

$$\mathcal{G}^{1\pm}_<(a) \;=\; \frac{R^2}{4\beta a^2}\sigma(\Omega)\sum_{n=1}^{N-1}\frac{q_{1n}}{q_{1n}J^2_2(q_{1n})}\,. \tag{I.5}$$

To address $\mathcal{G}^{1\pm}$ (I.4c), we note that n may be considered large throughout the range of summation and m is bounded. We may therefore employ the McMahon expansion (H.6) and asymptotic behaviour (H.10), leading to

$$\mathcal{G}_{>}^{1\pm}(a) = \frac{\pi}{2a}\sum_{m\in\mathcal{C}^{1\pm}}\sum_{n=N}^{N^{\pm}_{\max}} n\big(\tfrac{\beta}{a}X_{|m|}(\pi\alpha_{|m|n})\big)\, J^2_{|m|}\big(\tfrac{R}{a}X_{|m|}(\pi\alpha_{|m|n})\big) \times X'_{|m|}(\pi\alpha_{|m|x})\sigma\big(\pm\big(m\Omega-\tfrac{1}{a}X_{|m|}(\pi\alpha_{|m|n})\big)\big)\,. \tag{I.6}$$

The summand in (I.6) vanishes for $n > N^{\pm}_{\max}$. As such, we may extend the range of summation to infinity and appeal to the Euler-Maclaurin formula (H.16) with $l = 3$,

$$\mathcal{G}_{>}^{1\pm}(a) = I_1 + I_2 + I_3 + I_4\,, \tag{I.7a}$$

$$I_1 = \frac{\pi}{2a}\sum_{m\in\mathcal{C}^{1\pm}}\int_N^\infty \mathrm{d}x\, n\big(\tfrac{\beta}{a}X_{|m|}(\pi\alpha_{|m|x})\big)\, J^2_{|m|}\big(\tfrac{R}{a}X_{|m|}(\pi\alpha_{|m|x})\big) \times X'_{|m|}(\pi\alpha_{|m|x})\sigma\big(\pm\big(m\Omega-\tfrac{1}{a}X_{|m|}(\pi\alpha_{|m|x})\big)\big)\,, \tag{I.7b}$$

$$I_2 = \frac{\pi}{4a}\sum_{m\in\mathcal{C}^{1\pm}} n\big(\tfrac{\beta}{a}X_{|m|}(\pi\alpha_{|m|N})\big)\, J^2_{|m|}\big(\tfrac{R}{a}X_{|m|}(\pi\alpha_{|m|N})\big) \times X'_{|m|}(\pi\alpha_{|m|N})\sigma\big(\pm\big(m\Omega-\tfrac{1}{a}X_{|m|}(\pi\alpha_{|m|N})\big)\big)\,, \tag{I.7c}$$

$$I_3 = -\frac{\pi}{24a}\sum_{m\in\mathcal{C}^{1\pm}}\frac{\mathrm{d}}{\mathrm{d}x}\Big[n\big(\tfrac{\beta}{a}X_{|m|}(\pi\alpha_{|m|x})\big)\, J^2_{|m|}\big(\tfrac{R}{a}X_{|m|}(\pi\alpha_{|m|x})\big) \times X'_{|m|}(\pi\alpha_{|m|x})\sigma\big(\pm\big(m\Omega-\tfrac{1}{a}X_{|m|}(\pi\alpha_{|m|x})\big)\big)\Big]\Big|_{x=N}\,, \tag{I.7d}$$

$$I_4 = \frac{\pi}{12a}\sum_{m\in\mathcal{C}^{1\pm}}\int_N^\infty \mathrm{d}x\,\widetilde{B}_3(1-x)\frac{\mathrm{d}^3}{\mathrm{d}x^3}\Big[n\big(\tfrac{\beta}{a}X_{|m|}(\pi\alpha_{|m|x})\big) \times J^2_{|m|}\big(\tfrac{R}{a}X_{|m|}(\pi\alpha_{|m|x})\big)\, X'_{|m|}(\pi\alpha_{|m|x})\sigma\big(\pm\big(m\Omega-\tfrac{1}{a}X_{|m|}(\pi\alpha_{|m|x})\big)\big)\Big]\,. \tag{I.7e}$$

Elementary estimates, using (H.7) and $0 < p < \frac{1}{3}$, give

$$I_1 = I_0 + \Delta I_1\,, \tag{I.8a}$$

$$I_0 = \sum_{m\in\mathcal{C}^{1\pm}}\int_0^\infty \mathrm{d}z\,\frac{1}{2}n(\beta z)J^2_{|m|}(Rz)\sigma(\pm(m\Omega-z))\,, \tag{I.8b}$$

$$\Delta I_1 = -\frac{R^2}{16\beta a^2}\sigma(\Omega)\big(\pi^2(N+\tfrac{1}{4})^2-\tfrac{3}{4}\big)+o(a^{-2})\,, \tag{I.8c}$$

$$I_2 = \frac{\pi^2R^2}{16\beta a^2}\sigma(\Omega)(N+\tfrac{1}{4})+o(a^{-2})\,, \tag{I.8d}$$

$$I_3 = -\frac{\pi^2R^2}{96\beta a^2}\sigma(\Omega)+o(a^{-2})\,, \tag{I.8e}$$

$$I_4 = o(a^{-2})\,. \tag{I.8f}$$

Adding $\mathcal{G}^{1\pm}_{<}$ (I.5) and $\mathcal{G}^{1\pm}_{>}$ (I.8), we find

$$\begin{aligned}\mathcal{G}^{1\pm}(a) \;&=\; \sum_{m\in\mathcal{C}^{1\pm}}\int_0^\infty \mathrm{d}z\,\frac{1}{2}n(\beta z)J^2_{|m|}(Rz)\sigma(\pm(m\Omega-z))\\ &-\frac{R^2}{4\beta a^2}\sigma(\Omega)\left[\sum_{n=1}^{N-1}\left(\frac{\pi^2}{2}(n+\tfrac{1}{4})-\frac{q_{1n}}{q_{1n}J_2^2(q_{1n})}\right)+\frac{(23\pi^2-36)}{192}\right]+o(a^{-2})\,. \qquad \text{(I.9)}\end{aligned}$$

We address the N-dependence of (I.9),

$$\begin{aligned}\sum_{n=1}^{N-1}\left(\frac{\pi^2}{2}(n+\tfrac{1}{4})-\frac{q_{1n}}{q_{1n}J_2^2(q_{1n})}\right) \;&=\; \sum_{n=1}^{\infty}\left(\frac{\pi^2}{2}(n+\tfrac{1}{4})-\frac{q_{1n}}{q_{1n}J_2^2(q_{1n})}\right)\\ &-\sum_{n=N}^{\infty}\left(\frac{\pi^2}{2}(n+\tfrac{1}{4})-\frac{q_{1n}}{q_{1n}J_2^2(q_{1n})}\right)\,. \qquad \text{(I.10)}\end{aligned}$$

The McMahon expansion (H.6) and (H.10) show that

$$\frac{q_{1n}}{q_{1n}J_2^2(q_{1n})} \;\sim\; \frac{\pi^2}{2}(n+\tfrac{1}{4})+\mathcal{O}(n^{-2})\,. \qquad \text{(I.11)}$$

As such, we see that the second term in (I.10) is $\mathcal{O}(N^{-1})$.

The leading and subleading terms in $\mathcal{G}^{1\pm}$ (I.3b) are hence given by

$$\begin{aligned}\mathcal{G}^{1\pm}(a) \;&=\; \sum_{m\in\mathcal{C}^{1\pm}}\int_0^\infty \mathrm{d}z\,\frac{1}{2}n(\beta z)J^2_{|m|}(Rz)\sigma(\pm(m\Omega-z))\\ &-\frac{R^2}{4\beta a^2}\sigma(\Omega)\left[\sum_{n=1}^{\infty}\left(\frac{\pi^2}{2}(n+\tfrac{1}{4})-\frac{q_{1n}}{q_{1n}J_2^2(q_{1n})}\right)+\frac{(23\pi^2-36)}{192}\right]+o(a^{-2})\,. \qquad \text{(I.12)}\end{aligned}$$

I.3 $\mathcal{G}^{2\pm}$

We consider next $\mathcal{G}^{2\pm}$ (I.3c). To decompose the sum over m, we fix a constant $q\in(0,1)$ and set $M\coloneqq\lfloor\left(\frac{a}{R}\right)^q\rfloor$. We write

$$\mathcal{G}^{2\pm}(a) \;=\; \mathcal{G}^{2\pm}_{<}(a)+\mathcal{G}^{2\pm}_{>}(a)\,, \qquad \text{(I.13a)}$$

$$\mathcal{G}^{2\pm}_{<}(a) \;=\; \frac{1}{a}\sum_{\substack{m\in\mathcal{C}^{2\pm},\\ m\le M-1}}\sum_{n=N^{\pm}_{\min}}^{N^{\pm}_{\max}}\frac{J^2_{|m|}\left(\frac{R}{a}q_{|m|n}\right)}{q_{|m|n}J^2_{|m|+1}(q_{|m|n})}\sigma(\pm(m\Omega-\omega_{mn}))\,, \qquad \text{(I.13b)}$$

$$\mathcal{G}^{2\pm}_{<}(a) \;=\; \frac{1}{a}\sum_{m=M}^{\infty}\sum_{n=N^{\pm}_{\min}}^{N^{\pm}_{\max}}\frac{J^2_{|m|}\left(\frac{R}{a}q_{|m|n}\right)}{q_{|m|n}J^2_{|m|+1}(q_{|m|n})}\sigma(\pm(m\Omega-\omega_{mn}))\,. \qquad \text{(I.13c)}$$

To address $\mathcal{G}^{2\pm}_{>}$ (I.13c), we appeal again to the observations of Section H.3.

Elementary estimates, using (H.33), show

$$|\mathcal{G}^{2\pm}_{>}(a)| \;<\; \frac{A}{4\sqrt{1-v^2}}\frac{\mathrm{e}^{-(\beta\Omega\pi+2\xi(v))M}}{1-\mathrm{e}^{-(\beta\Omega\pi+2\xi(v))M}} \;=\; \mathcal{O}\big(\mathrm{e}^{-(\beta\Omega\pi+2\xi(v))\lfloor(a/R)^q\rfloor}\big)\;, \tag{I.14}$$

where A is a positive constant and $\xi(v)$ is defined below (H.33). In particular, $\mathcal{G}^{2\pm}_{>}(a) = o(a^{-2})$.

To address $\mathcal{G}^{2\pm}_{<}$ (I.13b), we note that n is large relative to m and use the McMahon expansion (H.6) and the asymptotic expansion (H.10). By the support of σ, we may extend the range of summation to $N^{\pm}_{\mathsf{min}} - 1 \le n \le N^{\pm}_{\mathsf{max}} + 1$. Then, the Euler-Maclaurin formula (H.16) gives

$$\mathcal{G}^{2\pm}_{<}(a) \;=\; J_1 + J_2\,, \tag{I.15a}$$

$$J_1 \;=\; \frac{\pi}{a}\sum_{\substack{m\in\mathcal{C}^{2\pm},\\ m\le M-1}}\int_{N^{\pm}_{\mathsf{min}}-1}^{N^{\pm}_{\mathsf{max}}+1}\mathrm{d}x\,\frac{1}{2}n\big(\tfrac{\beta}{a}X_{|m|}(\pi\alpha_{|m|x})\big)\,J^2_{|m|}\big(\tfrac{R}{a}X_{|m|}(\pi\alpha_{|m|x})\big) \times X'_{|m|}(\pi\alpha_{|m|x})\sigma\big(\pm\big(m\Omega-\tfrac{1}{a}X_{|m|}(\pi\alpha_{|m|x})\big)\big)\;, \tag{I.15b}$$

$$J_2 \;=\; \frac{\pi}{12a}\sum_{\substack{m\in\mathcal{C}^{2\pm},\\ m\le M-1}}\int_{N^{\pm}_{\mathsf{min}}-1}^{N^{\pm}_{\mathsf{max}}+1}\mathrm{d}x\,\widetilde{B}_3(1-x)\frac{\mathrm{d}^3}{\mathrm{d}x^3}\Big[n\big(\tfrac{\beta}{a}X_{|m|}(\pi\alpha_{|m|x})\big) \times J^2_{|m|}\big(\tfrac{R}{a}X_{|m|}(\pi\alpha_{|m|x})\big)\,X'_{|m|}(\pi\alpha_{|m|x})\sigma\big(\pm\big(m\Omega-\tfrac{1}{a}X_{|m|}(\pi\alpha_{|m|x})\big)\big)\Big]\,. \tag{I.15c}$$

To address J_2 (I.15c), we recall $X_{|m|}(\pi\alpha_{|m|x}) = \pi\alpha_{|m|x} + f_{|m|}(\pi\alpha_{|m|x})$. For $x \in (N^{\pm}_{\mathsf{min}} - 1, N^{\pm}_{\mathsf{max}} + 1)$, we have $|f_{|m|}(\pi\alpha_{|m|x})| \ll 1$. To leading order, we have $X_{|m|}(\pi\alpha_{|m|x}) \sim \pi\alpha_{|m|x}$. We perform the change of variables $s = \frac{\pi}{a}\alpha_{|m|x}$,

$$J_2 \;\sim\; \frac{1}{24}\Big(\frac{\pi}{a}\Big)^3\sum_{\substack{m\in\mathcal{C}^{2\pm},\\ m\le M-1}}\int_{\frac{\pi}{a}\alpha_{|m|N^{\pm}_{\mathsf{min}}-1}}^{\frac{\pi}{a}\alpha_{|m|N^{\pm}_{\mathsf{max}}+1}}\mathrm{d}s\,\widetilde{B}_3(\tfrac{a}{\pi}s-\alpha_{|m|0})\frac{\mathrm{d}^3}{\mathrm{d}s^3}\Big[n(\beta s)J^2_{|m|}(Rs) \times\sigma(\pm(m\Omega-s))\Big]\,. \tag{I.16}$$

The observations of Section H.3 inform us that the upper and lower limits of integration are order m. Elementary estimates then give

$$|J_2| \;<\; A\frac{1}{a^3}M \;=\; \mathcal{O}(a^{q-3}) \;=\; o(a^{-2})\,, \tag{I.17}$$

where A is a positive constant and we have used $0 < q < 1$.

To address J_1 (I.15b), we extend the range of integration to the positive real line by the support of σ and perform the change of variables $z = \frac{1}{a}X_{|m|}(\pi\alpha_{|m|x})$. Elementary estimates then give

$$J_1 \;=\; \sum_{\substack{m\in\mathcal{C}^{2\pm},\\ m\le M-1}}\int_0^{\infty}\mathrm{d}z\,\frac{1}{2}n(\beta z)J^2_{|m|}(Rz)\sigma(\pm(m\Omega-z))\;. \tag{I.18}$$

By the estimation of $\mathcal{G}^{2\pm}_{>}$, we see that the summation of the integral over $m \geq M$ is exponentially small. We therefore extend the range of summation over m to the full set $\mathcal{C}^{2\pm}$,

$$J_1 \;=\; \sum_{m\in\mathcal{C}^{2\pm}} \int_0^\infty \mathrm{d}z\, \frac{1}{2} n(\beta z) J^2_{|m|}(Rz)\sigma(\pm(m\Omega - z)) \;. \tag{I.19}$$

The expansion of $\mathcal{G}^{2\pm}$ (I.3c) is given by

$$\mathcal{G}^{2\pm}(a) \;=\; \sum_{m\in\mathcal{C}^{2\pm}} \int_0^\infty \mathrm{d}z\, \frac{1}{2} n(\beta z) J^2_{|m|}(Rz)\sigma(\pm(m\Omega - z)) \;. \tag{I.20}$$

I.4 Combining $\mathcal{G}^{1\pm}$ and $\mathcal{G}^{2\pm}$

The full expression for the leading and next-to-leading terms for $\Delta\mathcal{G}_\beta(a)$ is now obtained by combining $\mathcal{G}^{1\pm}$ (I.12) and $\mathcal{G}^{2\pm}$ (I.20), with the result

$$\begin{aligned}\Delta\mathcal{G}_\beta(a) \;&=\; \sum_{m\in\mathbb{Z}} \frac{1}{2} \int_0^\infty \mathrm{d}z\, n(\beta z) J^2_{|m|}(Rz)[\sigma(m\Omega - z) + \sigma(-(m\Omega - z))] \\ &\quad - \frac{R^2}{2\beta a^2}\sigma(\Omega)\left[\sum_{n=1}^\infty \left(\frac{\pi^2}{2}(n+\tfrac{1}{4}) - \frac{q_{1n}}{q_{1n}J_2^2(q_{1n})}\right) + \frac{(23\pi^2 - 36)}{192}\right] + o(a^{-2})\,.\end{aligned} \tag{I.21}$$

To extract the thermal contribution to the response function from (I.21), we rewrite the limits of the integral and the summation, perform a change of variables, and take the subleading term under the integral. This gives

$$\begin{aligned}&\Delta\mathcal{G}_\beta(a) \;= \\ &\int_{\mathbb{R}} \mathrm{d}\overline{E}\, \overline{E}^{-2}\sigma(\overline{E})\Bigg(\frac{\overline{E}^2}{2} \sum_{m>\overline{E}/\Omega} n(\beta\varpi_+) J^2_{|m|}(\varpi_+ R) + \frac{\overline{E}^2}{2} \sum_{m>-\overline{E}/\Omega} n(\beta\varpi_-) J^2_{|m|}(\varpi_- R) \\ &- \frac{R^2\overline{E}^2}{2\beta a^2}\left[\sum_{n=1}^\infty \left(\frac{\pi^2}{2}(n+\tfrac{1}{4}) - \frac{q_{1n}}{q_{1n}J_2^2(q_{1n})}\right) + \frac{(23\pi^2 - 36)}{192}\right]\delta(\overline{E} - \Omega) + o(a^{-2})\Bigg)\,,\end{aligned} \tag{I.22}$$

where $\varpi_\pm = m\Omega \mp \overline{E}$.

Finally, we recall that the result (I.22) was obtained under the assumption $\mathrm{supp}\{\sigma\} \subset \mathbb{R}_{>0}$. When this assumption is relaxed to allow $\mathrm{supp}\{\sigma\} \subset \mathbb{R} \setminus \{0\}$, (I.22) is replaced by

$$\begin{aligned}&\Delta\mathcal{G}_\beta(a) \;= \\ &\int_{\mathbb{R}} \mathrm{d}\overline{E}\, \overline{E}^{-2}\sigma(\overline{E})\Bigg(\frac{\overline{E}^2}{2} \sum_{m>|\overline{E}|/\Omega} n(\beta\omega_+) J^2_{|m|}(\omega_+ R) + \frac{\overline{E}^2}{2} \sum_{m>-|\overline{E}|/\Omega} n(\beta\omega_-) J^2_{|m|}(\omega_- R)\end{aligned}$$

$$-\frac{R^2\overline{E}^2}{2\beta a^2}\left[\sum_{n=1}^{\infty}\left(\frac{\pi^2}{2}(n+\tfrac{1}{4})-\frac{q_{1n}}{q_{1n}J_2^2(q_{1n})}\right)+\frac{(23\pi^2-36)}{192}\right]\delta(|\overline{E}|-\Omega)+o(a^{-2})\Bigg), \tag{I.23}$$

where $\omega_\pm = m\Omega \mp |\overline{E}|$ and $\delta(|\overline{E}|-\Omega) = \delta(\overline{E}-\Omega) = \delta(\overline{E}+\Omega)$.

Appendix J

Large-α asymptotics in CAdS

In this Appendix, we demonstrate the asymptotic behaviour of the integrated response contribution due to finite temperature $\Delta\mathcal{G}_\beta$ (8.51) in the large-α regime leading to the results of 8.2.3. We note that the calculations in this Appendix parallel those in Appendix H and Appendix I.

J.1 Decomposition of integrated response due to finite temperature

The integrated response contribution due to finite temperature $\mathcal{G}$ (8.51) with $\Delta\mathcal{F}_\beta$ (8.50) reads

$$\begin{aligned}\Delta\mathcal{G}_\beta(\alpha) \;=\; & \frac{1}{\alpha}\frac{1}{\sqrt{1+\frac{R^2}{\alpha^2}}}\sum_{m=-\infty}^{\infty}\sum_{k=0}^{\infty}\Theta(\alpha\omega_k-|m|)n(\beta\omega_k)\frac{(2k+1+|m|)!}{(2k+1-|m|)!}\\ & \times\left[\mathrm{P}^{-|m|}_{2k+1}\left(\frac{1}{\sqrt{1+\frac{R^2}{\alpha^2}}}\right)\right]^2\left[\sigma(\gamma(\omega_k-m\Omega))+\sigma(-\gamma(\omega_k-m\Omega))\right]\,, \qquad \text{(J.1)}\end{aligned}$$

where $\omega_k=(2k+3/2)/\alpha$.

We recall that $\sigma\in C_0^\infty$. Let $\sigma_I=\inf\mathrm{supp}\{\sigma\}$ and $\sigma_S=\sup\mathrm{supp}\{\sigma\}$. We assume that the support of σ is chosen such that either $\mathrm{supp}\{\sigma\}\subset\mathbb{R}_{>0}$ with $0<\sigma_I<\Omega\Gamma<\sigma_S$ or $\mathrm{supp}\{\sigma\}\subset\mathbb{R}_{<0}$ with $\sigma_I<-\Omega\Gamma<\sigma_S<0$. Since $\Delta\mathcal{F}_\beta$ is even in E, we shall for now assume that $\mathrm{supp}\{\sigma\}\subset\mathbb{R}_{>0}$ and relax this assumption in (J.22).

We rewrite the integrated response contribution due to finite temperature to separate the two σ in (J.1),

$$\Delta\mathcal{G}_\beta(\alpha) \;=\; \mathcal{G}^+(\alpha)+\mathcal{G}^-(\alpha)\,, \qquad \text{(J.2a)}$$

$$\mathcal{G}^+(\alpha) \;=\; \frac{1}{\alpha}\frac{1}{\sqrt{1+\frac{R^2}{\alpha^2}}}\sum_{m=-\infty}^{\infty}\sum_{k=0}^{\infty}\Theta(\alpha\omega_k-|m|)n(\beta\omega_k)\frac{(2k+1+|m|)!}{(2k+1-|m|)!}$$

$$\times \left[\mathrm{P}_{2k+1}^{-|m|}\left(\frac{1}{\sqrt{1+\frac{R^2}{\alpha^2}}} \right) \right]^2 \sigma(\gamma(\omega_k - m\Omega))\,, \tag{J.2b}$$

$$\mathcal{G}^{-}(\alpha) \;=\; \frac{1}{\alpha}\frac{1}{\sqrt{1+\frac{R^2}{\alpha^2}}} \sum_{m=-\infty}^{\infty}\sum_{k=0}^{\infty} \Theta(\alpha\omega_k - |m|) n(\beta\omega_k) \frac{(2k+1+|m|)!}{(2k+1-|m|)!}$$
$$\times \left[\mathrm{P}_{2k+1}^{-|m|}\left(\frac{1}{\sqrt{1+\frac{R^2}{\alpha^2}}} \right) \right]^2 \sigma(-\gamma(\omega_k - m\Omega))\,. \tag{J.2c}$$

We recall that $\mathrm{supp}\{\sigma\} \subset [\sigma_I, \sigma_S]$. For fixed m in (J.2b) and (J.2c), the values of k in the sums over k are hence restricted by

$$\frac{\alpha}{2}\left(\frac{\sigma_I}{\gamma} + m\Omega\right) - \frac{3}{4} \;<\; k \;<\; \frac{\alpha}{2}\left(\frac{\sigma_S}{\gamma} + m\Omega\right) - \frac{3}{4}\,, \qquad \text{in } \mathcal{G}^{+}\,, \tag{J.3a}$$

$$\frac{\alpha}{2}\left(-\frac{\sigma_S}{\gamma} + m\Omega\right) - \frac{3}{4} \;<\; k \;<\; \frac{\alpha}{2}\left(-\frac{\sigma_I}{\gamma} + m\Omega\right) - \frac{3}{4}\,, \qquad \text{in } \mathcal{G}^{-}\,. \tag{J.3b}$$

Depending on the value of m, the conditions (J.3) fall into three different cases. For sufficiently large α, with the other parameters fixed, these cases are as follows.

In $\mathcal{G}^{+}$:

- For $m \leq -\frac{\sigma_S}{\gamma\Omega}$, no k satisfy (J.3a).
- For $-\frac{\sigma_S}{\gamma\Omega} < m \leq -\frac{\sigma_I}{\gamma\Omega}$, k satisfies $0 \leq k \leq K^{+}_{\mathrm{max}} := \frac{\alpha}{2}(\frac{\sigma_S}{\gamma} + m\Omega) - \frac{3}{4}$. We denote the set of these m by $\mathcal{C}^{1+}$.
- For $-\frac{\sigma_I}{\gamma\Omega} < m$, k satisfies $K^{+}_{\mathrm{min}} \leq k \leq K^{+}_{\mathrm{max}}$, where $K^{+}_{\mathrm{min}} := \frac{\alpha}{2}(\frac{\sigma_I}{\gamma} + m\Omega) - \frac{3}{4}$. We denote the set of these m by $\mathcal{C}^{2+}$.

In $\mathcal{G}^{-}$:

- For $m \leq \frac{\sigma_I}{\gamma\Omega}$, no k satisfy (J.3b).
- For $\frac{\sigma_I}{\gamma\Omega} < m \leq \frac{\sigma_S}{\gamma\Omega}$, k satisfies $0 \leq k \leq K^{-}_{\mathrm{max}} := \frac{\alpha}{2}(-\frac{\sigma_I}{\gamma} + m\Omega) - \frac{3}{4}$. We denote the set of these m by $\mathcal{C}^{1-}$.
- For $\frac{\sigma_S}{\gamma\Omega} < m$, k satisfies $K^{-}_{\mathrm{min}} \leq k \leq K^{-}_{\mathrm{max}}$, where $K^{-}_{\mathrm{min}} := \frac{\alpha}{2}(-\frac{\sigma_S}{\gamma} + m\Omega) - \frac{3}{4}$. We denote the set of these m by $\mathcal{C}^{2-}$.

We note that the sets $\mathcal{C}^{1\pm}$ are finite and $\pm 1 \in \mathcal{C}^{1\mp}$. Note also that the notation suppresses the dependence of $K^{\pm}_{\mathrm{max}}$ and $K^{\pm}_{\mathrm{min}}$ on α and m.

With this notation, we may split $\mathcal{G}^{\pm}$ as

$$\mathcal{G}^{\pm}(\alpha) \;=\; \mathcal{G}^{1\pm}(\alpha) + \mathcal{G}^{2\pm}(\alpha)\,, \tag{J.4a}$$

$$\mathcal{G}^{1\pm}(\alpha) \;=\; \frac{1}{\alpha}\frac{1}{\sqrt{1+\frac{R^2}{\alpha^2}}} \sum_{m\in\mathcal{C}^{1\pm}}\sum_{k=0}^{K^{\pm}_{\mathrm{max}}} \Theta(\alpha\omega_k - |m|) n(\beta\omega_k) \frac{(2k+1+|m|)!}{(2k+1-|m|)!}$$

$$\times \left[\mathrm{P}_{2k+1}^{-|m|} \left(\frac{1}{\sqrt{1+\frac{R^2}{\alpha^2}}} \right) \right]^2 \sigma(\pm\gamma(\omega_k - m\Omega)) \,, \tag{J.4b}$$

$$\mathcal{G}^{2\pm}(\alpha) = \frac{1}{\alpha} \frac{1}{\sqrt{1+\frac{R^2}{\alpha^2}}} \sum_{m\in\mathcal{C}^{2\pm}} \sum_{k=K_{\min}^{\pm}}^{K_{\max}^{\pm}} \Theta(\alpha\omega_k - |m|) n(\beta\omega_k) \frac{(2k+1+|m|)!}{(2k+1-|m|)!}$$
$$\times \left[\mathrm{P}_{2k+1}^{-|m|} \left(\frac{1}{\sqrt{1+\frac{R^2}{\alpha^2}}} \right) \right]^2 \sigma(\pm\gamma(\omega_k - m\Omega)) \,. \tag{J.4c}$$

J.2 $\mathcal{G}^{1\pm}$

We consider first $\mathcal{G}^{1\pm}$ (J.4b). To further decompose the sum over k, we fix a constant $p \in (0, \frac{1}{3})$ and set $K := \lfloor (\frac{\alpha}{R})^p \rfloor$, where $\lfloor\cdot\rfloor$ is the floor function [111]. For sufficiently large α, we then have $K < K_{\max}^{\pm}$, and we may write

$$\mathcal{G}^{1\pm}(\alpha) = \mathcal{G}_{<}^{1\pm}(\alpha) + \mathcal{G}_{>}^{1\pm}(\alpha) \,, \tag{J.5a}$$

$$\mathcal{G}_{<}^{1\pm}(\alpha) = \frac{1}{\alpha} \frac{1}{\sqrt{1+\frac{R^2}{\alpha^2}}} \sum_{m\in\mathcal{C}^{1\pm}} \sum_{k=0}^{K-1} \Theta(\alpha\omega_k - |m|) n(\beta\omega_k) \frac{(2k+1+|m|)!}{(2k+1-|m|)!}$$
$$\times \left[\mathrm{P}_{2k+1}^{-|m|} \left(\frac{1}{\sqrt{1+\frac{R^2}{\alpha^2}}} \right) \right]^2 \sigma(\pm\gamma(\omega_k - m\Omega)) \,, \tag{J.5b}$$

$$\mathcal{G}_{>}^{1\pm}(\alpha) = \frac{1}{\alpha} \frac{1}{\sqrt{1+\frac{R^2}{\alpha^2}}} \sum_{m\in\mathcal{C}^{1\pm}} \sum_{k=K}^{K_{\max}^{\pm}} \Theta(\alpha\omega_k - |m|) n(\beta\omega_k) \frac{(2k+1+|m|)!}{(2k+1-|m|)!}$$
$$\times \left[\mathrm{P}_{2k+1}^{-|m|} \left(\frac{1}{\sqrt{1+\frac{R^2}{\alpha^2}}} \right) \right]^2 \sigma(\pm\gamma(\omega_k - m\Omega)) \,. \tag{J.5c}$$

To address $\mathcal{G}_{<}^{1\pm}$ (J.5b), we observe that the hypergeometric representation of the associated Legendre function [111, (14.3.1)] gives

$$\mathrm{P}_l^{-|m|}(1-\delta) = \frac{1}{\Gamma(1+|m|)} \left(\frac{\delta}{2}\right)^{|m|/2} \left(1 + \mathcal{O}(\delta l^2)\right) \tag{J.6}$$

as $\delta \to 0^+$, with m fixed and l bounded relative to δ so that $\delta l^2 \to 0$. In (J.5b), $\delta = \frac{1}{2}(R/\alpha)^2 \left(1 + \mathcal{O}(R^2/\alpha^2)\right)$ and $l = 2k+1$, so that $\delta l^2 = \mathcal{O}(k^2/\alpha^2)$, and m takes values in the finite set $\mathcal{C}^{1\pm}$ that is independent of α and contains ∓ 1. Elementary

estimates, using $0 < p < \frac{1}{3}$ and the Laurent expansion

$$n(x) \;=\; \frac{1}{x} - \frac{1}{2} + \mathcal{O}(x)\,, \tag{J.7}$$

show that the contributions from the terms with $|m| > 1$ are $o(\alpha^{-2})$, and combining this with similar estimates for the $m = -1$ term in $\mathcal{G}^{1+}_<$ and the $m = 1$ term in $\mathcal{G}^{1-}_<$ gives

$$\begin{aligned}
\mathcal{G}^{1\pm}_<(\alpha) \;&=\; \frac{R^2}{4\alpha^2\beta}\sum_{k=0}^{K-1}\frac{(2k+1)(2k+2)}{(2k+\frac{3}{2})}\sigma(\Omega\Gamma) + o(\alpha^{-2}) \\
&=\; \frac{R^2}{4\alpha^2\beta}\sigma(\Omega\Gamma)\bigg(K^2 + \frac{1}{2}K - \frac{1}{8}\psi^{(0)}\Big(K+\frac{3}{4}\Big) - \frac{1}{6} + \frac{1}{8}\psi^{(0)}\Big(\frac{7}{4}\Big)\bigg) + o(\alpha^{-2}) \\
&=\; \frac{R^2}{4\alpha^2\beta}\sigma(\Omega\Gamma)\bigg(K^2 + \frac{1}{2}K - \frac{1}{8}\ln\Big(K+\frac{3}{4}\Big) - \frac{1}{6} + \frac{1}{8}\psi^{(0)}\Big(\frac{7}{4}\Big)\bigg) + o(\alpha^{-2})\,,
\end{aligned} \tag{J.8}$$

where in the first equality we have evaluated the sum over k in terms of the digamma function $\psi^{(0)}$ and in the second equality used the asymptotic formula $\psi^{(0)}(z) = \ln(z) + \mathcal{O}(1/z)$ as $z \to \infty$ [111].

To address $\mathcal{G}^{1\pm}_>$ (J.5c), we observe that Stirling's approximation [111] gives

$$\frac{(2k+1+|m|)!}{(2k+1-|m|)!} \;=\; \Big(2k+\frac{3}{2}\Big)^{2|m|}\bigg(1 - \frac{|m|(4|m|^2-1)}{12\big(2k+\frac{3}{2}\big)^2} + \mathcal{O}(k^{-4})\bigg)\,, \tag{J.9}$$

as $k \to \infty$, with m fixed.

The asymptotic behaviour of the associated Legendre function $\mathrm{P}_l^{-|m|}(\cos\varphi)$ uniformly in m in the double limit $l \to \infty$ and $\varphi \to 0$ is given by [208] [117, (8.722)]. Application of this to the associated Legendre function in $\mathcal{G}^{1\pm}_>$ (J.5c) gives

$$\begin{aligned}
\mathrm{P}^{-|m|}_{2k+1}\bigg(\frac{1}{\sqrt{1+\frac{R^2}{\alpha^2}}}\bigg) \;&=\; \Big(2k+\frac{3}{2}\Big)^{-|m|}\Big(1-\frac{R^2}{8\alpha^2}\Big)^{-|m|} \\
&\times\bigg(J_{|m|}(\omega_k R) + \frac{R^2}{4\alpha^2}\bigg(\frac{J_{|m|+1}(\omega_k R)}{2\omega_k R} - J_{|m|+2}(\omega_k R) + \frac{\omega_k R}{6}J_{|m|+3}(\omega_k R)\bigg)\bigg) \\
&+ \mathcal{O}(\alpha^{-4})\,.
\end{aligned} \tag{J.10}$$

Elementary estimates, using $0 < p < \frac{1}{3}$, the expansions (J.9) and (J.10), and the Euler-Maclaurin formula (H.16), give

$$\begin{aligned}
\mathcal{G}^{1\pm}_>(\alpha) \;&=\; \sum_{m\in\mathcal{C}^{1\pm}}\frac{1}{2}\int_0^\infty \mathrm{d}\omega\, n(\beta\omega)J^2_{|m|}(\omega R)\sigma(\pm\Gamma(\omega - m\Omega)) \\
&-\frac{R^2\sigma(\Omega\Gamma)}{4\beta\alpha^2}\bigg(K^2 + \frac{1}{2}K + \frac{103}{12} - \frac{1}{8}\ln(2)\bigg) + \frac{R^2}{32\beta\alpha^2}\ln(K+\tfrac{3}{4})\sigma(\Omega\Gamma) \\
&-\frac{R^2}{32\beta\alpha^2}\ln\Big(\frac{\alpha}{R}\Big)\,\sigma(\Omega\Gamma)
\end{aligned}$$

$$
\begin{aligned}
&\mp\frac{R^2\Gamma^3}{4\alpha^2}\sum_{m\in\mathcal{C}^{1\pm}}\int_0^\infty \mathrm{d}\omega\,\frac{\mathrm{d}}{\mathrm{d}\omega}\big[n(\beta\omega)(\omega-m\Omega)J^2_{|m|}(\omega R)\big]\,\sigma(\pm\Gamma(\omega-m\Omega))\\
&-\frac{1}{24\alpha^2}\sum_{m\in\mathcal{C}^{1\pm}\setminus\{\mp1\}}|m|(4|m|^2-1)\int_0^\infty \mathrm{d}\omega\,\frac{n(\beta\omega)}{\omega^2}J^2_{|m|}(\omega R)\sigma(\pm\Gamma(\omega-m\Omega))\\
&-\frac{1}{8\alpha^2}\int_0^\infty \mathrm{d}\omega\left\{\frac{n(\beta\omega)}{\omega^2}J_1^2(\omega R)\sigma(\pm\Gamma(\omega\pm\Omega))-\frac{R^2}{4\beta}\frac{1}{\omega}\sigma(\Omega\Gamma)\Theta\Big(\frac{1}{R}-\omega\Big)\right\}\\
&+\frac{R^2}{4\alpha^2}\sum_{m\in\mathcal{C}^{1\pm}}\int_0^\infty \mathrm{d}\omega\,n(\beta\omega)J_{|m|}(\omega R)\Big\{\Big(\frac{|m|}{2}-1\Big)J_{|m|}(\omega R)\\
&+\frac{1}{2\omega R}J_{|m|+1}(\omega R)-J_{|m|+2}(\omega R)+\frac{\omega R}{6}J_{|m|+3}(\omega R)\Big\}\sigma(\pm\Gamma(\omega-m\Omega))\\
&+o(\alpha^{-2})\,.
\end{aligned}
\tag{J.11}
$$

Adding $\mathcal{G}^{1\pm}_<$ (J.8) and $\mathcal{G}^{1\pm}_>$ (J.11), we find

$$
\begin{aligned}
\mathcal{G}^{1\pm}(\alpha)\;=\;&\sum_{m\in\mathcal{C}^{1\pm}}\frac{1}{2}\int_0^\infty \mathrm{d}\omega\,n(\beta\omega)J^2_{|m|}(\omega R)\sigma(\pm\Gamma(\omega-m\Omega))\\
&-\frac{R^2}{32\beta\alpha^2}\ln\Big(\frac{\alpha}{R}\Big)\,\sigma(\Omega\Gamma)-\frac{R^2\sigma(\Omega\Gamma)}{4\beta\alpha^2}\left(\frac{35}{4}-\frac{1}{8}\ln(2)-\frac{1}{8}\psi^{(0)}\Big(\frac{7}{4}\Big)\right)\\
&\mp\frac{R^2\Gamma^3}{4\alpha^2}\sum_{m\in\mathcal{C}^{1\pm}}\int_0^\infty \mathrm{d}\omega\,\frac{\mathrm{d}}{\mathrm{d}\omega}\big[n(\beta\omega)(\omega-m\Omega)J^2_{|m|}(\omega R)\big]\,\sigma(\pm\Gamma(\omega-m\Omega))\\
&-\frac{1}{24\alpha^2}\sum_{m\in\mathcal{C}^{1\pm}\setminus\{\mp1\}}|m|(4|m|^2-1)\int_0^\infty \mathrm{d}\omega\,\frac{n(\beta\omega)}{\omega^2}J^2_{|m|}(\omega R)\sigma(\pm\Gamma(\omega-m\Omega))\\
&-\frac{1}{8\alpha^2}\int_0^\infty \mathrm{d}\omega\left\{\frac{n(\beta\omega)}{\omega^2}J_1^2(\omega R)\sigma(\pm\Gamma(\omega\pm\Omega))-\frac{R^2}{4\beta}\frac{1}{\omega}\sigma(\Omega\Gamma)\Theta\Big(\frac{1}{R}-\omega\Big)\right\}\\
&+\frac{R^2}{4\alpha^2}\sum_{m\in\mathcal{C}^{1\pm}}\int_0^\infty \mathrm{d}\omega\,n(\beta\omega)J_{|m|}(\omega R)\Big\{\Big(\frac{|m|}{2}-1\Big)J_{|m|}(\omega R)\\
&+\frac{1}{2\omega R}J_{|m|+1}(\omega R)-J_{|m|+2}(\omega R)+\frac{\omega R}{6}J_{|m|+3}(\omega R)\Big\}\sigma(\pm\Gamma(\omega-m\Omega))\\
&+o(\alpha^{-2})\,.
\end{aligned}
\tag{J.12}
$$

Note that whilst $\mathcal{G}^{1\pm}_<$ (J.8) and $\mathcal{G}^{1\pm}_>$ (J.11) individually depend on the auxiliary function K, the K-dependence has cancelled out in $\mathcal{G}^{1\pm}$ (J.12).

The leading and subleading terms in (J.12) are given by

$$
\begin{aligned}
\mathcal{G}^{1\pm}(\alpha)\;=\;&\sum_{m\in\mathcal{C}^{1\pm}}\frac{1}{2}\int_0^\infty \mathrm{d}\omega\,n(\beta\omega)J^2_{|m|}(\omega R)\sigma(\pm\Gamma(\omega-m\Omega))\\
&-\frac{R^2}{32\beta\alpha^2}\ln\Big(\frac{\alpha}{R}\Big)\,\sigma(\Omega\Gamma)+\mathcal{O}(\alpha^{-2})\,.
\end{aligned}
\tag{J.13}
$$

J.3 $\mathcal{G}^{2\pm}$

We consider next $\mathcal{G}^{2\pm}$ (J.4). To decompose the sum over m, we fix a constant $q \in (0, \frac{1}{2})$ and set $M := \lfloor (\frac{\alpha}{R})^q \rfloor$. For sufficiently large α, the argument of the Heaviside theta is always positive and we may write

$$\mathcal{G}^{2\pm}(\alpha) \;=\; \mathcal{G}^{2\pm}_{<}(\alpha) + \mathcal{G}^{2\pm}_{>}(\alpha)\,, \tag{J.14a}$$

$$\mathcal{G}^{2\pm}_{<}(\alpha) \;=\; \frac{1}{\alpha}\frac{1}{\sqrt{1+\frac{R^2}{\alpha^2}}} \sum_{\substack{m\in\mathcal{C}^{2\pm}_{\mathrm{f}}\\ m\le M-1}} \sum_{k=K^{\pm}_{\min}}^{K^{\pm}_{\max}} n(\beta\omega_k)\frac{(2k+1+|m|)!}{(2k+1-|m|)!} \times \left[\mathrm{P}^{-|m|}_{2k+1}\left(\frac{1}{\sqrt{1+\frac{R^2}{\alpha^2}}}\right)\right]^2 \sigma(\pm\gamma(\omega_k - m\Omega))\,, \tag{J.14b}$$

$$\mathcal{G}^{2\pm}_{>}(\alpha) \;=\; \frac{1}{\alpha}\frac{1}{\sqrt{1+\frac{R^2}{\alpha^2}}} \sum_{m=M}^{\infty} \sum_{k=K^{\pm}_{\min}}^{K^{\pm}_{\max}} n(\beta\omega_k)\frac{(2k+1+|m|)!}{(2k+1-|m|)!} \times \left[\mathrm{P}^{-|m|}_{2k+1}\left(\frac{1}{\sqrt{1+\frac{R^2}{\alpha^2}}}\right)\right]^2 \sigma(\pm\gamma(\omega_k - m\Omega))\,. \tag{J.14c}$$

To address $\mathcal{G}^{2\pm}_{>}$ (J.14c), we observe that the connection formula for the associated Legendre function [111, (14.9.13)] gives

$$\frac{(2k+1+|m|)!}{(2k+1-|m|)!}\left[\mathrm{P}^{-|m|}_{2k+1}\left(\frac{1}{\sqrt{1+\frac{R^2}{\alpha^2}}}\right)\right]^2 \;=\; \frac{(2k+1-|m|)!}{(2k+1+|m|)!}\left[\mathrm{P}^{+|m|}_{2k+1}\left(\frac{1}{\sqrt{1+\frac{R^2}{\alpha^2}}}\right)\right]^2. \tag{J.15}$$

Application of the connection formula (J.15) and upper bound [209, (6)] gives

$$\frac{(2k+1-|m|)!}{(2k+1+|m|)!}\left[\mathrm{P}^{+|m|}_{2k+1}\left(\frac{1}{\sqrt{1+\frac{R^2}{\alpha^2}}}\right)\right]^2 \;<\; \frac{\Gamma^2\left(\frac{1}{4}\right)\mathrm{e}^{1/2}}{\pi^2}\,. \tag{J.16}$$

Elementary estimates, using (J.16), show

$$\left|\mathcal{G}^{2\pm}_{>}(\alpha)\right| \;<\; \frac{A}{2\beta}\frac{\mathrm{e}^{-\beta\Omega M}}{1-\mathrm{e}^{-\beta\Omega}} \;=\; \mathcal{O}(\mathrm{e}^{-\beta\Omega\lfloor(\alpha/R)^q\rfloor})\,, \tag{J.17}$$

where A is a positive constant. In particular, $\mathcal{G}^{2\pm}_{>}(\alpha) = o(\alpha^{-2})$.

To address $\mathcal{G}^{2\pm}_{<}$ (J.14b), we will make use of Stirling's approximation (J.9); however, we are unable to assume m is fixed and must include m in the error

bound,

$$\frac{(2k+1+|m|)!}{(2k+1-|m|)!} = \left(2k+\frac{3}{2}\right)^{2|m|}\left(1-\frac{|m|(4|m|^2-1)}{12\left(2k+\frac{3}{2}\right)^2}+o(k^{-2})\right), \tag{J.18}$$

as $k\to\infty$ with m bounded relative to k such that $m^3k^{-1}\to 0$.

We use the compact support of σ to extend the limits of summation over k in (J.14b) to $0\le k<\infty$. Elementary estimates, using $0<q<\frac{1}{2}$ to guarantee that $m^3k^{-1}\to 0$ as $k\to\infty$, asymptotic formulae (J.18) and (J.10) and the Euler-Maclaurin formula (H.16), give

$$\mathcal{G}^{2\pm}_{<}(\alpha) = \sum_{m\in\mathcal{C}^{2\pm}}\frac{1}{2}\int_0^\infty \mathrm{d}\omega\, n(\beta\omega)J^2_{|m|}(\omega R)\sigma(\pm\Gamma(\omega-m\Omega))+\mathcal{O}(\alpha^{-2}), \tag{J.19}$$

where we have extended the summation over m to $m\in\mathcal{C}^{2\pm}$ by using that in each term the integrand is exponentially suppressed such that the total sum of the added terms is exponentially suppressed for $m>M$.

J.4 Combining $\mathcal{G}^{1\pm}$ and $\mathcal{G}^{2\pm}$

The full expression for the leading and next-to-leading terms for $\mathcal{G}(\alpha)$ is now obtained by combining $\mathcal{G}^{1\pm}$ (J.13) and $\mathcal{G}^{2\pm}$(J.19), with the result

$$\begin{aligned}\Delta\mathcal{G}_\beta(\alpha) = \sum_{m=-\infty}^{\infty}\frac{1}{2}\int_0^\infty \mathrm{d}\omega\, n(\beta\omega)J^2_{|m|}(\omega R)[\sigma(\Gamma(\omega-m\Omega))+\sigma(-\Gamma(\omega-m\Omega))]\\ -\frac{R^2}{16\beta\alpha^2}\ln\left(\frac{\alpha}{R}\right)\sigma(\Omega\Gamma)+\mathcal{O}(\alpha^{-2}).\end{aligned} \tag{J.20}$$

To extract the response function from (J.20), we rewrite the limits of the integral and the summation, perform a change of variables, and take the subleading term under the integral. This gives

$$\begin{aligned}\Delta\mathcal{G}_\beta(\alpha) = \int_{\mathbb{R}}\mathrm{d}E\,E^{-2}\sigma(E)\Bigg(&\frac{E^2}{2\Gamma}\sum_{m>E/(\Gamma\Omega)}n(\beta\varpi_+)J^2_{|m|}(\varpi_+R)\\ &+\frac{E^2}{2\Gamma}\sum_{m>-E/(\Gamma\Omega)}n(\beta\varpi_+)J^2_{|m|}(\varpi_+R)-\frac{R^2E^2}{16\beta\alpha^2}\ln\left(\frac{\alpha}{R}\right)\delta(E-\Omega\Gamma)\Bigg)+\mathcal{O}(\alpha^{-2}),\end{aligned} \tag{J.21}$$

where $\varpi_\pm = m\Omega\mp E/\Gamma$.

We recall that the result (J.21) was obtained under the assumption $\mathrm{supp}\{\sigma\}\subset\mathbb{R}_{>0}$. When this assumption is relaxed to allow $\mathrm{supp}\{\sigma\}\subset\mathbb{R}\setminus\{0\}$, (J.21) is replaced by

$$\Delta\mathcal{G}_\beta(\alpha) = \int_{\mathbb{R}}\mathrm{d}E\,E^{-2}\sigma(E)\Bigg(\frac{E^2}{2\Gamma}\sum_{m>|E|/(\Gamma\Omega)}n(\beta\omega_+)J^2_{|m|}(\omega_+R)$$

$$+\frac{E^2}{2\Gamma}\sum_{m>-|E|/(\Gamma\Omega)} n(\beta\omega_+)J^2_{|m|}(\omega_+R) - \frac{R^2E^2}{16\beta\alpha^2}\ln\Big(\frac{\alpha}{R}\Big)\,\delta(|E|-\Omega\Gamma)\Big) + \mathcal{O}(\alpha^{-2})\,, \tag{J.22}$$

where $\omega_\pm = m\Omega \mp |E|/\Gamma$.

Appendix K

Euclidean vacuum response at small cosmological constant

In this Appendix, we verify the small-cosmological constant asymptotic form (8.73) of the detector response in the Euclidean vacuum in RdS.

Let $a \in \mathbb{R} \setminus \{0\}$, $0 < V < 1$, and $\eta > 0$. We define

$$I(\eta) \coloneqq \int_0^\infty \mathrm{d}z \frac{\sin(az)}{z} \frac{g(\eta z)}{\sqrt{1 - w^2(z) g^2(\eta z)}}, \tag{K.1}$$

where

$$g(z) \coloneqq \frac{z}{\sinh(z)}, \tag{K.2a}$$

$$w(z) \coloneqq V \operatorname{sinc}(z), \tag{K.2b}$$

and the notation suppresses the dependence of $I(\eta)$ on a and V. $I(\eta)$ is the integral that appears in (8.72) with $a = 2ER(\Gamma_V V)^{-1}$. We shall find first two terms in the asymptotic expansion of $I(\eta)$ as $\eta \to 0$ with a and V fixed.

For the rest of this Appendix, we assume $a > 0$. The outcome (K.11) holds also for $a < 0$ by parity.

To find the leading term, we split the integral (K.1) as

$$I(\eta) = \int_0^\infty \mathrm{d}z \, \frac{\sin(az)}{z} g(\eta z) + \int_0^\infty \mathrm{d}z \, \frac{\sin(az)}{z} \left[\frac{1}{\sqrt{1 - w^2(z) g^2(\eta z)}} - 1 \right] g(\eta z) \,. \tag{K.3}$$

Using [117, (3.981.1)], the first integral in (K.3) evaluates to $\frac{\pi}{2} \tanh(\frac{a\pi}{2\eta})$, which tends to $\pi/2$ with corrections of order $\mathcal{O}(\mathrm{e}^{-a\pi/\eta})$ as $\eta \to 0$. In the second integral in (K.3), a dominated convergence argument allows us to take the limit under the integral. Combining, we find

$$\lim_{\eta \to 0} I(\eta) = \int_0^\infty \mathrm{d}z \, \frac{\sin(az)}{z} \frac{1}{\sqrt{1 - w^2(z)}}, \tag{K.4}$$

where we have used the integral $\int_0^\infty \mathrm{d}z \sin(az)/z = \pi/2$.

To find the next-to-leading term, we split the integral (K.1) as

$$I(\eta) \;=\; I_0 + I_1 + I_2 + I_3\,, \tag{K.5a}$$

$$I_0 \;\coloneqq\; \int_0^\infty \mathrm{d}z\, \frac{\sin(az)}{z} g(\eta z) \left[\frac{1}{\sqrt{1-w^2(z)}} - 1 - \frac{1}{2} w^2(z) \right], \tag{K.5b}$$

$$I_1 \;\coloneqq\; \int_0^\infty \mathrm{d}z\, \frac{\sin(az)}{z} g(\eta z) \times \left[\frac{1}{\sqrt{1-w^2(z) g^2(\eta z)}} - \frac{1}{\sqrt{1-w^2(z)}} - \frac{1}{2} w^2\big(g^2(\eta z) - 1\big) \right], \tag{K.5c}$$

$$I_2 \;\coloneqq\; \int_0^\infty \mathrm{d}z \frac{\sin(az)}{z} g(\eta z)\,, \tag{K.5d}$$

$$I_3 \;=\; \frac{1}{2} \int_0^\infty \mathrm{d}z\, \frac{\sin(az)}{z} w^2(z) g^3(\eta z)\,. \tag{K.5e}$$

We consider first the integral I_0 in (K.5). We introduce the function $h(x) = (g(x)-1)/x^2$, which is bounded and tends to $-\frac{1}{6}$ as $x \to 0$. Writing $g(\eta z) = 1 + \eta^2 z^2 h(\eta z)$ and splitting the integral gives

$$\begin{aligned} I_0 \;&=\; \int_0^\infty \mathrm{d}z\, \frac{\sin(az)}{z} \left[\frac{1}{\sqrt{1-w^2(z)}} - 1 - \frac{1}{2} w^2(z) \right] \\ &\quad + \eta^2 \int_0^\infty \mathrm{d}z\, \sin(az) z h(\eta z) \left[\frac{1}{\sqrt{1-w^2(z)}} - 1 - \frac{1}{2} w^2(z) \right] \\ &= \int_0^\infty \mathrm{d}z\, \frac{\sin(az)}{z} \left[\frac{1}{\sqrt{1-w^2(z)}} - 1 - \frac{1}{2} w^2(z) \right] \\ &\quad - \frac{1}{6} \eta^2 \int_0^\infty \mathrm{d}z\, \sin(az) z \left[\frac{1}{\sqrt{1-w^2(z)}} - 1 - \frac{1}{2} w^2(z) \right] + o(\eta^2)\,, \end{aligned} \tag{K.6}$$

where the second equality holds by a dominated convergence argument.

We consider next the integral I_1 in (K.5). I_1 can be rearranged as

$$\begin{aligned} I_1 \;&= \eta^2 \int_0^\infty \mathrm{d}z\, \sin(az) w^2(z) g(\eta z)(g(\eta z)+1)\, h(\eta z) \\ &\quad \times \left[\frac{1}{\sqrt{1-w^2(z)}\sqrt{1-w^2(z)g^2(\eta z)}\Big(\sqrt{1-w^2(z)} + \sqrt{1-w^2(z)g^2(\eta z)}\Big)} - \frac{1}{2} \right] \\ &= -\frac{1}{6} \eta^2 \int_0^\infty \mathrm{d}z \sin(az) z w^2(z) \left[\frac{1}{(1-w^2(z))^{3/2}} - 1 \right] + o(\eta^2)\,, \end{aligned} \tag{K.7}$$

where we again used $g(\eta z) = 1 + \eta^2 z^2 h(\eta z)$, and in the second equality we have taken the limit under the integral by a dominated convergence argument.

We consider next the integral I_2 in (K.5). Using [117, (3.981.1)], the integral I_2 evaluates as

$$I_2 \;=\; \frac{\pi}{2} \tanh\left(\frac{a\pi}{2\eta} \right) \;=\; \frac{\pi}{2} + \mathcal{O}(\mathrm{e}^{-a\pi/\eta})\,. \tag{K.8}$$

We consider next the integral I_3 in (K.5). We extend the integral over the full real line by parity, perform a change of variables $z = u/\eta$, and deform the contour to $u = \mathrm{i}\frac{\pi}{2} + r$ with $r \in \mathbb{R}$, leading to

$$\begin{aligned} I_3 &= \frac{1}{16} V^2 \eta^2 \int_{-\infty}^{\infty} \mathrm{d}r \frac{1}{\cosh^3 r} \Bigg[\sinh\left(\frac{\pi(a+2)}{2\eta}\right) \cos\left(\frac{a+2}{\eta} r\right) \\ &\qquad + \sinh\left(\frac{\pi(a-2)}{2\eta}\right) \cos\left(\frac{a-2}{\eta} r\right) - 2\sinh\left(\frac{a\pi}{2\eta}\right) \cos\left(\frac{a}{\eta} r\right) \Bigg] \\ &= \frac{\pi}{32} V^2 \Bigg[\left((a+2)^2 + \eta^2\right) \tanh\left(\frac{\pi(a+2)}{2\eta}\right) + \left((a-2)^2 + \eta^2\right) \tanh\left(\frac{\pi(a-2)}{2\eta}\right) \\ &\qquad - 2(a^2 + \eta^2) \tanh\left(\frac{a\pi}{2\eta}\right) \Bigg] \\ &= \frac{\pi}{16} V^2 \left[4 - \left((a-2)^2 + \eta^2\right) \Theta(2-a)\right] + o(\eta^2)\,, \end{aligned} \tag{K.9}$$

where Θ is the Heaviside theta function with the convention $\Theta(0) = 1/2$. In the second equality, we have used [117, (3.985.1)] and [111, (5.4.4)] to evaluate the integrals. In the third equality, we have performed the elementary expansion as $\eta \to 0$.

Combining (K.6)-(K.9), we have

$$\begin{aligned} I(\eta) &= \int_0^{\infty} \mathrm{d}z \, \frac{\sin(az)}{z} \frac{1}{\sqrt{1 - w^2(z)}} \\ &\quad + \eta^2 \left(-\frac{1}{6} \int_0^{\infty} \mathrm{d}z \, z \sin(az) \left[\frac{1}{(1 - w^2(z))^{3/2}} - 1 - \frac{3}{2} w^2(z) \right] - \frac{\pi}{16} V^2 \Theta(2-a) \right) \\ &\quad + o(\eta^2)\,. \end{aligned} \tag{K.10}$$

The integral $\frac{1}{4} \int_0^{\infty} \mathrm{d}z \, z \sin(az) w^2(z)$ in the coefficient of η^2 may be evaluated by an elementary contour integral and is found to exactly cancel the term involving $\Theta(2-a)$. Therefore, we have

$$\begin{aligned} I(\eta) &= \int_0^{\infty} \mathrm{d}z \, \frac{\sin(az)}{z} \frac{1}{\sqrt{1 - w^2(z)}} - \frac{1}{6} \eta^2 \int_0^{\infty} \mathrm{d}z \, z \sin(az) \left[\frac{1}{(1 - w^2(z))^{3/2}} - 1 \right] \\ &\quad + o(\eta^2)\,. \end{aligned} \tag{K.11}$$

Bibliography

[1] C. R. D. Bunney and J. Louko, Class. Quant. Grav. **40**, 155001 (2023).

[2] C. R. D. Bunney, V. S. Barroso, S. Biermann, A. Geelmuyden, C. Gooding, G. Ithier, X. Rojas, J. Louko, and S. Weinfurtner, New J. Phys. **26**, 065001 (2024).

[3] C. R. D. Bunney, L. Parry, T. R. Perche, and J. Louko, Phys. Rev. D **109**, 065001 (2024).

[4] C. R. D. Bunney, J. Math. Phys. **65**, 052501 (2024).

[5] C. R. D. Bunney and J. Louko, Circular motion in (anti-)de Sitter spacetime: thermality versus finite size (2024), arXiv:2406.17643 [gr-qc] .

[6] A. Einstein, Sitzungsber. Preuss. Akad. Wiss. (Berlin) **1915**, 831 (1915).

[7] F. W. Dyson, A. S. Eddington, and C. Davidson, Philosophical Transactions of the Royal Society of London Series A **220**, 291 (1920).

[8] P. W. Higgs, Phys. Rev. Lett. **13**, 508 (1964).

[9] F. Englert and R. Brout, Phys. Rev. Lett. **13**, 321 (1964).

[10] G. S. Guralnik, C. R. Hagen, and T. W. B. Kibble, Phys. Rev. Lett. **13**, 585 (1964).

[11] G. Aad *et al.* (ATLAS), Phys. Lett. B **716**, 1 (2012).

[12] N. D. Birrell and P. C. W. Davies, *Quantum Fields in Curved Space*, Cambridge Monographs on Mathematical Physics (Cambridge University Press, 1982).

[13] R. M. Wald, *Quantum Field Theory in Curved Space-Time and Black Hole Thermodynamics*, Chicago Lectures in Physics (University of Chicago Press, Chicago, IL, 1995).

[14] L. E. Parker and D. Toms, *Quantum Field Theory in Curved Spacetime: Quantized Field and Gravity*, Cambridge Monographs on Mathematical Physics (Cambridge University Press, 2009).

[15] L. Parker, Phys. Rev. Lett. **21**, 562 (1968).

[16] L. Parker, Phys. Rev. **183**, 1057 (1969).

[17] L. Parker, Phys. Rev. D **3**, 346 (1971), [Erratum: Phys.Rev.D 3, 2546–2546 (1971)].

[18] L. Parker and J. Navarro-Salas, Fifty years of cosmological particle creation (2017), arXiv:1702.07132 [physics.hist-ph] .

[19] S. W. Hawking, Commun. Math. Phys. **43**, 199 (1975), [Erratum: Commun. Math. Phys. 46, 206 (1976)].

[20] K. Schwarzschild, Sitzungsber. Preuss. Akad. Wiss. (Berlin) **1916**, 189 (1916).

[21] W. G. Unruh, Phys. Rev. D **14**, 870 (1976).

[22] B. S. DeWitt, in *General Relativity: An Einstein Centenary Survey*, edited by S. W. Hawking and W. Israel (Cambridge University Press, Cambridge, 1979) pp. 680–745.

[23] L. Hodgkinson, J. Louko, and A. C. Ottewill, Phys. Rev. D **89**, 104002 (2014).

[24] S. S. Costa and G. E. A. Matsas, Phys. Rev. D **52**, 3466 (1995).

[25] W. G. Unruh and R. M. Wald, Phys. Rev. D **29**, 1047 (1984).

[26] S. Takagi, Prog. Theor. Phys. Supp. **88**, 1 (1986).

[27] L. C. B. Crispino, A. Higuchi, and G. E. A. Matsas, Rev. Mod. Phys. **80**, 787–838 (2008).

[28] W. G. Brenna, R. B. Mann, and E. Martín-Martínez, Phys. Lett. B **757**, 307 (2016).

[29] S. Vriend, D. Grimmer, and E. Martín-Martínez, Symmetry **13**, 1977 (2021).

[30] T. R. Perche, Phys. Rev. D **104**, 065001 (2021).

[31] B. A. Juárez-Aubry and J. Louko, Class. Quant. Grav. **31**, 245007 (2014).

[32] B. A. Juárez-Aubry and J. Louko, JHEP **2018**, 140 (2018).

[33] B. A. Juárez-Aubry and J. Louko, AVS Quantum Sci. **4**, 013201 (2022).

[34] L. Hodgkinson and J. Louko, Phys. Rev. D **86**, 064031 (2012).

[35] K. K. Ng, C. Zhang, J. Louko, and R. B. Mann, New J. Phys. **24**, 103018 (2022).

[36] M. R. Preciado-Rivas, M. Naeem, R. B. Mann, and J. Louko, Phys. Rev. D **110**, 025002 (2024).

[37] A. Valentini, Phys. Lett. A **153**, 321 (1991).

[38] B. Reznik, Found. Phys. **33**, 167 (2003).

[39] A. Pozas-Kerstjens and E. Martin-Martinez, Phys. Rev. D **92**, 064042 (2015).

[40] A. Pozas-Kerstjens and E. Martin-Martinez, Phys. Rev. D **94**, 064074 (2016).

[41] E. Tjoa and E. Martín-Martínez, Phys. Rev. D **104**, 125005 (2021).

[42] H. Maeso-García, T. R. Perche, and E. Martín-Martínez, Phys. Rev. D **106**, 045014 (2022).

[43] J. De Ramón, L. J. Garay, and E. Martín-Martínez, Phys. Rev. D **98**, 105011 (2018).

[44] T. R. Perche and E. Martín-Martínez, Phys. Rev. D **105**, 066011 (2022).

[45] M. Hotta, Phys. Rev. D **78**, 045006 (2008).

[46] R. H. Jonsson, E. Martin-Martinez, and A. Kempf, Phys. Rev. A **89**, 022330 (2014).

[47] R. H. Jonsson, E. Martin-Martinez, and A. Kempf, Phys. Rev. Lett. **114**, 110505 (2015).

[48] R. H. Jonsson, J. Phys. A **49**, 445402 (2016).

[49] R. H. Jonsson, J. Phys. A **50**, 355401 (2017).

[50] G. W. Gibbons and S. W. Hawking, Phys. Rev. D **15**, 2738 (1977).

[51] W. G. Unruh, Phys. Rev. Lett. **46**, 1351 (1981).

[52] G. K. Batchelor, *An Introduction to Fluid Dynamics*, Cambridge Mathematical Library (Cambridge University Press, 2000).

[53] R. P. Feynman, Feynman lectures on physics. Volume 2: Mainly electromagnetism and matter (Addison–Wesley, 1964).

[54] R. Schutzhold and W. G. Unruh, Phys. Rev. D **66**, 044019 (2002).

[55] M. Visser and S. E. C. Weinfurtner, Class. Quant. Grav. **22**, 2493 (2005).

[56] M. Novello, M. Visser, and G. Volovik, eds., *Artificial black holes* (World Scientific, 2002).

[57] G. Volovik, *The Universe in a Helium Droplet*, International Series of Monographs on Physics (Oxford University Press, 2009).

[58] T. G. Philbin, C. Kuklewicz, S. Robertson, S. Hill, F. Konig, and U. Leonhardt, Science **319**, 1367 (2008).

[59] G. Rousseaux, C. Mathis, P. Maissa, T. G. Philbin, and U. Leonhardt, New J. Phys. **10**, 053015 (2008).

[60] S. Weinfurtner, E. W. Tedford, M. C. J. Penrice, W. G. Unruh, and G. A. Lawrence, Phys. Rev. Lett. **106**, 021302 (2011).

[61] T. Torres, S. Patrick, A. Coutant, M. Richartz, E. W. Tedford, and S. Weinfurtner, Nature Phys. **13**, 833 (2017).

[62] T. Torres, S. Patrick, M. Richartz, and S. Weinfurtner, Phys. Rev. Lett. **125**, 011301 (2020).

[63] P. Švančara, P. Smaniotto, L. Solidoro, J. F. MacDonald, S. Patrick, R. Gregory, C. F. Barenghi, and S. Weinfurtner, Nature **628**, 66 (2024).

[64] J. S. Bell and J. M. Leinaas, Nuclear Physics B **212**, 131 (1983).

[65] J. D. Jackson, in *15th Advanced ICFA Beam Dynamics Workshop on Quantum Aspects of Beam Physics* (1998) pp. 622–625.

[66] W. G. Unruh, Phys. Rept. **307**, 163 (1998).

[67] S. A. Fulling and G. E. A. Matsas, Scholarpedia **9**, 31789 (2014).

[68] J. Louko, Class. Quant. Grav. **35**, 205006 (2018).

[69] S. Biermann, S. Erne, C. Gooding, J. Louko, J. Schmiedmayer, W. G. Unruh, and S. Weinfurtner, Phys. Rev. D **102**, 085006 (2020).

[70] C. Gooding, S. Biermann, S. Erne, J. Louko, W. G. Unruh, J. Schmiedmayer, and S. Weinfurtner, Phys. Rev. Lett. **125**, 213603 (2020).

[71] J. R. Letaw, Phys. Rev. D **23**, 1709 (1981).

[72] M. Good, B. A. Juárez-Aubry, D. Moustos, and M. Temirkhan, JHEP **06**, 059 (2020).

[73] C. R. D. Bunney and J. Louko, Circular motion in Minkowski spacetime: thermality versus finite size (2024), (In preparation).

[74] S. A. Fulling, Phys. Rev. D **7**, 2850 (1973).

[75] P. C. W. Davies, J. Phys. A: Math. Gen. **8**, 609 (1975).

[76] E. Poisson, *A Relativist's Toolkit: The Mathematics of Black-Hole Mechanics* (Cambridge University Press, 2009).

[77] J. M. Bardeen, B. Carter, and S. W. Hawking, Commun. Math. Phys. **31**, 161 (1973).

[78] B. S. Kay and R. M. Wald, Phys. Rept. **207**, 49 (1991).

[79] S. A. Fulling and S. N. M. Ruijsenaars, Phys. Rept **152**, 135 (1987).

[80] R. Kubo, J. Phys. Soc. Jap. **12**, 570 (1957).

[81] P. C. Martin and J. S. Schwinger, Phys. Rev. **115**, 1342 (1959).

[82] S. W. Hawking, Phys. Rev. D **13**, 191 (1976).

[83] T. Jacobson, Phys. Rev. Lett. **75**, 1260 (1995).

[84] S. W. Hawking and G. F. R. Ellis, *The Large Scale Structure of Space-Time*, Cambridge Monographs on Mathematical Physics (Cambridge University Press, 2023).

[85] J. J. Bisognano and E. H. Wichmann, J. Math. Phys. **16**, 985 (1975).

[86] J. J. Bisognano and E. H. Wichmann, J. Math. Phys. **17**, 303 (1976).

[87] P. A. Cherenkov, Dokl. Akad. Nauk SSSR **2**, 451 (1934).

[88] J. D. Jackson, *Classical Electrodynamics* (Wiley, 1998).

[89] Y. Décanini and A. Folacci, Phys. Rev. D **78**, 044025 (2008).

[90] C. J. Fewster, B. A. Juárez-Aubry, and J. Louko, Class. Quant. Grav. **33**, 165003 (2016).

[91] J. R. Letaw and J. D. Pfautsch, Phys. Rev. D **22**, 1345 (1980).

[92] A. Einstein, Phys. Z. **18**, 121 (1917).

[93] D. ter Haar, *The Old Quantum Theory* (Elsevier, 1967).

[94] J. I. Korsbakken and J. M. Leinaas, Phys. Rev. D **70**, 084016 (2004).

[95] L. Parry and J. Louko, Circular and drifted Rindler Unruh effects: Two sides of the same coin (2024), arXiv:2409.19799 [gr-qc] .

[96] J. Doukas and B. Carson, Phys. Rev. A **81**, 062320 (2010).

[97] Y. Jin, J. Hu, and H. Yu, Annals of Physics **344**, 97 (2014).

[98] Y. Jin, J. Hu, and H. Yu, Phys. Rev. A **89**, 064101 (2014).

[99] J. S. Bell and J. M. Leinaas, Nucl. Phys. B **284**, 488 (1987).

[100] J. M. Leinaas, in *15th Advanced ICFA Beam Dynamics Workshop on Quantum Aspects of Beam Physics*, edited by P. Chen (World Scientific, 1999) pp. 577–593.

[101] K. Lochan, H. Ulbricht, A. Vinante, and S. K. Goyal, Phys. Rev. Lett. **125**, 241301 (2020).

[102] A. Retzker, J. I. Cirac, M. B. Plenio, and B. Reznik, Phys. Rev. Lett. **101**, 110402 (2008).

[103] J. Marino, G. Menezes, and I. Carusotto, Phys. Rev. Res. **2**, 042009 (2020).

[104] C. Barcelo, S. Liberati, and M. Visser, Living Rev. Rel. **8**, 12 (2005).

[105] V. S. Barroso, C. R. D. Bunney, and S. Weinfurtner, J. Phys. Conf. Ser. **2531**, 012003 (2023).

[106] M. J. Jacquet, S. Weinfurtner, and F. König, Phil. Trans. Roy. Soc. Lond. A **378**, 20190239 (2020).

[107] V. S. Barroso, A. Geelmuyden, Z. Fifer, S. Erne, A. Avgoustidis, R. J. A. Hill, and S. Weinfurtner, Primary thermalisation mechanism of Early Universe observed from Faraday-wave scattering on liquid-liquid interfaces (2022), arXiv:2207.02199 [gr-qc] .

[108] W. G. Unruh, J. Low Temp. Phys. **208**, 196 (2022).

[109] F. Belgiorno, S. L. Cacciatori, M. Clerici, V. Gorini, G. Ortenzi, L. Rizzi, E. Rubino, V. G. Sala, and D. Faccio, Phys. Rev. Lett. **105**, 203901 (2010).

[110] T. G. Philbin, C. Kuklewicz, S. Robertson, S. Hill, F. König, and U. Leonhardt, Science **319**, 1367 (2008).

[111] DLMF, *NIST Digital Library of Mathematical Functions*, https://dlmf.nist.gov/, Release 1.2.0 of 2024-03-15, f. W. J. Olver, A. B. Olde Daalhuis, D. W. Lozier, B. I. Schneider, R. F. Boisvert, C. W. Clark, B. R. Miller, B. V. Saunders, H. S. Cohl, and M. A. McClain, eds.

[112] S. Knight, Robin Hood: A Mythic Biography (Cornell University Press, 2003) p. 43, 1st ed.

[113] D. J. Raine, D. W. Sciama, and P. G. Grove, Proc. R. Soc. Lond. A **435**, 205 (1991).

[114] A. Raval, B. L. Hu, and J. Anglin, Phys. Rev. D **53**, 7003 (1996).

[115] Q. Wang and W. G. Unruh, Phys. Rev. D **89**, 085009 (2014).

[116] N. N. Bogolyubov, J. Phys. (USSR) **11**, 23 (1947).

[117] I. S. Gradshteyn and I. M. Ryzhik, *Table of Integrals, Series, and Products*, seventh ed. (Elsevier/Academic Press, Amsterdam, 2007) pp. xlviii+1171.

[118] G. Amelino-Camelia, Living Rev. Rel. **16**, 5 (2013).

[119] Weinfurtner S, private communication (2022).

[120] P. Kapitza, Nature **141**, 74 (1938).

[121] L. Landau, Phys. Rev. **60**, 356 (1941).

[122] R. J. Donnelly and C. F. Barenghi, JPCRD **27**, 1217 (1998).

[123] E. L. Andronikashvili, Zhur. Ekxp. Theor. Fiz **16**, 780 (1946).

[124] L. D. Landau and E. M. Lifshitz, *Fluid Mechanics* (Pergamon Press, 1959).

[125] K. R. Atkins, Phys. Rev. **113**, 962 (1959).

[126] K. R. Atkins and I. Rudnick, Prog. Low Temp. Phys. **6**, 37 (1970).

[127] C. W. F. Everitt, K. R. Atkins, and A. Denenstein, Phys. Rev. **136**, A1494 (1964).

[128] C. G. Baker, G. I. Harris, D. L. McAuslan, Y. Sachkou, X. He, and W. P. Bowen, New J. Phys. **18**, 123025 (2016).

[129] D. R. Tilley and J. Tilley, *Superfluidity and Superconductivity* (Adam Hilger, Bristol, 1990).

[130] J. E. Rutledge, W. L. McMillan, J. M. Mochel, and T. E. Washburn, Phys. Rev. B **18**, 2155 (1978).

[131] P. V. E. Mc McClintock, D. J. Meredith, and J. K. Wigmore, Liquid helium-4, in *Low-temperature physics: An introduction for scientists and engineers* (Springer Netherlands, Dordrecht, 1992) pp. 151–189.

[132] I. White, *Third sound in thin film superfluid ^3He*, Ph.D. thesis, University of Manchester (2006).

[133] V. S. Barroso, A. Geelmuyden, S. C. Ajithkumar, A. J. Kent, and S. Weinfurtner, Appl. Opt. **62**, 7175 (2023).

[134] D. L. McAuslan, G. I. Harris, C. Baker, Y. Sachkou, X. He, E. Sheridan, and W. P. Bowen, Phys. Rev. X **6**, 021012 (2016).

[135] G. I. Harris, D. L. McAuslan, E. Sheridan, Y. Sachkou, C. Baker, and W. P. Bowen, Nature Phys. **12**, 788 (2016).

[136] Y. P. Sachkou, C. G. Baker, G. I. Harris, O. R. Stockdale, S. Forstner, M. T. Reeves, X. He, D. L. McAuslan, A. S. Bradley, M. J. Davis, *et al.*, Science **366**, 1480 (2019).

[137] V. S. Barroso, *Classical and quantum fluid interfaces as simulators for gravity and the early Universe*, Ph.D. thesis, University of Nottingham (2023).

[138] G. S. Agarwal and S. S. Jha, Phys. Rev. A **90**, 023812 (2014).

[139] E. G. Flekkøy and D. H. Rothman, Phys. Rev. Lett. **75**, 260 (1995).

[140] E. G. Flekkøy and D. H. Rothman, Phys. Rev. E **53**, 1622 (1996).

[141] P. Roche, G. Deville, K. O. Keshishev, N. J. Appleyard, and F. I. B. Williams, Phys. Rev. Lett. **75**, 3316 (1995).

[142] D. F. Walls and G. J. Milburn, *Quantum Optics* (Springer, 2008).

[143] M. S. Ali, S. Bhattacharya, and K. Lochan, JHEP **03**, 220 (2021).

[144] D. Jennings, Class. Quant. Grav. **27**, 205005 (2010).

[145] J. Louko and A. Satz, Class. Quant. Grav. **25**, 055012 (2008).

[146] E. Patterson and R. B. Mann, JHEP **06**, 214 (2023).

[147] F. Frenet, J Math Pures Appl , 437 (1852).

[148] J. A. Serret, J Math Pures Appl , 193 (1851).

[149] C. Jordan, C. R. Acad. Sci., Paris **79**, 795 (1874).

[150] L. H. Ford, Proc. Roy. Soc. Lond. A **364**, 227 (1978).

[151] C. J. Fewster, Class. Quant. Grav. **17**, 1897 (2000).

[152] C. J. Fewster and J. Thompson, Class. Quant. Grav. **40**, 175008 (2023).

[153] M. P. do Carmo, *Differential Geometry of Curves and Surfaces*, 2nd ed. (Dover Publications Inc, 2017).

[154] S. M. Carroll, *Spacetime and Geometry: An Introduction to General Relativity* (Cambridge University Press, 2019).

[155] T. Frankel, *The Geometry of Physics: An Introduction*, 3rd ed. (Cambridge University Press, 2011).

[156] A. F. Beardon, *The Geometry of Discrete Groups*, 1st ed. (Springer New York, 1983).

[157] G. Abraham, Proc. Indian Acad. Sci. (Math. Sci.) **28**, 87 (1948).

[158] J. Cirici, Linear Algebra Appl. **450**, 250 (2014).

[159] M. Mars and C. Peón-Nieto, Class. Quant. Grav. **38**, 035005 (2021).

[160] M. Mars and C. Peón-Nieto, Class. Quant. Grav. **38**, 125009 (2021).

[161] P. M. Neumann, The mathematical writings of Évariste Galois (European Mathematical Society, 2011) 1st ed.

[162] R. C. Myers and M. J. Perry, Annals Phys. **172**, 304 (1986).

[163] R. C. Myers, Myers–Perry black holes, in *Black holes in higher dimensions*, edited by G. T. Horowitz (Cambridge University Press, 2012).

[164] R. Emparan and H. S. Reall, Living Rev. Rel. **11**, 6 (2008).

[165] M. Banados, M. Henneaux, C. Teitelboim, and J. Zanelli, Phys. Rev. D **48**, 1506 (1993), [Erratum: Phys.Rev.D 88, 069902 (2013)].

[166] I. Lovrekovic, Holography of new conformal higher spin gravities in 3d (2023), arXiv:2312.12301 [hep-th] .

[167] P. C. W. Davies, T. Dray, and C. A. Manogue, Phys. Rev. D **53**, 4382 (1996).

[168] T. R. Perche and M. H. Zambianco, Phys. Rev. D **108**, 045017 (2023).

[169] J. Louko and S. D. Upton, Phys. Rev. D **97**, 025008 (2018).

[170] Nemes G, private communication (2024).

[171] W. de Sitter, Mon. Not. Roy. Astron. Soc. **76**, 699 (1916).

[172] W. de Sitter, Mon. Not. Roy. Astron. Soc. **77**, 155 (1916).

[173] W. de Sitter, Mon. Not. Roy. Astron. Soc. **78**, 3 (1917).

[174] S. Deser and O. Levin, Class. Quant. Grav. **14**, L163 (1997).

[175] T. Jacobson, Class. Quant. Grav. **15**, 251 (1998).

[176] B.-W. Xiao, Phys. Lett. B **665**, 173 (2008).

[177] S. J. Avis, C. J. Isham, and D. Storey, Phys. Rev. D **18**, 3565 (1978).

[178] N. A. Chernikov and E. A. Tagirov, Ann. Inst. H. Poincare A Phys. Theor. **9**, 109 (1968).

[179] T. S. Bunch and P. C. W. Davies, Proc. Roy. Soc. Lond. A **360**, 117 (1978).

[180] A. S. Lapedes, J. Math. Phys. **19**, 2289 (1978).

[181] A. Ishibashi and R. M. Wald, Class. Quant. Grav. **21**, 2981 (2004).

[182] V. E. Ambrus, C. Kent, and E. Winstanley, Int. J. Mod. Phys. D **27**, 1843014 (2018).

[183] C. Dappiaggi, H. R. C. Ferreira, and B. A. Juárez-Aubry, Phys. Rev. D **97**, 085022 (2018).

[184] J. P. M. Pitelli, Phys. Rev. D **99**, 108701 (2019).

[185] V. S. Barroso and J. P. M. Pitelli, Gen. Rel. Grav. **52**, 29 (2020).

[186] T. Morley, P. Taylor, and E. Winstanley, Class. Quant. Grav. **38**, 035009 (2020).

[187] C. Dappiaggi, B. A. Juárez-Aubry, and A. Marta, Phys. Rev. D **105**, 105017 (2022).

[188] G. Lifschytz and M. Ortiz, Phys. Rev. D **49**, 1929 (1994).

[189] E. C. Titchmarsh, *Introduction to the theory of Fourier integrals* (Oxford University Press, Oxford, 1937).

[190] J. S. Dowker and G. Kennedy, J. Phys. A **11**, 895 (1978).

[191] M. Castagnino and R. Ferraro, Phys. Rev. D **40**, 4188 (1989).

[192] M. Castagnino and R. Ferraro, Phys. Rev. D **34**, 497 (1986).

[193] L. H. Ford, Phys. Rev. D **11**, 3370 (1975).

[194] R. C. Tolman, Phys. Rev. **35**, 904 (1930).

[195] R. C. Tolman and P. Ehrenfest, Phys. Rev. **36**, 1791 (1930).

[196] R. C. Tolman, *Relativity, Thermodynamics and Cosmology* (Clarendon Press, Oxford, 1934).

[197] E. T. Akhmedov, K. V. Bazarov, D. V. Diakonov, and U. Moschella, Phys. Rev. D **102**, 085003 (2020).

[198] A. Higuchi, Class. Quant. Grav. **4**, 721 (1987).

[199] B. Allen, Phys. Rev. D **32**, 3136 (1985).

[200] J. Bros, H. Epstein, and U. Moschella, Phys. Rev. D **65**, 084012 (2002).

[201] L. Hodgkinson and J. Louko, J. Math. Phys. **53**, 082301 (2012).

[202] G. N. Watson, *A Treatise on the Theory of Bessel Functions*, 2nd ed. (Cambridge University Press, Cambridge, 1944).

[203] M. Reed and B. Simon, *Functional Analysis*, revised ed. (Academic Press, 1981).

[204] S. Barman, B. R. Majhi, and L. Sriramkumar, Phys. Rev. D **109**, 105025 (2024).

[205] G. Nemes, SIMA **53**, 4328 (2021).

[206] V. G. Kac and P. Cheung, *Quantum Calculus*, 1st ed. (Springer New York, 2002).

[207] O. Costin, N. Falkner, and J. D. McNeal, Am. Math. Mon. **123**, 387 (2016).

[208] W. Magnus and F. Oberhettinger, *Formeln und Sätze für die speziellen Funktionen der mathematischen Physik*, 2nd ed. (Springer-Verlag Berlin, 1948).

[209] G. Lohöfer, J. Approx. Theory **95**, 178 (1998).